Fall 2015

Synthesis, Characterisation, Electrochemical, and Spectroscopic Studies of Cobaloximes: Unique Clues of Cobalt(I) Species in Various Solvents

Michael John Celestine
Old Dominion University, michaeljc2003@hotmail.com

SYNTHESIS, CHARACTERISATION, ELECTROCHEMICAL, AND SPECTROSCOPIC STUDIES OF COBALOXIMES: UNIQUE CLUES OF COBALT(I) SPECIES IN VARIOUS SOLVENTS

by

Michael John Celestine
B.S. Chemistry, May 2012, University of the Virgin Islands

A Thesis Submitted to the Faculty of
Old Dominion University in Partial Fulfillment of the
Requirements for the Degree of

MASTER OF SCIENCE

CHEMISTRY

OLD DOMINION UNIVERSITY
August 2015

Approved by:

_____
Alvin A. Holder (Director)

_____
Craig A. Bayse (Member)

_____
John B. Cooper (Member)

_____
Patricia Pleban (Member)

ABSTRACT

SYNTHESIS, CHARACTERISATION, ELECTROCHEMICAL, AND SPECTROSCOPIC STUDIES OF COBALOXIMES: UNIQUE CLUES OF COBALT(I) SPECIES IN VARIOUS SOLVENTS

Michael John Celestine
Old Dominion University, 2015
Director: Dr. Alvin A. Holder

With the dwindling amount of fossil fuels in the world's reserve is said to run out in the future. The use of alternative fuels such as hydrogen can be produced from renewable sources. One source is the use of first row transition metal complexes that can harness the power of the sun to reduce protons to hydrogen. In this thesis we investigated a well-known hydrogen evolution catalyst in a quest to understand the behavior of different oxidation states that occur during the catalytic cycle.

In an attempt to synthesize a binuclear ruthenium(II) complex, $[\{Ru(phen)_2\}_2\{\mu\text{-}mes(1,4\text{-}phO\text{-}Izphen)_3\}](PF_6)_4$, as a possible photosensitizer for the production of hydrogen from the reduction of protons in various media. The expected product was not synthesized according to the reported procedure that was followed. The reaction was carried out in refluxing ethylene glycol due to low solubility of 2,4,6-trimethyl-1,3,5-tris(4-oxymethyl-1-yl(1H-imidazo-2yl-[4,5-f][1,10]phenanthroline)phenyl)benzene in organic solvents such as acetonitrile, DMSO, and DMF. In the first attempt, two (2) equivalents of complex to one (1) equivalence of ligand was first used, which resulted in the formation of a trinuclear complex, $[\{Ru(phen)_2\}_3\{\mu\text{-}mes(1,4\text{-}phO\text{-}Izphen)_3\}](PF_6)_6\bullet CH_3CN\bullet 10H_2O$, with a yield of 48%. In another procedure with 1.5 equivalences of the ruthenium(II) precursor to 1 equivalence of the ligand, $[\{Ru(phen)_2\}_3\{\mu\text{-}mes(1,4\text{-}phO\text{-}Izphen)_3\}](PF_6)_6\bullet xH_2O$ was isolated with a yield of 58%. The fomula of the trinuclear complex was ascertained by elemental analysis, ESI MS, UV-visible and ^1H NMR spectroscopies, along with electrochemical studies.

In another study $[Co(dmgBF_2)_2(H_2O)_2]$ (where $dmgBF_2$ = difluoroboryldimethylglyoximato) was reacted with triethylamine in either acetone or acetonitrile in an attempt to identify the products that were formed in situ during photocatalytic production of hydrogen when triethylamine was used as a sacrificial reductant. Techniques such as elemental analysis, ESI MS, and UV-visible spectroscopy were used in an attempt to characterize the resulting products from the respective solvents. Futher characterization of the unknown isolated product will be carried out in the near future.

$[Co(dmgBF_2)_2(H_2O)_2]$ was used to synthesize $[Co(dmgBF_2)_2(H_2O)(py)]\bullet 0.5(CH_3)_2CO$ in acetone. The formulation of $[Co(dmgBF_2)_2(H_2O)(py)]\bullet 0.5(CH_3)_2CO$ was confirmed by elemental analysis, high resolution ESI MS, and FT IR spectroscopy. Equilibrium studies carried out on $[Co(dmgBF_2)_2(H_2O)_2]$ proved the formation of a monopyridine species, with formation constants, log K = 5.5, 5.1, 5.0, 4.4, and 3.1 in 2-butanone, dichloromethane, acetone, 1,2-difluorobenzene/acetone (4:1, v/v), and acetonitrile, respectively, at 20 ^oC. In strongly coordinating solvents, such as acetonitrile, the magnitude of K is observed to be lower, and this phenomenon was also observed in the electrochemical studies and in the other spectroscopic studies as well.

A larger formation constant, log K = 4.6 vs 3.1, as calculated for the pyridine coordinated to a cobalt(I) species relative to the cobalt(II) species in acetonitrile at 20 ^oC. The electrosynthesis of hydrogen by $[Co(dmgBF_2)_2(H_2O)_2]$ and $[Co(dmgBF_2)_2(H_2O)(py)]\bullet 0.5(CH_3)_2CO$ in various solvents demonstrated the dramatic effect of the axial ligand on the turn over number of the catalyst, which eventually will assist in the development of the next generation of H_2 producing catalysts.

This thesis is dedicated to my Mom and Dad

ACKNOWLEDGMENTS

I would like to thank my family for all their love and support. I would like to thank Dr. A. A. Holder my mentor, who gave me a chance to further my education. I would like to also thank my fellow lab mates; Jimmie L. Bullock, Mark A.W. Lawrence, Raj Gurung, Edward T. Artis, Deisy L. Esquivel, Lorne S. Joseph, the other undergraduate students, and Professor Chee-Hun Kwak, who offered guidance and support. I would also like to thank the chemistry administrative staff for all their help. I would like to thank Dr. Jim Hall for his assistance with the ^{19}F NMR spectroscopic acquisitions.

I would like to thank the NSF for an NSF CAREER Award (awarded to Dr. Alvin A. Holder), which allowed the successful execution of the completion of this thesis, as this material is based upon work supported by the National Science Foundation under CHE-1431172 (formerly CHE – 1151832). I would also like to thank Old Dominion University for the help and support in completion of this work. Also this research was supported partially by an appointment to the Student Research Participation Program at the U.S. Army Engineer Research and Development Center, Construction Engineering Research Laboratory, administered by the Oak Ridge Institute for Science and Education through an interagency agreement between the U.S. Department of Energy and ERDC-CERL. This work was also partially supported by the Center Directed Research Program at the U.S. Army Corps of Engineers.

TABLE OF CONTENTS

LIST OF TABLES

LIST OF FIGURES

CHAPTER I

INTRODUCTION[1]

GENERAL INTRODUCTION

Chemistry of Cobalt

Cobalt is a Group 8 (Group VIII)metal that has the symbol Co, an atomic number of 27 (electronic configuration = [Ar] $3d^7$ $4s^2$), an atomic weight of 59.93 g mol^{-1}, and one naturally occurring isotope (^{59}Co, 100%).[1] Cobalt was used in Egypt pottery dating back to 2600 BC,[1] and has oxidation states ranging from -1 to +5, with the most common being the +2 and +3 oxidation states.[2] An impure cobalt product was isolated by G. Brandt in 1735, but it was not classified as a new element until T. O. Bergman classified it as such in 1780.[1]

Cobalt(I)

Five-coordinate cobalt(I) (d^8) species have been reported to form square pyramidal and trigonal bipyrimidal geometric isomers[3] and tetrahedral complexes are also known (Figure 1). Depending on the ligands coordinated to cobalt(II) metal centers, mainly phosphites, they can disproportionate to form a cobalt(I) complex and also a cobalt(III) complex.[4] Two other ways for the formation of a cobalt(I) metal center are by photochemical or by chemical reduction.[4]

---

[1] The text of this thesis was modeled after the *Journal of American Chemical Society*.

Figure 1. Cobalt(I)-containing complexes.[4]

Cobalt(II)

Cobalt(II) (d^7) complexes generally have octahedral or tetrahedral geometry, however, five coordinated and square planar geometries are known.[2] Figure 2 shows two cobalt(II) complexes of different geometries. The first structure is of $[Co(NH_3)_6]^{2+}$ which has the classic octahedral geometry which many cobalt(II) complexes possess. Table 1 lists a few examples of cobalt in different geometries and oxidation states.[2] From that table we see that cobalt(II) metal complexes have a wide range of geometries when compared to the other oxidation states. One of the best known cobalt(II) halide complexes is $CoCl_2 \cdot xH_2O$. In its anhydrous form the solid $CoCl_2$ has a blue coloration when compared to its hydrated form ($6H_2O$) which has a red/pink coloration.[1] When placed in a aqueous solution, the chlorides are aquated to produce an octahedral hexaaqua complex which is in equilibrium with the tetrahedral tetraaqua species, but the octahedral is much more favored.[1]

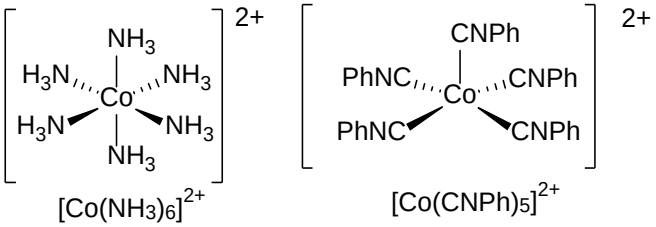

Figure 2. Cobalt(II)-containing complexes.[4]

Cobalt(III)

Low-spin cobalt(III) (d^6) complexes are known for their relative inertness when compared to cobalt(II).[2] The majority of cobalt(III) complexes are reported to be octahedral in shape.[2] Alfred Werner won the The Nobel Prize in Chemistry in 1913 for his work and experiments with cobalt(III) complexes solving the basic coordination chemistry in transition metal compounds.[5] Figure 3 displays three cobalt(III) complexes with the third complex being the of the first complexes that helped give rise to modern coordination chemistry.[5-6]

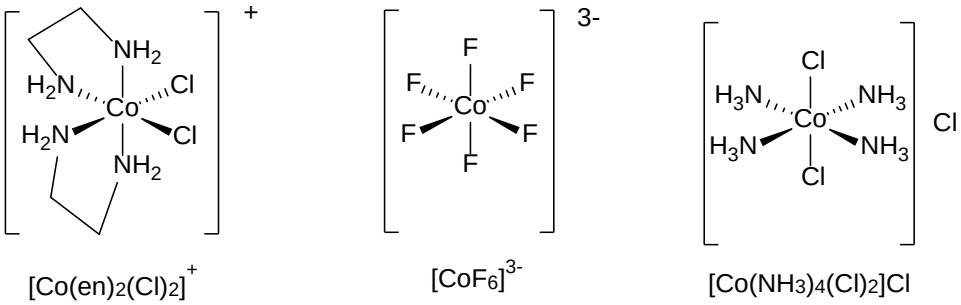

Figure 3. Cobalt(III)-containing complexes.[4, 6]

Cobalt(IV) and Cobalt(V)

The cobalt(IV) (d^5) complexes are low spin paramagnetic with tetrahedral geometry,[4] and are rarely seen. From ligand field splitting we know that tetrahedral complexes are normally high spin. Cobalt(IV) has been reported to be an intermediate in the oxidation of water to form oxygen.[7] In the work of Brunschwig *et al.*,[7] the cobalt(IV) intermediate was formed as a result of an electron transfer from the cobalt complex to an acceptor, which in their case was a ruthenium photosensitizer.

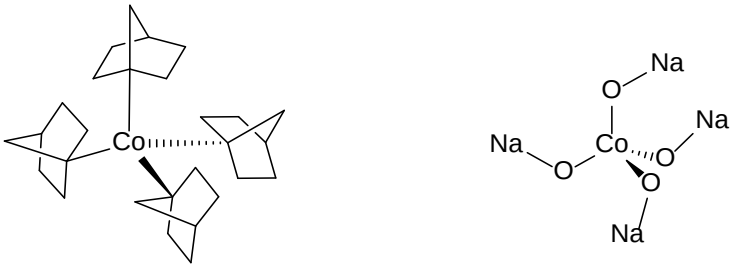

[Co(1-norboynyl)$_4$] Na_4CoO_4

Figure 4. Cobalt(IV)-containing complexes.[4]

Cobalt (V) (d^4) complexes are diamagnetic in nature with a tetrahedral geometry.[4] These complexes are typically formed from the oxidation of cobalt(IV) complexes.[4]

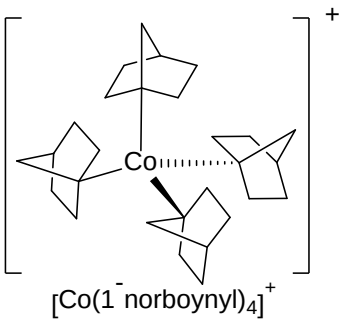

Figure 5. Cobalt(V)-containing complex.[4]

Table 1. Select oxidation states and stereochemistry of cobalt[2]

Oxidation state	Coordination number	Geometry	Examples
Co^{I}, d^8	3	Planar	$[(tempo)Co(CO)_2]$
	4	Tetrahedral	$[CoBr(PR_3)_3]$
	5	Trigonal bipyrimidal	$[Co(CO)_3(PR_3)_2]^+$
	5	Square pyrimidal	$[Co(NCPh)_5]ClO_4$
	6	octahedral	$[Co(bpy)_3]^+$
Co^{II}, d^7	3	Trigonal	$[Co_2(NPh_2)_4]$
	4	Tetrahedral	$[CoCl_4]^{2-}$
	4	Square planar	$[(Ph_3P)_2N]_2[Co(CN)_4]$
	5	Trigonal bipyrimidal	$[Co(Me_6tren)Br]^+$
	5	Square pyrimidal	$[Co(CNPh)_5]^{2+}$
	6	Octahedral	$[Co(NH_3)_6]^{2+}$
	8	Dodecahedral	$(Ph_4As)_2[Co(NO_3)_4]$
Co^{III}, d^6	4	Tetrahedral	--
	4	Square planar	$[Co(SR)_4]^-$
	5	Square pyramidal	[RCo(saloph)]
	5	Trigonal bipyrimidal	[CoCl(TC-4,4)]
	6	Octahedral	$[CoF_6]^{3-}$
Co^{IV}, d^5	4	Tetrahedral	$[Co(1\text{-norbornyl})_4]$
	6	Octahedral	$[CoF_6]^{2-}$
Co^{V}, d^4	4	Tetrahedral	$[Co(1\text{-norbornyl})_4]^+$

The cobalt(III) species are known for their stability compared to cobalt(II) due to their slow ligand exchange rates.[2] In Table 2 the standard reduction potentials ($E°$) for some $Co^{III/II}$ redox couples are given. Generally, the reduction potentials are more negative than the proton couple reduction of oxygen to produce water.

Table 2. Standard reduction potential for some Co^{III}/Co^{II} couples in acid.[1]

Redox couple	E°/V
$[Co(OH_2)_6]^{3+} + e^- \rightleftharpoons [Co(OH_2)_6]^{2+}$	+1.83
$[Co(C_2O_4)_3]^{3-} + e^- \rightleftharpoons [Co(C_2O_4)_3]^{4-}$	+0.57
$[Co(EDTA)]^- + e^- \rightleftharpoons [Co(EDTA)]^{2-}$	+0.37
$[Co(dpy)_3]^{3+} + e^- \rightleftharpoons [Co(dpy)_3]^{2+}$	+0.31
$[Co(en)_3]^{3+} + e^- \rightleftharpoons [Co(en)_3]^{2+}$	+0.18
$[Co(NH_3)_6]^{3+} + e^- \rightleftharpoons [Co(NH_3)_6]^{2+}$	+0.11
$[Co(CN)_6]^{3-} + H_2O + e^- \rightleftharpoons [Co(CN)_5(OH_2)]^{3-} + CN^-$	-0.80
$½O_2 + 2H^+ + e^- \rightleftharpoons H_2O$	+1.23

Chemistry of Ruthenium

Ruthenium is a Group 8 (Group VIII) metal with the symbol Ru, an atomic number of 44 (electronic configuration = [Kr] $3d^7$ $4s^1$), an atomic weight of 101.07 g mol^{-1}, and

seven naturally occurring isotope (Table 3).[1, 8] Ruthenium was discovered in 1844 as a byproduct of purifying platinum.[1] It is known that ruthenium possesses a wide range of oxidation states; ranging from -2, and 0 to +8, with the most common being the +3 state. [1-2]

Table 3. A table of naturally occurring ruthenium isotopes and their abundances.[8]

Isotope	% Abundance
^{96}Ru	5.51
^{98}Ru	1.87
^{99}Ru	12.72
^{100}Ru	12.62
^{101}Ru	17.07
^{102}Ru	31.61
^{104}Ru	18.58

Ruthenium(I)

Apart from the short lived $[Ru(CN)_6]^{5-}$ and $[Ru(bpy)_3]^{+}$ complexes (Figure 6), most ruthenium(I) containing complexes have been reported to be either bimeric or polymeric.[9] Ruthenium(I) complexes are said to react and behave just like ruthenium(II) complexes, and in the case of $[Ru(bpy)_3]^{+}$ the metal center is actually ruthenium(II) and the electron is delocalized on one of the bpy.[9]

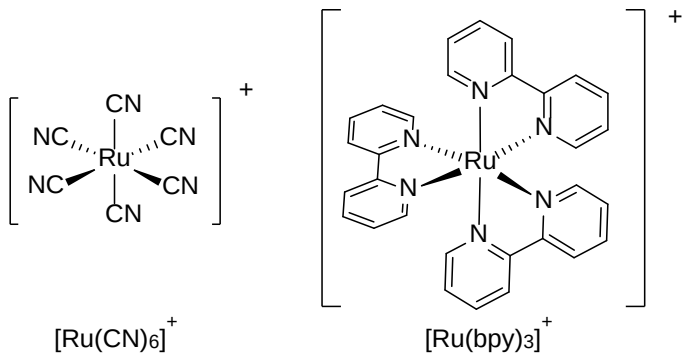

Figure 6. Ruthenium(I)-containing complexes.[4, 9]

Ruthenium(II)

Ruthenium(II) complexes have been reported to have tetrahedral, square planar, or octahedral geometries.[1] Many ruthenium complexes are known for a pronounced metal-to-ligand-charge transfer band, that when excited gives the metal center the ability to undergo an electron transfer process.[10-12] An electron from the ruthenium(II) metal center is first excited from the t_{2g} to the π^* of one of the ligands, that electron can then be transferred either by colliding with an electron acceptor, or by transfer through a bridging ligand.[4, 10-11] The first complex which is shown in Figure 7 is a photosensitizer typically used in solar cells. The second complex in Figure 7, when the chloro-ligands are substituted with a bridging ligand, can participate in electron transfers form the excited complex to electron acceptor without collision.

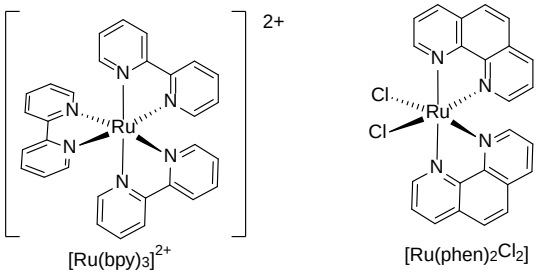

Figure 7. Ruthenium(II)-containing complexes.[4]

Ruthenium(III)

Ruthenium(III) complexes tend to have an octahedral geometry as seen in Figure 8 and listed in Table 4. Many ruthenium complexes are synthesized using $RuCl_3 \cdot xH_2O$, has an oxidation state of +3 as one of the starting materials.[4] Ru(III) complexes have varying substitution rates. Starting from $[RuCl_6]^{3-}$, e.g., in the presence of water the aquation of the first chloro ligand happens within seconds and the rate slows down to about a year for the aquation of the sixth chloro ligand.[4]

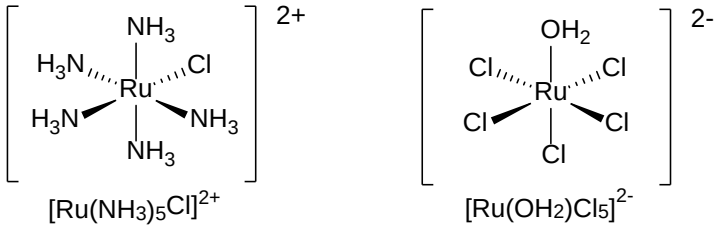

Figure 8. Ruthenium(III)-containing complexes.[4]

Table 4. Selected oxidation states and stereochemistry of ruthenium[2]

Oxidation state	Coordination number	Geometry	Examples
Ru^{I}, d^7	6	--	$[\eta^5\text{-}C_5H_5Ru(CO)_2]_2$
Ru^{II}, d^6	5	Trigonal bipyrimidal	$RuHCl(PPh_3)_3$
	6	Octahedral	$[RuNOCl_4]^{2-}$
Ru^{III}, d^5	4	Distorted tetrahedral	
	6	Octahedral	

Table 5. Standard reduction potential for some ruthenium species in acidic aqueous solution.[1]

Redox couple	E°/V
$Ru^{2+} + 2e^- \rightleftharpoons Ru^0$	+0.455
$Ru^{3+} + e^- \rightleftharpoons Ru^{2+}$	+0.249
$RuO_2 + 4H^+ + 2e^- \rightleftharpoons Ru^{2+} + 2H_2O$	+1.120
$[RuO_4]^{2-} + 8H^+ 4e^- \rightleftharpoons Ru^{2+} + 4H_2O$	+1.563
$[RuO_4]^- + 8H^+ 5e^- \rightleftharpoons Ru^{2+} + 4H_2O$	+1.368
$[RuO_4] + 4H^+ 4e^- \rightleftharpoons RuO_2 + 2H_2O$	+1.387

Cobalt-containing complexes as catalysts for hydrogen evolution

$[Co(dmgBF_2)_2(OH_2)_2]$ and numerous cobalt-containing macrocyclic compounds (**Figure 9**) are usually considered as models of the coenzyme, vitamin B_{12}. Studies performed on these cobalt containing macrocyclic compounds have allowed for the postulation of various mechanisms involving vitamin B_{12} within living organisms.[13] Cobaloximes have an octahedral geometry, with two equatorial glyoximato ligands and two interchangeable axial ligands, as shown in by the structures A-E in Figure 9. Cobaloximes and similar cobalt complexes with ligands such as the tetraazamacrocyles, imine/oxime functionalities are utilizes to stabilize the cobalt(III) species and to some extent the cobalt(II) species.

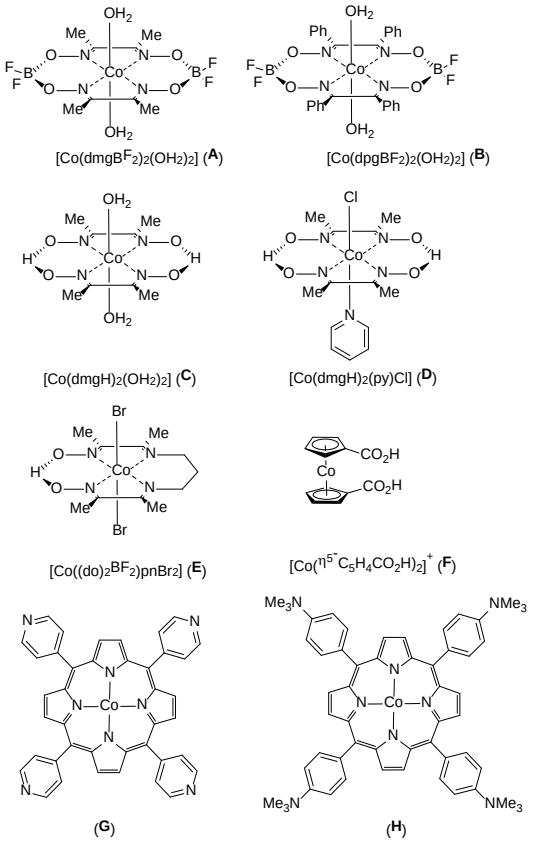

Figure 9. Some cobalt catalysts used for the generation of hydrogen.[14]

Cobaloximes and similar tetraazamacrocyles have been reported to have the ability to reduce protons in solution to form hydrogen,[14] and the project relies on this as a catalytic center. From the literature, the most acceptable route in the catalytic evolution of hydrogen first involves the formation of a cobalt(I) species.[15-16] Recent studies have been geared towards studying the cobalt(I) intermediate through NMR spectroscopy[17] and XAS[18] and HFEPR[19] techniques. Other studies[16, 20-21] have employed bridged binuclear cobaloxime systems in an effort to understand and enhance the catalyst performance. For photocatalytic processes involving molecular systems with metal-containing photosensitizers linked by pyridine type systems to a cobaloxime catalytic center,[22-23] the effect of bridging ligand in the axial position on the electron transfer relative to the "free" cobaloxime center is unclear.

Little is known on the effects the sacrificial electron donors, such as triethanolamine, diethanolamine, monoethanolamine, triethylamine, MeOH, EtOH, $EDTA^{4-}$, *L*-ascorbic acid, and phenol, on the chemistry of several cobalt-containing complexes as reported in the literature. [24]

Various electrocatalytic studies,[15, 17, 20, 25-29] have focused on the variation of the equatorial ligands, however, it is still unclear as to how the axial ligand influences the redox chemistry and catalytic activities of these cobalt systems towards the reduction of protons. Pyridine-type linker groups form an important template in the synthesis of photocatalytic systems reported for the reduction of protons to form hydrogen.[14, 22, 30]

Other studies involving cobaloxime have explored their redox activities. Bakac *et al.*[13] for example, carried out studies involving the oxidation of $[Co(dmgBF_2)(OH_2)_2]$ in the presence of $[Fe(OH_2)_6]^{3+}$ using UV-visible spectroscopy (Scheme 1). From the reaction, it was concluded that the electron transfer process occurs after the formation of $[(OH_2)_5Fe(OH)Co(dmgBF_2)_2(OH_2)]^{2+}$ as an intermediate.[13] This reaction was reversible in the presence of chromium(II), i.e., most of the cobaloximes were reduced back to the cobalt(II) metal center.[13] The equilibrium studies of that report, suggests that redox reaction between iron(III) and the cobalt(II) species of scheme 1 lies to right the reaction.

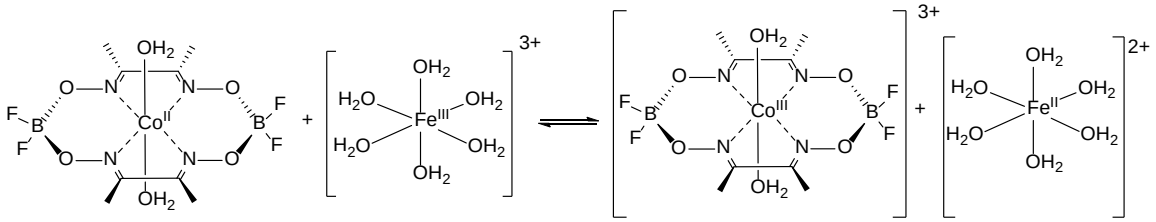

Scheme 1. Oxidation of a cobalt(II) metal center in the presence of $[Fe(OH_2)_6]^{3+}$.

The reduction of alkyl-cobalt(II) complex causes homolytic cleavage of the metal-alkyl bond which then results in the formation of the cobalt(I) species and an alkyl free radical, Scheme 2.[31] Similar single electron-transfer reactions have also been reported between metal hydrides and aromatic ketones.[31] The stability and nucleophilicity of the cobalt(I) species that is formed is based on the absolute energy of the $3d_{z^2}$ orbital and the charge density of the cobalt metal center which arises from the ligands in the equatorial position.[9]

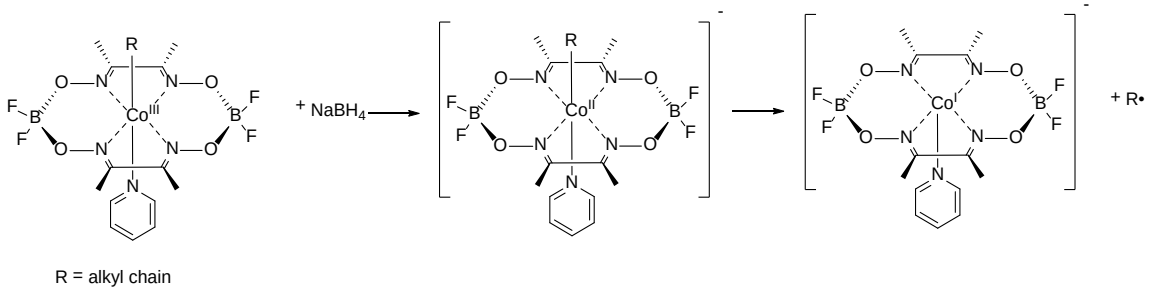

Scheme 2. Reduction of a cobaloxime in the presence of $NaBH_4$.

Radiolytic studies of cobalt-containing complexes

In an effort to assist in understanding the electron transfer process and the substitution kinetics of the Co(II) and Co(III) oxidation states, radiolytic studies were carried out on some cobalt(III) complexes, for example, $[Co(dmgH)_2(py)(Cl)]$.[32-34] Radiolytic and high-pressure kinetic studies of cobalt(III) compounds such as $[Co(NH_3)_5(CH_3)]^{2+}$ and $[Co(phendione)_2Cl_2]Cl$, directed towards the lability of the ligands on the resulting Co(II) species,[35-37] and other studies involving Co(II)[38] and Co(III)[34, 36] complexes bearing polypyridyl ligands such as $[Co(pic)_2(bpy)]$ (where pic^- = 2-picolinato ligand), $[Co(bpy)_3]^{3+}$, $[Co(phen)_3]^{3+}$, $[Co(en)_2(bpy)]^{3+}$, and $[Co(en)_2(phen)]^{3+}$ show the formation of a ligand radical anion species, which decays by either protonation of the ligand,[39-40] or by reduction of the metal center via intramolecular electron transfer. Kumar and co-workers[37] have attempted to distinguish between $[Co^I(dmgBF_2)_2]^-$ species and the pyridine coordinated species. In their work, radiolysis and chemical means of reduction in $MeOH/H_2O$, were presented as evidence of the various oxidation states of cobalt. However, in their report, the effect of solvent on the coordination of pyridine to the Co(II) state was not investigated. These studies are of interest, because the stability of the different oxidation states of the cobaloxime and its coordination sphere are believed to have a significant effect on its catalytic properties. In strongly coordinating solvents (as determined from solvent exchange rate constants[41-42] for example), or in the presence of various nucleophiles, the axial ligands of the cobaloxime may be easily substituted by the solvent,[18, 43] which is expected to influence the redox and substitution chemistries of the cobalt center. Acetonitrile has proven to be a very convenient solvent for the electrocatalytic and photocatalytic studies of cobaloximes, however the influence of this

solvent (and other coordinating solvents) from its ability to substitute the axial ligands have been neglected.

Electrochemical studies on cobaloxime complexes

Cobaloximes are known for their ability to reduce protons to hydrogen in solutions at comparatively modest overpotentials.[44] The potential needed for the onset of the catalytic current is important because, in water, if the potential needed to produce hydrogen is very negative, the result can lead to the electrode splitting the water instead of the catalyst reducing protons. In 2014, Wakerley and Reisner[45] carried out a study on how the electrocatalytic effects are influenced by the ligands in the axial position as seen in the image below. It was noted that electron donating groups on the pyridine ring, even if it was just one, gave a better catalytic response when compared to that of pyridine as the axial ligand. When 3,5-dimethylpyridine was used as the axial ligand a large response was recorded, but it was noted the complex would degrade with consecutive scans which is attributed to the inadequate electrostability of the complex.[45] From the studies as carried out by Wakerley and Reisner,[45] it was also reported that imidazole containing ligands increase the observed catalytic current, but also increased the overpotential needed for the reduction of a cobalt(II) metal center to form a cobalt(I) metal center.

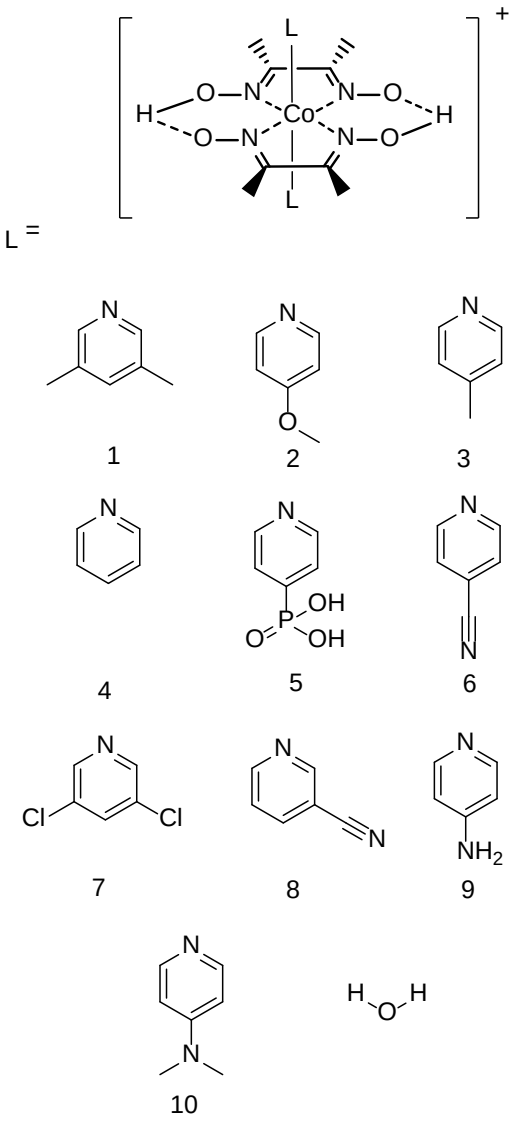

Figure 10. Cobaloximes with different pyridine analogues or water coordinated in the axial position of the complex.

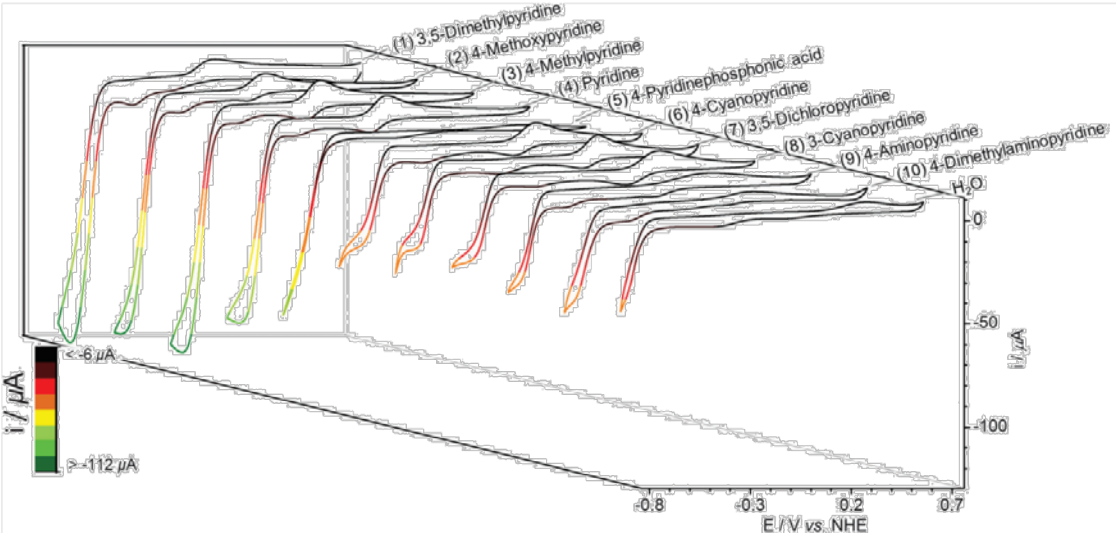

Figure 11. Cyclic voltammagrams of a series of cobaloximes in a phosphate buffer solution at a pH of 7.0. Published by the PCCP Owner Societies.[45]

SOLAR FUELS

The rapid consumption of fossil fuels as a primary fuel source is causing major environmental problems, with the potential to alter the global climate by the emission of the greenhouse gas, CO_2.[46-47] Furthermore it could be inferred that the increase in the average global temperature is believed to be due to the increasing amount of greenhouse gasses that are released during the combustion of fossil fuels. Solar energy is an energy source that has been gaining much attention as a potential alternative to fossil fuels.[47] The conversion of solar to chemical energy via the production of

hydrogen from water offers a fuel source which is clean and renewable, and could potentially reduce the amount of harmful greenhouse gases emitted through the burning of fossil fuels.[48-54] The process of splitting water into hydrogen and oxygen requires a multi-electron redox process, all while overcoming the large energy barriers which can be lowered with the use of a catalyst.[55] The most effective catalysts for water splitting to produce hydrogen as a fuel source are rare noble metals such as platinum, palladium, and rhodium, to name a few, but the costs to produce such catalysts are extreme, making these catalysts less attractive alternatives when compared to the use of fossil fuels.[56-58] Recent major advancements and enhancements in hydrogen fuel cell technologies allows for storage in transportation, stationary and portable applications thus opening the door for hydrogen production.[59]

Due to the demand for fossil fuels being as high as it is currently and the dwindling amount of fossil fuels in the World's reserves, the search of alternative non-fossil fuels is expanding. As shown in Figure 12, the renewable fuel energy sources such as wind, solar, tide, and wave are on the borderline of non-existence when compared to fossil fuels which make up about 83% of the energy produced worldwide.

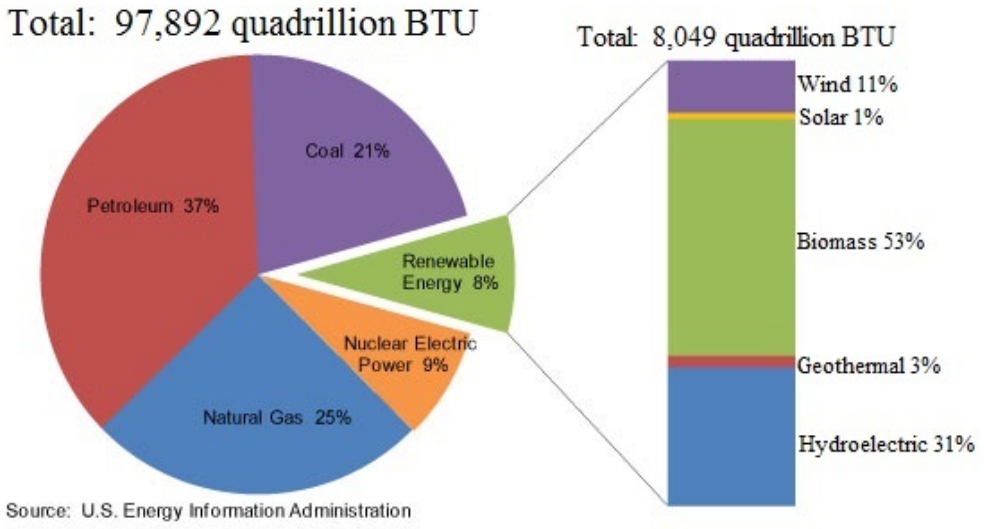

Figure 12. United States of America's energy consumption for 2010.[60]

The world's consumption of fossil fuel through combustion is known to produce carbon dioxide, which is a known greenhouse gas; a gas that is believed to be the cause of global warming and the current climate change. In the last four decades, we have evidence to show that the world's temperatures are rising when compared to the year 1850. Figure 13 shows the temperature anomalies from 1850 to 2010 where from about 1910 onwards there seems to be a steady increase number of these anomalies. Figure 14 shows the **c**arbon dioxide emissions in the U.S.A. by source, where non-fossil fuel consumption accounts for 5% of such emissions. There have been many strives for alternative energy sources that are carbon-neutral or free.[61] Carbon neutral or fossil free energy sources may have the ability to steady these anomalies. Large scale use of alternative fossil fuel sources have the potential to return the average temperature to the averages seen in a pre-1910 era. One of the best routes for the development of alternative energy sources would be to expand on

research involving solar energy capture and the development of cheaper catalysts to produce alternative energy sources to that of fossil fuels.

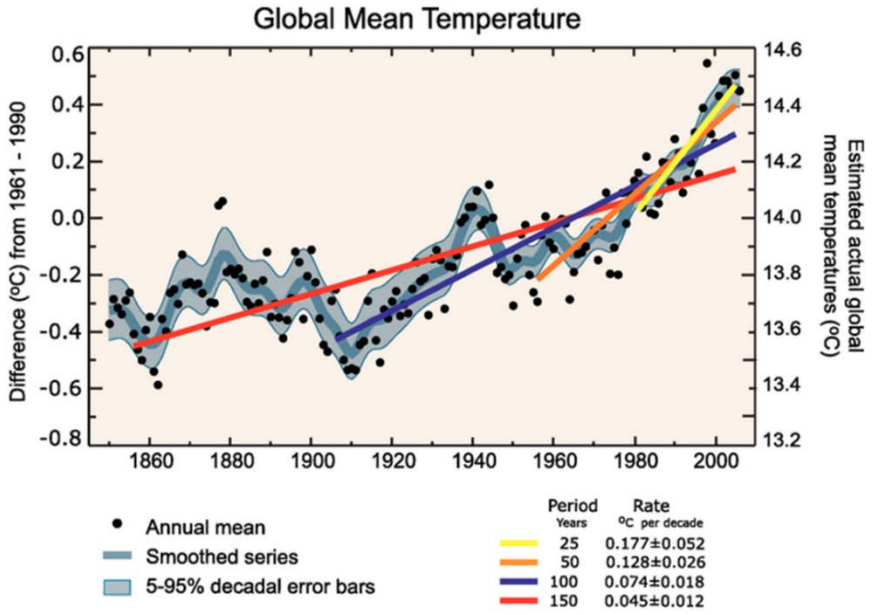

Figure 13. Global annual average temperature and carbon dioxide concentration measured over land and oceans from 1850 to 2010.[62]

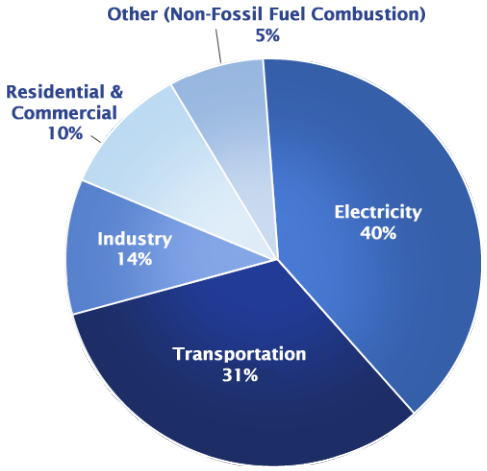

Figure 14. Carbon dioxide emissions in the U.S.A. by source.[63]

In light of the problems, we need to discuss hydrogen's role in an uncertain energy future as energy use in this century and beyond faces deep uncertainties. There are widely conflicting opinions on the size of ultimately recoverable fossil fuel reserves, and the extent to which unconventional resources can be tapped. If, as expected in most forecasts, fossil fuel use continues to grow, the sequestration of vast amounts of CO_2 would be needed if we are to limit global warming. Large emitters such as power plants could probably only capture around a third of the amount needed, requiring the deployment of air capture, untried, and energy-intensive technology. Carbon free sources face their own uncertainties. The future of nuclear energy depends heavily on the successful and timely development of either breeder reactors or fusion energy. Yet, after nearly half a century of effort, neither is near commercialization, and fission technologies face deep public opposition. Ongoing climate change will adversely affect hydro and biomass energy expansion. The potential for intermittent renewable energy sources, wind and solar, is far

greater, but is unevenly distributed spatially, and both face orders of magnitude scale-up to be major energy suppliers. They will eventually also need conversion and storage, which will greatly raise the costs of delivered energy. For all these reasons, we have argued that a low energy future is more likely. There is a need to use ruthenium- containing complexes and similar types of systems in solar energy capture and as photosensitizers for the production of hydrogen in various solvent media. In the following sections, we will explore some advances towards cheaper methods of catalytically producing molecular hydrogen with ruthenium and cobalt complexes; and through their coupled use in solar energy capture and production of hydrogen.

Ruthenium-based photosensitizers

For many years, ruthenium(II) polypyridyl complexes have been reported in the literature for their roles in photochemistry, photocatalysis, photoelectrochemistry, and electron and energy transfer.[64-72] The production of efficient solar cells which are capable of harnessing and storing the sun's energy for future use have the potential to reduce the amount of greenhouse gases produced through the burning of fossil fuels. Polypyridyl ruthenium(II) complexes are reported as being powerful sensitizers due to strong metal-to-ligand charge transfer and the lowering of the π^* energy level which can be tuned by functionalizing the polypyridyl ligands.[73] In the case of photosensitized TiO_2 particles, the lowering of the π^* energy level allows for a more efficient electron injection into the conductance band of the TiO_2 particles.[73]

A clear example is the ruthenium dye-sensitized of the type N3 solar cells, as shown in Figure 15, which were first reported by O'Regan and Grätzel with the N3 photo sensitizer being unmatched by any other known sensitizer in the early 1990s.[74-75] When

treated on TiO_2, the ruthenium dyes act as proficient charge-transfer sensitizers for nanocrystalline TiO_2 films.[75] As a result many ruthenium based solar cells are reported to work very efficiently in areas of low light. During photosynthesis only about 10% of the solar radiation captured by plants is converted into chemical energy, but there were reports that porous nanocrystaline TiO_2 films that were sensitized by polypyridyl ruthenium dyes have an efficiency that exceeds 11%.[76] In 2013 Nath *et al.*[77] reported that when the carboxylic acids of the N3 ruthenium dyes are capped with 1-methyl-3-phenylpropylamine they were able to achieve an efficiency of 15%, thus placing such ruthenium solar cells on par with some of the more expensive silicon-based solar cells.

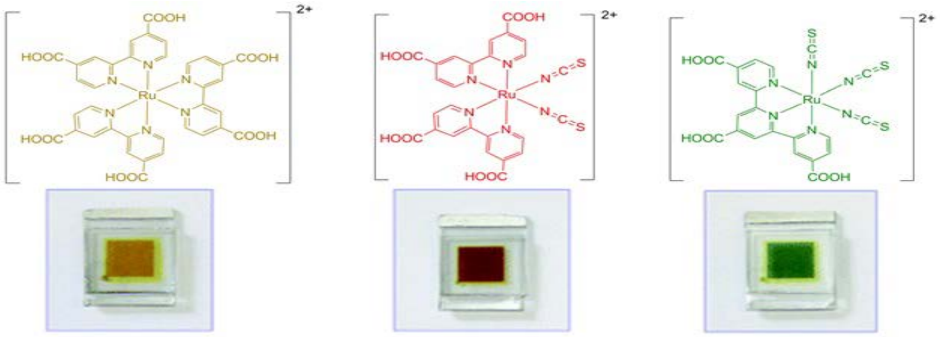

Figure 15. Solar cells coated with ruthenium dye-sensitized TiO_2. Reprinted (adapted) with permission from Grätzel, M., *Inorg. Chem.* **2005**, *44* (20), 6841. Copyright 2005 American Chemical Society.[76]

The formation of the covalent Ti-O-C, Ti-O-P, or Ti-S linkages between the TiO_2 and the ligand improves binding and promotes faster charge transfer between the photoexcited photosensitizer and the nanoparticle.[78-80] A study reported by Shahroosvand *et al*.[81] showed that by increasing the amount of carboxylate attached to the dye, one can obtain better penetration of the dye into the porous TiO_2 nanostructure. It was concluded that their dyes had an efficiency of 13% for light with a wavelength of 510 nm.[81] Studies conducted on dyes with thiol functional groups binding to metal oxides showed that there was an increase in the bonding affinity and current when the thiol was deprotonated.[80] Complex **5** was shown to be an efficient solar energy converter with an efficiency of ~5.6% followed closely by complexes **2**, **1**, **3**, and **4** with efficiencies of 2.6%, 2.1%, 0.9%, and 0.3%, respectively.[79-80]

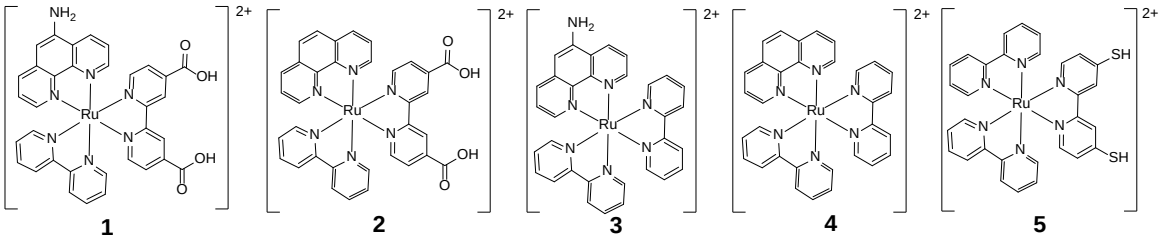

Complexes **6-9** were synthesized with the tridentate bipyridine-pyrazolate ancillary ligands in order to increase the π-conjugation of the system as well as increase the dye

uptake onto the TiO_2 nanoparticles.[82] The solar energy uptake of the ruthenium dyes with the tridentate bipyridine-pyrazolate ancillary ligands was larger than that of the N3 type, with their conversion of solar energy to electricity being comparable around 6%.[82] It was believed that the increased thermal and light absorption stability could lead to an extension in the life spans of solar devices.[82]

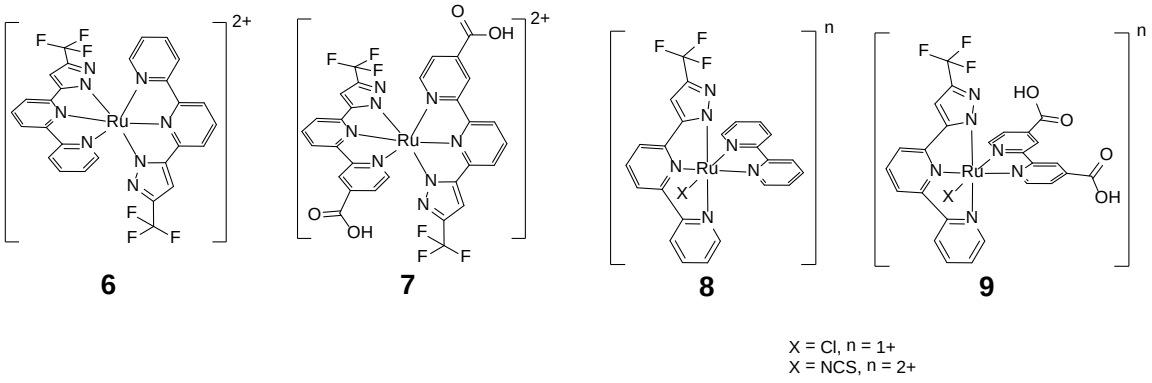

Based on mechanistic studies, photoexcitation of $[Ru(bpyR_2)_2XY]^{n+}$ (where X = Y = NCS^-, or a bpy analogue), occurred when an electron was excited into a MLCT state.[64, 83] This transpired when the electron from the d-orbital of ruthenium was transferred to the π^* orbital of one of its ligands.[64, 83] The MLCT excited state of the photosensitizer was reductively quenched by sacrificial electron donors such as Et_3N and TEOA.[84] Upon photoexcitation an electron was transferred from the dye into the conductance band of the

conductor.[85] Ruthenium-containing complexes were also reported to be able to transfer an electron after it was excited to TiO_2 creating a charge separation.[86-87] The electron donor thus reduced the oxidized ruthenium photosensitizer which generally enhanced the lifetime of the electron as it moves through the TiO_2.[88]

There has been an substantial amount of research to develop an effective converter of light to electricity with nanometer-sized semiconductor.[87] Polypyridyl-ruthenium complexes have been shown to be very successful charge transfer sensitizers in photovoltaics.[89] Effective charge separation is important in the conversion of light to a suitable energy source similar to what is observed in photosynthesis.[87] This process occurs when the electron is transferred from the photoexcited photosensitizer to the TiO_2 nanoparticle creating a hole confined around the photosensitizer.[87] The efficiency of solar cells are dependent on the time it takes for the electron and hole to recombine and return to the ground state.[87]

In 1993, it was reported that a device created from a simple molecular light absorber achieved a conversion efficiency comparable to that of the conventional silicon-based photovoltaic cells.[75] That is really phenomenal. The researchers with the aid of Figure 16 demonstrated how a solar cell with a ruthenium dye functions in the presence of light. First the ruthenium dye is excited in the presence of light and when it relaxes; an electron is transferred to the conducting glass via the nanocrystaline TiO_2 film generating a current and leaving a hole on the ruthenium dye.[**90**] The spent electron is returned to cathode where it reduces the mediator, in which the electrolyte mixture is normally I^-/I_3^-, which transfers an electron to reduce the ruthenium dye while taking the hole to the cathode to begin the

catalytic process over again.[90] The final solar cell would resemble the cell shown in Figure 17.

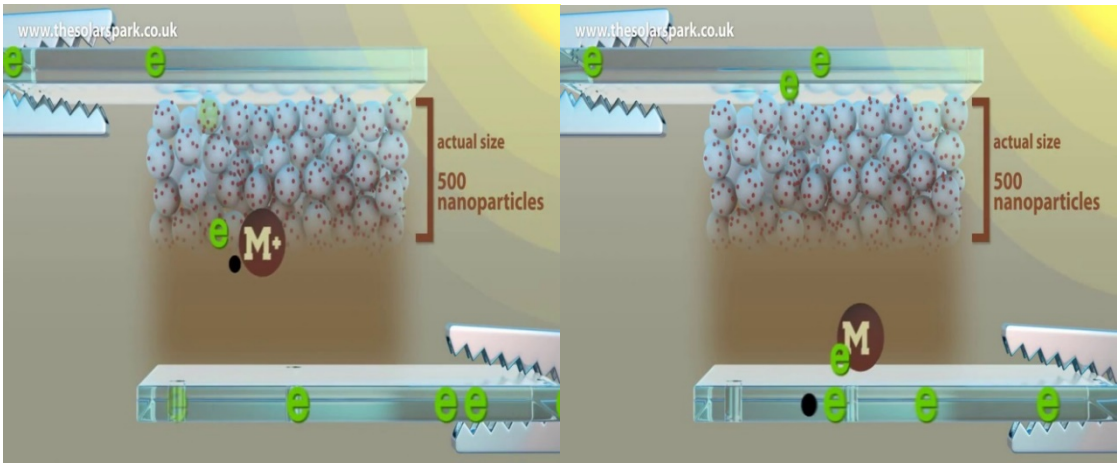

Figure 16. Cross section of a TiO_2 dye-sensitized solar cell.[90]

Dyesol™ engineered a ruthenium dye-sensitized solar panels which by their predictions should be more cost effective to produce and use versus the traditional silicon based solar panels.[91] Dyesol's panels were reported to have a lifetime of approximately 20 years with an efficiency of ~15% and can produce energy in conditions where sunlight is limited unlike silicon-based solar panels that need direct sunlight.[91] Other researchers have reported the use of ruthenium in solar energy conversion.[92-104]

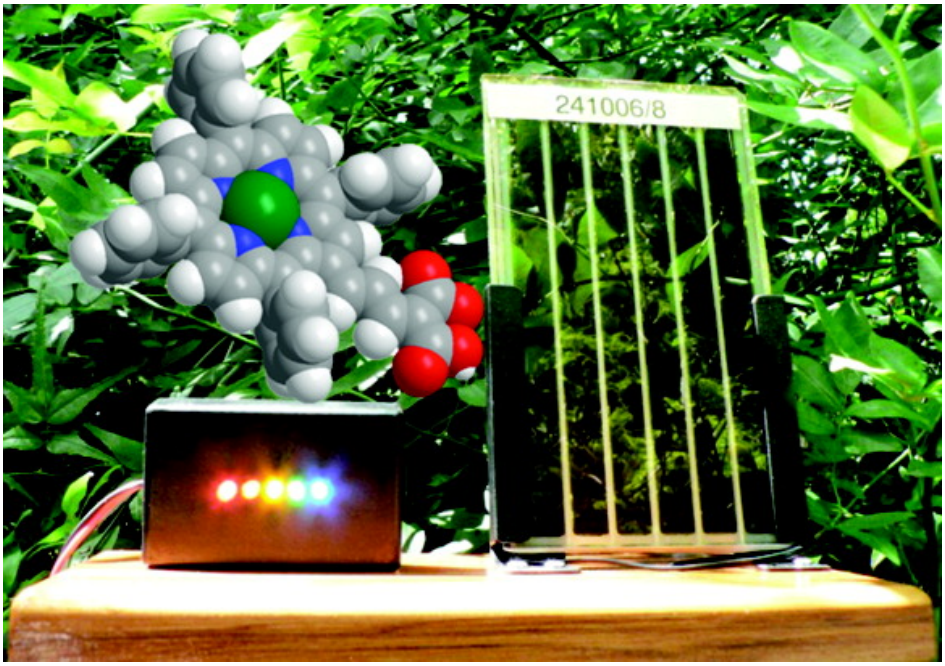

Figure 17. A ruthenium-containing porphyrin dye sensitized solar cell. Reprinted with permission.[105]

Ruthenium photosensitzers used for H_2 production

It was reported by Cao *et al.*,[106] that the transfer of an electron from $[*Ru(bpy)_3]^{2+}$ to a hydrogenase mimic (scheme 3) was thermodynamically unfavorable. The hydrogen ascorbate (HA^-) anion was reported to be able to reduce the excited $[*Ru(bpy)_3]^{2+}$ to form $[Ru(bpy)_3]^+$ which then transfers an electron to the hydrogenase mimic.[106-108] Control

experiments conducted in the absence of *L*-ascorbic acid showed a reduction in the lifetime of the Ru(I) species.[109] The solution was also shown to affect the efficiency of the system, where H_2O had the highest TON (TON = turnover number), which was almost double that of solutions of CH_3CN/H_2O or CH_3OH.[106] The same effect was also reported when comparing the solution mixture of H_2O with ascorbate to a mixture of CH_3CN with acetic acid.[106] In water the TON was more than 88 which is higher than what was observed from CH_3CN.[106]

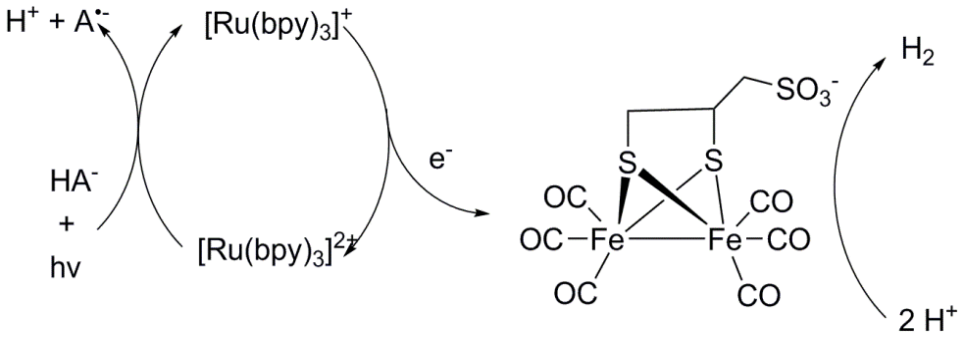

Scheme 3. The photocatalytic pathway for H_2 evolution by [FeFe]-H_2ases mimic with $[Ru(bpy)_3]^{2+}$ and *L*-ascorbic acid.

The binuclear mixed-metal nickel–ruthenium complexes $[Ni(xbsms)Ru(Cp)(L)]PF_6$ (where L = DMSO (**10**) , CO (**11**), PPh_3 (**12**), and PCy_3 (**13**)) were designed to mimic the active site of NiFe hydrogenases.[110] From the reported experiments, it was concluded that there is an increase in the electron density around the

metal centers, which allowed complexes like [Ni(xbsms)Ru(Cp)(DMSO)]PF_6 **10** to be able to produce hydrogen in DMF with $[Et_3NH]^+$ being used as a proton source.[110] It was reported that the complexes' overpotential were reduced by 180 mV compared to previous NiRu complexes thus making them efficient NiFe hydrogenase mimics.[110] DFT calculations were used to propose a mechanism which involved a possible bridging hydride that is formed after a two electron reduction of a proton.[111]

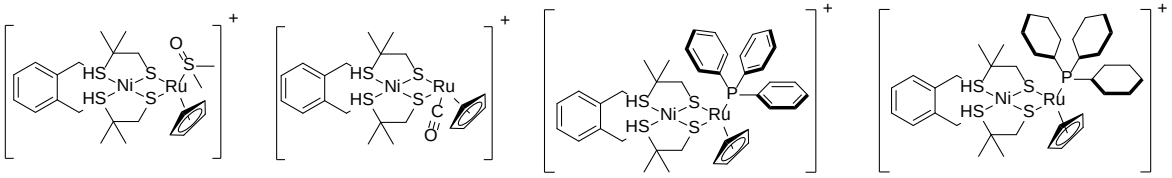

10 **11** **12** **13**

Complexes with ruthenium and rhodium metal centers

The binuclear mixed metal complexes, $[(bpy)_2Ru(dpp)Rh(COD)](PF_6)_3$ and $[(Me_2bpy)_2Ru(dpp)Rh(COD)](PF_6)_2(BF_4)$, were reported to produce H_2 when compared to the sterically hindered complex **16**.[112] Steric hindrance played an important role in the production of H_2 in the binuclear complexes during photoreduction, where complexes such **23** can dimerize and impede contact with the substrates.[112] It was reported that by tuning the sterics and electronics of the binuclear complexes through the terminal ligands a point

is reached where complexes **14** and **15** were able to produce H_2 from H_2O.[112-113] Ruthenium-rhodium-ruthenium trinuclear mixed-metal complexes such as complex **17** were recognized for their ability to reduce H_2O to form H_2 through a photoreduction process, whereas the binuclear mixed-metal ruthenium-rhodium complexes were shown not to be able to catalyze H_2O reduction to form H_2.[113]

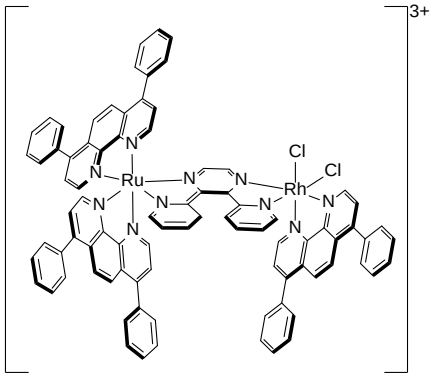

14

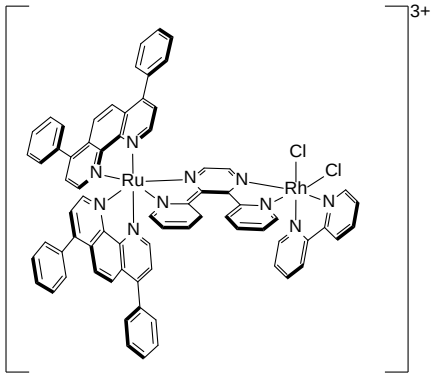

15

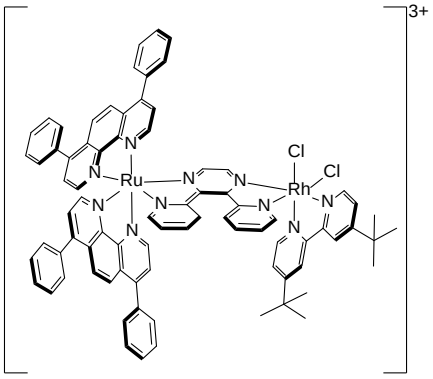

16

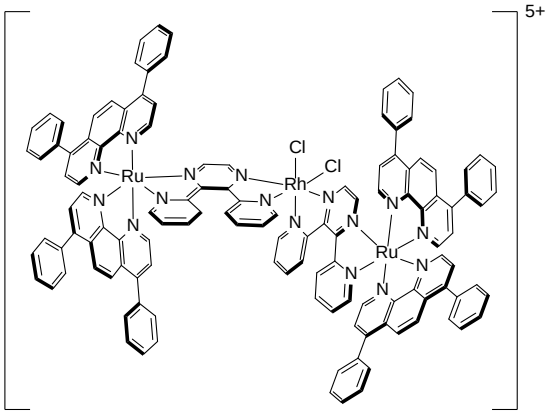

17

Complexes with ruthenium and palladium metal centers

A study with a complex such as $[(tbbpy)_2Ru(tpphz)Pd]^{2+}$ (shown in scheme **4**) showed that the electron-transfer process in the tpphz ligand was potentially able to

produce hydrogen, from the possibility of water forming hydrogen bonds with the phenazine's nitrogen, followed by a reduction when the phenazine was replaced by the acridine unit.[114] It was reported that $[(tbbpy)_2Ru(tpac)Pd]^{2+}$ had a TON of 0.15, but in the presence of water, TON of 139 and 238 were reported for $[(tbbpy)_2Ru(tpac)Pd]^{2+}$ and $[(tbbpy)_2Ru(tpphz)Pd]^{2+}$, respectively.[114-115]

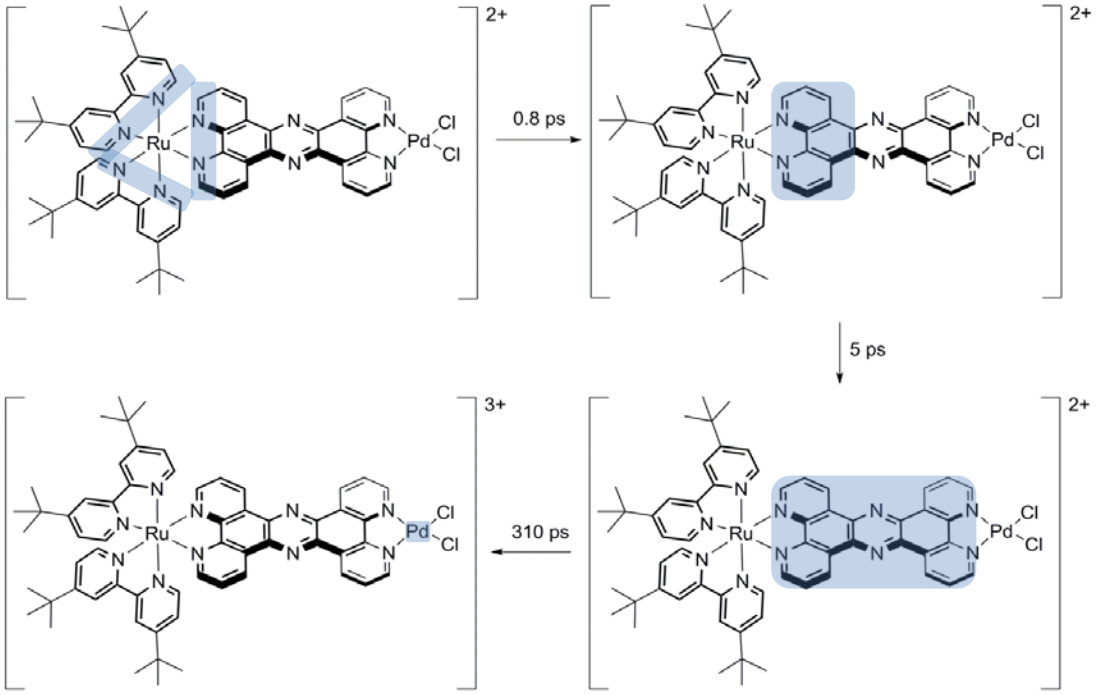

Scheme 4. Intra-molecular electron transfer from the photoactive Ru(II) center to the catalytic Pd(II) metal center.[116]

Complex **18** was reported to have a TON of 400 in the presence of water.[117] It is reported that water plays a major role in the production of hydrogen.[117] Vos *et al.*[117] deduced that water had three functions which are as follows: (i) being a proton source, (ii) enable in proton transfer, and (iii) to stabilize any polar intermediate that may be formed throughout the catalytic process.

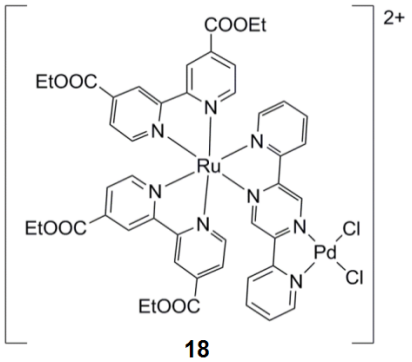

18

It is noted that when complex **19** is photo-excited, the palladium metal center is reduced from Pd(II) to Pd(0).[118] The Pd(0) then dissociates from the ligand to form colloid nanoparticles in solution, which become the site for hydrogen evolution.[118]

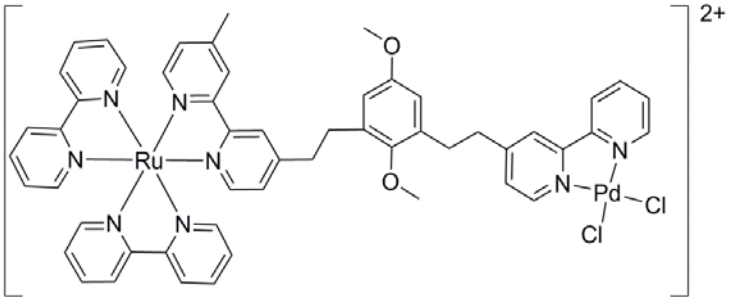

19

Complexes with ruthenium and platinum metal centers

The photocatalytic activities of two binuclear mixed-metal ruthenium(II)-platinum(II) complexes, $[(bpy)_2Ru(dpp)PtCl_2]^{2+}$ (**20**) and $[(bpy)_2Ru(pmcbpy)PtCl_2]^{2+}$ (**21**), were tested for their ability to produce H_2 in the presence of $[Ru(bpy)_3]^{2+}$ and methylviologen.[119] Complexes **20** and **21** were reported to display catalytic properties for the production of hydrogen.[119]

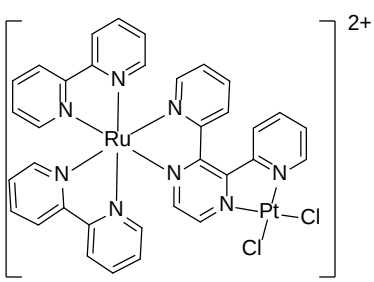

20

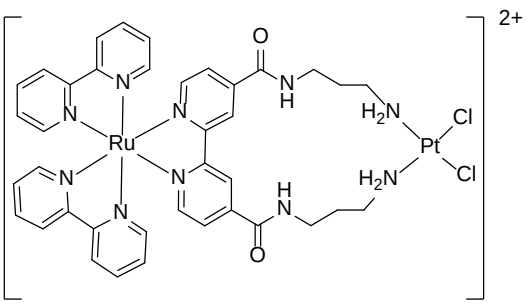

21

Complex **23** was reported to photocatalytically reduce protons to hydrogen in the presence of light and $EDTA^{4-}$ as a sacrificial electron donor.[120] When **22** was compared to **23,** it was reported that the rate of reduction doubled which could be due to the covalent linkage between the two complexes.[120]

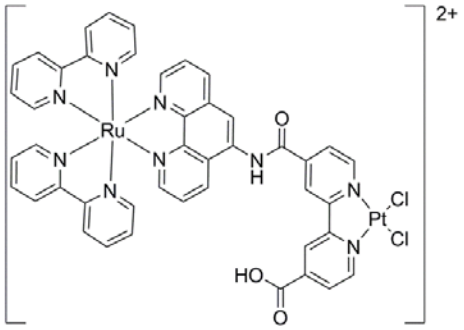

22

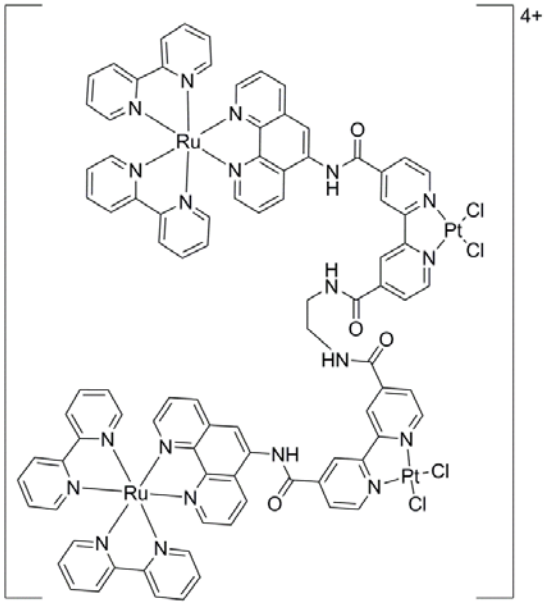

23

Electrochemical studies conducted on the tetranuclear complexes, $[((Ph_2phen)_2Ru(dpp))_2Ru(dpp)PtCl_2](PF_6)_6$ (**24**), $[((Ph_2phen)_2Ru(dpp))_2Ru(dpq)PtCl_2](PF_6)_6$ (**25**) and $[((phen)_2Ru(dpp))_2Ru(dpq)PtCl_2](PF_6)_6$ (**26**) showed that the HOMO orbitals are based on the terminal ligands and the LUMO orbitals are based on the bridging ligand.[121] The tetranuclear complexes were reported as active photocatalysts and are able to produce H_2 from H_2O, with complex **25** having the largest TON of 94 in 10 hours.[121] The environment produced by the BL have a significant impact on the catalytic activity, whereas the terminal ligands affect the wavelength of light that is absorbed.[121]

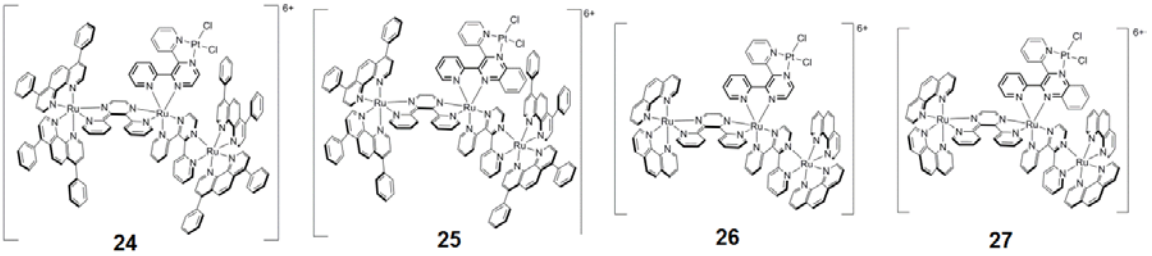

Photocatalytic studies of photosensitized cobaloximes

Recently there is an interest in the use of mixed-metal complexes (with a photoactive metal center bridged via a bridging ligand (BL) to the catalytic active subunit) for the production of hydrogen in various media.[116] In another classic piece of published research by Fihri and co-workers, [122] a BL can be an electron reservoir, whereby it transfers the electron from a ruthenium(II) photoactive center to a cobalt(II) catalyst via an intra-molecular transfer process (see figure 9).[122] In Figure 18, the proton source is the $[Et_3NH]^+$ cation, while the sacrificial reductant is Et_3N. During the catalytic process, a Co(I) species is formed, followed by its reaction with protons to form H_2.[122]

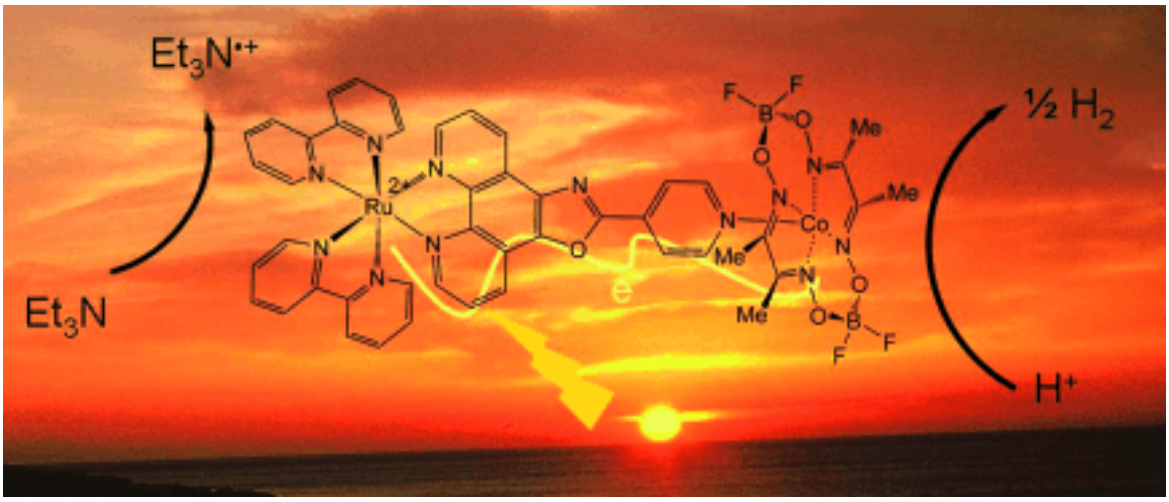

Figure 18. Photocatalytic reduction of protons through an intra-molecular electron transfer from ruthenium(II) photosensitizer to a cobalt(II) catalytic center via the bridging ligand in the presence of Et_3N as a sacrificial electron donor. (Reprinted with permission)[122]

As mentioned above, due to the fact that fossil fuel reserves are rapidly diminishing, emphasis has been placed on the use of renewable energy to meet the fuel needs of the world. Solar to chemical energy conversion is one of the most attractive for sustainable development; thus there is a growing need for the direct generation of molecular hydrogen from water as a result of a convenient and clean energy vector, while utilising renewable resources, for example, water and sunlight.[48-53] However, splitting water into hydrogen and oxygen is a complex multi-electron redox process[55] involving high energy barriers that requires either an electric potential or a catalyst to lower energy barriers. It must be reemphasized that he splitting of water into oxygen and hydrogen has utilised catalysts that are derived from expensive and rare noble metals, for example, Pt, Pd, Rh, *etc.*,[56-57] which are not competitive to fossil fuels, and

unsuitable to meet global demands.[123] More recently and in the past, efforts in research have shifted from heterogeneous to the use of homogeneous catalytic processes that are based on cheaper and abundant first-row transition metals.[23, 122, 124-130]

The entire water-to-hydrogen process first requires the oxidation of water to protons and O_2 followed by the reduction of protons to hydrogen. Success has been achieved on water oxidation,[131-133] however, our focus is on the latter reaction designed to produce H_2. While one approach is to mimic the core of natural hydrogenases,[134-137] there have also been reports of cobaloxime-containing complexes that are efficient electrocatalysts for hydrogen evolution.[15, 55, 138-149] Cobaloximes are composed of a Co(II) center, two equatorial glyoxime ligands and two exchangeable axial ligands, which influence the catalytic activity.[148] Lehn and co-workers pioneered the first studies on homogeneous photogeneration of hydrogen using $[Co(dmgH)_2(OH_2)_2]$ (where $dmgH^-$ = dimethylglyoximato) as a catalyst with $[Ru(bpy)_3]^{2+}$ as photosensitizer and triethanolamine (TEOA) as a sacrificial electron donor in a DMF solution.[126]

Connolly *et al.*,[139] Razavet *et al.*,[148] and more recently, Dempsey *et al.*[15, 55] have carried out thorough investigations of the mechanisms and kinetics of H_2 reduction by cobaloximes. Whereas three different pathways were postulated, all proceed through the same intermediate, a Co(III)-hydride (Co(III)-H) complex that possesses a high hydridic character. Depending on the relative concentrations of protons and Co(I), Co(III)-H is either protonated and releases H_2 in a heterolytic pathway or Co(III)-H is reduced by Co(I) to form Co(II)-H, followed by protonation and H_2 release.[15] The former pathway is energetically unfavourable since the formation of Co(III) involves high energy barriers. A third, homolytic and energetically more favourable pathway

was suggested in which two Co(III)-H species release H_2 and form Co(II) in a reductive elimination step.[15, 148] More recently, Muckerman and Fujita[150] carried out theoretical studies of the reduction potentials of $[Co(dmgBF_2)_2(H_2O)_2]$ in an acetonitrile solution so as to shed light on its electrocatalytical mechanism for hydrogen production. Muckerman and Fujita[150] proposed three mechanisms, all of which were believed to proceed through the formation of Co(III)-H. Their results indicated that the mechanism involving a Co(II)-H intermediate was the most likely.

In an approach to couple an H_2 evolution catalyst to a photosensitizer for photocatalytic H_2 generation, Fihri *et al.*[23, 122] synthesized a series of supramolecular catalysts comprising a cobaloxime-based catalytic center and a Ru(II)-based photosensitizer. The coupling was performed by replacing one of the axial H_2O ligands of the cobaloxime with a pyridine-functionalized ruthenium(II)-polypyridine complex. These complexes were tested for photochemical hydrogen generation from $[Et_3NH]BF_4$, where it was found that the mixed-metal binuclear ruthenium(II)-cobalt(II) complexes were more efficient in hydrogen production than their corresponding multi-component systems under the same conditions. A complex containing a BF_2-capped Co(II) metal center was found to be superior when compared to those with an H-capped Co(III) metal center because the +2 oxidation state in the former is more easily reducible and more resistant towards side reactions, for example, acidic hydrolysis and hydrogenation.[23, 122]

Li *et al.*[151] also studied related mixed-metal binuclear ruthenium(II)-cobalt(II) complexes with and without linker conjugation in order to determine which of the two compounds were better photocatalysts for the generation of hydrogen under homogeneous conditions. While both complexes were more active than the

corresponding multi-component systems, the non-conjugated bridge was found to exhibit higher activity for hydrogen production.[151] My project focus is on the synthesis of binuclear mixed-metal complexes where the catalyst used will be a first row transition metal bridged to a photosensitizer. Many researchers expressed interest in the synthesis and characterisation mixed-metal complexes with a ruthenium(II) metal photocenter for a means of increasing the rate of catalysis Therefore I will brief disscussion on these binuclear mixed-metal ruthenium(II) complexes that are capable of producing hydrogen in acidic media.

Studies that involve the linking of cobalt HEC like cobaloximes to ruthenium photoactive catalytic complexes give rise to binuclear mixed-metal complexes such as $[Ru(pbt)_2(L\text{-pyr})Co(dmgBF_2)_2(OH_2)]^{2+}$ (where = 2-(2′-pyridyl)benzothiazole and L-pyr = (4-pyridine)oxazolo[4,5-*f*]phenanthroline), complex **32**, as reported by Cropek *et al.*[152] Upon irradiation, the binuclear mixed-metal complexes **28-34** in acidic acetonitrile undergo an intra-molecular electron transfer from the photoexcited ruthenium(II) photosensitizer to the cobalt(II) metal center which then leads to the production of H_2.[15] These Ru(II)-Co(II) mixed-metal complexes are reported to have efficiencies up to 8.5 time more than analogous systems under similar conditions.[15] Studies on complexes **33** and **34** showed that complex **34** had a higher TON when compared to complex **33** which is surprising since **33** is conjugated while **34** is not.[15, 151] Complex **32** showed that its TOF varied depending on the sacrificial electron donor, where in Et_3N the TOF was ~1 h^{-1} and in TEOA has a TOF of ~2 h^{-1} as reported in Figure 19.[152] Figure 19 also shows a comparison complex **14** and the mononuclear photocatalyst in solution with the

cobaloxime that there is little to no production of H_2 from the latter, which could be attributed to the BL facilitating in the electron transfer process.

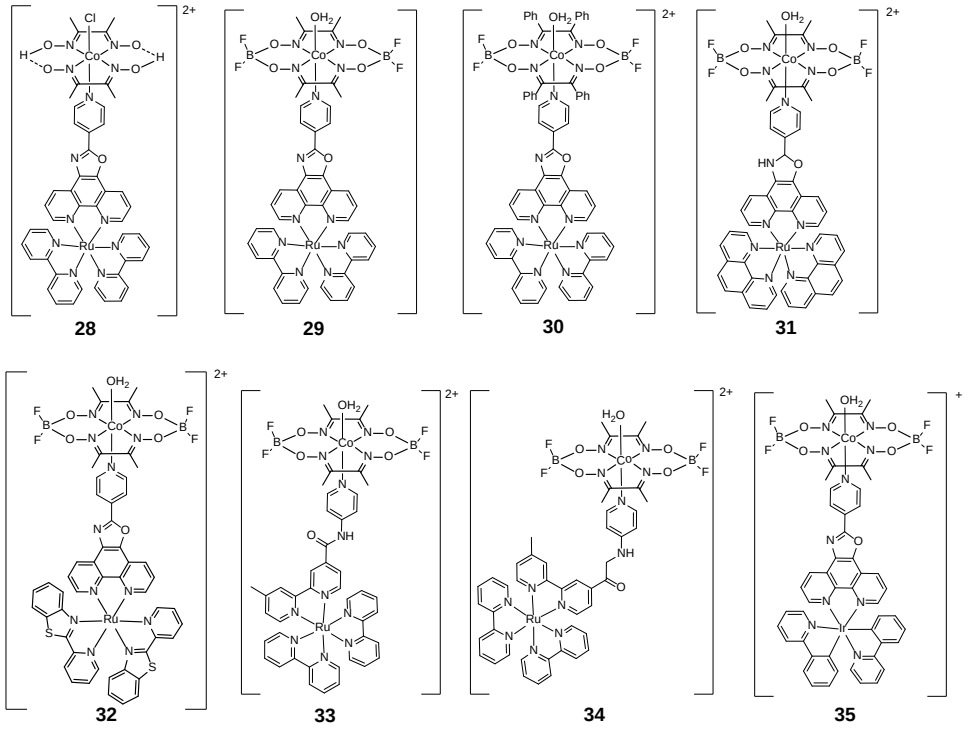

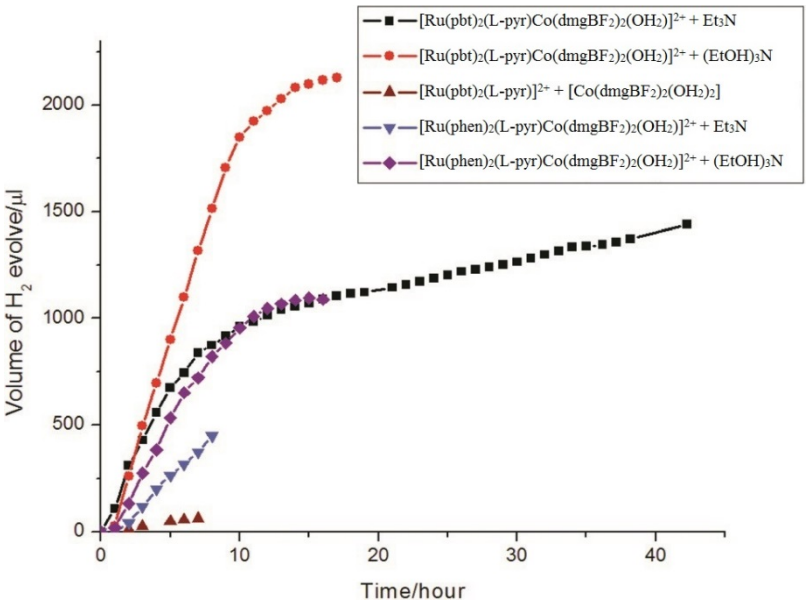

Figure 19**.** Photocatalytic H_2 production in acidic acetonitrile with 300 µM complex and Et_3N as a sacrificial electron donor and *p*-cyanoanilinium tetrafluoroborate as an proton source (Reproduced with permission).[152]

Two binuclear mixed-metal complexes $Ru[(bpy)_2(bpy\text{-}4\text{-}CH_3,4'\text{-}CONH(4\text{-}py))Co(dmgBF_2)_2(OH_2)](PF_6)_2$ **33** and $[(bpy)_2Ru(bpy\text{-}4\text{-}CH_3,4'\text{-}CONHCH_2(4\text{-}py)Co(dmgBF_2)_2(OH_2)](PF_6)_2$ **34** were synthesized with a polypyridyl ruthenium photosensitizer and the cobaloxime catalyst connected by a BL that was either conjugated or unconjugated. [151] Complexes **33** and **34** were tested for their ability to produce H_2. The maximum TON for hydrogen evolution were 38 for complex **33**, and 48 for complex **16** in the presence of both Et_3N, a sacrificial electron donor, and $[Et_3NH]BF_4$, a proton source, in acetone for eight hours of irradiation under visible light.[151] Complex **34** with the

unconjugated BL was reported to generate H_2 more efficiently when compared to complex **33**.[151]

As reported by Cropek and co-workers,[152] photocatalytic studies involving complex **32** were carried out in acidified acetonitrile revealed that H_2 was continuously produced longer than 42 hours and was detected by gas chromatography. Cropek *et al.*[152] proposed a mechanism for hydrogen production with binuclear mixed-metal Ru(II)-BL-Co(II) complexes, where the initial step is the photoexcitation of the ruthenium photosensitizer, followed by the intra-molecular transfer of an electron to the cobalt metal center thus forming the reactive Co(I) species. The Co(I) metal center then reacts with a proton to form a Co(III) species which transfers two electrons to the proton to form a hydride that reacts with another proton. The Co(III)-H bond cleaves through heterolytic fission. The two electrons are then replaced by Et_3N allowing the cycle to be repeated. Time resolved spectroscopic measurements performed on complex **32** confirmed that an intramolecular electron transfer from the excited Ru(II) metal center to the Co(II) metal center via the bridging L-pyr ligand.[152] The formation of the cobalt(I)-containing species is vital for the production of H_2 in the presence of H^+ ions. A proposed mechanism for the generation of hydrogen is shown in scheme **5**.

$[Ru^{II}(pbt)_2(L\text{-}pyr)Co^{II}(dmgBF_2)_2(H_2O)]^{2+} + hv \rightarrow [*Ru^{II}(pbt)_2(L\text{-}pyr)Co^{II}(dmgBF_2)_2(H_2O)]^{2+}$ (**1**)

$[*Ru^{II}(pbt)_2(L\text{-}pyr)Co^{II}(dmgBF_2)_2(H_2O)]^{2+} \rightleftharpoons [Ru^{III}(pbt)_2(L\text{-}pyr)Co^{I}(dmgBF_2)_2(H_2O)]^{2+}$ (**2**)

$[Ru^{III}(pbt)_2(L\text{-}pyr)Co^{I}(dmgBF_2)_2(H_2O)]^{2+} + H \rightleftharpoons [Ru^{III}(pbt)_2(L\text{-}pyr)Co^{III}H(dmgBF_2)_2(H_2O)]^{3+}$ (**3**)

$[Ru^{III}(pbt)_2(L\text{-}pyr)Co^{III}H(dmgBF_2)_2(H_2O)]^{3+} + H \rightleftharpoons [Ru^{III}(pbt)_2(L\text{-}pyr)Co^{III}(dmgBF_2)_2(H_2O)]^{4+} + H_2$ (**4**)

$[Ru^{III}(pbt)_2(L\text{-}pyr)Co^{III}(dmgBF_2)_2(H_2O)]^{4+} + Et_3N \rightleftharpoons [Ru^{II}(pbt)_2(L\text{-}pyr)Co^{III}(dmgBF_2)_2(H_2O)]^{3+} + Et_3N^{\bullet+}$ (**5**)

$[Ru^{II}(pbt)_2(L\text{-}pyr)Co^{III}(dmgBF_2)_2(H_2O)]^{3+} + hv \rightarrow [*Ru^{II}(pbt)_2(L\text{-}pyr)Co^{III}(dmgBF_2)_2(H_2O)]^{3+}$ (**6**)

$[*Ru^{II}(pbt)_2(L\text{-}pyr)Co^{III}(dmgBF_2)_2(H_2O)]^{3+} \rightleftharpoons [Ru^{III}(pbt)_2(L\text{-}pyr)Co^{II}(dmgBF_2)_2(H_2O)]^{3+}$ (**7**)

$[Ru^{III}(pbt)_2(L\text{-}pyr)Co^{II}(dmgBF_2)_2(H_2O)]^{3+} + Et_3N \rightleftharpoons [Ru^{II}(pbt)_2(L\text{-}pyr)Co^{II}(dmgBF_2)_2(H_2O)]^{2+} + Et_2N^{\bullet+}$ (**8**)

Scheme 5. The proposed mechanism for the generation of hydrogen from acidified acetonitrile using $[Ru(pbt)_2(L\text{-}pyr)Co(dmgBF_2)_2(H_2O)$. Reproduced by permission of The Royal Society of Chemistry.[152]

A cobaloxime anchored to TiO_2 nanoparticles was tested for its ability to produce H_2 as an alternative to a platinum catalyst.[153] As shown in Figure 20, upon photoexcitation of the ruthenium photosensitizer, the electron is transferred from the π^* transition state of the photosensitizer to the conduction band of the nanoparticle. The electrons were then transferred from the nanoparticle to the cobaloximes which then reduces protons to form H_2. The nanoparticles were shown to have a TON of 100 under irradiation of visible light.[153-154]

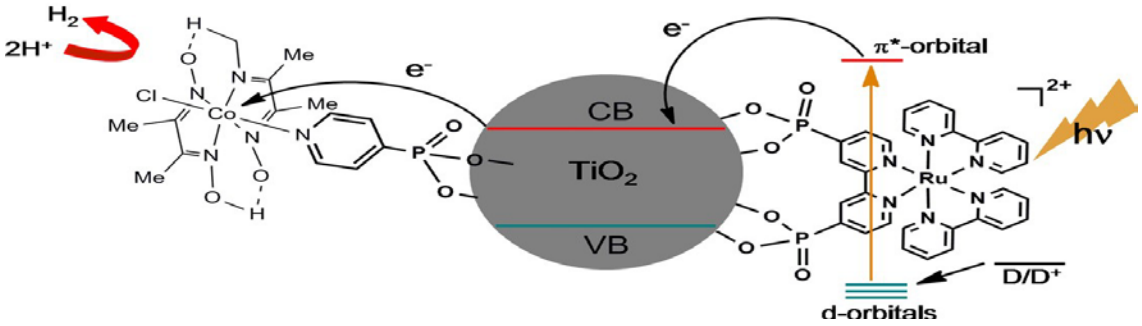

Figure 20. Structure of the TiO_2-based material for H_2 photoproduction using cobaloxime as catalyst. (Reprinted with permission)[153-154]

PROJECT AIMS AND HYPOTHESES

For many years, my mentor has been interested in the development of transition metal complexes that contain at least one cobalt metal center,[155-162] and also inorganic reaction mechanisms that involve electron transfer processes.[156-157, 163-164] Recently, Cropek *et al.*[155] reported the synthesis, characterization, and photocatalytic studies of novel mixed-metal binuclear ruthenium(II)–cobalt(II) photocatalysts ($[Ru(pbt)_2(L\text{-}pyr)Co(dmgBF_2)_2(H_2O)](PF_6)_2$ (where pbt = 2-(2′-pyridyl)benzothiazole, L-pyr = (4-pyridine)oxazolo[4,5-*f*]phenanthroline, and $dmgBF_2$ = difluoroboryldimethylglyoximato), $[Ru(Me_2bpy)_2(L\text{-}pyr)Co(dmgBF_2)_2(OH_2)](PF_6)_2$ (where Me_2bpy = 4,4′-dimethyl-2,2′-bipyridine), and $[Ru(phen)_2(L\text{-}pyr)Co(dmgBF_2)_2(OH_2)](PF_6)_2$) for hydrogen evolution in acidic acetonitrile. Photocatalytic studies carried out in acidified acetonitrile demonstrated constant hydrogen generation longer than a 42 hour period as detected by gas chromatography. Time resolved spectroscopic measurements on $[Ru(pbt)_2(L\text{-}pyr)Co(dmgBF_2)_2(H_2O)](PF_6)_2$, proved an intramolecular electron transfer from an excited

ruthenium(II) metal center to the cobalt(II) metal center via the bridging L-pyr ligand. This resulted in the formation of a cobalt(I)-containing species that was essential for the production of H_2 gas in the presence of H^+ ions. Based on the fact, this thesis will be focused on mechanistic studies involving the role of the cobalt(I) metal center during the course of the production of hydrogen in various solvent media. As such, this thesis will describe the isolation and characterization of a new cobaloxime, $[Co(dmgBF_2)_2(OH_2)(py)]\bullet 0.5(CH_3)_2CO$, together with electrochemical and spectroelectrochemical studies in both strongly and weakly coordinating solvents to assess the effect of solvent on the extent of coordination of the pyridine in the axial position to $[Co(dmgBF_2)_2(OH_2)_2]$, and how this influences the cobaloxime's reactivity in the production of hydrogen. The thesis will also examine the extent of pyridine's coordination to a cobalt(I) metal center in various solvents which will serve as a model for its analogues. This is a critical step to understand the electron transfer process and the stability of a pyridine-cobalt(I) species that is likely to be formed in reduced cobaloximes.

Traditional studies for the photocatalytic production of hydrogen in an acidified media tend to ignore the effects between the catalyst and the sacrificial electron donor. As such, a study to observe the interaction of $[Co(dmgBF_2)_2(H_2O)_2]$ with triethylamine will be monitored spectroscopically for any observable changes. Due to the fact that triethylamine can act as a reductant it can be **hypothesized** that $[Co(dmgBF_2)_2(H_2O)_2]$ in the presence of triethylamine will be reduced to form a cobalt(I)-containing cobaloxime.

Another aspect of the thesis will focus on the attempted synthesis characterization of a new photosensitizer, $Ru(phen)_2\}_2\{\mu\text{-mes}(1,4\text{-phO-Izphen})_3\}](PF_6)_4$, also an intial

study involving the reaction involving Et_3N and $[Co(dmgBF_2)_2(H_2O)_2]$ in both acteonitrile and acetone.

CHAPTER II

ATTEMPTED SYNTHESIS OF A BINUCLEAR RUTHENIUM(II) PHOTOSENSITIZER

METHODS AND MATERIAL

Analytical or reagent grade chemicals obtained from commercial sources were used as received throughout this study. Microanalyses (C, H, N, B, Co, and N) were performed by Columbia Analytical Services (Tucson, AZ), Galbraith Laboratory, Inc. (Knoxville, TN), Intertek Pharmaceutical Services (Whitehouse, NJ), and the University of Illinois Urbana-Champaign (Urbana, IL).

Physical measurements

^{1}H spectra were acquired on a Varian 400 MHz spectrometer where all samples were dissolved in their appropritate solvents.

All electrochemical experiments were performed on a BASi® Epsilon C3 under an argon atmosphere in the respective solvents thoroughly purged with Ar before analysis at room temperature (ca 20 ^{o}C) and are uncorrected for junction potentials. A standard three electrode configuration was employed consisting of a glassy carbon working electrode (diameter = 3 mm), Pt wire auxiliary electrode and a Ag wire as reference electrode in non-aqueous solvents; against which the ferrocenium/ferrocene couple showed a reversible wave at +0.29 V in acetonitrile.

Absorbance measurements were performed on an Agilent® 8453A diode array spectrophotometer.

High-resolution ESI MS spectra were acquired via positive electrospray ionization on a Bruker 12 Tesla APEX –Qe FTICR-MS with and Apollo II ion source. Samples were dissolved in acetonitrile; followed by direct injection using a syringe pump with a flow rate of 2 μL s^{-1}. The data was processed using Bruker Daltonics Data Analysis Version 3.4.

EXPERIMENTAL

Synthesis of 2,4,6-trimethyl-1,3,5-tris(4-oxymethyl-1-yl(1H-imidazo-2yl-[4,5-f][1,10]phenanthroline)phenyl)benzene

The following method was adapted from Samy and Alexander.[67] A hot solution of 1,10-phenanthroline-5,6-dione (0.0590 g, 0.281 mmol) and ammonium acetate (0.4414 g, 5.727 mmol) in glacial acetic acid (957 μL) was added slowly (dropwise) to a mixture of 2,4,6-trimethyl-1,3,5-tris(4-oxymethyl-1-formylphenyl)benzene (0.0529 g, 0.101 mmol) and glacial acetic acid (479 μL) with constant stirring. The reaction mixture was left to reflux for five hours. The reaction mixture was then left to cool to room temperature, before it was poured into water (4.785 mL). Ammonium hydroxide (29%) was added dropwise with stirring. The product was filtered and washed with water and left to dry. Yield = 0.0850 g (77%).

Synthesis of $[\{Ru(phen)_2\}_3\{\mu\text{-}mes(1,4\text{-}phO\text{-}Izphen)_3\}](PF_6)_6 \bullet MeCN \bullet 10H_2O$

2,4,6-Trimethyl-1,3,5-tris(4-oxymethyl-1-yl(1H-imidazo-2yl-[4,5-f][1,10]phenanthroline)phenyl)benzene (0.5040 g, 0.46 mmol) and $[Ru(phen)_2Cl_2]$ (0.4862 g, 0.91 mmol) , along with ethylene glycol (40 mL) were mixed in a 100 ml RB flask; then the mixture was refluxed with stirring for three days under argon. The reaction mixture was then cooled to room temperature; then water (50 mL) was added. Upon addition of

NH_4PF_6 (2.01 g, 12.33 mmol) the solution color changed from dark brown to an orange with an immediate precipitation of the crude product. Filtered aqueous saturated KPF_6 (200 mL) was then added to the reaction mixture; then the reaction mixture was cooled at -20 °C for 90 minutes. Additional NH_4PF_6 (1.01 g, 6.20 mmol) was added to the mixture while it was cooling. The product was filtered by use of a fine frit; then left to dry overnight in a fume hood. The crude product was dissolved in the minimum volume of acetonitrile; then the mixture was filtered in a fine frit.. The filtrate was collected and loaded onto a Sephadex LH-20 column (length = 46 cm, inner diameter = 14.5 cm); then elution was carried out with acetonitrile. The respective fractions that came off the column were monitored via UV-visible spectrophotometry. The suspect fractions with the product were combined; then the solvent was rotary evaporated. The purification process on the combined fractions was repeated with acetonitrile as the eluent on the Sephadex LH-20 column (length = 46 cm, inner diameter = 14.5 cm); then the main fraction was collected, and the solvent was rotary evaporated to leave an orange solid. Yield= 0.79 g (48%). Calc. for $C_{143}H_{119}F_{36}N_{25}O_{13}P_6Ru_3$: C, 48.13; H, 3.36; N, 9.81%. Found: C, 47.98; H, 3.09; N, 10.06%. HRMS (ESI, positive mode): m/z = 387.07 ([M-({Ru(phen)$_2$}$_2${μ-mes(1,4-phO-Izphen)$_2$}) - 6PF_6]$^{6+}$), 773.14 ([M-({Ru(phen)$_2$}$_2${μ-mes(1,4-phO-Izphen)$_2$}) - H^+ - 6PF_6]$^{5+}$). δ_H (400 MHz, DMSO-d_6): 7.02 (d), 7.77 (dd), 7.98 - 8.03 (m), 8.09 (d), 8.11 - 8.20 (m), 8.35 - 8.46 (m), 8.77 (d), 9.04 (d), 10.13 (br. s.) Lit.[166] δ_H(500 MHz; DMSO-d_6; 298 K) 2.07 (s,9H, -CH_3), 4.54 (s, 6H, -CH_2-), 7.01 (d, 6H, J = 8.5 Hz, H_f),7.73–7.79 (m, 18H, H_2, H_7, H_b), 7.98 (d, 6H, J = 4.5 Hz, H_1), 8.06 (d, 6H, J = 5 Hz, H_8), 8.11–8.14 (m, 12H, H_a, H_e), 8.36 (s, 12H, H_5, H_4), 8.74 (d, 12H, J = 8 Hz, H_3, H_6), 9.03 (d, 6H, J = 8.5 Hz, H_c).

Attempted synthesis of [{Ru(phen)$_2$}$_3$(μ-mes(1,4-phO-Izphen)$_3$}](PF$_6$)$_6$

2,4,6-Trimethyl-1,3,5-tris(4-oxymethyl-1-yl(1H-imidazo-2yl-[4,5-f][1,10]phenanthroline)phenyl)benzene (0.3537 g, 0.32 mmol) and [Ru(phen)$_2$Cl$_2$] (0.258 g, 0.48 mmol), along with ethylene glycol (30 mL) were mixed in a 100 ml RB flask; then the mixture was refluxed with stirring for three days under argon. The reaction mixture was then cooled to room temperature; then water (50 mL) was added. The solution was then added to a mixture containing filtered aqueous saturated KPF_6 (200 ml) with added NH_4PF_6 (3.03 g, 18.6 mmol). The mixture was then cooled at -20 °C for one hour; then filtered. The crude product was air dried; then dissolved in the minimum volume of acetonitrile. The resulting mixture was filtered to remove any undissolved KPF_6. The filtrate was collected and loaded onto a Sephadex LH-20 column (length = 46 cm, inner diameter = 14.5 cm); then elution was carried out with acetonitrile. The respective fractions that came off the column were monitored via UV-visible spectrophotometry. The suspect fractions with the product were combined; then the solvent was rotary evaporated to leave an orange solid which was then dried overnight in an oven set at 110 °C. Yield = 0.28 g (58%). Based on elemental analysis, where found: C, 48.46; H, 2.67; N, 9.93%, the complex was formulated as [{Ru(phen)$_2$}$_2${μ-mes(1,4-phO-Izphen)$_3$}](PF$_6$)$_6$•xH_2O. MS (ESI, positive mode): m/z = 387.07 ([M-({Ru(phen)$_2$}$_2${μ-mes(1,4-phO-Izphen)$_2$}) - 6PF_6]$^{6+}$). δ_H (400 MHz, DMSO-d$_6$): 7.01 (d) 7.77 (dd) 7.98 - 8.21 (m) 8.39 (s) 8.77 (d) 10.14 (s).

RESULTS AND DISCUSSION

Synthesis and characterisation of [{Ru(phen)$_2$}$_3$(μ-mes(1,4-phO-Izphen)$_3$}](PF$_6$)$_6$•MeCN•10H_2O

This study was carried out to synthesize a binuclear ruthenium(II) complex that can be used as a possible photosensitizer for the production of hydrogen from the reduction of protons in various media. 2,4,6-trimethyl-1,3,5-tris(4-oxymethyl-1-yl(1H-imidazo-2yl-[4,5-f][1,10]phenanthroline)phenyl)benzene or mes(1,4-phO-Izphen)$_3$ was synthesized using the methods as reported by Samy *et al*.[166] The trinuclear ruthenium(II) complex in scheme 6, was synthesised serendipitously from 2,4,6-trimethyl-1,3,5-tris(4-oxymethyl-1-yl(1H-imidazo-2yl-[4,5-f][1,10]phenanthroline)phenyl)benzene.

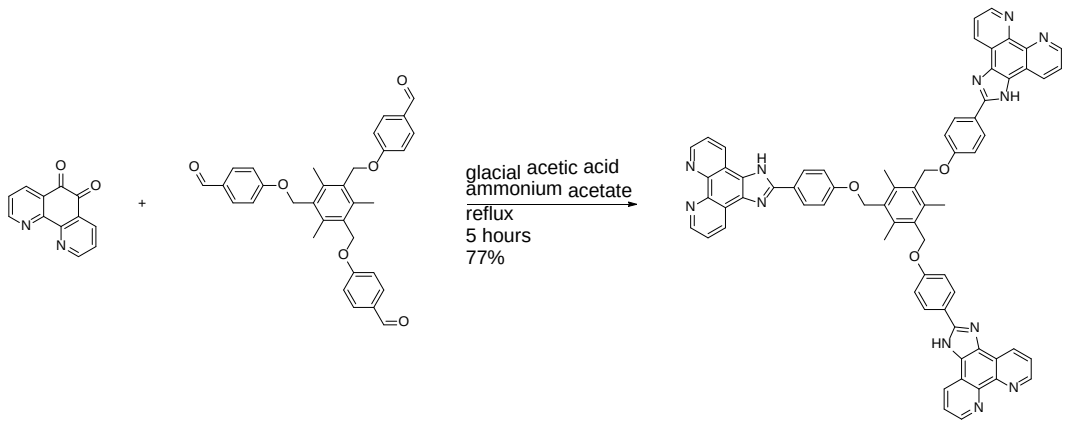

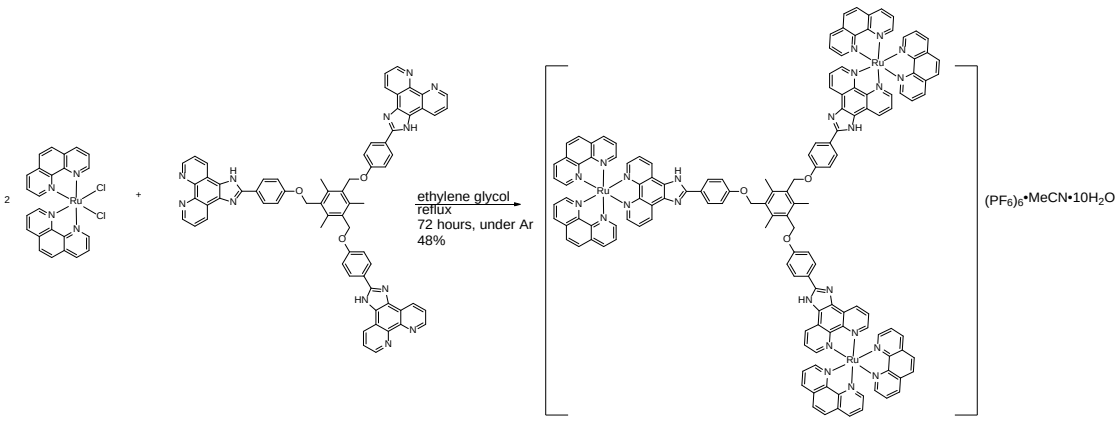

Scheme 6. Synthesis of $[\{Ru(phen)_2\}_3\{\mu\text{-mes}(1,4\text{-phO-Izphen})_3\}](PF_6)_6\bullet MeCN\bullet 10H_2O$

Analysis of the ligand via any type of NMR spectroscopy was futile due to the insolubility of the product in many solvents such as acetonitrile, DMSO, and DMF, a physical property which was also reported by Samy *et al.*[166] The solubility also proved to be an issue in our first attempt to synthesize a novel binuclear ruthenium(II) complex. Though the reaction was carried out as a 2:1 ratio (ruthenium precursor:ligand), a complex which corresponded to the trinuclear ruthenium(II) complex was isolated (see in scheme 6). When the resulting complex was analyzed via ESI MS in the positive moder (see Figure 21), the m/z peaks at 387.07 and 773.13 are the result of fragmentation, which corresponded to the $[Ru(phen)_2(1,4\text{-phO-Izphen})]^{2+}$ and $[Ru(phen)_2(1,4\text{-phO-Izphen}) - H^+]^+$ cations, respectively. Upon analysis of the electronic spectrum (Figure 22), the following wavelengths and molar extinction coeffiecents ($\varepsilon \times 10^4\ M^{-1}\ cm^{-1}$) were observed; 200 (202), 224 (222), 264 (264), 285 (286), and 458 (455) 30.8 (22.9), 31.6 (24.4), 38.0

(29.3), 24.7 (20.1), and 7.6 (5.4), respectively. ^{1}H NMR spectroscopic shifts observed in Figure 23 are the same as those values observed in the literature.[166]

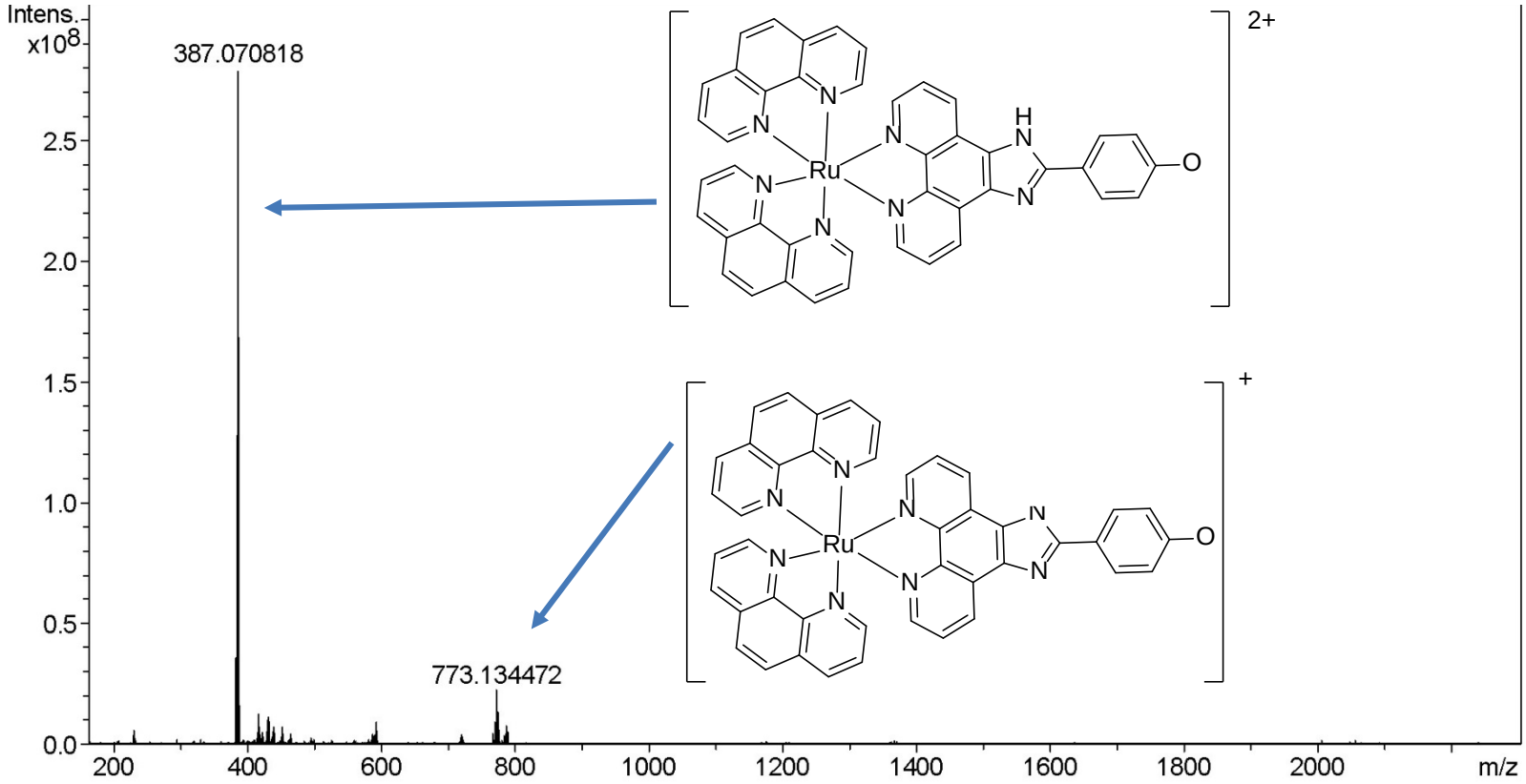

Figure 21. HRMS of the cations formed from [{Ru(phen)$_2$}$_3$(μ-mes(1,4-phO-Izphen)$_3$}](PF$_6$)$_6$•MeCN•10H$_2$O in acetonitrile.

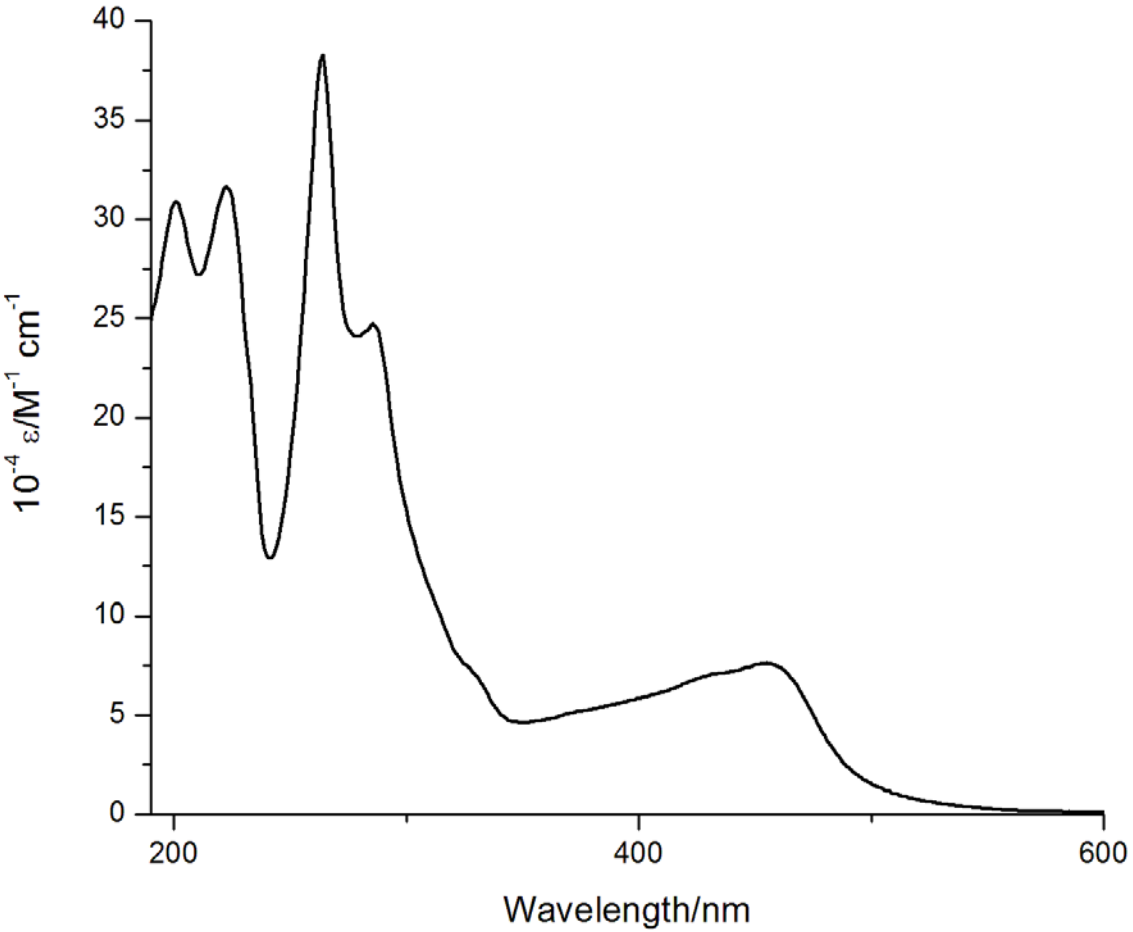

Figure 22. A plot of the molar extinction coefficient versus wavelength of [{Ru(phen)$_2$}$_3$(μ-mes(1,4-phO-Izphen)$_3$}](PF$_6$)$_6$•MeCN•10H$_2$O in acetonitrile.

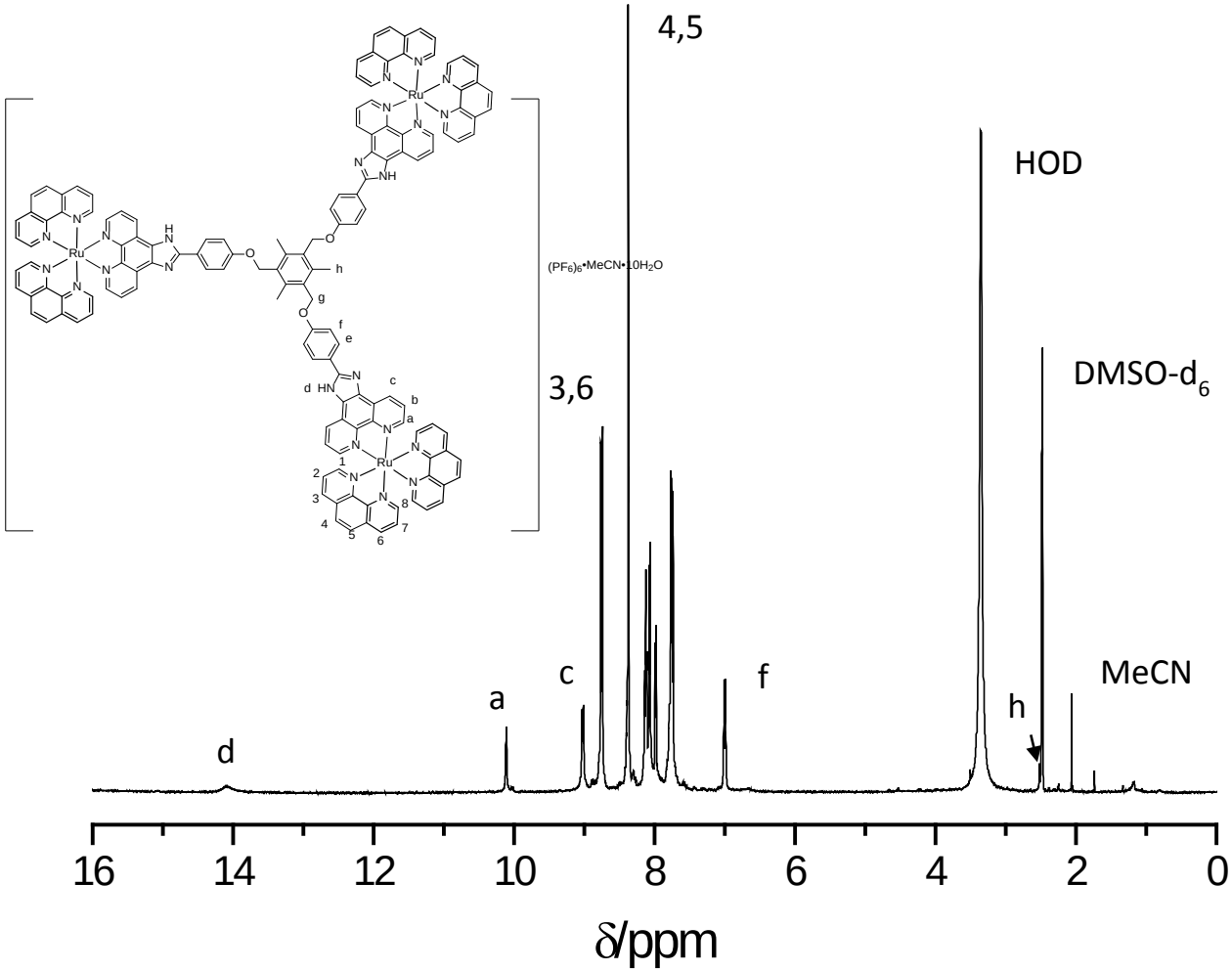

Figure 23. A ^{1}H NMR spectrum of [{Ru(phen)$_2$}$_3${μ-mes(1,4-phO-Izphen)$_3$}](PF$_6$)$_6$•MeCN•10H$_2$O in DMSO-d$_6$.

Figure 24 shows a cyclic voltammogram of [{Ru(phen)$_2$}$_3${μ-mes(1,4-phO-Izphen)$_3$}](PF$_6$)$_4$•MeCN•10H$_2$O, where the redox couple of $Ru^{II/III}$ is observed to have an E½ value of +1.37 V, and when compared to the literature, the value of the $Ru^{II/III}$ redox couple (E½ = +1.34 V), is very close. The ligand reductions of -1.34 V (-1.37 V) and -1.79 V (-1.63 V) were also observed, and are comparable to the value observed for the complex with three ruthenium(II) metal centers. The synthesis was repeated using 1.5 equivalents of the ruthenium precursor (scheme 7), in an attempt to limit the formation of the trinuclear complex.

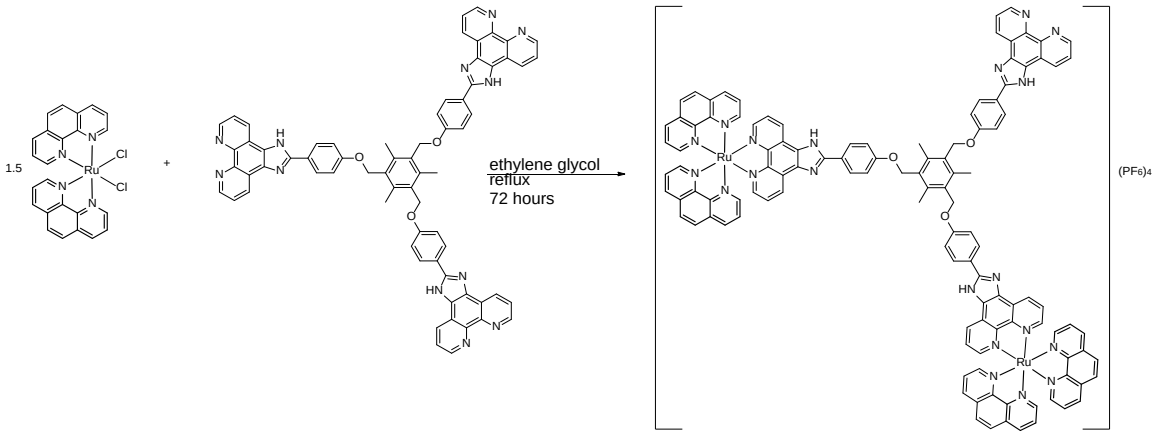

Scheme 7. Attempted synthesis of [{Ru(phen)$_2$}$_3${μ-mes(1,4-phO-Izphen)$_3$}](PF$_6$)$_6$

Upon analysis of the mass spectrum the m/z peak at 387.07 was again classified as the [Ru(phen)$_2$(1,4-phO-Izphen)]$^{2+}$. Form the UV-visible spectrum in Figure 26, the following wavelengths and molar extinction coefficients (ε x 10^4 M^{-1} cm^{-1}) were observed;

200 (202), 224 (222), 264 (264), 287 (286), and 458 (455); 24.1 (22.9), 24.8 (24.4), 30.0 (29.3), 19.5 (20.1), and 6.3 (5.4), respectively. The fact that molar extinction coefficients and the wavelength observed are comparable to what was reported for the trinuclear complex. The ^{1}H NMR spectrum, Figure 27, is also rather identical to Figure 23 and what is reported in literature, and should be considered as proof that we were unable to synthesize and isolate the binuclear ruthenium(II) complex. Figure 24 also shows an identical CV for $[\{Ru(phen)_2\}_2\{\mu\text{-mes91,4-phO-Izphen})_3\}](PF_6)_6$ which implies that both synthetic procedures produce the same complex.

(A)

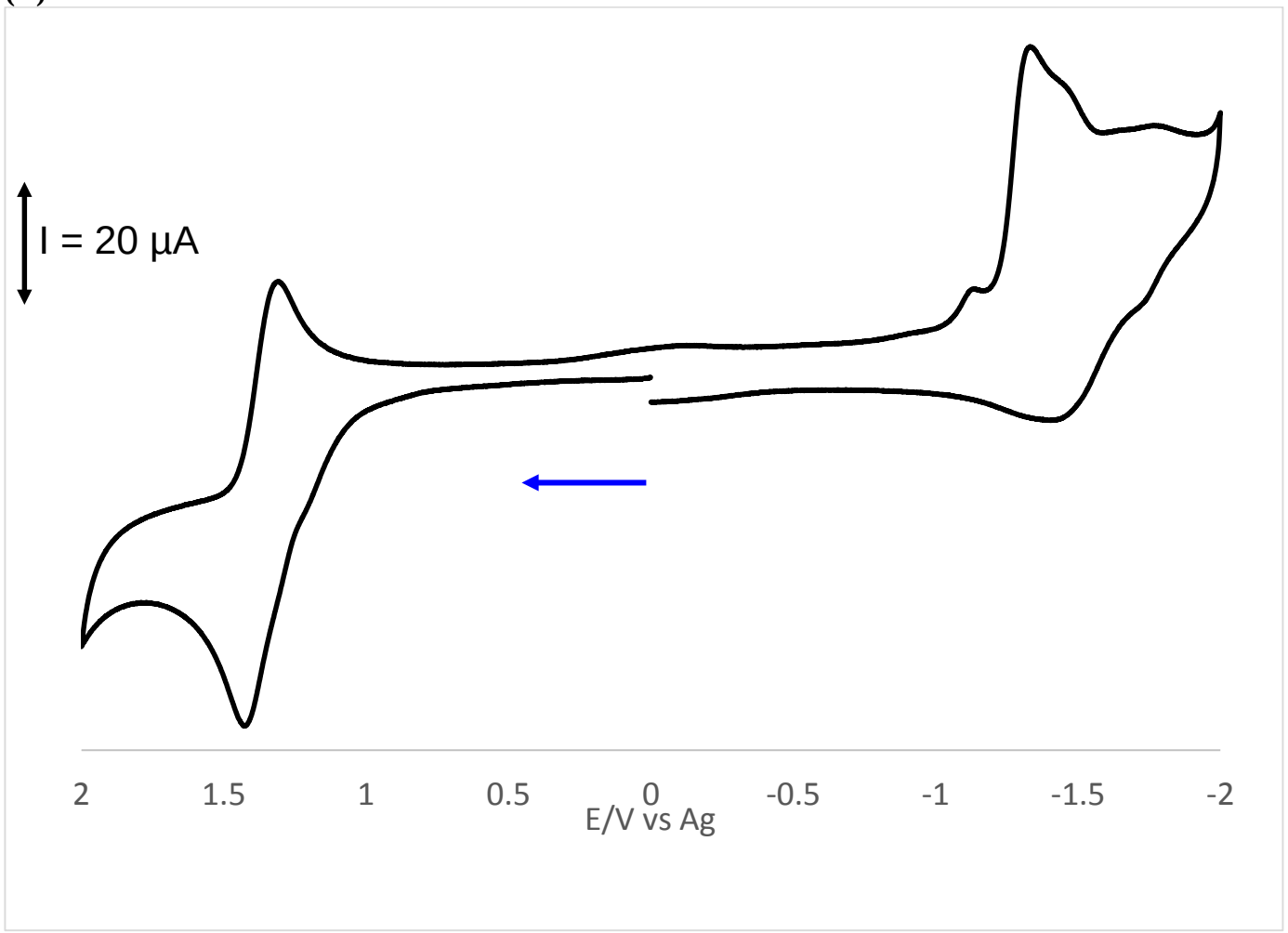

(B)

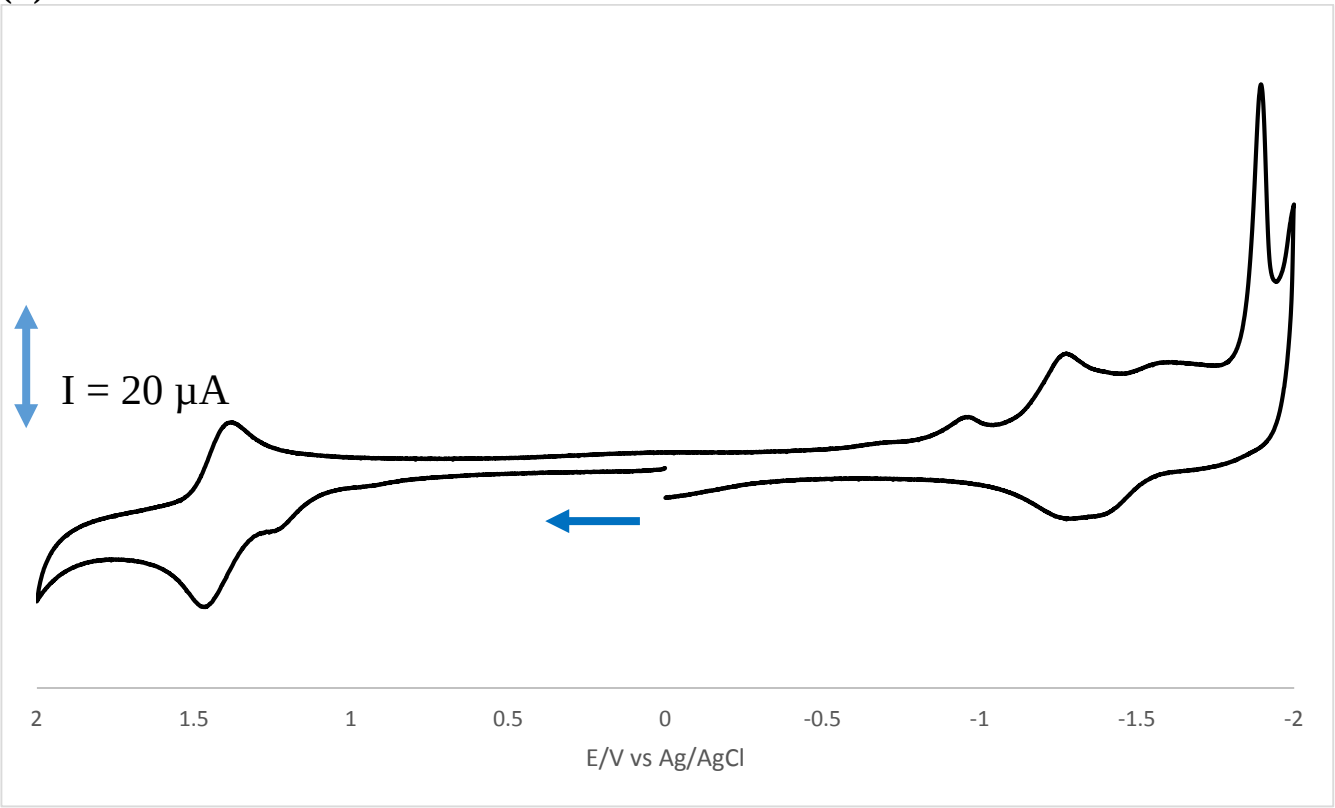

Figure 24. Cyclic voltammograms of $[\{Ru(phen)_2\}_2\{\mu\text{-mes91,4-phO-Izphen})_3\}](PF_6)_6 \bullet MeCN \bullet 10H_2O$ (A) and $[\{Ru(phen)_2\}_2\{\mu\text{-mes91,4-phO-Izphen})_3\}](PF_6)_6$ (B) in the potential range of +2 to -2 V on a glassy carbon electrode in acetonitrile (tetrabutylammonium perchlorate = 0.1 mM) versus Ag wire at 25 °C, scan rate = 100 mV s^{-1}.

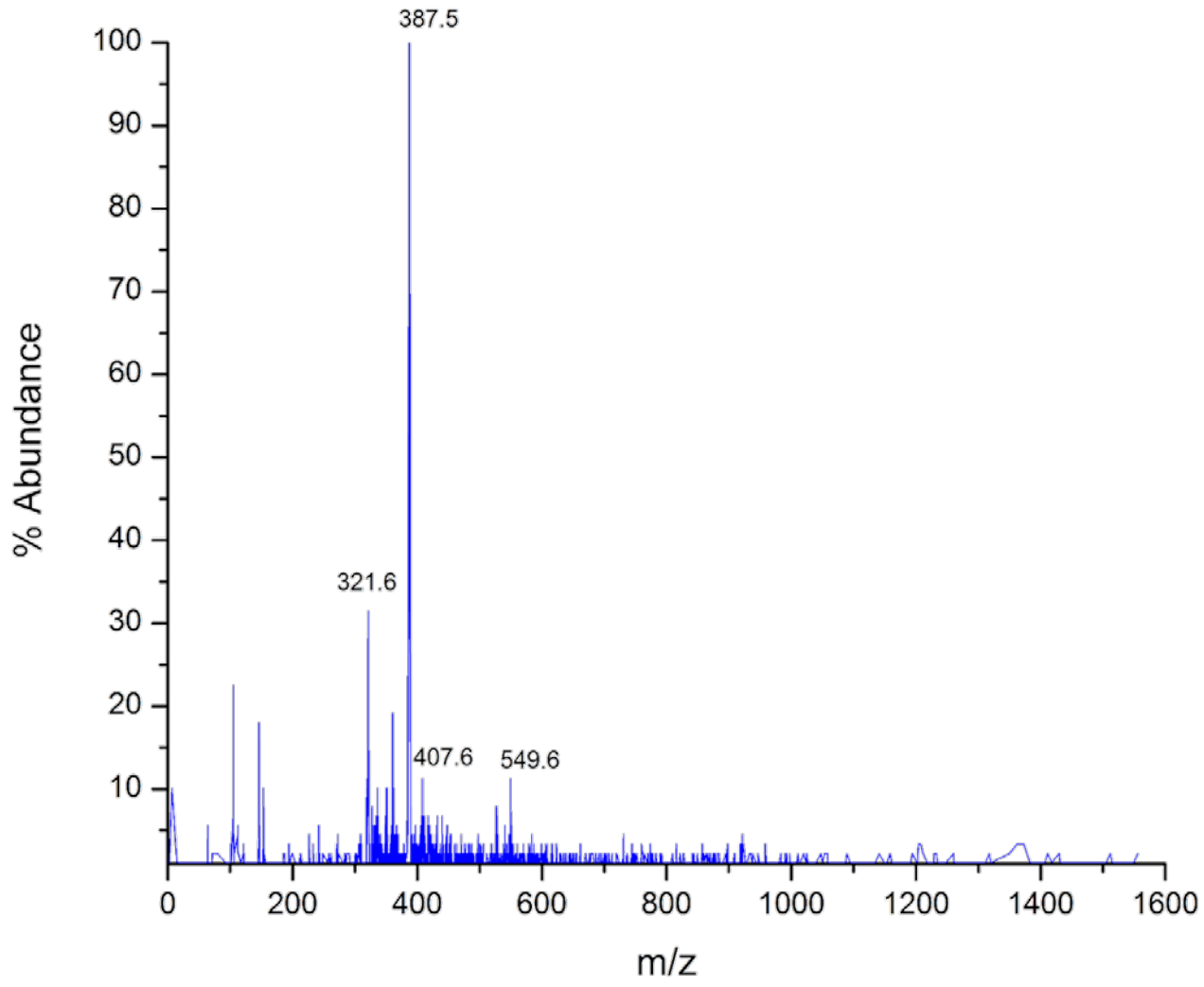

Figure 25. ESI MS of [{Ru(phen)$_2$}$_3$(μ-mes(1,4-phO-Izphen)$_3$}](PF$_6$)$_6$ in acetonitrile.

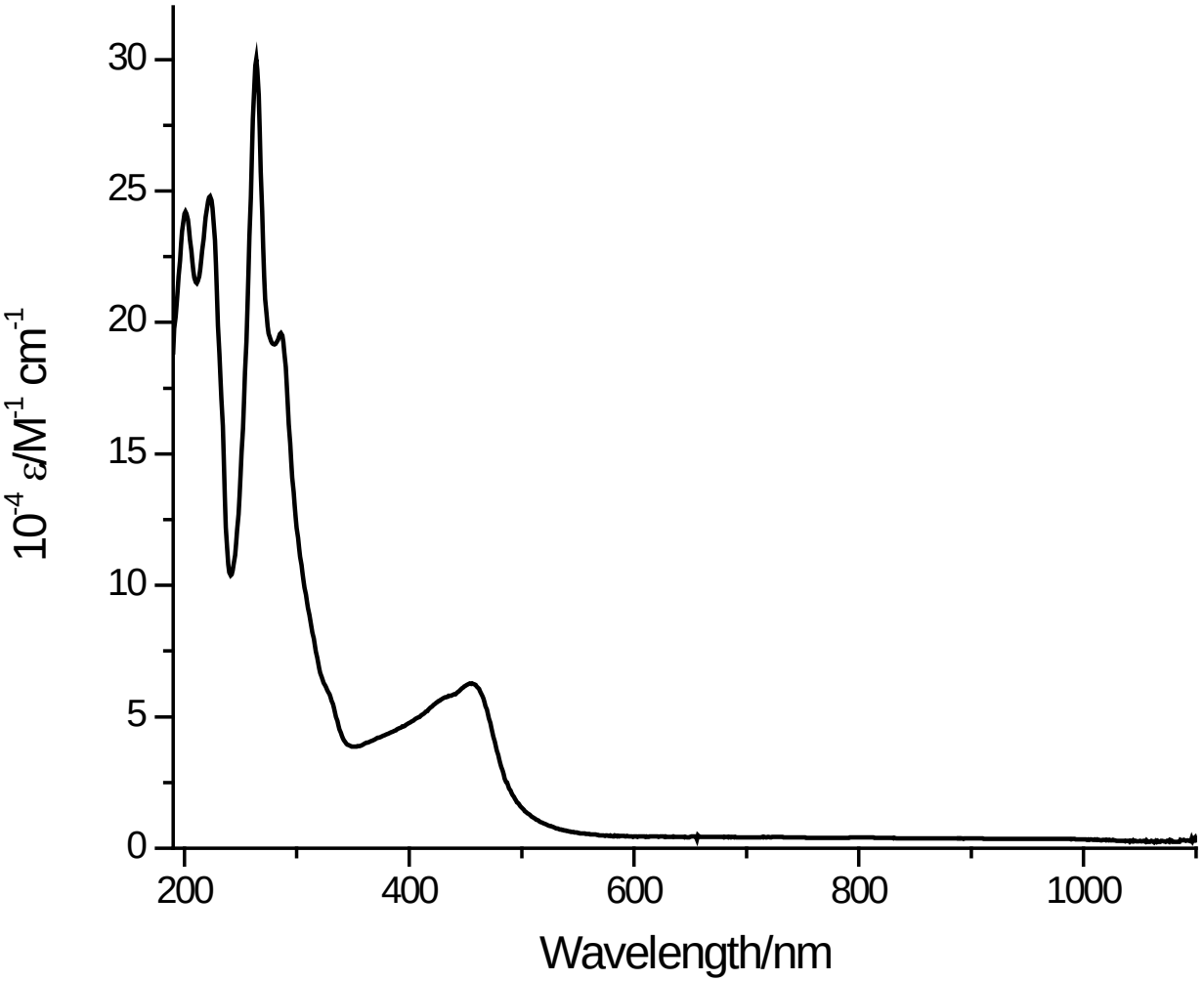

Figure 26. A plot of the molar extinction coefficient versus wavelength of [{Ru(phen)$_2$}$_3$(μ-mes(1,4-phO-Izphen)$_3$}](PF$_6$)$_6$ in acetonitrile.

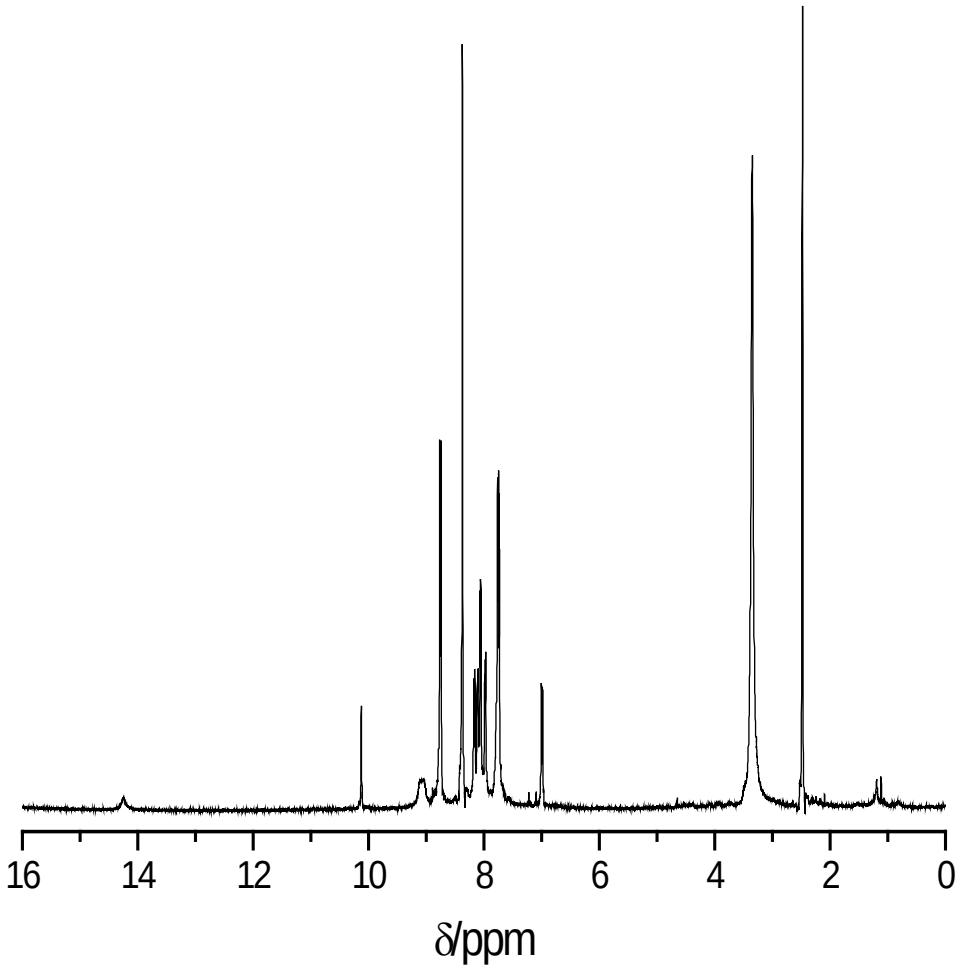

Figure 27. A ^{1}H NMR spectrum of $[\{Ru(phen)_2\}_3\{\mu\text{-mes}(1,4\text{-phO-Izphen})_3\}](PF_6)_6$ in DMSO-d_6.

CHAPTER III

SPECTROSCOPIC STUDIES USING COBALOXIMES IN DETERMINATION OF THE COORDINATION OF PYRIDINE TO THE COBALT(I) METAL CENETER

METHODS AND MATERIALS

Analytical or reagent grade chemicals obtained from commercial sources were used as received throughout this study. Microanalyses (C, H, N, B, Co, and N) were performed by Columbia Analytical Services (Tucson, AZ), Galbraith Laboratory, Inc. (Knoxville, TN), Intertek Pharmaceutical Services (Whitehouse, NJ), and the University of Illinois Urbana-Champaign (Urbana, IL).

Physical measurements

Magnetic susceptibility measurements were acquired on a Johnson Matthey® magnetic susceptibility balance, Mark I, at ambient temperature. ^{19}F NMR spectra were acquired on a Burker 400 MHz spectrometer with acetonitrile-d_3 as solvent, CF_3CO_2H (δ = -76.55 ppm[165]) as an external reference at room temperature. ^{1}H and ^{13}C NMR spectra were acquired on a Varian 400 MHz spectrometer where all samples were dissolved in their appropritate solvents.

All electrochemical experiments were performed on a BASi® Epsilon C3 under an argon atmosphere in the respective solvents thoroughly sparged with Ar before analysis at room temperature (ca 20 ^{o}C) and are uncorrected for junction potentials. A standard three electrode configuration was employed consisting of a glassy carbon working electrode (diameter = 3 mm), Pt wire auxiliary electrode and a Ag wire as reference electrode in non-aqueous solvents; against which the ferrocenium/ferrocene couple showed a reversible

wave at +0.29 V in acetonitrile, +0.40 V in acetone, +0.55 V in 2-butanone, and +0.44 V in 1,2-difluorobenzene/acetone (4:1, v/v), and a AgCl/Ag (BASi, 3.0 M NaCl which was separated from the analytical solution by a Vicor® frit) in aqueous media. The ionic strength was maintained with 0.10 M ($[^{n}Bu_4N]ClO_4$ in non-aqueous media and $NaClO_4$ in aqueous media). The $NaClO_4$ was standardized as shown in this protocol. $HClO_4$ (70 ml, 11.36 M) was diluted with water, and was neutralized with $NaHCO_3$ to produce an aqueous solution of $NaClO_4$, which was then diluted to give a concentration of ~4 M. $NaClO_4$ (1.00 ml) from the stock solution was diluted with deionised water in a 25.00 ml volumetric flask. A column with Dowex® 50WX@-200 (H) ion-exchange resin was soaked with 0.10 M $HClO_4$, to charge the column for ion exchange, followed by water (15 – 18 ml) to elute the excess 0.10 M $HClO_4$. A portion of the diluted solution of $NaClO_4$ (5 ml) was loaded onto the column; then elution was carried with deinonised water (25.00 ml). The eluted $HClO_4$ was then titrated with standardized NaOH. From this point onwards, the concentration of the stock $NaClO_4$ was determined to be 3.85 M

Spectroelectrochemical measurements were carried out at 20 ^{o}C with a thermostated water bath/circulator (Thermo Scientific®). Absorbance measurements were performed on an Agilent® 8453A diode array spectrophotometer. A Pt gauze and Pt wire were employed as working and auxiliary electrodes, respectively, and Ag wire was used as a quasi-reference electrode. The ionic strength was maintained at 0.10 M as stated above. Each solution was purged with argon for at least two minutes in the spectroelectrochemical cuvette (path length = 0.1 cm) prior to the measurement, and the spectra are acquired over 200–1000 s at a constant potential.

Other electronic spectra were recorded using quartz cuvettes on a Cary 5000 UV/Vis/NIR spectrophotometer, Spectramax M5 (Molecular Devices) or an Agilent 8453 diode array spectrophotometers in the respective solvent(s). High-resolution ESI MS spectra were acquired via positive electrospray ionization on a Bruker 12 Tesla APEX – Qe FTICR-MS with and Apollo II ion source. Samples were dissolved in 1:1 dichloromethane (DCM)/MeOH; followed by direct injection using a syringe pump with a flow rate of 2 μL s^{-1}. The data was processed using Bruker Daltonics Data Analysis Version 3.4.

EXPERIMENTAL

Synthesis of $[Co(dmgBF_2)_2(H_2O)_2]$

$[Co(dmgBF_2)_2(H_2O)_2]$ was synthesized using the methods of Bakac *et al.*[13] Calculated magnetic moment, μ_{eff} = 1.84 B.M., Lit.[13]: , μ_{eff} = 1.92 B.M.

Synthesis of $[Co(dmgBF_2)_2(H_2O)(py)]\bullet 0.5CH_3COCH_3$

$[Co(dmgBF_2)_2(H_2O)_2]$ (0.30 g, 0.71 mmol), along with pyridine (79 mg, 1.0 mmol) and acetone (400 mL) were mixed in a 500 mL RB flask; and the reaction mixture was stirred at room temperature for 21.5 hours. The reaction mixture was rotary evaporated to dryness; and more acetone was added to the mixture. The mixture was once more rotary evaporated, and the resulting solid was washed with diethyl ether and a dry solid was recovered. Yield = 0.33 g (89%). Calc. for $C_{14.5}H_{22}B_2CoF_4N_5O_{5.5}$: C, 34.09; H, 4.34; B, 4.23; Co, 11.53; N, 13.71%. Found: C, 33.79; H, 3.71; B, 4.48; Co, 11.71; N, 13.79%. HRMS (ESI, positive mode) *m/z* = of 482.083653 ($[Co(dmgBF_2)_2(H_2O)(py)]^+$). FTIR ($\nu/cm^{-1}$): 537.6 (s) (Co-N(O-B)), 689.8 (m) (py), 758.3 (m) (py), 822.8 (vs) (B-F), 1100.8

(s) (N-O), 1163.5 (s) (B-F), 1225.1 (m) (N-O), and 1622.0 (m) (C=N). UV-visible spectrum (acetonitrile), $\lambda_{max.}$/nm (10^{-3} ε/M^{-1} cm^{-1}): 198 (24.3), 260 sh (4.8), 323 sh (4.1), 425 (4.8), and 1144 (0.15). Calculated magnetic moment, μ_{eff} = 1.28 ± 0.02 B.M.

An investigation of the reaction between $[Co(dmgBF_2)_2(H_2O)_2]$ and triethylamine in acetone and acetonitrile

Reaction of $[Co(dmgBF_2)_2(H_2O)_2]$ with triethylamine in acetone

$[Co(dmgBF_2)_2(H_2O)_2]$ (0.1004 g, 0.24 mmol) was dissolved in acetone (40 mL). Et_3N (0.1202 g, 116 µL, 1.89 mmol) was added to the reaction mixture and it was left to stir for 73.4 hours in the dark. The reaction mixture started out rusty red-brown, and upon the addition of Et_3N the solution darkened instantly. The solution was rotary evaporated to dryness. Product has a brown coloration. Ether was added to the round bottom flask and the product was scraped of the sides and was left to settle. The ether was decanted and centrifuged to collect any suspended particles. The ether layer was brown-orange in color color. Yield = 0.1891 g. As determined by elemental analysis: CHN, found: C, 41.84; H, 5.95; N, 11.38%. The exact formula of the product is yet to be determined.

Reaction of $[Co(dmgBF_2)_2(H_2O)_2]$ with triethylamine in acetonitrile in air

$[Co(dmgBF_2)_2(H_2O)_2]$ (0.0992 g, 0.24 mmol) was dissolved in acetonitrile (40 mL). Et_3N (0.1202 g, 166 µL, 1.89 mmol) was added and the reaction mixture was left stirring in the dark for 73.9 hours. The solution started out as transparent brown, and upon addition of Et_3N the solution darkened over the course of 30 seconds. Some of the product precipitated out of solution coating the round bottom flask. The solution was rotary evaporated to dryness. The product is black in color. Ether was added to the round bottom

flask and the product was scraped off and poured into a beaker. The product was allowed to settle and the ether was decanted and centrifuged to remove any particles that may have been suspended. The ether layer was clear in color. Yield= 0.0988 g. The exact formula of the product is yet to be determined.

Reaction of $[Co(dmgBF_2)_2(H_2O)_2]$ with triethylamine in acetonitrile with evaporation under N_2

$[Co(dmgBF_2)_2(H_2O)_2]$ (0.0995 g, 0.24 mmol) was dissolved in acetonitrile (40 mL). Et_3N (0.1202 g, 166 µL, 1.89 mmol) was added and the reaction mixture was left in the dark for 26.5 hours. The solution started out as transparent brown, and upon addition of Et_3N the solution darkened over the course of 30 seconds. Some of the product precipitated out of solution coating the round bottom flask. The solution was purged with argon for 20 minutes before it placed in the glovebox (nitrogen atmosphere) to evaporate. Yield = 0.1244 g. The exact formula of the product is yet to be determined.

Spectrophotometric titration of $[Co(dmgBF_2)_2(H_2O)_2]$ with pyridine and perfluoropyridine in various solvents

$[Co(dmgBF_2)_2(H_2O)_2]$ (0.0105 g, 0.025 mmol) was dissolved in a 50 ml volumetric flask with the appropriate solvent, producing a solution with a concentration of 0.500 mM. The solution was sonicated to ensure that all solids were dissolved. Pyridine (80.9 µl, 1 mmol) was diluted in a 5 ml volumetric flask with the appropriate solvent to produce a stock solution with a concentration of 200 mM. Using the stock 200 mM pyridine solution, a 2.00 mM pyridine solution was prepared by diluting 500 µl of the 200 mM stock in a 50 mL volumetric flask. Both stocks were measured out according to Table 6, and was added

to a 10 ml volumetric flask and diluted to the final concentration before the spectrum of each solution was acquired.

Table 6. Spectrophotometric titration solution preparation table for $[Co(dmgBF_2)_2(H_2O)_2]$ and pyridine in 10 ml volumetric flasks.

[py]/[Complex]	**[Complex]/mM**	**Volume of 0.50 mM Complex/µl**	**[pyridine]/mM**	**Volume of 2.00 mM pyridine/µl**
0:0	0.100	2000	0.00	0.00
0.25:1.00	0.100	2000	0.025	125
0.33:1.00	0.100	2000	0.033	165
0.40:1.00	0.100	2000	0.040	200
0.50:1.00	0.100	2000	0.050	250
0.65:1.00	0.100	2000	0.065	325
0.75:1.00	0.100	2000	0.075	375
0.87:1.00	0.100	2000	0.087	435
1.00:1.00	0.100	2000	0.100	500
1.12:1.00	0.100	2000	0.112	560
1.25:1.00	0.100	2000	0.125	625
1.50:1.00	0.100	2000	0.150	750
1.75:1.00	0.100	2000	0.175	875
2.00:1.00	0.100	2000	0.200	1000
2.25:1.00	0.100	2000	0.225	1130
2.50:1.00	0.100	2000	0.250	1250
2.75:100	0.100	2000	0.275	1380
3.00:1.00	0.100	2000	0.300	1500
4.00:1.00	0.100	2000	0.400	2000
5.00:1.00	0.100	2000	0.500	2500

$[Co(dmgBF_2)_2(H_2O)_2]$ (0.0105 g, 0.025 mmol) was dissolved in a 50 ml volumetric flask with the appropriate solvent, producing a solution with a concentration of 0.500 mM. The solution was sonicated to ensure that all solids were dissolved. Pyridine (161.8 µl, 2 mmol) was diluted in a 50 ml volumetric flask with the appropriate solvent to produce a stock solution with a concentration of 40 mM. Both stocks were measured out according to *Table 7,* and was added to a 10 ml volumetric flask and diluted to the final concentration before the spectrum of each solution was acquired.

Table 7. Spectrophotometric titration solution preparation table for $[Co(dmgBF_2)_2(H_2O)_2]$ and pyridine in 10 ml volumetric flasks.

[py]/[Complex]	**[Complex]/mM**	**Volume of 0.50 mM Complex/µl**	**[pyridine]/mM**	**Volume of 40.00 mM pyridine/µl**
0.00:0.00	2.00	4000	0.00	0.00
0.25:1.00	2.00	4000	0.50	125
0.33:1.00	2.00	4000	0.66	165
0.40:1.00	2.00	4000	0.80	200
0.50:1.00	2.00	4000	1.00	250
0.65:1.00	2.00	4000	1.30	325
0.75:1.00	2.00	4000	1.50	375
0.87:1.00	2.00	4000	1.74	435
1.00:1.00	2.00	4000	2.00	500
1.12:1.00	2.00	4000	2.24	560
1.25:1.00	2.00	4000	2.50	625
1.50:1.00	2.00	4000	3.00	750
1.75:1.00	2.00	4000	3.50	875
2.00:1.00	2.00	4000	4.00	1000
2.25:1.00	2.00	4000	4.50	1130
2.50:1.00	2.00	4000	5.00	1250
2.75:100	2.00	4000	5.50	1380
3.00:1.00	2.00	4000	6.00	1500
4.00:1.00	2.00	4000	8.00	2000
5.00:1.00	2.00	4000	10.00	2500

Spectrophotometric Titration of $[Co(dmgBF_2)_2(H_2O)_2]$ with triethylamine in acetonitrile

The titrant (triethylamine) was prepared in acetonitrile as the solvent. Measured amounts of the triethylamine was mixed with aliquots of $[Co(dmgBF_2)_2(H_2O)_2]$ in 10 ml volumetric flasks and was diluted acetonitrile to a final complex concentration of 2.0 mM for NIR studies (Table 7) and 0.1 mM for UV-visible studies (Table 6). The triethylamine concentration ranged from zero equivalence to five equivalences. All samples were equilibrated at 20 ^oC and their absorbances were recorded after 10 minutes and then 24 hours.

Spectroelectrochemical measurements of $[Co(dmgBF_2)_2(OH_2)_2]$ and $[Co(dmgBF_2)_2(OH_2)(py)]\bullet 0.5(CH_3)_2CO$ in various solvents

Safety Reminder: perchlorate salts are highly explosive especially when dried. Please use in small quanities.

Spectroelectrochemical measurements were regulated at 20 ^oC with a thermostated water bath/circulator (Thermo Scientific®). Absorbance measurements were aquired on an Agilent® 8453A diode array spectrophotometer. A Pt gauze and Pt wire were employed as working and auxiliary electrodes, respectively, and Ag wire was used as a quasi-reference electrode. The ionic strength was maintained at 0.10 M as stated above. Each solution was purgrd with Ar for at least two minutes in the spectroelectrochemical cuvette (1 mm path

length) prior to the measurement, and the spectra are acquired over a time of 200–1000 s at a constant potential of -1.0 V.

RESULTS AND DISCUSSION

Spectrophotometric titration of $[Co(dmgBF_2)_2(H_2O)_2]$ with triethylamine in acetonitrile

This study was conducted to verify whether there is any interaction between $[Co(dmgBF_2)_2(H_2O)_2]$ and triethylamine. It was observed that a color change occurred faster at high concentrations of Et_3N were utilized after carrying out near infrared studies, and the color changes were very dramatic (Figure 32). The data that was gathered spectrophotometric titration involving $[Co(dmgBF_2)_2(H_2O)_2]$ in the presence of triethylamine (Figure 33) within the first hour mixing, appeared as if there was no reaction between $[Co(dmgBF_2)_2(H_2O)_2]$ and triethylamine. Twenty four hours later, a color change was apparent in the solutions containing the triethylamine. The solutions had changed from a translucent gold to a purple coloration upon standing at room temperature for 24 hours.

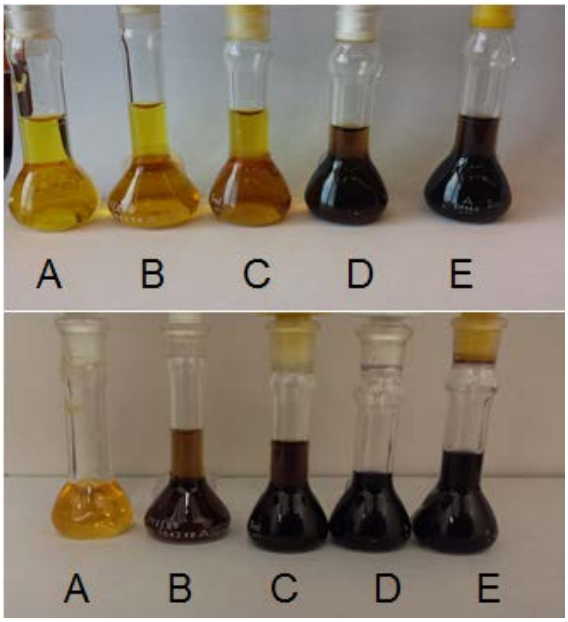

Figure 28. Image of reaction mixtures from the spectrophotometric titration of 2.0 mM $[Co(dmgBF_2)_2(OH_2)_2]$ with trimethylamine.(A) 0 equivalence, (B) 0.5 equivalence, (C) 1.0 equivalence, (D) 5.0 equivalences, and (E) 10 equivalences of triethylamine; Time = 5 minutes (top), 30 minutes (bottom)

In Figure 34, two peaks at 560 and 650 nm were observed with their absorbance increasing as the concentration of triethylamine is increased. It should be noted that absorbance in that region is normally due to cobalt(I). The absorbance change for the peak that appears at 1162 nm, Figure 35, remains unchanged up to the addition of one equivalent of triethylamine. At five and ten equivalence, the peak is seen to have blue shifted, with the peaks broadening to produce shoulders.

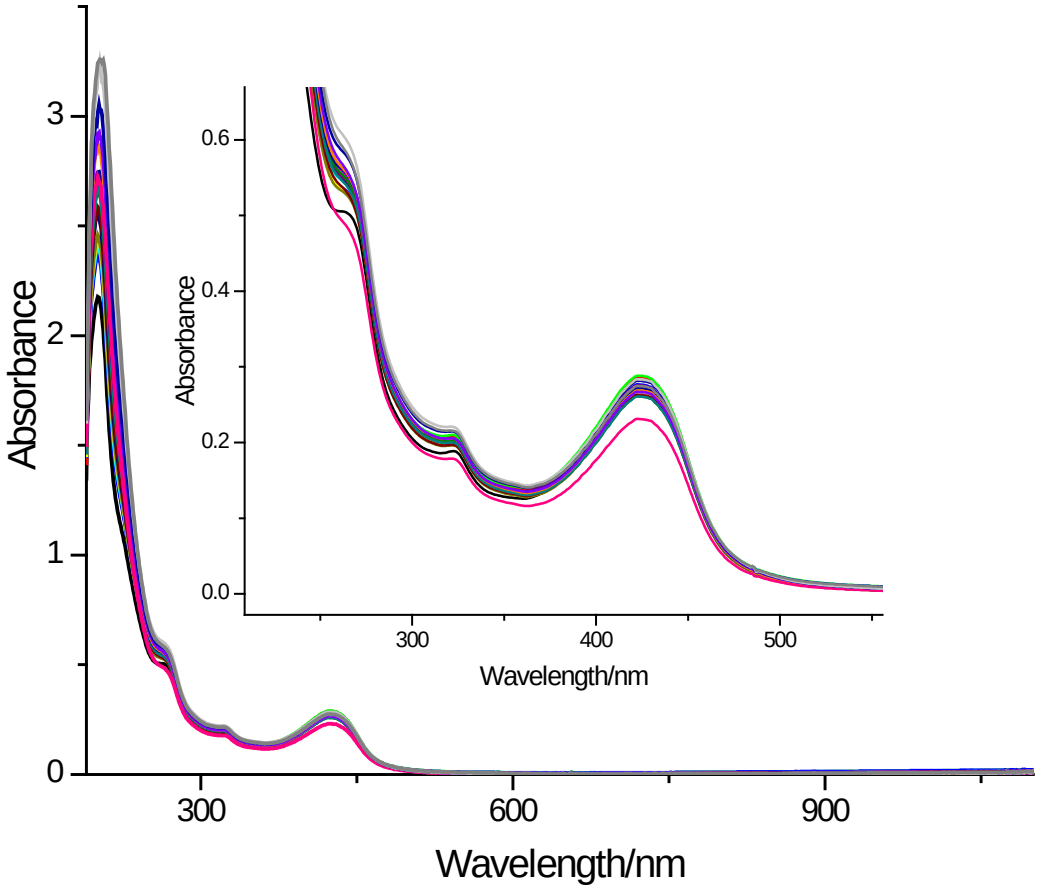

Figure 29. A plot of absorbance versus wavelength for the spectrophotometric titration of $[Co(dmgBF_2)_2(H_2O)_2]$ with Et_3N in acetonitrile. [Complex] = 0.1 mM. Time = 0 hours.

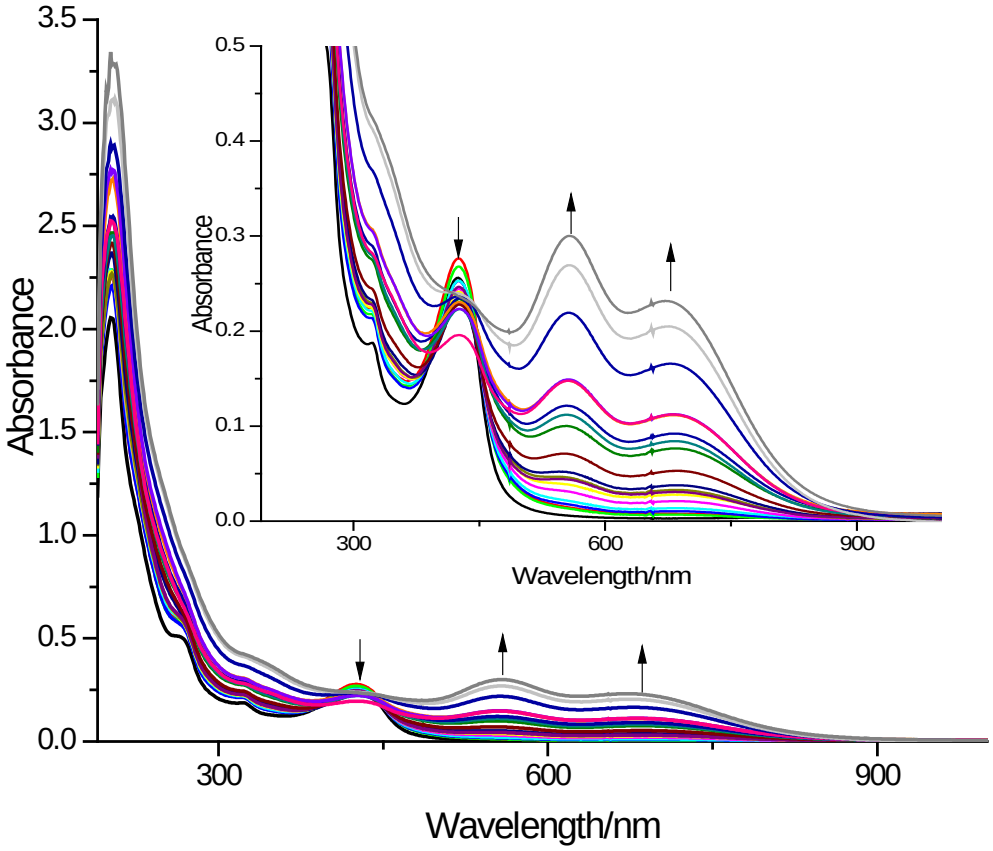

Figure 30. A plot of absorbance versus wavelength for the spectrophotometric titration of $[Co(dmgBF_2)_2(H_2O)_2]$ with Et_3N in acetonitrile. [Complex] = 0.1 mM. Time = 24 hours later.

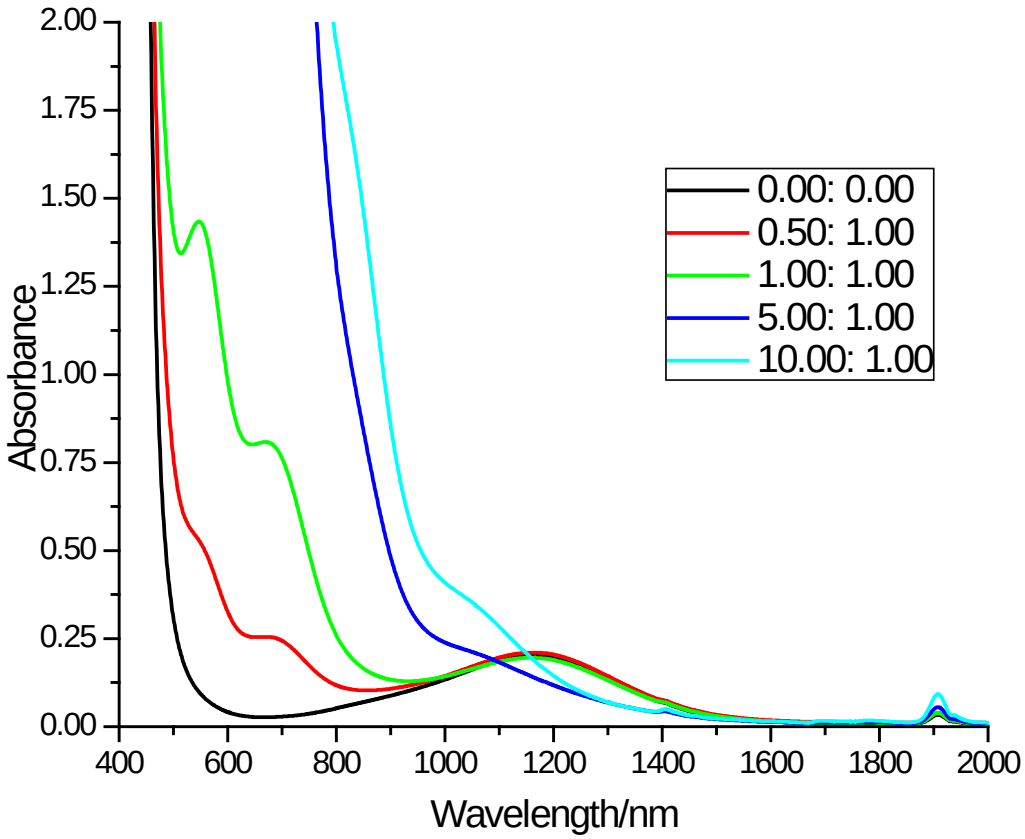

Figure 31. A plot of absorbance versus wavelength of the spectrophotometric titration of $[Co(dmgBF_2)_2(H_2O)_2]$ with Et_3N in acetonitrile. [Complex] = 2.00 mM.

Spectroscopic and electrochemical studies involving $[Co(dmgBF_2)_2(H_2O)_2]$

3.3.1 Synthesis of $[Co(dmgBF_2)_2(H_2O)(py)]\bullet 0.5CH_3COCH_3$

$[Co(dmgBF_2)_2(H_2O)_2]$ was reacted with 1.4 equivalents of pyridine in acetone as a solvent to produce $[Co(dmgBF_2)_2(H_2O)(py)]\bullet 0.5(CH_3)_2CO$ (see Scheme 8) The formulation of pyridine coordinating to the cobalt(II) metal center is supported by the M^+ parent ion of high-resolution MS, the elemental analysis, as well as the other spectroscopic characterizations (see Figures A1-A4). In the FTIR spectrum there are distinct blue shifts (see Figure A2) in the C=N, N-O, and B-F stretching frequencies of $[Co(dmgBF_2)_2(H_2O)_2]$ compared to $[Co(dmgBF_2)_2(H_2O)(py)]\bullet 0.5(CH_3)_2CO$, as well as two peaks at 689.8 and 758.3 cm^{-1} all consistent with the coordination of pyridine.[167] Additionally the magnetic moment μ_{eff} = 1.28 ± 0.02 B.M. for $[Co(dmgBF_2)_2(H_2O)(py)]\bullet 0.5(CH_3)_2CO$ (at ambient temperature) is consistent with low spin Co(II). Both $[Co(dmgBF_2)_2(H_2O)_2]$ and $[Co(dmgBF_2)_2(H_2O)(py)]\bullet 0.5(CH_3)_2CO$ are reasonably soluble in acetonitrile, acetone, butanone, moderately soluble in water, and are soluble at < 0.1 mM in 1,2-difluorobenzene. $[Co(dmgBF_2)_2(H_2O)_2]$ is known to have an enhanced solubility in acetone relative to alcohols.[42] Acetone generally behaves as a polar weakly coordinating solvent, and this nature was evident from the synthetic protocol of $[Co(dmgBF_2)_2(H_2O)(py)]\bullet 0.5(CH_3)_2CO$, where the axial water molecule is retained in the solid as shown in the ESI-MS. The absorbance spectra of $[Co(dmgBF_2)_2(H_2O)_2]$ and $[Co(dmgBF_2)_2(H_2O)(py)]\bullet 0.5(CH_3)_2CO$, in various solvents are given in the ESI and the molar extinction coefficients are given in Table 8.

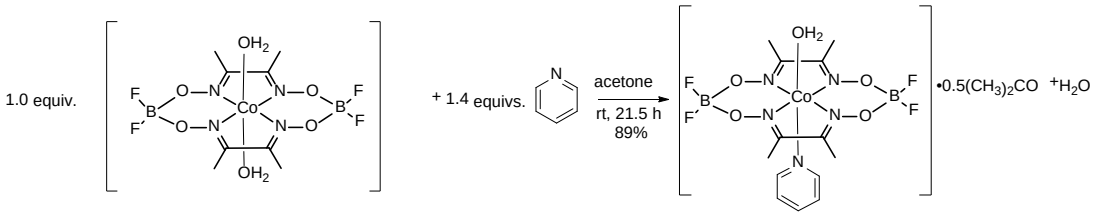

$[Co(dmgBF_2)_2(OH_2)_2]$ $[Co(dmgBF_2)_2(OH_2)(py)]\bullet 0.5(CH_3)_2CO$

Scheme 8. Synthesis of $[Co(dmgBF_2)_2(H_2O)(py)]\bullet 0.5(CH_3)_2CO$.

Table 8. The absorption maxima (nm) and molar extinction coefficients (M^{-1} cm^{-1}) of $[Co(dmgBF_2)_2(OH_2)_2]$ and $[Co(dmgBF_2)_2(py)(OH_2)]\bullet 0.5(CH_3)_2CO$.

solvent	complex	λ ($10^{-3}\varepsilon$)	λ ($10^{-3}\varepsilon$)	λ ($10^{-3}\varepsilon$)	λ ($10^{-3}\varepsilon$)	λ ($10^{-2}\varepsilon$)
acetonitrile	$[Co(dmgBF_2)_2(OH_2)_2]$	201 (23.6)	264 sh (6.5)	323 sh (2.5)	425 (3.6)	1162 (1.1)
water	$[Co(dmgBF_2)_2(OH_2)_2]$	198 (20.8)	261 (5.1)	--	455 (2.7)	--
acetone	$[Co(dmgBF_2)_2(OH_2)_2]$	--	--	--	446 (2.7)	1294 (0.7)
2-butanone	$[Co(dmgBF_2)_2(OH_2)_2]$	--	--	--	449 (2.9)	1319 (0.6)
1,2-difluorobenzene:acetone (4:1 v/v)	$[Co(dmgBF_2)_2(OH_2)_2]$	--	--	--	444 (2.7)	1170 (1.3)
acetonitrile	$[Co(dmgBF_2)_2(H_2O)(py)]\bullet 0.5(CH_3)_2CO$	199 (47.6)	256 sh (15.0)	323 sh (4.1)	425 (4.8)	1144 (1.5)
water	$[Co(dmgBF_2)_2(H_2O)(py)]\bullet 0.5(CH_3)_2CO$			--	454 (3.2)	--
acetone	$[Co(dmgBF_2)_2(H_2O)(py)]\bullet 0.5(CH_3)_2CO$	--	--	--	436 (2.8)	1135 (2.7)
2-butanone	$[Co(dmgBF_2)_2(H_2O)(py)]\bullet 0.5(CH_3)_2CO$	--	--	--	431 (2.6)	1131 (2.7)
1,2-difluorobenzene:acetone (4:1 v/v)	$[Co(dmgBF_2)_2(H_2O)(py)]$			--	420 (3.9)	1138 (2.6)

In the UV-visible portion of the spectrum, the band between 420 and 450 nm shows the most variation between $[Co(dmgBF_2)_2(H_2O)_2]$ and $[Co(dmgBF_2)_2(H_2O)(py)]\bullet 0.5(CH_3)_2CO$. When $[Co(dmgBF_2)_2(H_2O)(py)]\bullet 0.5(CH_3)_2CO$ is dissolved in weakly coordinating solvents (acetone, 2-butanone, etc.), this band observed at ca 450 nm in $[Co(dmgBF_2)_2(H_2O)_2]$ and at ca 430 nm for $[Co(dmgBF_2)_2(H_2O)(py)]\bullet 0.5(CH_3)_2CO$. For $[Co(dmgBF_2)_2(H_2O)(py)]\bullet 0.5(CH_3)_2CO$ the tail and the band into the NIR are also more pronounced. These changes can be interpreted as additional evidence for the coordination of pyridine to the Co(II) complex. Additionally, the band in the NIR is characteristic of, and confirms, the low spin nature of the cobalt(II) metal center in both species.[155]

The complex, $[Co(dmgBF_2)_2(H_2O)_2]$, has a very rapid solvent exchange rate that is comparable to the hexasolvated high-spin Co(II) species.[41-42] Thus, it is expected that the axial water ligand(s) are substituted with coordinating solvents. In weakly coordinating solvents (Figures A5-A7), the addition of pyridine causes a blue shift of the 450 nm band and the resulting band at ca 430 nm coincides with the band observed in the ketone solutions of $[Co(dmgBF_2)_2(H_2O)(py)]\bullet 0.5(CH_3)_2CO$. In the NIR, there is an increase in the intensity of the absorbance and a blue shift in λ_{max} in going from $[Co(dmgBF_2)_2(H_2O)_2]$ to $[Co(dmgBF_2)_2(H_2O)(py)]\bullet 0.5(CH_3)_2CO$. In acetonitrile (see Figure 36), this transformation is best observed in the NIR region as the changes the UV region are masked by an excess of pyridine. In water (not shown), the changes in the UV-visible region of the spectrum of $[Co(dmgBF_2)_2(H_2O)_2]$ upon the addition of pyridine, are difficult to interpret. In an unbuffered environment, there is the possibility of deprotonating the axial water molecule at higher pH values (induced by the addition of pyridine). Additionally, it was

observed that the complex interacts with all the buffer systems we have tried[2] which limited our ability to interpret the changes at higher ratios of pyridine to complex. The poor solubility of the complexes in water prevents the acquisition of reasonable spectral data in the NIR region. These observations in the non-aqueous solvents point to the formation of $[Co(dmgBF_2)_2(H_2O)(py)]\bullet 0.5(CH_3)_2CO$ from $[Co(dmgBF_2)_2(H_2O)_2]$ in situ upon the addition of pyridine. Using these spectral transformations, the stoichiometry of the interaction between pyridine and $[Co(dmgBF_2)_2(H_2O)_2]$ in acetonitrile (and other solvents) was determined from mole ratio plots (see ESI Figures A8–A18) and was found to be 1:1 (Eq. 3) with up to five times excess pyridine.

$$[Co(dmgBF_2)_2(OH_2)_2] + py \underset{}{\overset{K_1}{\rightleftharpoons}} [Co(dmgBF_2)_2(OH_2)(py)] + H_2O \quad (1)$$

From this data, the formation constant[168-169] for $[Co(dmgBF_2)_2(OH_2)(py)]$ from $[Co(dmgBF_2)_2(OH_2)_2]$ was determined (see Table 9). In all the solvents explored, the mole ratio and log plots also indicate that the monopyridine species is the major species over the concentration range studied (see Figures A8–A18). The stoichiometry and equilibrium constants are consistent with analogous systems reported by Nonaka and Hamada.[169] In water, and other coordinating solvents, the equilibrium between $[Co(dmgBF_2)_2(X)_2]$ or $[Co(dmgH)_2X_2]$ and pyridine (and analogous Lewis bases) have been found to be relatively small and the propensity to form a stoichiometry greater than 1:1 is even smaller.[37, 169-170] From the magnitude of the equilibrium constant in acetonitrile (1.3×10^3 at 20 ^oC), it can be easily deduced that the dissociation of the pyridine from $[Co(dmgBF_2)_2(X)(py)]$ is

[2] Holder et al. unpublished work

significant at 20 °C. This dissociation that can occur with the pyridine linker systems employed in bridging binuclear systems has been largely ignored in the interpretation of data presented in the literature. In the case of acetone and 2-butanone, there is a much larger formation constant for the monopyridine complex ($[Co(dmgBF_2)_2(H_2O)(py)]\bullet 0.5(CH_3)_2CO$) compared to acetonitrile and represent suitable solvents for studying $[Co(dmgBF_2)_2(H_2O)(py)]\bullet 0.5(CH_3)_2CO$.

Table 9. Formation constants for some pyridine coordinated Co(II) complexes at 20 ± 1 °C.

Compound	solvent	K_1	Ref.
$[Co(dmgBF_2)_2(OH_2)_2]$	2-butanone	1.26×10^3	This work
$[Co(dmgBF_2)_2(OH_2)_2]$	Acetone	1.00×10^5	This work
$[Co(dmgBF_2)_2(OH_2)_2]$	dichloromethane	3.16×10^5	This work
$[Co(dmgBF_2)_2(OH_2)_2]$	1,2-difluorobenzene/acetone (4:1 v/v)	2.51×10^4	This work
$[Co(dmgBF_2)_2(OH_2)_2]$	Acetonitrile	1.26×10^5	This work
$[Co(dmgBF_2)_2(OH_2)_2]$	DMF	2.00×10^2*	[169]
$[Co(dmgH)_2(OH_2)_2]$	methanol	1.26×10^2	[170]
$[Co(dpgBF_2)_2(OH_2)_2]$	DMF	1.58×10^4*	[169]
$[Co(dpgH)_2(OH_2)_2]$	DMF	7.94×10^2*	[169]

* At 25 °C

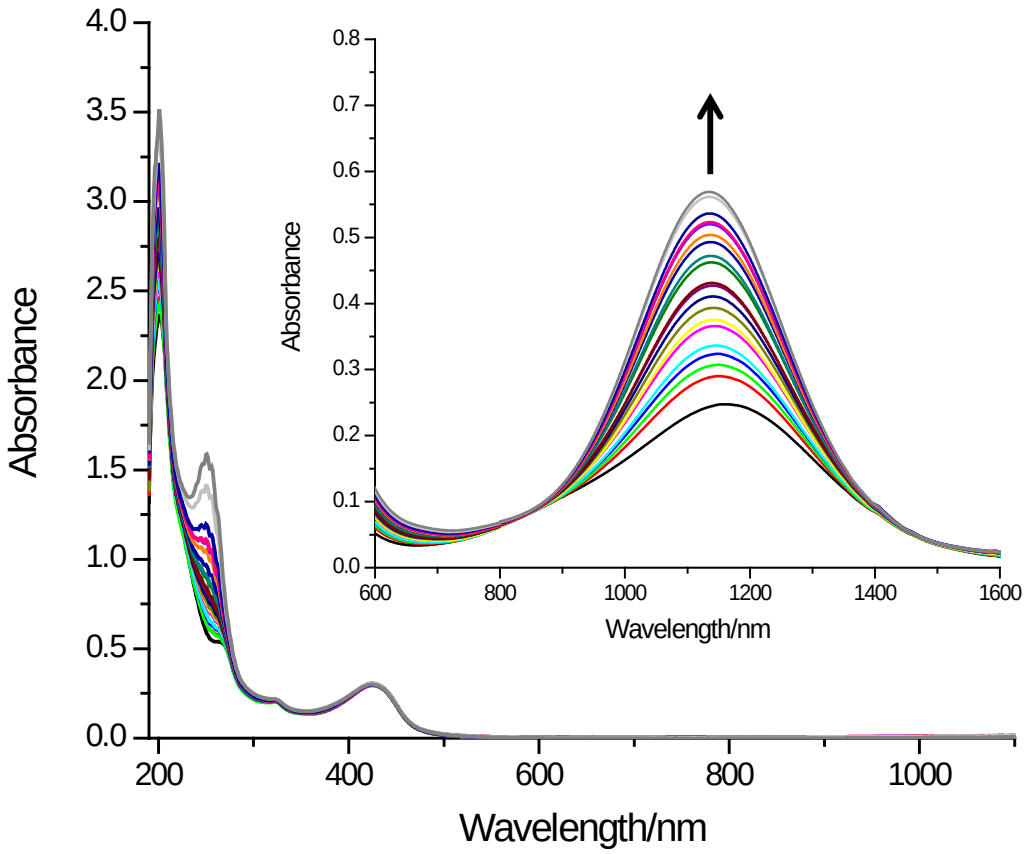

Figure 32. Spectrophotometric titration of $[Co(dmgBF_2)_2(H_2O)_2]$ with pyridine in acetonitrile. [complex **1**] = 0.1 mM, NIR region shown in inset ([complex **1**] = 2 mM), path length = 1 cm. Arrow represents increasing [pyridine], see Table S1.

Electrochemical and chemical reduction studies

In acetonitrile, on oxidatively or reductively initiated scans, the cyclic voltammograms of $[Co(dmgBF_2)_2(H_2O)_2]$ and $[Co(dmgBF_2)_2(H_2O)(py)]\bullet 0.5(CH_3)_2CO$ (Figure 37) shows a quasi-reversible wave for the $Co^{III/II}$ redox couple, reversible waves corresponding to the $Co^{II/I}$ redox couple,[155] as well as quasi-reversible waves corresponding to the $Co^{I/0}$ redox couple and to the reduction of the ligand (most likely reduction of the C=N bonds). The behavior of the cobalt center is comparable to what has been reported for

$[Co(dmgBF_2)_2(H_2O)_2]$ in the literature.[26] The equilibrium established in strongly coordinating solvents, as described above, between the $[Co(dmgBF_2)_2(OH_2)_2]$ and $[Co(dmgBF_2)_2(OH_2)(py)]$ species results in the profile of the cyclic voltammograms of both species being very similar as shown in Figure 37. In acetone and 2-butanone, the cyclic voltammograms for $[Co(dmgBF_2)_2(OH_2)_2]$ can be clearly distinguished from $[Co(dmgBF_2)_2(OH_2)(py)]$ via the absence of the cathodic peak in the region of the $Co^{I/0}$ redox couple for $[Co(dmgBF_2)_2(OH_2)(py)]$ (as shown in Figure 38a and Figure A22). The addition of five equivalences of pyridine to $[Co(dmgBF_2)_2(OH_2)_2]$, in any of the solvents studied, as discussed above, shifts the equilibrium towards $[Co(dmgBF_2)_2(OH_2)(py)]$ species, and the $Co^{I/0}$ redox couple is not observed. It is likely that the absence of the cathodic wave (see Figure 38b) is related to the coordination of the pyridine to the Co(II), which in turn affects the $Co^{I/0}$ redox couple. The addition of sterically encumbering pyridines (2-methylpyridine and 2,6-dimethylpyridine) up to fifteen equivalences to an acetonitrile solution of $[Co(dmgBF_2)_2(OH_2)_2]$ did not affect peak potentials in the cyclic voltammogram (Figure A26-A27). This indicates that the change observed in the cyclic voltammogram of $[Co(dmgBF_2)_2(H_2O)_2]$ in the presence of pyridine is not the result of a Brønsted acid-base behavior. The inability of these sterically hindered substituted pyridines to coordinate was also observed for the $[Co(dmgH)_2(OH_2)_2]$ system.[45] On the other hand, the addition of 4-aminopyridine resulted in similar changes to what was observed with the addition of pyridine and further validates the use of cyclic voltammetry to assess the coordination of pyridine. Interestingly, in the weakly coordinating solvents, where the integrity of $[Co(dmgBF_2)_2(H_2O)(py)]\bullet 0.5(CH_3)_2CO$ is retained, the addition of an excess (five equivalences) of pyridine did not result in an enhancement of the peak

currents, any shift in the peak potentials, or the appearance of any additional peaks in the cyclic or square wave voltammograms (not shown) of $[Co(dmgBF_2)_2(H_2O)(py)]\bullet 0.5(CH_3)_2CO$. This point to the dominance of the monopyridine species over these concentration ranges. The values of the reduction potentials are summarized in Table 10 for comparative purposes. To the best of our knowledge, this is the first time that a cobaloxime is being studied by cyclic voltammetry in either ketone solvents or 1,2-difluorobenzene. Like the UV-visible measurements, cyclic voltammetry also shows the effect of the solvent coordinating ability on the extent of the pyridine substitution.

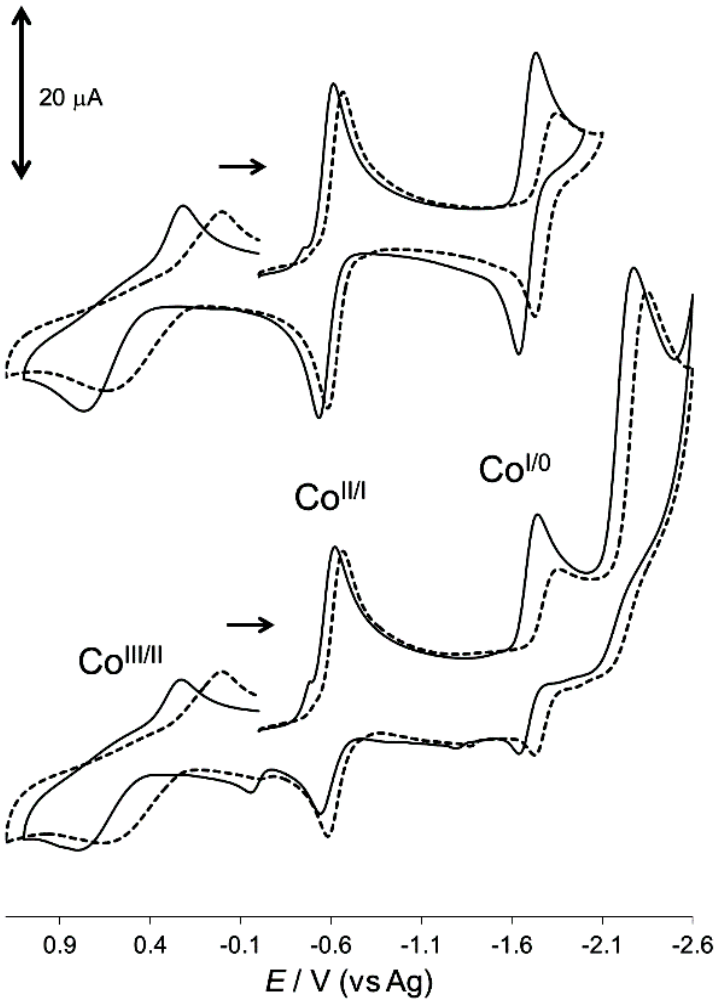

Figure 33. A comparison of the cyclic voltammograms of $[Co(dmgBF_2)_2(H_2O)_2]$ and $[Co(dmgBF_2)_2(H_2O)(py)]\bullet 0.5(CH_3)_2CO$ in acetonitrile on a glassy carbon working electrode vs Ag quasi-reference electrode. $[Co(dmgBF_2)_2(H_2O)_2]$ = 1.04 mM (solid lines) and $Co(dmgBF_2)_2(H_2O)(py)\bullet 0.5(CH_3)_2CO]$ = 1.02 mM (broken lines), I = 0.10 M ($[^nBu_4N]ClO_4$), and scan rate = 100 mV s^{-1}. The effect of the scan range on the shapes of cobalt peaks is shown above.

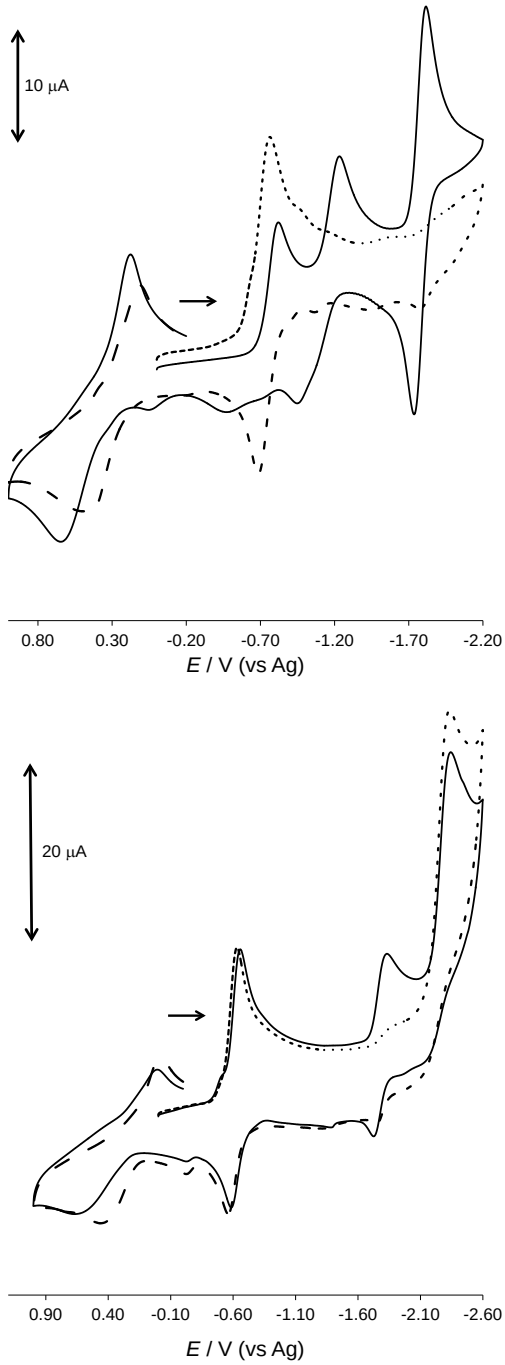

Figure 34. Cyclic voltammograms of $[Co(dmgBF_2)_2(H_2O)_2]$ and $[Co(dmgBF_2)_2(H_2O)(py)]\bullet 0.5(CH_3)_2CO$ on a glassy carbon working electrode vs Ag quasi-reference electrode, I = 0.10 M ($[^nBu_4N]ClO_4$), and scan rate = 100 mV s^{-1}. (a) In acetone, [complex **1**] = 1.12 mM (solid lines) and [complex **2**] = 1.04 mM (broken lines)

Figure 38 continued. and (b) in acetonitrile, [complex **2**] = 1.02 mM (solid lines) and [complex **2**] = 1.02 mM with 5.09 mM pyridine (broken lines).

Table 10. Comparison of the reduction potentials of $[Co(dmgBF_2)_2(H_2O)_2]$ and $[Co(dmgBF_2)_2(H_2O)(py)]\bullet 0.5(CH_3)_2CO$ at a glassy carbon working electrode vs Ag^+/Ag.

Entry	**Species**	**Solvent**	**$Co^{III/II}$/V**	**$Co^{II/I}$/V**	**$Co^{I/0}$/V**	**$dmgBF_2^{0/-}$ /V**
1	$[[Co(dmgBF_2)_2(OH_2)_2]$	acetonitrile	+0.70	−0.58	−1.69	−2.21
2	$[Co(dmgBF_2)_2(H_2O)(py)]\bullet 0.5(CH_3)_2CO$	acetonitrile	+0.60	−0.63	−1.77	−2.30
3	$[Co(dmgBF_2)_2(H_2O)(py)]\bullet 0.5(CH_3)_2CO$‡	acetonitrile	+0.46	−0.60	--	−2.30
4	$[Co(dmgBF_2)_2(OH_2)_2]$	acetone	+0.65	−0.82	−1.20	−1.79
5	$[Co(dmgBF_2)_2(H_2O)(py)]\bullet 0.5(CH_3)_2CO$	acetone	+0.50	−0.73	--	--
6	$[Co(dmgBF_2)_2(OH_2)_2]$	water	+0.48*	−0.60*	−0.85*	--
7	$[Co(dmgBF_2)_2(H_2O)(py)]\bullet 0.5(CH_3)_2CO$	water	+0.31*	−0.50*	--	--
8	$[Co(dmgBF_2)_2(OH_2)_2]$	2-butanone	+0.88	−0.58	−0.99	−1.58
9	$[Co(dmgBF_2)_2(H_2O)(py)]\bullet 0.5(CH_3)_2CO$	2-butanone	+0.64	−0.66	--	--
10	$[Co(dmgBF_2)_2(OH_2)_2]$	1,2-difluorobenzene/acetone (4:1, v/v)	+0.36	−0.82	−1.20	−1.82
11	$[Co(dmgBF_2)_2(H_2O)(py)]\bullet 0.5(CH_3)_2CO$	1,2-difluorobenzene/acetone (4:1, v/v)	+0.38	−0.80	--	--

‡ in five times excess pyridine, *values are vs AgCl/Ag. All the potentials quoted are determined from square wave voltammetry.

In acetonitrile where an excess of pyridine is added to force the formation $[Co(dmgBF_2)_2(H_2O)(py)]\bullet 0.5(CH_3)_2CO$(Table 10, entry 3), only the potentials for the cobalt couples are affected, but not the potential for the ligand. Using the potential of the ligand as reference, it is fair to assume that the addition of the pyridine does affect the cobalt center. In the other solvent systems, where $[Co(dmgBF_2)_2(H_2O)(py)]\bullet 0.5(CH_3)_2CO$ is stable without excess pyridine, a similar effect is also observed. Generally, the potential for the cobalt couples are more negative in $[Co(dmgBF_2)_2(H_2O)(py)]\bullet 0.5(CH_3)_2CO$ compared to $[Co(dmgBF_2)_2(H_2O)_2]$. From these findings, we have clearly shown that cyclic voltammetry can be used to qualitatively assess the coordination of pyridine to the Co(II) center.

Pyridine is known for its electron donating ability and has been used to stabilize low oxidation states as evidenced in its application in pyridine-enhanced pre-catalyst preparation stabilization and initiation (PEPPSI) complexes.[171-174] In water, the $Co^{II/I}$ redox couple illustrated a quasi-reversible behavior for $[Co(dmgBF_2)_2(H_2O)_2]$, but in the presence of an excess pyridine the behavior became reversible (i_{pa}/i_{pc} = 0.97, see Figure A25 vs A21). This behavior in addition to the absence of the $Co^{I/0}$ cathodic wave is quite intriguing, and is also observed in the ketone solvents. The transition of the cyclic voltammogram in going from $[Co(dmgBF_2)_2(H_2O)_2]$ to $[Co(dmgBF_2)_2(H_2O)(py)]\bullet 0.5(CH_3)_2CO$ is consistent in all the solvents used here (in terms of the absence of $Co^{I/0}$ redox couple in the cyclic voltammograms of $[Co(dmgBF_2)_2(H_2O)(py)]\bullet 0.5(CH_3)_2CO$). Repetitive cycling did not result in the appearance of any new peaks in the cyclic voltammograms of $[Co(dmgBF_2)_2(H_2O)(py)]\bullet 0.5(CH_3)_2CO$. It therefore appears that the coordination of the

pyridine causes the reduction of $Co^{I/0}$ couple to become more negative than the potential window of the solvent, and thus inaccessible. This we attribute to the electron donating ability of the pyridine, and validates the use of cyclic voltammetry to qualitatively identify the coordination of pyridine to $[Co(dmgBF_2)_2(H_2O)_2]$.

It is unclear from the electrochemical studies if the pyridine has a dissociation/association equilibrium with the Co(I) metal center as is established with the Co(II) state. Indeed, it has been suggested that the pyridine coordinates more strongly to the Co(I) than it does to the Co(II) state in $[Co(dmgH)_2(OH_2)_2]$ and $[Co(dmgBF)_2(OH_2)_2]$ complexes.[37] Both $[Co(dmgBF_2)_2(H_2O)_2]$ and $[Co(dmgBF_2)_2(H_2O)(py)]\bullet 0.5(CH_3)_2CO$ were reduced in acetonitrile under an argon atmosphere using $[^nBu_4N]BH_4$ (or powdered $NaBH_4$), and their spectra are given in Figure 39. The addition of $[^nBu_4N]BH_4$ resulted in an increase in the absorbance between 500 and 800 nm, which corresponds to the formation of a Co(I) species.[26, 37, 175-176] An analogous Co(I) species of $[Co(dmgBF_2)_2(H_2O)_2]$ (i.e. $[Co(dpgBF_2)_2(CH_3CN)]^-$, where $dpgBF_2$ = difluoroboryldiphenylglyoxime) and the pyridine coordinated anion of $[Co(dmgBF_2)_2(H_2O)(py)]\bullet 0.5(CH_3)_2CO$ have been isolated with a pentacoordinate geometry.[26, 177] It is evident that the differences between the UV-visible spectra of the reduced forms of $[Co(dmgBF_2)_2(H_2O)_2]$ and $[Co(dmgBF_2)_2(H_2O)(py)]\bullet 0.5(CH_3)_2CO$ are due to the presence of the pyridine in the axial position in place of the solvent molecule. These Co(I) species are very sensitive to oxygen and are unstable at low to moderate pH values ($pH < 10$).[37] In our experiments, we found that if the reduced cobalt species (Co(I)) is exposed to air, the change is irreversible and the Co(I) will not reform in an excess of the reducing agent under inert atmosphere. The exact nature of the species formed upon exposure to oxygen is unclear at this point.

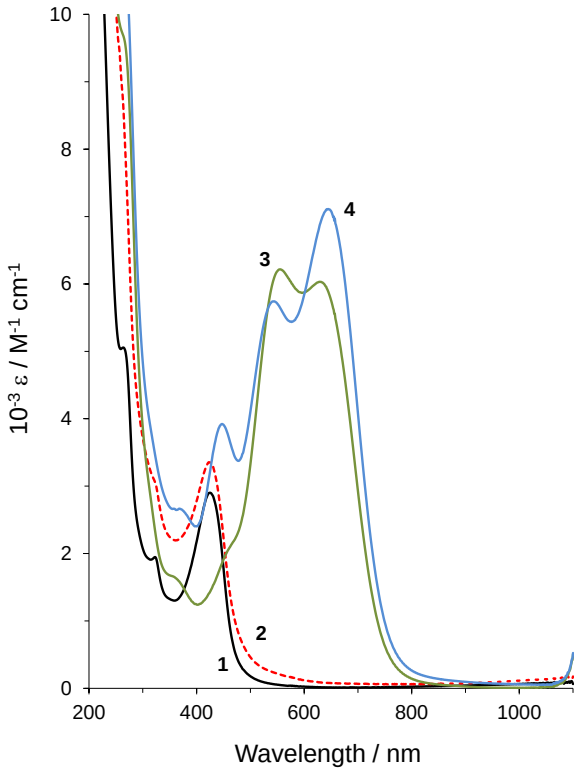

Figure 35. UV-visible spectra (acetonitrile solutions) of $[Co(dmgBF_2)_2(H_2O)_2]$ (black, (1)), $[Co(dmgBF_2)_2(H_2O)(py)]\bullet 0.5(CH_3)_2CO$ (broken/red, (2)), $[Co(dmgBF_2)_2(H_2O)_2]$ in excess $[^nBu_4N]BH_4$ (green, (3)), $[Co(dmgBF_2)_2(H_2O)(py)]\bullet 0.5(CH_3)_2CO$ in excess $[^nBu_4N]BH_4$ (blue, (4)).

The addition of pyridine to the acetonitrile Co(I) solution of $[Co(dmgBF_2)_2(OH_2)]^-$ (produced by reducing $[Co(dmgBF_2)_2(H_2O)_2]$ in excess BH_4^- salt) caused spectral transformations that resemble those of a borohydride reduced solution of $[Co(dmgBF_2)_2(H_2O)(py)]\bullet 0.5(CH_3)_2CO$ (i.e., the $[Co(dmgBF_2)_2(py)]^-$ species) as shown in Figure 40. It is quite clear that the sequential addition of the pyridine results in distinct changes to the spectra of the solution and provides evidence for the formation of a Co^I-

pyridine coordination compound. The data also indicates that less than stoichiometric amounts of pyridine will cause significant transformation in the visible region of the spectrum (unlike the Co(II) state). The changes in the absorbance values upon the addition of pyridine are also suggestive of an equilibrium between the "pyridine-bound" and the "free" Co(I) species in acetonitrile. From the mole ratio plot, the stoichiometry was found to be 1:1 (pyridine:complex), consistent with the formation of a monopyridine species. Using the method of Nonaka and Hamada,[169] log K = 3.94 x 10^4 (see Appendix) for the Co(I) species as compared to 1.26 x 10^4 for the Co(II) species. These results provide evidence that the Co(I) metal center has a stronger affinity for pyridine than the Co(II). Indeed, the crystal structure of the anion of $[Co(dmgBF_2)_2(H_2O)(py)]\bullet 0.5(CH_3)_2CO$ [177] reveals a shorter Co-N bond than for the corresponding Co(II) species[13] and supports the larger formation constants obtained.

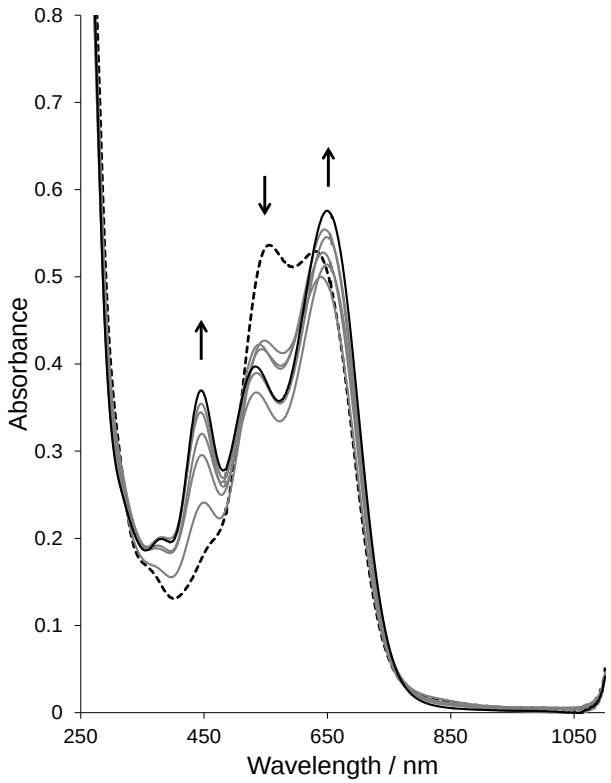

Figure 36. UV-visible spectra (acetonitrile solutions) of cobalt(I) species produced in situ using $[^{n}Bu_4N]BH_4$ as a reductant [complex] = 1.0 mM (broken line), and with various equivalences (0.50, 1.0, 1.5, 2.0, 2.5, and 4.0) of pyridine, path length = 1 mm. Arrows indicate the absorbance change with increasing [pyridine].

^{19}F NMR spectroscopic studies

Transition metal NMR chemical shifts are useful probes of the structure and reactivity of many coordination complexes, since those chemical shifts are sensitive to tiny variations at the coordination metal center under investigation.[178] Previous, we had used NMR spectroscopic studies (with ^{11}B, ^{19}F, and ^{59}Co) to verify coordination of a (4-pyridine)oxazolo[4,5-*f*]phenanthroline (L-pyr) bridging ligand to a Co(II) metal center by

the environmental effect on the BF_2-capped $dmgBF_2$ ligand.[155] In our current study, ^{19}F NMR spectra were acquired in CD_3CN at ambient temperature for $[Co(dmgBF_2)_2(H_2O)_2]$ and $[Co(dmgBF_2)_2(H_2O)(py)]\bullet 0.5(CH_3)_2CO$ in the absence and presence of pyridine and pentafluoropyridine, as well as solutions that were treated with excess $[^nBu_4N]BH_4$ to generate the corresponding Co(I) species. Studies of the Co(II) and Co(I) species of $[Co(dmgBF_2)_2(H_2O)_2]$ and $[Co(dmgBF_2)_2(H_2O)(py)]\bullet 0.5(CH_3)_2CO$ (see Table 11, Figure A31 and Figure 41) corroborated our equilibrium and electrochemical studies. It must be noted that the ^{19}F NMR spectra of $[Co(dmgBF_2)_2(H_2O)_2]$ in acetonitrile-d_3 show chemical shifts at –142.4, –150.1, –151.9, –168.4, and –189.2 ppm (Table 11, entry 1). Like our electrochemical studies vide supra, the addition of five equivalences of pyridine to complex **1** is expected to shift the equilibrium towards that of $[Co(dmgBF_2)_2(H_2O)(py)]\bullet 0.5(CH_3)_2CO$. A mixture of complex **1** and five equivalences of pyridine gave three predominant peaks resonating at –147.3, –151.8, and –189.1 ppm (Figure A31). Comparing the spectrum of $[Co(dmgBF_2)_2(H_2O)(py)]\bullet 0.5(CH_3)_2CO$ dissolved in CD_3CN (Table 11, entry 2) with the mixture $[Co(dmgBF_2)_2(H_2O)_2]$ and five equivalences of pyridine (Table 11, entry 3), it was evident that $[Co(dmgBF_2)_2(H_2O)(py)]\bullet 0.5(CH_3)_2CO$ had a dissociation/association equilibrium with $[Co(dmgBF_2)_2(H_2O)_2]$ as shown in Eq. 3 above.

Secondly, the addition of ten equivalences of the reducing $[^nBu_4N]BH_4$ to the complexes to produce Co(I) species (Table 11, entries 4-6), resulted in the disappearance of the peak resonating at ~ –189 ppm in both $[Co(dmgBF_2)_2(H_2O)_2]$ (Figure 41a) and $[Co(dmgBF_2)_2(H_2O)(py)]\bullet 0.5(CH_3)_2CO$ (Figure 41b). Also, the reduced form of $[Co(dmgBF_2)_2(H_2O)_2]$ had two additional peaks when compared to that of

$[Co(dmgBF_2)_2(H_2O)(py)]\bullet 0.5(CH_3)_2CO$, as was observed with the Co(II) species. The reduction in the number of resonances observed point to a reduction in the number of conformations of the BF_2-capped $dmgBF_2$ ligand upon the coordination of pyridine. When $[Co(dmgBF_2)_2(H_2O)_2]$ was reduced in the presence of five equivalences of pyridine (Figure 41c), a very similar spectrum to that of the reduced $[Co(dmgBF_2)_2(H_2O)(py)]\bullet 0.5(CH_3)_2CO$ was obtained, and further confirms the similarity of the species formed.

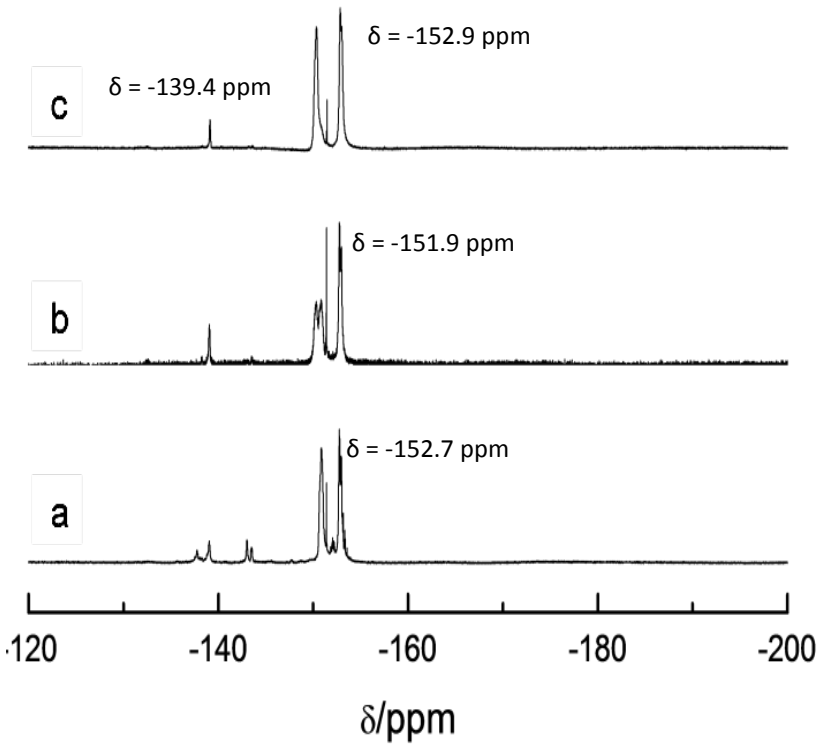

Figure 37. ^{19}F NMR spectra acquired in acetonitrile-d_3 of (a) 50 mM $[Co(dmgBF_2)_2(H_2O)_2]$ with 500 mM $[Bu_4N]BH_4$; (b) 50 mM $[Co(dmgBF_2)_2(H_2O)(py)]\bullet 0.5(CH_3)_2CO$ with 500

Figure 41 continued. mM $[Bu_4N]BH_4$; and (c) 50 mM $[Co(dmgBF_2)_2(H_2O)_2]$ with 250 mM pyridine and 500 mM $[Bu_4N]BH_4$.

A polyfluorinated pyridine such as pentafluoropyridine (pyF_5) should be a very useful spectroscopic probe for ^{19}F NMR measurements on pyridine coordinated to the cobalt metal center. The coordination of pyF_5 should result in changes in the chemical shifts of the *ortho*- and *para*-fluorine due to the inductive effect. The addition of five equivalences of pyF_5 to $[Co(dmgBF_2)_2(H_2O)_2]$ did not result in noticeable changes in the spectra (Figure 42). This is consistent with our observations using UV-visible absorbance and cyclic voltammetry measurements (in acetonitrile or the ketone solvents (not shown)) in which no changes were observed, and possibly points to no reaction or a small equilibrium constant. The pyF_5 species is defluorinated at the *para* position (to give 2,3,5,6-tetrafluoropyridine, pyF_4) in the presence of $[Bu_4N]BH_4$ (see Figure A32) and this type of reaction with a borohydride salt is well documented in the literature.[179-180] The addition of ten equivalences of the reducing agent $[^nBu_4N]BH_4$ to $[Co(dmgBF_2)_2(H_2O)_2]$ along with five equivalences of the pyF_5 yielded some intriguing results. Apart from the disappearance of the resonance for the *para*-fluorine at –162.3 ppm, of note is the appearance of a resonance at –102.1 ppm which is about 12 and 9 ppm up field of the *ortho*-fluorine of pyF_5 and pyF_4, respectively. This shift in the resonance of the *ortho*-fluorine is believed to be indicative of coordination of pyF_4 to the Co(I) metal center to produce the complex as shown in Scheme 9. With the appearance of the a peak circa -75 ppm which corresponds to the tetrabutylammonium fluoride salt in acetonitrile-d_3 according to literature which puts

that value at -72 ppm.[181] The peak circa -75 ppm is not as intense as the other peaks that are observed downfield which could be due to the formation of fluorinated borohydrides.

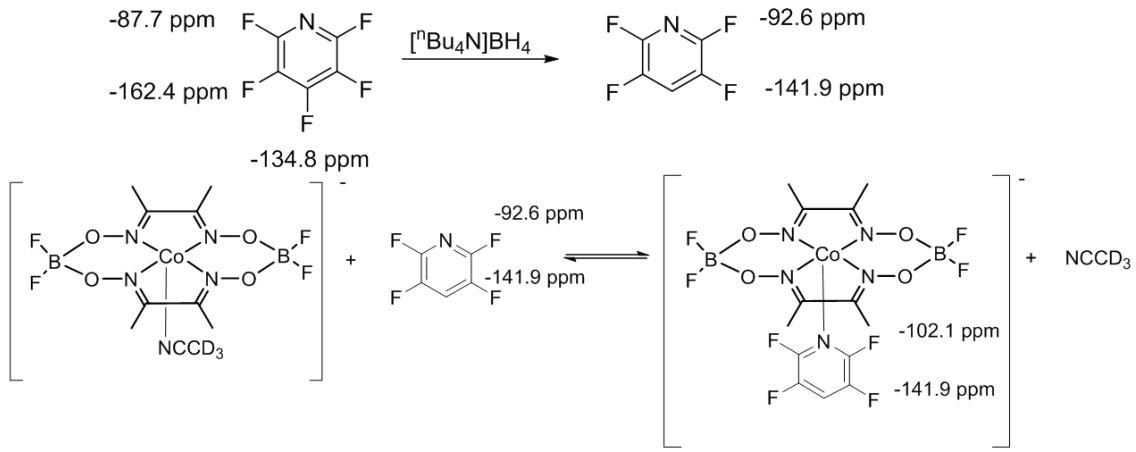

Scheme 9. Proposed reaction between the Co(I) species (produced in situ) and pyF_4. [179-180]

Additional peaks are observed when compared to the pyridine coordinated analogue (Table 11, entry 8 vs 6) which is further indicative of possible association/dissociation equilibria and the presence of conformers involving the $dmgBF_2$ ligand.[155] Here again we see that the Co(I) species has a higher affinity for the pyridine type species compared to the Co(II) species, as no coordination was observable between the Co(II) and the fluorinated pyridine. The extent of the coordination to the Co(I) center is, however, difficult to decipher at this point as the effect of coupling as well as the quality of the baseline makes integration unsuitable, typical of ^{19}F NMR spectroscopic data.

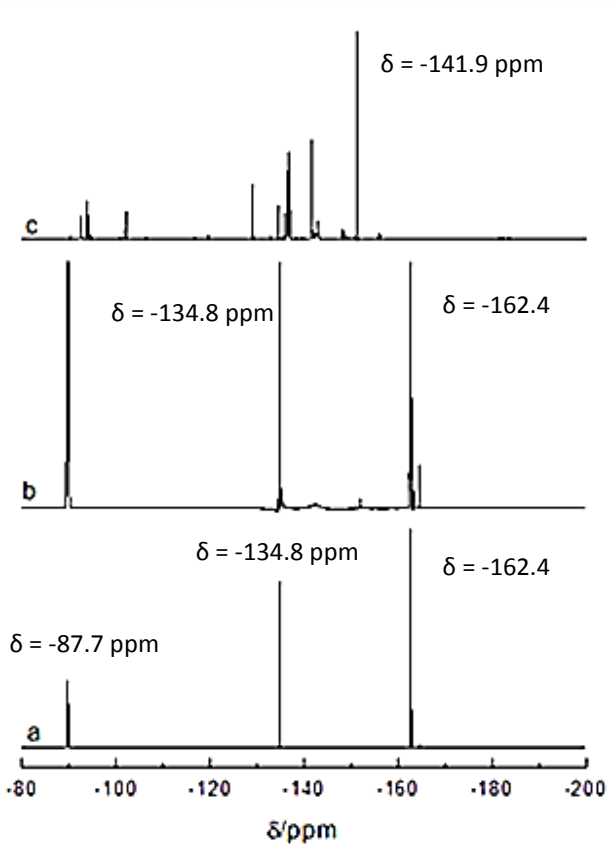

Figure 38. ^{19}F NMR spectra in acetonitrile-d_3 for (a) 250 mM pyF_5, (b) 50 mM complex **1** and 250 mM pyF_5 and (c) 50 mM complex **1**, 250 mM pyF_5 and 500 mM $[^nBu_4N]BH_4$.

Table 11. ^{19}F NMR chemical shifts for $[Co(dmgBF_2)_2(H_2O)_2]$ and $[Co(dmgBF_2)_2(H_2O)(py)]\bullet 0.5(CH_3)_2CO$ in acetonitrile-d_3.

Entry	Species/mixture	δ/ ppm	Ref.
1	$[Co(dmgBF_2)_2(H_2O)_2]$	–142.4, –150.1, –151.9, –168.4, –189.2	This work
2	$[Co(dmgBF_2)_2(H_2O)(py)]\bullet 0.5(CH_3)_2CO$	–141.5, –142.4, –144.8, –147.7, –151.7, –154.9, –156.2, –188.9	This work
3	$[Co(dmgBF_2)_2(H_2O)_2]$ + py	–147.3, –151.8, –189.1	This work
4	$[Co(dmgBF_2)_2(H_2O)_2]$ + $[^nBu_4N]BH_4$	–137.8, –138.3, –143.5, –150.8, –151.4 , –152.7	This work
5	$[Co(dmgBF_2)_2(H_2O)(py)]\bullet 0.5(CH_3)_2CO$ + $[^nBu_4N]BH_4$	–139.1, –150.7, –151.4, –152.8	This work
6	$[Co(dmgBF_2)_2(H_2O)_2]$ + $[^nBu_4N]BH_4$ + py	–139.4, –150.4, –151.5, –152.9	This work
7	$[Co(dmgBF_2)_2(H_2O)_2]$ + pyF_5	–89.7, –134.9, –142.5, –150.3, –151.9, –162.7, –168.5, –189.1	This work
8	$[Co(dmgBF_2)_2(H_2O)_2]$ + $[^nBu_4N]BH_4$ + pyF_5	–92.6, –94.6, –102.1, –119.7, –129.0, –134.4, –135.7, –136.5, –136.9, –141.9, –148.2, –150.7, –151.4, –156.1	This work
9	pyF_5 (lit. [a])	–89.7 (–87.7), –134.8 (–134.3), –162.7 (–162.4)	[179-180]
10	pyF_4 (lit. [a])	–92.6 (–92.6), –141.9 (–141.3)	[179-180]
11	$[Co(dmgBF_2)_2(H_2O)_2]$ [b]	–145.6 , –146.6, –148.4	[155]

[a] tetrachloromethane, [b] DMSO-d_6

Spectroelectrochemical studies

From cyclic voltammetric and chemical reduction studies, it is clear that the pyridine does influence the reduction of the $Co^{II/I}$ redox couple, as well as the spectrum of the Co(I) species. This difference is most pronounced in relatively weakly coordinating solvents. To provide further insight, and to justify our assignments for the $Co^{II/I}$ redox couple, studies of the spectral changes under cathodic potentials in the various solvents were performed. In acetonitrile (Figure 43), absorption spectrum changes of $[Co(dmgBF_2)_2(H_2O)_2]$ at a constant potential of −1.0 V vs Ag, resulted in spectral characteristics similar to the Co(I) species reported by Pantani et al.,[175] also generated by electrochemical methods. Comparing the reduced spectra formed from $[Co(dmgBF_2)_2(H_2O)_2]$ and $[Co(dmgBF_2)_2(H_2O)(py)]\bullet 0.5(CH_3)_2CO$, there are subtle differences. For $[Co(dmgBF_2)_2(H_2O)_2]$, the peak at ca 430 nm decreases in absorbance upon reduction whereas in $[Co(dmgBF_2)_2(H_2O)(py)]\bullet 0.5(CH_3)_2CO$, this absorbance increases. Additionally, the relative intensities of the peaks assigned to the formation of the Co(I) species at ca 550 and 640 nm differ between $[Co(dmgBF_2)_2(H_2O)_2]$ and $[Co(dmgBF_2)_2(H_2O)(py)]\bullet 0.5(CH_3)_2CO$. The addition of excess pyridine to acetonitrile solutions of $[Co(dmgBF_2)_2(H_2O)_2]$ or $[Co(dmgBF_2)_2(H_2O)(py)]\bullet 0.5(CH_3)_2CO$ yields enhanced absorbance for the Co(I) state relative to a solution of only $[Co(dmgBF_2)_2(H_2O)(py)]\bullet 0.5(CH_3)_2CO$ (see Figure 44 and Figures A33−A35 vs Figure 43b). This further confirms the extent of the equilibration in acetonitrile as given in Eq. 3. In water, only one broad band with λ_{max} at 640 nm develops when $[Co(dmgBF_2)_2(H_2O)_2]$ is reduced (see Figure A37), which is consistent with the spectrum observed by Kumar et al.[37] In the presence of an excess of pyridine, similar features to the acetonitrile solution (i.e., the dual band for the Co(I) species) are observed (Figure A38), and here also our

findings are consistent with the report of Kumar et al.[37] in aqueous media. In the weakly coordinating solvents, acetone, 2-butanone and 1,2-difluorobenzene/acetone, the reduction of $[Co(dmgBF_2)_2(H_2O)_2]$ at the $Co^{II/I}$ redox couple develops a similar band to that of water, but red shifted by ~100 nm, , whereas $[Co(dmgBF_2)_2(H_2O)(py)]\bullet 0.5(CH_3)_2CO$ gave the same spectral features that were observed in acetonitrile (and water) as shown in Figure 45 (and Figures A39–A46). Like the acetonitrile and water solutions, the reduction of $[Co(dmgBF_2)_2(H_2O)_2]$ in the presence of excess pyridine resulted in the spectral characteristics of $[Co(dmgBF_2)_2(H_2O)(py)]\bullet 0.5(CH_3)_2CO$ under reduction. Interestingly, the addition of excess pyridine to the ketone solutions of $[Co(dmgBF_2)_2(H_2O)(py)]\bullet 0.5(CH_3)_2CO$ did not enhance the absorbance change upon reduction. This strongly supports the idea that the dissociation of $[Co(dmgBF_2)_2(H_2O)(py)]\bullet 0.5(CH_3)_2CO$ is insignificant in these solvents, and the monopyridine species is the predominant species. It is very important that the differences in the spectra of Co(I) species of $[Co(dmgBF_2)_2(H_2O)_2]$ in these solvents are highlighted. In water and the ketone solvents, only a single band develops between 600 and 900 nm in the absence of pyridine, however, in acetonitrile, a dual band develops for Co(I) species of $[Co(dmgBF_2)_2(H_2O)_2]$. It can be speculated that the coordination of the nitrogen from the acetonitrile solvent causes the splitting of the Co(I) band, in a manner similar to pyridine. This splitting may be the result of back bonding from the electron rich Co(I) to the sp^2 or sp hybridized nitrogen. This idea was also postulated by Espenson and co-workers.[177] Evidence for this is seen when the acetonitrile spectra are compared to those obtained in from weak to moderately coordinating solvents, Figures 43 and 45.

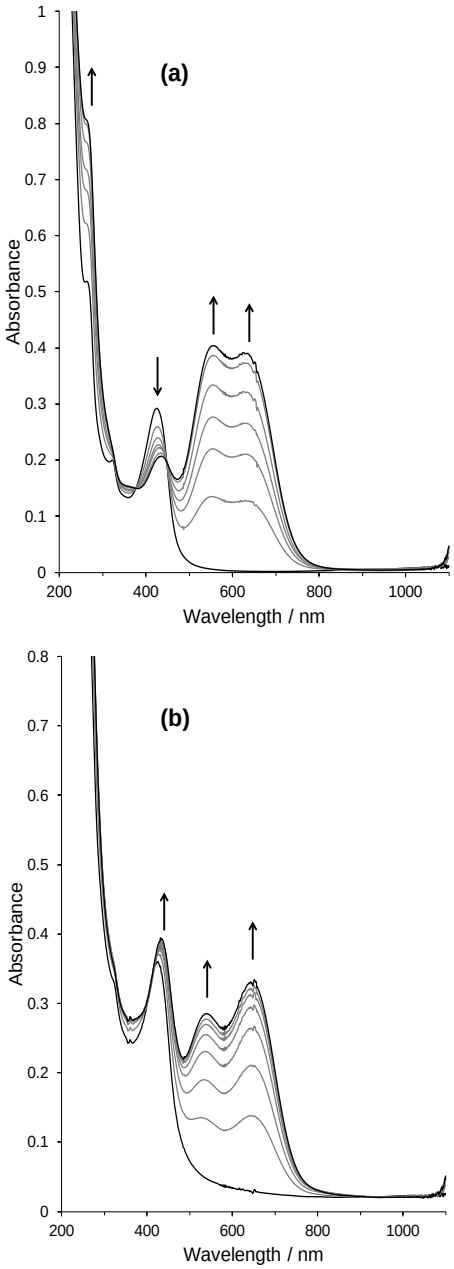

Figure 39. Absorbance changes in the UV-visible spectra of $[Co(dmgBF_2)_2(H_2O)_2]$ and $[Co(dmgBF_2)_2(H_2O)(py)]\bullet 0.5(CH_3)_2CO$ in acetonitrile at a constant potential of −1.0 V vs Ag, I = 0.10 M ($[^nBu_4N]ClO_4$), path length = 1 mm. (a) [complex **1**] = 1.05 mM and, (b) [complex **2**] = 1.02 mM.

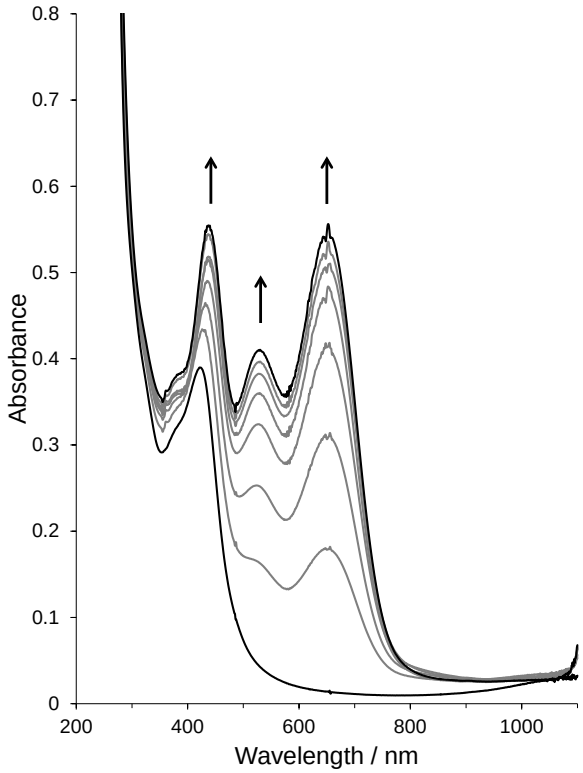

Figure 40. Absorbance changes in the UV-visible spectra of $[Co(dmgBF_2)_2(H_2O)(py)]\bullet 0.5(CH_3)_2CO$ with pyridine in acetonitrile at a constant potential of −1.0 V vs Ag, I = 0.10 M ($[^nBu_4N]ClO_4$), path length = 1 mm. [complex **2**] = 1.02 mM and [pyridine] = 5.09 mM.

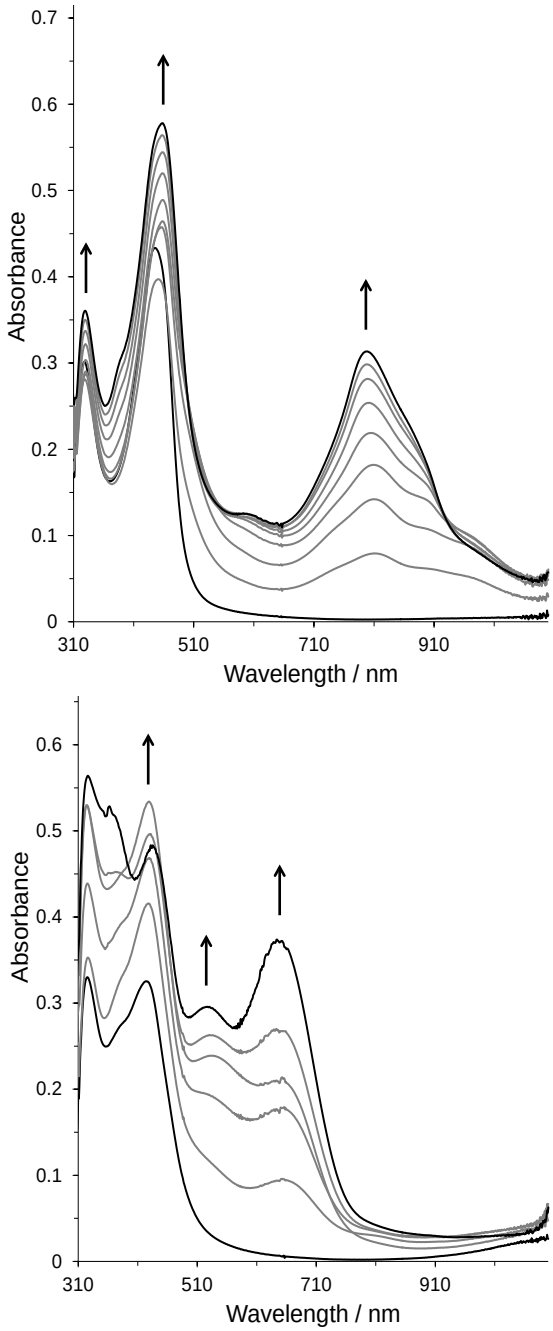

Figure 41. Absorbance changes in the UV-visible spectra of $[Co(dmgBF_2)_2(H_2O)_2]$ and $[Co(dmgBF_2)_2(H_2O)(py)]\bullet 0.5(CH_3)_2CO$ in acetone at a constant potential of −0.90 V vs Ag, I = 0.10 M ($[^nBu_4N]ClO_4$), path length = 1 mm. (a) [complex **1**] =1.14 mM, (b) [complex **2**] =1.08 mM.

Electrochemical behavior of $[Co(dmgBF_2)_2(H_2O)_2]$ and $[Co(dmgBF_2)_2(H_2O)(py)]\bullet 0.5(CH_3)_2CO$ for the production of hydrogen in the presence of *p*-cyanoanilinium tetrafluoroborate in various solvents

Complex **1** has been used as a benchmark for the activity of cobaloxime and other cobalt complexes employed in the electrocatalytic reduction of protons to form hydrogen, with the following mechanism being proposed (Scheme 10).[21, 26]

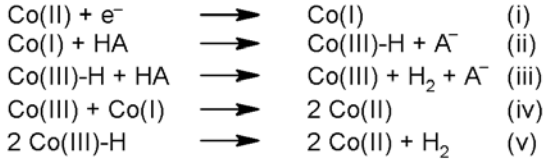

Scheme 10. Proposed mechanism for the electrocatalytic reduction of protons (from an acid source such as *p*-cyanoanilinium tetrafluoroborate, HA) by cobaloximes.[26]

There is very little doubt that a Co(I) species is involved in the catalytic process. As such, a comparative study of complexes **1** and **2** under similar conditions was undertaken to determine if the pyridine influences the catalytic reduction of protons, and to simultaneously establish the effect of the relatively non-coordinating solvents on the apparent rate constant[26] for the electrocatalytic transformation. Controlled-potential electrolysis measurements for the production of hydrogen were conducted in a sealed two-chambered H-cell (Figure A53). These results are summarized in Table 12. The electrochemical behavior of $[Co(dmgBF_2)_2(H_2O)_2]$and $[Co(dmgBF_2)_2(H_2O)(py)]\bullet 0.5(CH_3)_2CO$ in acetonitrile is an exact feature similar to what has been observed for $[Co(dmgBF_2)_2(H_2O)_2]$ in the literature (Figures A47-A49).[26] Under these conditions, $[Co(dmgBF_2)_2(H_2O)_2]$, based on the amount of hydrogen produced, had a turnover number (TON) of nearly five (5) whereas

$[Co(dmgBF_2)_2(H_2O)(py)]\bullet 0.5(CH_3)_2CO$ (generated by adding five times excess pyridine to $[Co(dmgBF_2)_2(H_2O)_2]$, had a TON of 3.3 after 2.5 h in acetonitrile. In acetone and 2-butanone, the TONs were less than half the values obtained in acetonitrile, which follows from the values for k_{app}. To the best of our knowledge, this represents the first such study in ketone solvents. The results of the electrocatalytic reduction of the protons in these solvent systems have provided some clear conclusions. There is a linear correlation between the dielectric constant[182] of the non-aqueous solvent and the apparent rate constant for the reduction of the proton (Figures A51 & A52). This retardation points to the possible role of the solvent in stabilizing the transition states involved in the catalytic process, as the Co(I) species will be ionic, and ion-pairing is likely to retard the catalytic cycle. It is also evident that $[Co(dmgBF_2)_2(H_2O)(py)]\bullet 0.5(CH_3)_2CO$ has a slower rate constant than $[Co(dmgBF_2)_2(H_2O)_2]$ in solvent systems explored. The reasons for this may be two-fold. The first is the reduction of the available catalytic sites[14] upon coordination of the axial pyridine. Secondly, the electron donating ability of the pyridine is likely to result in a more stable Co^{III}-H species in $[Co(dmgBF_2)_2(H_2O)(py)]\bullet 0.5(CH_3)_2CO$ than that formed in $[Co(dmgBF_2)_2(H_2O)_2]$, which will retard the rate of hydrogen production.

These findings clearly demonstrate the influence of the axial pyridine on performance of the catalyst and has a significant role in the development of the BF_2-capped cobaloxime based systems.

Table 12. Summary of electrocatalytic and controlled-potential electrolysis experiments.

complex	Solvent	k_{app} / M^{-1} s^{-1}	10^4 n_{acid} / mol	10^6 n_{cat} / mol	V_{H2} / µL	TON	TOF / h^{-1}
$[Co(dmgBF_2)_2(H_2O)_2]$	acetonitrile	2068 ± 143	2.18	10.2	1122	4.6	1.8
$[Co(dmgBF_2)_2(H_2O)(py)]\bullet 0.5(CH_3)_2CO$	acetonitrile	1571 ± 25	--	--	--	--	--
$[Co(dmgBF_2)_2(H_2O)(py)]\bullet 0.5(CH_3)_2CO$*	acetonitrile	1384 ± 241	2.16	8.14	639	3.3	1.3
$[Co(dmgBF_2)_2(H_2O)_2]$	acetone	254 ± 21	2.16	10.3	420	1.7	0.68
$[Co(dmgBF_2)_2(H_2O)(py)]\bullet 0.5(CH_3)_2CO$	acetone	183 ± 23	2.15	8.06	285	1.5	0.59
$[Co(dmgBF_2)_2(H_2O)_2]$	2-butanone	177 ± 25	2.15	10.2	255	1.0	0.42
$[Co(dmgBF_2)_2(H_2O)(py)]\bullet 0.5(CH_3)_2CO$	2-butanone	123 ± 9	2.19	9.32	211	0.94	0.38

Note: * $[Co(dmgBF_2)_2(H_2O)(py)]\bullet 0.5(CH_3)_2CO$ in 5 times excess pyridine which should force the equilibrium towards **2**; Controlled potential experiments are performed at 20 °C for 2.5 h at a constant potential of −0.75 V in acetonitrile, −1.0 V in acetone and 2-butanone vs Ag.

The data strongly supports the retention of the pyridine in the coordination sphere upon reduction. This supposition is also supported by the chemical and electrochemical reductions and the pyridine titrations. The retention of pyridine in the coordination sphere may also be inferred from the retardation of the rate constants for the reduction of protons by $[Co(dmgBF_2)_2(H_2O)(py)]\bullet 0.5(CH_3)_2CO$ relative to $[Co(dmgBF_2)_2(H_2O)_2]$. Further studies are required and are underway to explore the electronic effects of pyridine's coordination to the reduced cobalt center.

CHAPTER IV

CONCLUSIONS AND FUTURE STUDIES

In the course of this research project it became apparent that the protocol used for the synthesis of the binuclear ruthenium(II) complex will need to be adjusted to ensure that the binuclear product is obtained in high yields over the trinuclear product. Thus studies into the development of another ligand that can act as a bridge to connect a ruthenium photosensitizer to potential cobalt-containing catalysts is needed. With the development of these new potential photocatalyst, studies into their stability and ability to produce hydrogen will be needed. This will also lead to investigations into make photocatalyst that are highly soluble in water and stable over a wide range of pH values.

The equilibrium studies carried out on $[Co(dmgBF_2)_2(OH_2)_2]$ in various solvents showed that the ability of the solvent to coordinate with the metal center plays a vital role in the formation of $[Co(dmgBF_2)_2(OH_2)(py)]$. From the data it was observed that strongly coordinating solvents such as acetonitrile compete with pyridine in substituting the waters in the axial position of the cobaloxime, thus having an equilibrium constant that is not very favorable for the formation of $[Co(dmgBF_2)_2(OH_2)(py)]$. On the other hand moderately to weakly coordinating solvents like acetone was observed to have equilibrium constants that favored the formation of the monopyridine cobaloxime. The equilibrium studies that were carried out on the cobalt(I) species revealed that there was a preference for pyridine to be coordinated to the metal center after reduction over its cobalt(II) counterpart.

From the electrochemical data it is observed that in acetonitrile because the equilibrium does not favor the monopyridine product, the redox potential of $[Co(dmgBF_2)_2(OH_2)_2]$ and $[Co(dmgBF_2)_2(OH_2)(py)]\bullet 0.5(CH_3)_2CO$ were very similar to

each other. In the other solvents tested, different redox potentials were observed between the diaqua complex and the monopyridine complex where the potentials for the monopyridine complex was observed to be more cathodic compared to the diaqua complex. Interestingly enough it is also observed that the $Co^{I/0}$ redox couple is suppressed when pyridine is coordinated versus when it is not. This phenomenon was also observed in acetonitrile when additional pyridine was added to either solutions of the monopyridine or the diaqua complex.

From the spectroelectrochemical studies it was observed that the solutions that contained $[Co(dmgBF_2)_2(OH_2)_2]$ produced a different spectra from the solutions that contained $[Co(dmgBF_2)_2(OH_2)(py)]\bullet 0.5(CH_3)_2CO$. Interestingly enough upon addition of five equivalents of pyridine to the $[Co(dmgBF_2)_2(OH_2)(py)]\bullet 0.5(CH_3)_2CO$ in acetonitrile revealed an enhancement in the absorbance. That effect was not seen in the other solvents used which leads back to the equilibrium studies which concluded that the monopyridine complex was favored in moderately to weakly coordinating solvents.

The ^{19}F NMR spectroscopic studies further confirmed that pyridine remains coordinated upon reduction. This is observed through the limiting number of peaks observed, since pyridine is much larger than water which in turn limits the amount of stable conformers possible. Since pentafluoropyridine reacts with the reducing agent at this time it is unclear what is formed in solution and more studies on this system will be warranted.

The electrocatalytic production of hydrogen showed that the solvent affects the amount of hydrogen that is produced, and that amoung all of the solvents tested acetonitrile was seen to be the most efficient. This could arise from the possibility of the solvent's ability to stabilize the transition states that are involved in the catalytic process. An

example of this would be ion-pairing that may occur which can retard the catalytic cycle. When pyridine is coordinated to the metal center, the amount of hydrogen produced is much lower compared to the diaqua complex. An explanation for this is the possibility that the electron donating ability of pyridine stabilizes the Co^{III}-H which in turn would slow the reaction and thus producing less hydrogen.

Equilibrium studies involving $[Co(dmgBF_2)_2(H_2O)_2]$ and pyridine analogues are warranted. These studies will give a better insight on how substitution a pyridine ligand will affect the binding affinity to cobalt-containing metal center.

REFERENCES

1. Greenwood, N. N.; Earnshaw, A., *Chemistry of the Elements*. Elsevier: **2012**.
2. Cotton, F. A.; Wilkinson, G.; Murillo, C. A.; Bochmann, M.; Grimes, R., *Advanced inorganic chemistry*. Wiley New York: **1999**; Vol. 5.
3. Zhao, D.; Brammer, L., *Inorg. Chem.* **1994,**
4. Cotton, F. A.; Czuchajowska, J., *Polyhedron* **1990,** *9* (21),2553-2566.
5. Bowman-James, K., *Acc. Chem. Res.* **2005,** *38* (8),671-678.
6. Werner, A., *New Ideas on Inorganic Chemistry*. Longmans, Green, and Company: 1911.
7. Brunschwig, B. S.; Chou, M. H.; Creutz, C.; Ghosh, P.; Sutin, N., *J. Am. Chem. Soc.* **1983,** *105* (14),4832-3.
8. http://www.webelements.com/ruthenium/isotopes.html
9. Seddon, E. A.; Seddon, K. R., *The chemistry of ruthenium*. Elsevier: 2013.
10. Lin, C. T.; Boettcher, W.; Chou, M.; Creutz, C.; Sutin, N., *JACS* **1976,** *98* (21),6536-6544.
11. Bock, C. R.; Meyer, T. J.; Whitten, D. G., *JACS* **1974,** *96* (14),4710-4712.
12. Fuchs, Y.; Lofters, S.; Dieter, T.; Shi, W.; Morgan, R.; Strekas, T. C.; Gafney, H. D.; Baker, A. D., *JACS* **1987,** *109* (9),2691-2697.
13. Bakac, A.; Brynildson, M. E.; Espenson, J. H., *Inorg. Chem.* **1986,** *25* (23),4108-4114.
14. Artero, V.; Chavarot-Kerlidou, M.; Fontecave, M., *Angew. Chem. Int. Ed.* **2011,** *50* (32),7238-7266.
15. Dempsey, J. L.; Brunschwig, B. S.; Winkler, J. R.; Gray, H. B., *Acc. Chem. Res.* **2009,** *42* (12),1995-2004.
16. McNamara, W. R.; Han, Z.; Yin, C.-J.; Brennessel, W. W.; Hollan, P. L.; Eisenberg, R., *Proc. Natl. Acad. Sci. USA* **2012,** *109* (39),15594–15599.
17. Marinescu, S. C.; Winkler, J. R.; Gray, H. B., *Proc. Natl. Acad. Sci. USA* **2012,** *109* (38),15127-15131.
18. Smolentsev, G.; Guda, A. A.; Janousch, M.; Frieh, C.; Jud, G.; Zamponi, F.; Chavarot-Kerlidou, M.; Artero, V.; van Bokhoven, J. A.; Nachtegaal, M., *Faraday Discuss.* **2014,** *171* (0),259-273.
19. Krzystek, J.; Ozarowski, A.; Zvyagin, S. A.; Telser, J., *Inorg. Chem.* **2012,** *51* (9),4954-64.
20. Laga, S. M.; Blakemore, J. D.; Henling, L. M.; Brunschwig, B. S.; Gray, H. B., *Inorg. Chem.* **2014,** *53* (24),12668-12670.
21. Valdez, C. N.; Dempsey, J. L.; Brunschwig, B. S.; Winkler, J. R.; Gray, H. B., *Proc. Natl. Acad. Sci. USA* **2012,** *109* (39),15589–15593.
22. Cropek, D. M.; Metz, A.; Muller, A. M.; Gray, H. B.; Horne, T.; Horton, D. C.; Poluektov, O.; Tiede, D. M.; Weber, R. T.; Jarrett, W. L.; Phillips, J. D.; Holder, A. A., *Dalton Trans.* **2012,** *41* (42),13060-73.
23. Fihri, A.; Artero, V.; Pereira, A.; Fontecave, M., *Dalton Trans.* **2008,** (41),5567-5569.
24. Pal, U.; Ghosh, S.; Chatterjee, D., *Transition Met. Chem.* **2012,** *37* (1),93-96.
25. Bacchi, M.; Berggren, G.; Niklas, J.; Veinberg, E.; Mara, M. W.; Shelby, M. L.; Poluektov, O. G.; Chen, L. X.; Tiede, D. M.; Cavazza, C.; Field, M. J.; Fontecave, M.; Artero, V., *Inorg. Chem.* **2014,** *53* (15),8071-8082.

26. Hu, X.; Brunschwig, B. S.; Peters, J. C., *J. Am. Chem. Soc.* **2007,** *129*,8988-8998.
27. McCrory, C. C. L.; Uyeda, C.; Peters, J. C., *J. Am. Chem. Soc.* **2012,** *134* (6),3164-3170.
28. Stubbert, B. D.; Peters, J. C.; Gray, H. B., *J. Am. Chem. Soc.* **2011,** *133* (45),18070-18073.
29. Zhang, P.; Wang, M.; Dong, J.; Li, X.; Wang, F.; Wu, L.; Sun, L., *J. Phys. Chem. C* **2010,** *114* (37),15868-15874.
30. Varma, S.; Castillo, C. E.; Stoll, T.; Fortage, J.; Blackman, A. G.; Molton, F.; Deronzier, A.; Collomb, M. N., *Phys. Chem. Chem. Phys.* **2013,** *15* (40),17544-52.
31. Pasto, D. J.; Timmers, D. A.; Huang, N. Z., *Inorg. Chem.* **1984,**
32. Creutz, C.; Schwarz, H. A.; Sutin, N., *J. Am. Chem. Soc.* **1984,** *106* (10),3036-3037.
33. Kahnt, A.; Peuntinger, K.; Dammann, C.; Drewello, T.; Hermann, R.; Naumov, S.; Abel, B.; Guldi, D. M., *J. Phys. Chem. A* **2014,** *118* (25),4382-4391.
34. Kawade, V. A.; Ghosh, S.; Sapre, A. V.; Kumbhar, A. S., *J. Chem. Sci.* **2010,** *122* (2),225-232.
35. Ducker-Benfer, C.; Hamza, M. S. A.; Eckhardt, C.; Van Eldik, R., *Eur. J. Inorg. Chem.* **2000,** (7),1563-1569.
36. Funston, A. M.; McFadyen, W. D.; Tregloan, P. A., *J. Chem. Soc. Dalton Trans.* **2002,** (9),2053-2060.
37. Kumar, M.; Natarajan, E.; Neta, P., *J. Phys. Chem.* **1994,** *98*,8024-8029.
38. Kawade, V. A.; Kumbhar, A. S.; Naik, D. B.; Butcher, R. J., *Dalton Trans.* **2010,** *39* (24),5664-5675.
39. Mulazzani, Q. G.; Emmi, S.; Fuochi, P. G.; Venturi, M.; Hoffman, M. Z.; Simic, M. G., *J. Phys. Chem.* **1979,** *83* (12),1582-1590.
40. Simic, M.; Ebert, M., *Int. J. Radiat. Phys. Chem.* **1971,** *3* (3),259-272.
41. Helm, L.; Merbach, A. E., *Chem. Rev.* **2005,** *105* (6),1923-1960.
42. Wang, K.; Jordan, R. B., *Inorg. Chem.* **1995,** *34* (22),5672-9.
43. Bakac, A.; Espenson, J. H., *J. Am. Chem. Soc.* **1984,** *106* (18),5197-5202.
44. Marinescu, S. C.; Winkler, J. R.; Gray, H. B., *Proc. Natl. Acad. Sci.* **2012,** *109* (38),15127-15131.
45. Wakerley, D. W.; Reisner, E., *Phys. Chem. Chem. Phys.* **2014,** *16* (12),5739-5746.
46. Royer, D. L.; Berner, R. A.; Park, J., *Nature* **2007,** *446* (7135),530-532.
47. Lewis, N. S.; Nocera, D. G., *Proc. Natl. Acad. Sci. U. S. A.* **2006,** *103* (43),15729-15735.
48. Armaroli, N.; Balzani, V., *Angew. Chem. Int. Ed.* **2007,** *46* (1+2),52-66.
49. Eisenberg, R.; Nocera, D. G., *Inorg. Chem.* **2005,** *44* (20),6799-6801.
50. Gray, H. B., *Nat. Chem.* **2009,** *1* (2),112.
51. Hoffert, M. I.; Caldeira, K.; Jain, A. K.; Haites, E. F.; Harvey, L. D. D.; Potter, S. D.; Schlesinger, M. E.; Schneider, S. H.; Watts, R. G.; Wigley, T. M. L.; Wuebbles, D. J., *Nature* **1998,** *395* (6705),881-884.
52. Lubitz, W.; Tumas, W., *Chem. Rev.* **2007,** *107* (10),3900-3903.
53. Service, R. F., *Science* **2005,** *309* (5734),548-551.
54. Kerr, R. A.; Service, R. F., *Science* **2005,** *309* (5731),101.
55. Dempsey, J. L.; Esswein, A. J.; Manke, D. R.; Rosenthal, J.; Soper, J. D.; Nocera, D. G., *Inorg. Chem.* **2005,** *44* (20),6879-6892.
56. Du, P.; Knowles, K.; Eisenberg, R., *J. Am. Chem. Soc.* **2008,** *130* (38),12576-12577.
57. Esswein, A. J.; Nocera, D. G., *Chem. Rev.* **2007,** *107* (10),4022-4047.

58. Gordon, M. A.; Zhang, W.; Lenz, H.-J., *Curr. Pharmacogenomics* **2006,** *4* (4),277-283.
59. Baykara, S. Z., *Int. J. Hydrogen Energy* **2005,** *30* (5),545-553.
60. http://www.eia.gov/renewable/annual/preliminary/
61. Karkas, M. D.; Johnston, E. V.; Verho, O.; Akermark, B., *Acc. Chem. Res.* **2014,** *47* (1),100-11.
62. Stewart, S.; Priore, R. J.; Nelson, M. P.; Treado, P. J., *Annu. Rev. Anal. Chem.* **2012,** *5*,337-360.
63. Gordon, K. C.; McGoverin, C. M., *Int. J. Pharm.* **2011,** *417* (1),151-162.
64. Juris, A.; Balzani, V.; Barigelletti, F.; Campagna, S.; Belser, P.; von Zelewsky, A., *Coord. Chem. Rev.* **1988,** *84* (0),85-277.
65. Amao, Y., *Kokagaku* **2008,** *39* (3),169-176.
66. Zeitler, K., *Angew. Chem., Int. Ed.* **2009,** *48* (52),9785-9789.
67. Stafford, N., *Chem. World* **2007,** *4* (2),14-15.
68. Xie, P.; Guo, F., *Curr. Org. Chem.* **2007,** *11* (14),1272-1286.
69. Adeloye, A. O.; Ajibade, P. A., *Molecules* **2014,** *19* (8),12421-12460, 40 pp.
70. Bozic-Weber, B.; Constable, E. C.; Housecroft, C. E., *Coord. Chem. Rev.* **2013,** *257* (21-22),3089-3106.
71. Giarikos, D. G. In *Artificial photosynthesis: ruthenium complexes*, John Wiley & Sons, Inc.: 2013; pp 143-171.
72. Higashino, T.; Imahori, H., *Dalton Trans.* **2015,** *44* (2),448-463.
73. Mishra, A.; Fischer, M. K. R.; Bäuerle, P., *Angew. Chem. Int. Ed.* **2009,** *48* (14),2474-2499.
74. O'regan, B.; Grfitzeli, M., *Nature* **1991,** *353*,737-740.
75. Nazeeruddin, M.; Kay, A.; Rodicio, I.; Humphry-Baker, R.; Mueller, E.; Liska, P.; Vlachopoulos, N.; Graetzel, M., *J. Am. Chem. Soc.* **1993**,6382–6390.
76. Grätzel, M., *Inorg. Chem.* **2005,** *44* (20),6841-6851.
77. Nath, N. C. D.; Kim, J. C.; Kim, K. P.; Yim, S.; Lee, J.-J., *J. Mater. Chem. A* **2013,** *1* (43),13439-13442.
78. Reisner, E.; Powell, D.; Cavazza, C.; Fontecilla-Camps, J.; Armstrong, F., *J. Am. Chem. Soc.* **2009,** *131* (51),18457-18466.
79. Kim, Y. G.; Mosurkal, R.; Li, L.; Walker, J.; He, J.; Samuelson, L. A.; Kumar, J., *J. Macromol. Sci., Part A* **2007,** *44* (12),1255-1260.
80. Ohlsson, J.; Wolpher, H.; Hagfeldt, A.; Grennberg, H., *J. Photochem. Photobiol., A* **2002,** *148* (1–3),41-48.
81. Shahroosvand, H.; Nasouti, F.; Sousaraei, A., *Dalton Trans.* **2014,** *43* (13),5158-5167.
82. Chen, K.-S.; Liu, W.-H.; Wang, Y.-H.; Lai, C.-H.; Chou, P.-T.; Lee, G.-H.; Chen, K.; Chen, H.-Y.; Chi, Y.; Tung, F.-C., *Adv. Funct. Mater.* **2007,** *17* (15),2964-2974.
83. Zadvornyy, O.; Lucon, J.; Gerlach, R.; Zorin, N.; Douglas, T.; Elgren, T.; Peters, J., *J. Inorg. Biochem.* **2012,** *106* (1),151-155.
84. Summers, P. A.; Dawson, J.; Ghiotto, F.; Hanson-Heine, M. W. D.; Vuong, K. Q.; Stephen Davies, E.; Sun, X.-Z.; Besley, N. A.; McMaster, J.; George, M. W.; Schroder, M., *Inorg. Chem.* **2014,** *53* (9),4430-4439.
85. Tennakone, K.; Kumara, G.; Kottegoda, I.; Wijayantha, K.; Perera, V., *J. Phys. D: Appl. Phys.* **1998**,1492–1496.
86. Neupane, L. N.; Han, S. Y.; Lee, K.-H., *Chem. Commun.* **2014,** *50* (44),5854-5857.

87. Argazzi, R.; Bignozzi, C. A.; Heimer, T. A.; Castellano, F. N.; Meyer, G. J., *J. Am. Chem. Soc.* **1995,** *117* (47),11815-11816.
88. Argazzi, R.; Bignozzi, C.; Heimer, T.; Castellano, F.; Meyer, G., *J. Phys. Chem. B* **1997**,2591–2597.
89. Humphry-Baker, R.; Grätzel, M.; Murrer, B., *Chem. Comm.* **1998**,719-720.
90. Baird, J. A.; Taylor, L. S., *Adv. Drug Delivery Rev.* **2012,** *64* (5),396-421.
91. Park, C.-W.; Rhee, Y.-S.; Vogt, F. G.; Hayes, D.; Zwischenberger, J. B.; DeLuca, P. P.; Mansour, H. M., *Adv. Drug Delivery Rev.* **2012,** *64* (4),344-356.
92. Brewster, T. P.; Konezny, S. J.; Sheehan, S. W.; Martini, L. A.; Schmuttenmaer, C. A.; Batista, V. S.; Crabtree, R. H., *Inorg. Chem.* **2013,** *52* (11),6752-64.
93. Chitra, S.; Somasundaram, N.; Easwaramoorthy, D., *Arch. Appl. Sci. Res.* **2013,** *5* (1),112-119.
94. Giribabu, L.; Kanaparthi, R. K., *Curr. Sci.* **2013,** *104* (7),847-855.
95. Gonzalez-Pedro, V.; Zarazua, I.; Barea, E. M.; Fabregat-Santiago, F.; de la Rosa, E.; Mora-Sero, I.; Gimenez, S., *J. Phys. Chem. C* **2014,** *118* (2),891-895.
96. Honda, M.; Yanagida, M.; Han, L., *AIP Adv.* **2013,** *3* (7),072113/1-072113/6.
97. Hou, Y.; Chen, Z. P.; Wang, D.; Zhang, B.; Yang, S.; Wang, H. F.; Hu, P.; Zhao, H. J.; Yang, H. G., *Small* **2014,** *10* (3),484-492.
98. Kim, Y.-H.; Lee, I.-K.; Song, Y.-S.; Lee, M.-H.; Kim, B.-Y.; Cho, N.-I.; Lee, D. Y., *Electron. Mater. Lett.* **2014,** *10* (2),445-449.
99. Kley, C. S.; Dette, C.; Rinke, G.; Patrick, C. E.; Cechal, J.; Jung, S. J.; Baur, M.; Duerr, M.; Rauschenbach, S.; Giustino, F.; Stepanow, S.; Kern, K., *Nano Lett.* **2014,** *14* (2),563-569.
100. Krysova, H.; Zukal, A.; Trckova-Barakova, J.; Chandiran, A. K.; Nazeeruddin, M. K.; Gratzel, M.; Kavan, L., *Chimia* **2013,** *67* (3),149-54.
101. Noh, Y.; Song, O., *Electron. Mater. Lett.* **2014,** *10* (1),263-266.
102. Noh, Y.; Song, O., *Electron. Mater. Lett.* **2014,** *10* (1),271-273.
103. Singh, V. K.; Kanaparthi, R. K.; Giribabu, L., *RSC Adv.* **2014,** *4* (14),6970-6984.
104. Tang, G.; Li, R.; Kou, S.; Tang, T.; Zhang, Y.; Wang, Y., *Opt. Spectrosc.* **2014,** *116* (2),263-273.
105. Campbell, W. M.; Jolley, K. W.; Wagner, P.; Wagner, K.; Walsh, P. J.; Gordon, K. C.; Schmidt-Mende, L.; Nazeeruddin, M. K.; Wang, Q.; Graetzel, M.; Officer, D. L., *J. Phys. Chem. C* **2007,** *111* (32),11760-11762.
106. Cao, W.-N.; Wang, F.; Wang, H.-Y.; Chen, B.; Feng, K.; Tung, C.-H.; Wu, L.-Z., *Chem. Comm.* **2012,** *48* (65),8081-3.
107. Fisher, J. R.; Cole-Hamilton, D. J., *Dalton Trans.* **1984,** (5),809-813.
108. Streich, D.; Astuti, Y.; Orlandi, M.; Schwartz, L.; Lomoth, R.; Hammarström, L.; Ott, S., *Chem. Eur. J.* **2010,** *16* (1),60-63.
109. Hammarström, L.; Styring, S., *Nature* **2009,** *1* (3),185-186.
110. Canaguier, S.; Vaccaro, L.; Artero, V.; Ostermann, R.; Pécaut, J.; Field, M. J.; Fontecave, M., *Chem.--Eur. J.* **2009,** *15* (37),9350-9364.
111. Vaccaro, L.; Artero, V.; Canaguier, S.; Fontecave, M.; Field, M. J., *Dalton Trans.* **2010,** *39* (12),3043-3049.
112. Zhou, R.; Sedai, B.; Manbeck, G. F.; Brewer, K. J., *Inorg. Chem.* **2013,** *52* (23),13314-13324.

113. White, T. A.; Whitaker, B. N.; Brewer, K. J., *J. Am. Chem. Soc.* **2011,** *133* (39),15332-15334.
114. Karnahl, M.; Kuhnt, C.; Heinemann, F. W.; Schmitt, M.; Rau, S.; Popp, J.; Dietzek, B., *Chem. Phys.* **2012,** *393* (1),65-73.
115. Rau, S.; Schäfer, B.; Gleich, D.; Anders, E.; Rudolph, M.; Friedrich, M.; Görls, H.; Henry, W.; Vos, J. G., *Angew. Chem. Int. Ed.* **2006,** *45* (37),6215-6218.
116. Tschierlei, S.; Presselt, M.; Kuhnt, C.; Yartsev, A.; Pascher, T.; Sundström, V.; Karnahl, M.; Schwalbe, M.; Schäfer, B.; Rau, S.; Schmitt, M.; Dietzek, B.; Popp, J., *Chem. Eur. J.* **2009,** *15* (31),7678-7688.
117. Singh Bindra, G.; Schulz, M.; Paul, A.; Soman, S.; Groarke, R.; Inglis, J.; Pryce, M. T.; Browne, W. R.; Rau, S.; Maclean, B. J.; Vos, J. G., *Dalton Trans.* **2011,** *40* (41),10812-10814.
118. Lei, P.; Hedlund, M.; Lomoth, R.; Rensmo, H.; Johansson, O.; Hammarstroem, L., *J. Am. Chem. Soc.* **2008,** *130* (1),26-27.
119. Ozawa, H.; Yokoyama, Y.; Haga, M.-a.; Sakai, K., *Dalton Trans.* **2007,** (12),1197-1206.
120. Ozawa, H.; Kobayashi, M.; Balan, B.; Masaoka, S.; Sakai, K., *Chem. - Asian J.* **2010,** *5* (8),1860-1869.
121. Knoll, J. D.; Higgins, S. L. H.; White, T. A.; Brewer, K. J., *Inorg. Chem.* **2013,** *52* (17),9749-9760.
122. Fihri, A.; Artero, V.; Razavet, M.; Baffert, C.; Leibl, W.; Fontecave, M., *Angew. Chem., Int. Ed.* **2008,** *47* (3),564-567.
123. Gordon, R. B.; Bertram, M.; Graedel, T. E., *Proc. Natl. Acad. Sci. USA* **2006,** *103* (5),1209-1214.
124. Elvington, M.; Brown, J.; Arachchige, S. M.; Brewer, K. J., *J. Am. Chem. Soc.* **2007,** *129* (35),10644-10645.
125. Fisher, J. R.; Cole-Hamilton, D. J., *J. Chem. Soc., Dalton Trans.* **1984,** (5),809-813.
126. Hawecker, J.; Lehn, J. M.; Ziessel, R., *Nouveau J. Chimie* **1983,** *7* (5),271-277.
127. Wang, M.; Na, Y.; Gorlov, M.; Sun, L., *Dalton Trans.* **2009,** (33),6458-6467.
128. Brown, G. M.; Brunschwig, B. S.; Creutz, C.; Endicott, J. F.; Sutin, N., *J. Am. Chem. Soc.* **1979,** *101* (5),1298-1300.
129. Krishnan, C. V.; Brunschwig, B. S.; Creutz, C.; Sutin, N., *J. Am. Chem. Soc.* **1985,** *107* (7),2005-15.
130. Krishnan, C. V.; Sutin, N., *J. Am. Chem. Soc.* **1981,** *103* (8),2141-2.
131. Huang, Z.; Luo, Z.; Geletii, Y. V.; Vickers, J. W.; Yin, Q.; Wu, D.; Hou, Y.; Ding, Y.; Song, J.; Musaev, D. G.; Hill, C. L.; Lian, T., *J. Am. Chem. Soc.* **2011,** *133* (7),2068-2071.
132. McCool, N. S.; Robinson, D. M.; Sheats, J. E.; Dismukes, G. C., *J. Am. Chem. Soc.* **2011,** *133* (30),11446-11449.
133. Reece, S. Y.; Hamel, J. A.; Sung, K.; Jarvi, T. D.; Esswein, A. J.; Pijpers, J. J. H.; Nocera, D. G., *Science* **2011,** *334* (6056),645-648.
134. Li, X.; Wang, M.; Zhang, S.; Pan, J.; Na, Y.; Liu, J.; Aakermark, B.; Sun, L., *J. Phys. Chem. B* **2008,** *112* (27),8198-8202.
135. Na, Y.; Pan, J.; Wang, M.; Sun, L., *Inorg. Chem.* **2007,** *46* (10),3813-3815.
136. Na, Y.; Wang, M.; Pan, J.; Zhang, P.; Akermark, B.; Sun, L., *Inorg. Chem.* **2008,** *47* (7),2805-2810.

137. Barton, B. E.; Olsen, M. T.; Rauchfuss, T. B., *Curr. Opin. Biotechnol.* **2010,** *21* (3),292-297.
138. Baffert, C.; Artero, V.; Fontecave, M., *Inorg. Chem.* **2007,** *46* (5),1817-1824.
139. Connolly, P.; Espenson, J. H., *Inorg. Chem.* **1986,** *25* (16),2684-2688.
140. Dempsey, J. L.; Winkler, J. R.; Gray, H. B., *J. Am. Chem. Soc.* **2010,** *132* (47),16774-16776.
141. Dempsey, J. L.; Winkler, J. R.; Gray, H. B., *J. Am. Chem. Soc.* **2010,** *132* (3),1060-1065.
142. Gong, L.; Wang, J.; Li, H.; Wang, L.; Zhao, J.; Zhu, Z., *Catal. Commun.* **2011,** *12* (12),1099-1103.
143. Hu, X.; Cossairt, B. M.; Brunschwig, B. S.; Lewis, N. S.; Peters, J. C., *Chem. Commun.* **2005,** (37),4723-4725.
144. Hu, X. L.; Brunschwig, B. S.; Peters, J. C., *J. Am. Chem. Soc.* **2007,** *129* (29),8988-8998.
145. Losse, S.; Vos, J. G.; Rau, S., *Coord. Chem. Rev.* **2010,** *254* (21-22),2492-2504.
146. Pantani, O.; Anxolabehere-Mallart, E.; Aukauloo, A.; Millet, P., *Electrochem. Commun.* **2006,** *9* (1),54-58.
147. Probst, B.; Kolano, C.; Hamm, P.; Alberto, R., *Inorg. Chem.* **2009,** *48* (5),1836-1843.
148. Razavet, M.; Artero, V.; Fontecave, M., *Inorg. Chem.* **2005,** *44* (13),4786-4795.
149. Zhang, P.; Wang, M.; Li, C.; Li, X.; Dong, J.; Sun, L., *Chem. Commun.* **2010,** *46* (46),8806-8808.
150. Muckerman, J. T.; Fujita, E., *Chem. Commun.* **2011,** *47* (46),12456-12458.
151. Li, C.; Wang, M.; Pan, J.; Zhang, P.; Zhang, R.; Sun, L., *J. Organomet. Chem.* **2009,** *694* (17),2814-2819.
152. Cropek, D. M.; Metz, A.; Mueller, A. M.; Gray, H. B.; Horne, T.; Horton, D. C.; Poluektov, O.; Tiede, D. M.; Weber, R. T.; Jarrett, W. L.; Phillips, J. D.; Holder, A. A., *Dalton Trans.* **2012,** *41* (42),13060-13073.
153. Lakadamyali, F.; Reisner, E., *Chem. Commun.* **2011,** *47* (6),1695-1697.
154. Artero, V.; Fontecave, M., *C. R. Chim.* **2011,** *14* (9),799-810.
155. Cropek, D. M.; Metz, A.; Muller, A. M.; Gray, H. B.; Horne, T.; Horton, D. C.; Poluektov, O.; Tiede, D. M.; Weber, R. T.; Jarrett, W. L.; Phillips, J. D.; Holder, A. A., *Dalton Trans.* **2012,** *41* (42),13060-13073.
156. Holder, A. A.; Dasgupta, T. P., *Inorg. Chim. Acta* **2002,** *331* (1),279-289.
157. Holder, A. A.; Dasgupta, T. P.; Im, S.-C., *Transition Met. Chem.* **1997,** *22* (2),135-140.
158. Holder, A. A.; Dasgupta, T. P., *J. Chem. Soc. Dalton Trans.* **1996,** (13),2637-2643.
159. Holder, A. A.; Dasgupta, T. P.; McFarlane, W.; Rees, N. H.; Enemark, J. H.; Pacheco, A.; Christensen, K., *Inorg. Chim. Acta* **1997,** *260* (2),225-228.
160. Moody, L. M.; Balof, S.; Smith, S.; Rambaran, V. H.; VanDerveer, D.; Holder, A. A., *Acta Crystallogr. Sect. E: Struct. Rep. Online* **2008,** *E64*,m262-m263.
161. Rambaran, V. H.; Erves, T. R.; Grover, K.; Balof, S.; Moody, L. V.; Ramsdale, S. E.; Seymour, L. A.; VanDerveer, D.; Cropek, D. M.; Weber, R. T.; Holder, A. A., *J. Chem. Crystallogr.* **2013,** *43* (10),509-516.
162. Yuan, H.; Newton, D. A. L.; Seymour, L. A.; Metz, A.; Cropek, D.; Holder, A. A.; Ofoli, R. Y., *Catal. Commun.* **2014,** *56*,76-80.
163. Varey, J. E.; Lamprecht, G. J.; Fedin, V. P.; Holder, A.; Clegg, W.; Elsegood, M. R. J.; Sykes, A. G., *Inorg. Chem.* **1996,** *35* (19),5525-5530.

164. Holder, A. A.; Brown, R. F. G.; Marshall, S. C.; Payne, V. C. R.; Cozier, M. D.; Alleyne, W. A.; Bovell, C. O., *Transition Met. Chem.* **2000,** *25* (5),605-611.
165. *http://chemnmr.colorado.edu/manuals/19F_NMR_Reference_Standards.pdf*
166. Samy, N. A.; Alexander, V., *Dalton Trans.* **2011,** *40* (34),8630-8642.
167. Yamazaki, N.; Hohokabe, Y., *Bull. Chem. Soc. Jpn.* **1971,** *44*,63-69.
168. Vilakazi, S. L.; Nyokong, T., *Polyhedron* **1998,** *17* (25–26),4415-4423.
169. Nonaka, Y.; Hamada, K., *Bull. Chem. Soc. Jpn.* **1981,** *54* (10),3185-3190.
170. Rockenbauer, A.; Budo-Zahonyi, E.; Simandi, L. I., *J. Chem. Soc., Dalton Trans.* **1975,** (18),1729-1737.
171. Green, K.-A.; Maragh, P. T.; Abdur-Rashid, K.; Lough, A. J.; Dasgupta, T. P., *Eur. J. Inorg. Chem.* **2014,** *2014* (22),3600-3607.
172. Larrosa, I.; Somoza, C.; Banquy, A.; Goldup, S. M., *Org. Lett.* **2011,** *13* (1),146-149.
173. Organ, M. G.; Abdel-Hadi, M.; Avola, S.; Hadei, N.; Nasielski, J.; O'Brien C, J.; Valente, C., *Chem. Eur. J.* **2007,** *13* (1),150-157.
174. Valente, C.; Belowich, M. E.; Hadei, N.; Organ, M. G., *Eur. J. Org. Chem.* **2010**,4343–4354.
175. Pantani, O.; Anxolabéhère-Mallart, E.; Aukauloo, A.; Millet, P., *Electrochem. Commun.* **2007,** *9* (1),54-58.
176. Du, P.; Schneider, J.; Luo, G.; Brennessel, W. W.; Eisenberg, R., *Inorg. Chem.* **2009,** *48* (11),4952-4962.
177. Shi, S.; Daniels, L. M.; Espenson, J. H., *Inorg. Chem.* **1991,** *30* (18),3407-3410.
178. von Philipsborn, W., *Chem. Soc. Rev.* **1999,** *28* (2),95-105.
179. Bobbio, C.; Rausis, T.; Schlosser, M., *Chem. Eur. J.* **2005,** *11* (6),1903-1910.
180. Coe, P. L.; Holton, A. G.; Tatlow, J. C., *J. Fluorine Chem.* **1982,** *21* (2),171-189.
181. Sun, H.; DiMagno, S. G., *JACS* **2005,** *127* (7),2050-2051.
182. *CRC Handbook of Chemistry and Physics*. 82 ed.; CRC Press LLC: 2001.

APPENDIX

A1. Abbreviations

BL = bridging ligand

bpy-4-CH_3,4′-CONH(4-py) = 4-methyl-*N*-4′-pyridinyl[2,2'-bipyridine]-4-carboxamide-κN^1,κ$N^{1'}$

COD = 1,5-cyclooctadiene

Cp^- = cyclopentadienyl

DMF = N,N-dimethylformamide

dmgBF_2 = difluoroboryldimethylglyoximato

dpp = 2,3-bis(2-pyridyl)pyrazine

dpq = 2,3-bis(2-pyridyl)quinoxaline

$EDTA^{4-}$ = ethylenediaminetetraacetic acid

H_2ase = hydrogenase

HEC = hydrogen evolution catalyst

L-pyr = (4-pyridine)oxazolo[4,5-*f*]phenanthroline

Me_2bpy = 4,4'-dimethyl-2,2'-bipyridine

mes-1,4(phO-Izphen)$_3$ = 2,4,6-trimethyl-1,3,5-tris(4-oxymethyl-1-yl(1H-imidazo-2yl-[4,5-f][1,10]phenanthroline)phenyl)benzene

MLCT = metal-to-ligand-charge-transfer

N3 = [*cis*-di(thiocyanato)bis(2,2'-bipyridyl-4,4'-dicarboxylate)ruthenium(II)]

NPh_2 = diphenylamido

Ph_2phen = 4,7-diphenyl-1,10-phenanthroline

pbt = 2-(2-pyridinyl)benzothiazole

PCy_3 = tricyclohexylphosphine

pdt = propyldithiolate

pmcbpy = 4,4’-bis(N-(4-pyridyl)methylcarbamoyl)-2,2’-bipyridine

PPh_3 = triphenylphosphine

saloph = N,N’-disalicylidene-o-phenylenediaminate

tbbpy = 4,4'-bis(*tert*-butyl)-2,2'-bipyridine

TC-4,4 = tropocoronand

tempo = 2,2,6,6-tetramethylpiperidine-N-oxide

TEOA = triethanolamine

TOF = turnover frequency

TON = turnover numbers

tpac = tetrapyrido[3,2-a:2',3'-c:3",2"-h:2"',3"'-j]acridine

tpphz = tetrapyrido[3,2-a:2',3'-c:3",2"-h:2"',3"'-j] phenazine

A2. Characterization of $[Co(dmgBF_2)_2(H_2O)_2]$ and $[Co(dmgBF_2)_2(H_2O)(py)]\bullet 0.5(CH_3)_2CO$

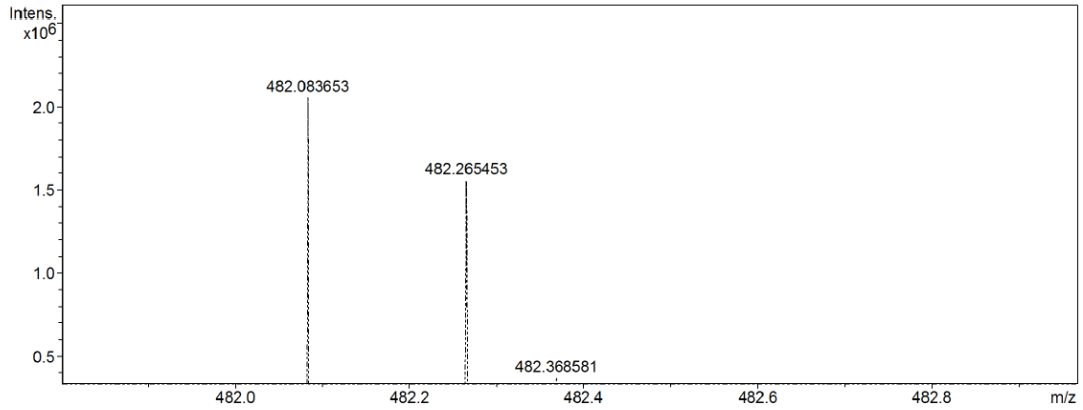

Figure A 1. HRMS of $[Co(dmgBF_2)_2(H_2O)(py)]^+$ in dichloromethane:methanol (1:1, v/v).

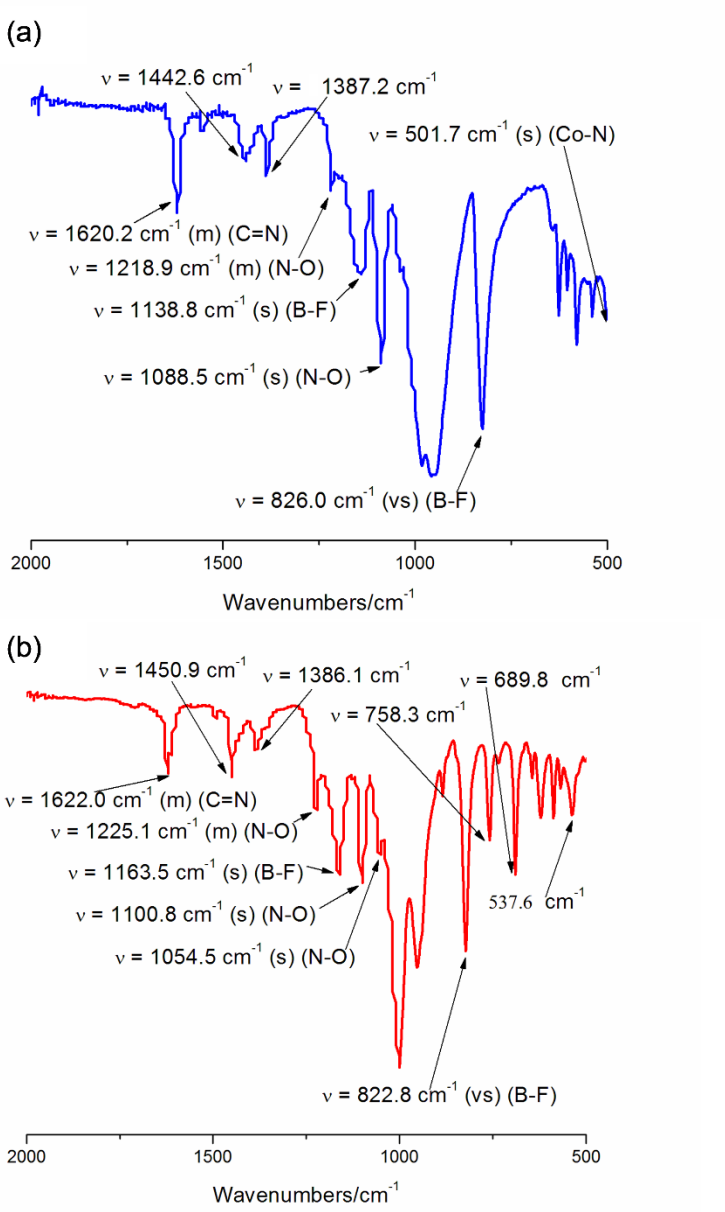

Figure A 2. Assignment of selected FTIR bands of (a) $[Co(dmgBF_2)_2(H_2O)_2]$ and (b) $[Co(dmgBF_2)_2(H_2O)(py)]\bullet 0.5(CH_3)_2CO$.

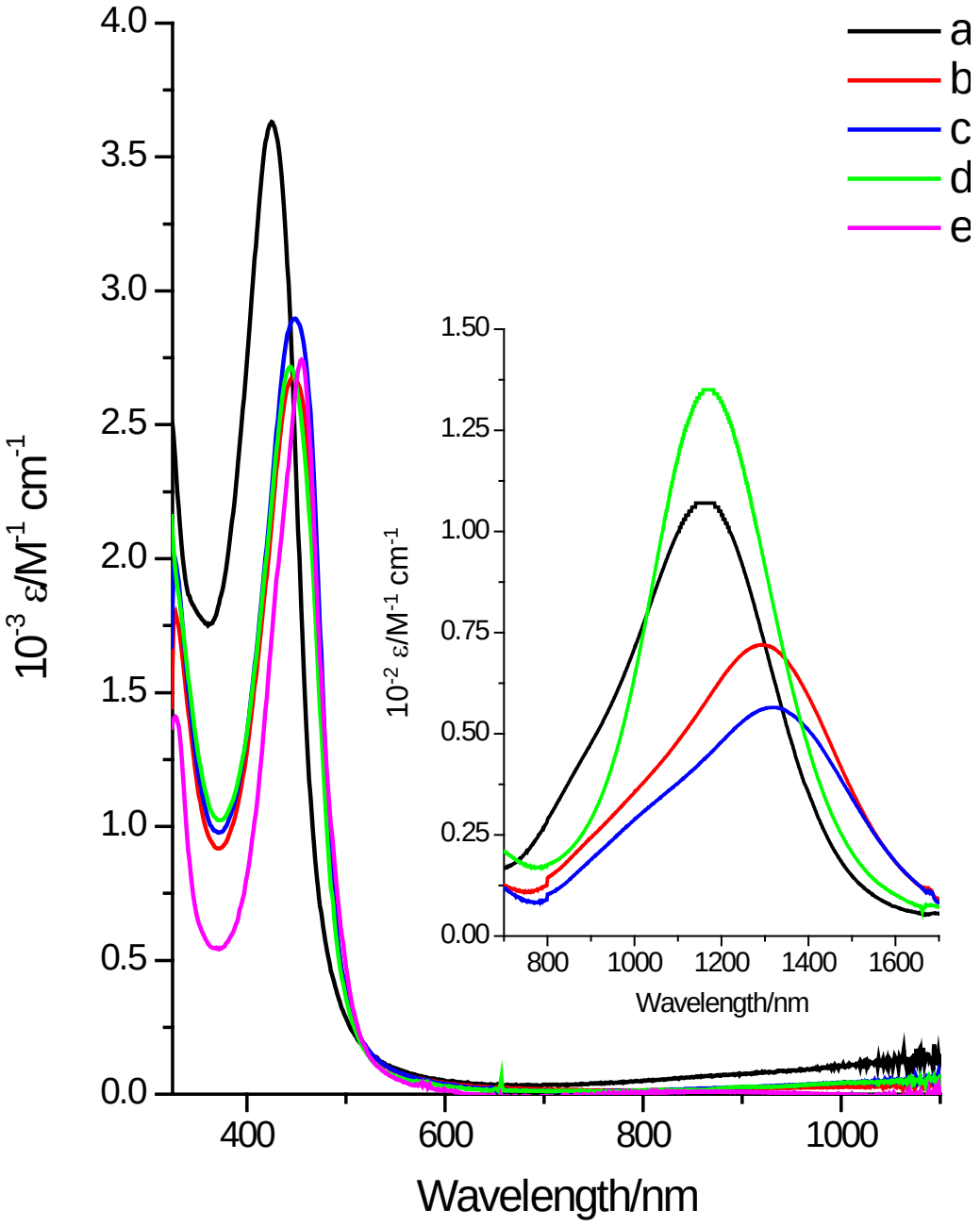

Figure A 3. A plot of the molar extinction coefficient versus wavelength of complex 1. Solvent = acetonitrile (a), acetone (b), 2-butanone (c), 1,2-difluorobenzene/acetone (4:1, v/v) (d), and water (e). NIR spectrum shown in inset.

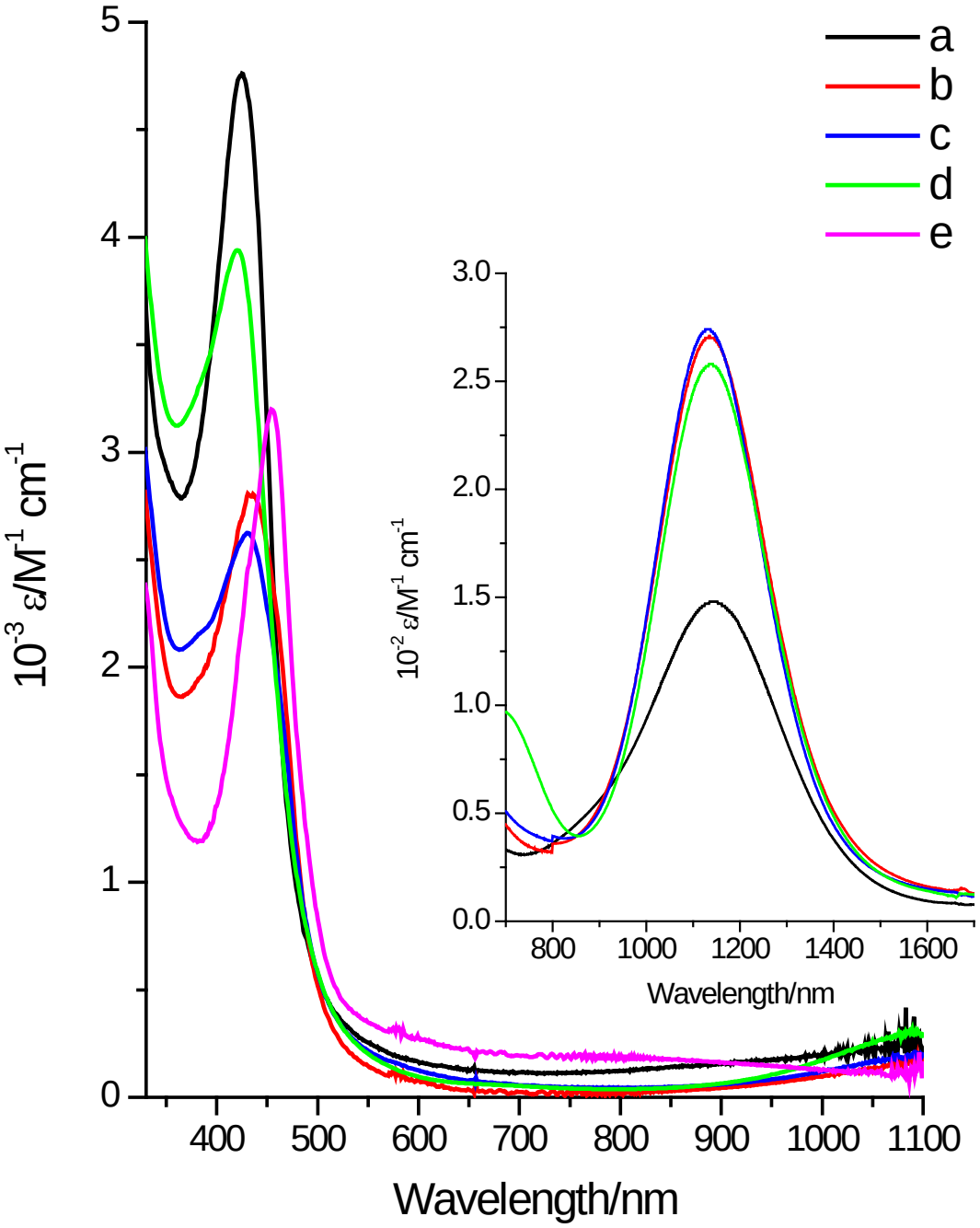

Figure A 4. A plot of the molar extinction coefficient versus wavelength of $[Co(dmgBF_2)_2(H_2O)(py)]\bullet 0.5(CH_3)_2CO$. Solvent = acetonitrile (a), acetone (b), 2-butanone (c), 1,2-difluorobenzene/acetone (4:1, v/v) (d), and water (e), NIR shown in inset.

A3. Mole ratio plots and equilibria

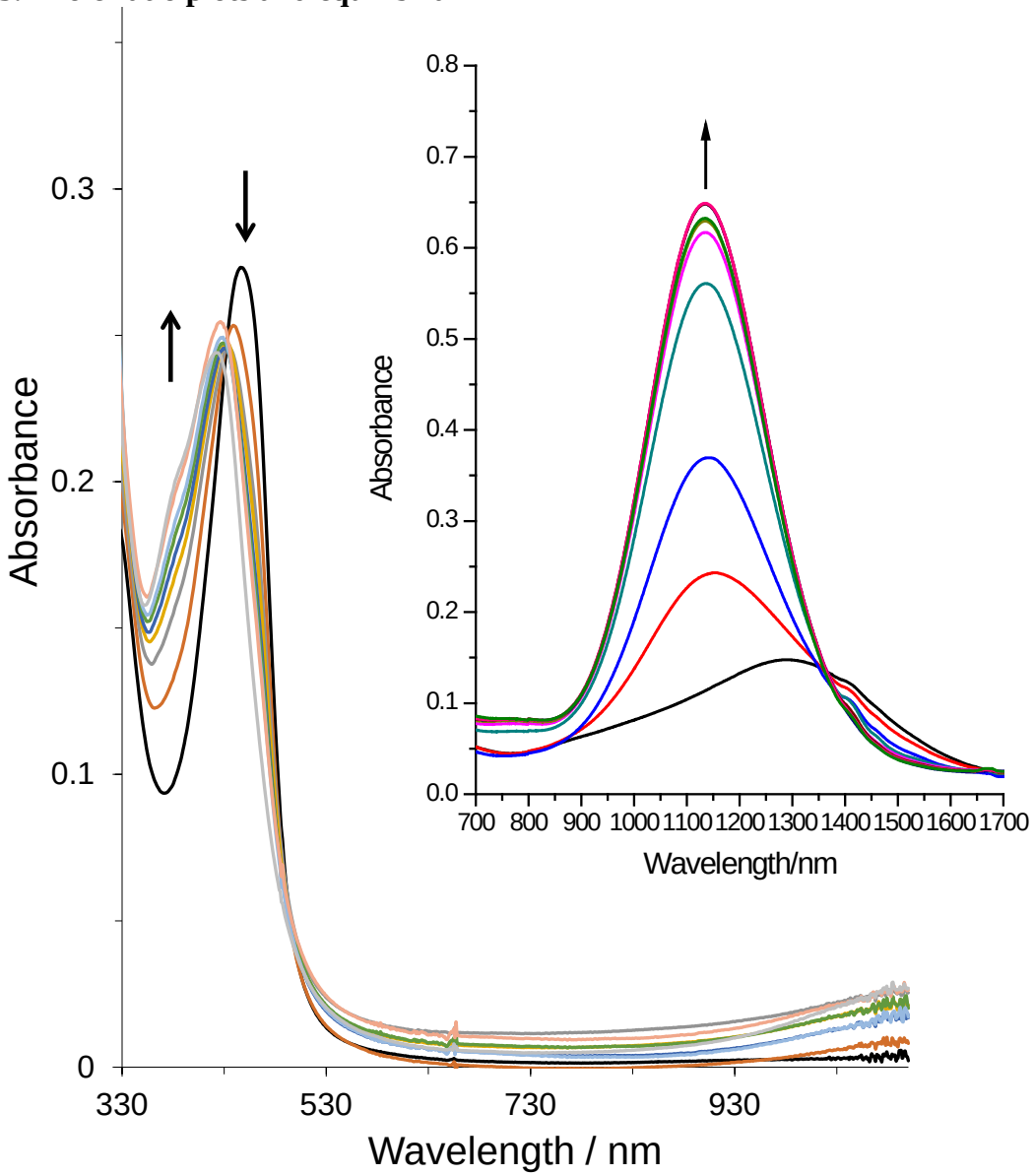

Figure A 5. The effect of pyridine addition to $[Co(dmgBF_2)_2(H_2O)_2]$ in the UV-visible spectrum (NIR shown in inset) in acetone. [complex] = 0.1 mM (2.0 mM fo NIR measurements) and 0.0 mM ≥ [pyridine] ≥ 0.5 mM (0.0 mM ≥ [pyridine] ≥ 4.0 mM for NIR measurements), path length = 1.0 cm.

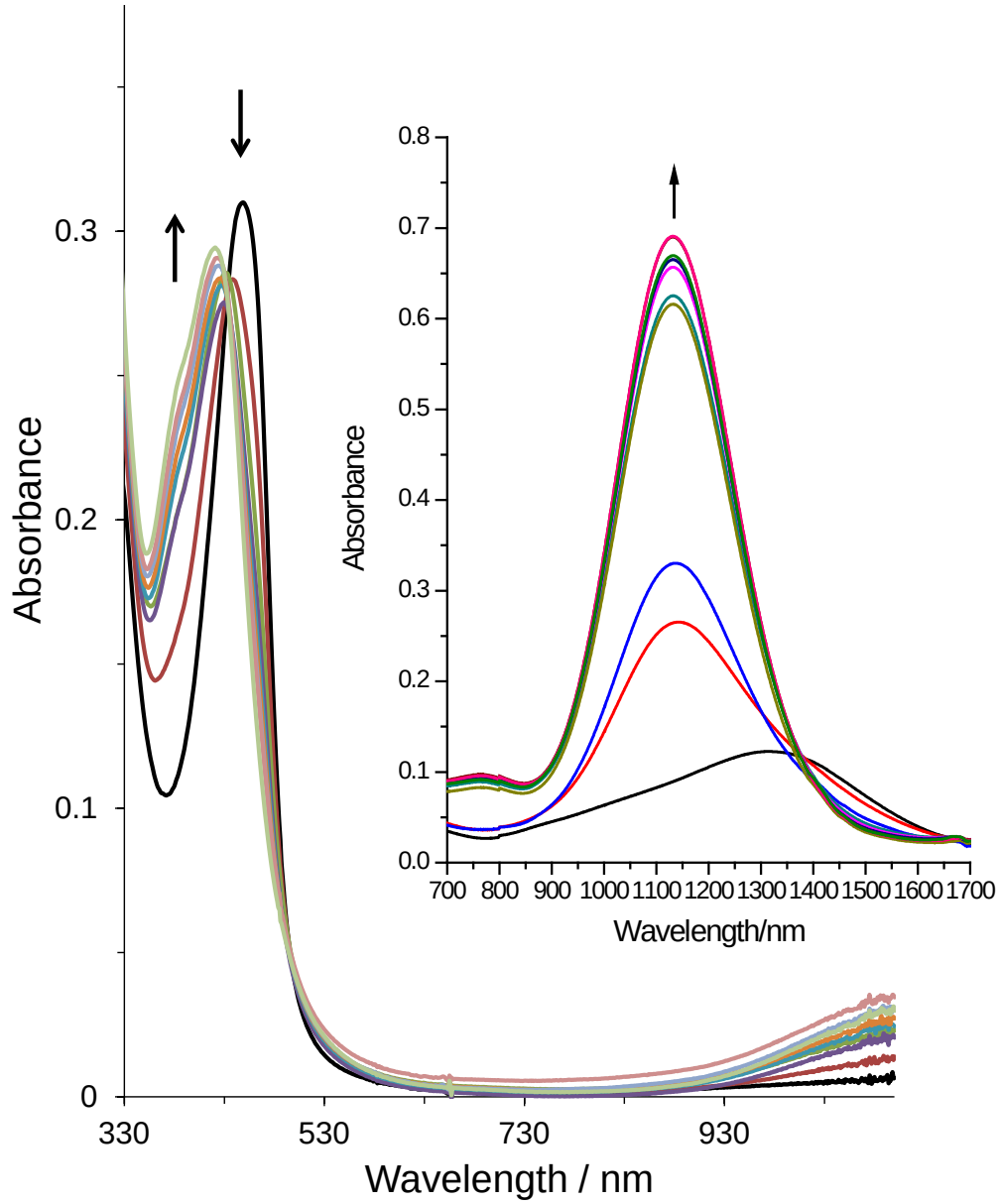

Figure A 6. The effect of pyridine addition to $[Co(dmgBF_2)_2(H_2O)_2]$ in the UV-visible spectrum (NIR shown in inset) in 2-butanone. [complex] = 0.1 mM (2.0 mM fo NIR measurements) and 0.0 mM ≥ [pyridine] ≥ 0.5 mM (0.0 mM ≥ [pyridine] ≥ 4.0 mM for NIR measurements), path length = 1.0 cm.

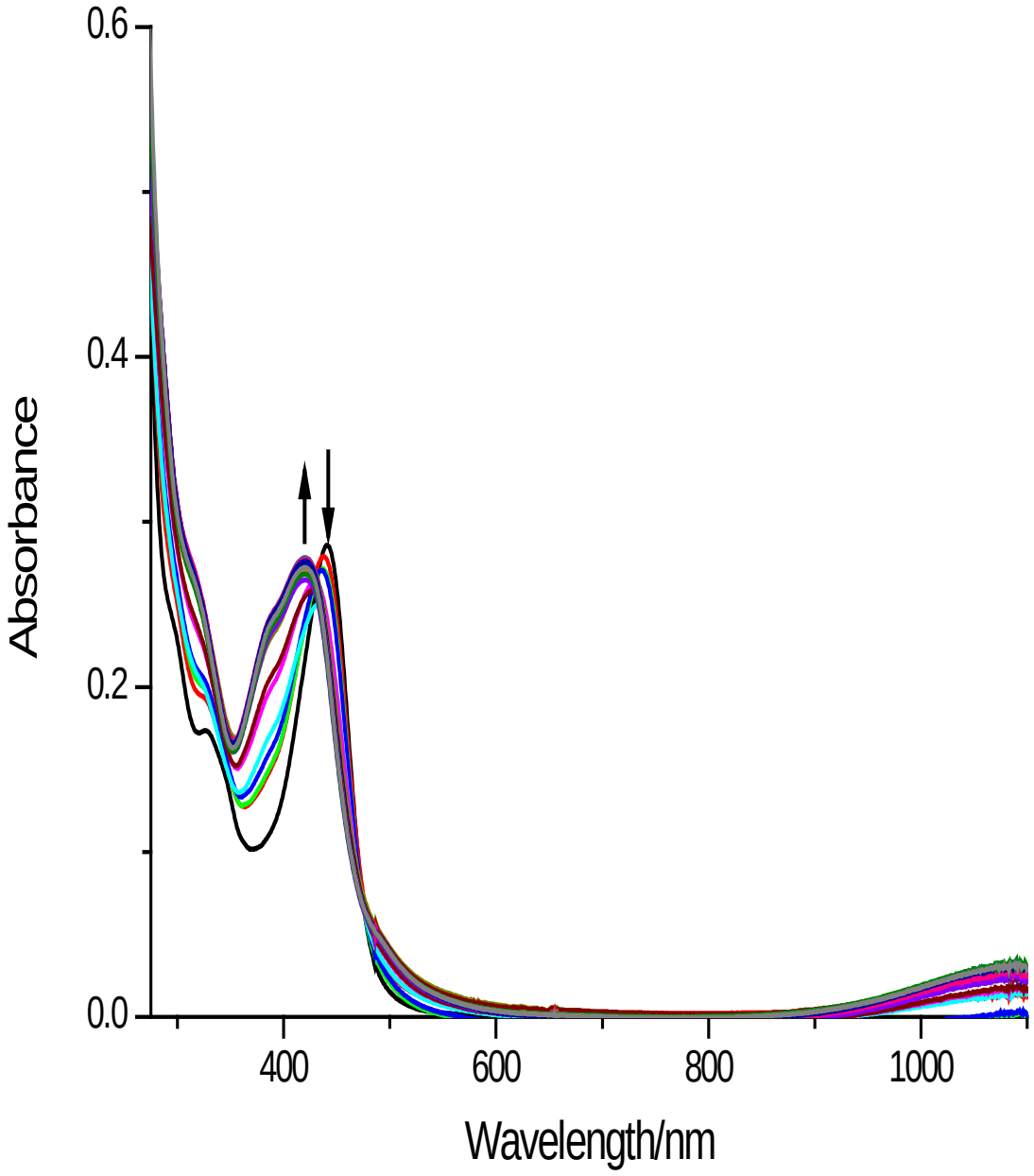

Figure A 7. A plot of absorbance vs wavelength for a titration of $[Co(dmgBF_2)_2(H_2O)_2]$ with pyridine in dichloromethane at 20 °C. [Complex] = 0.10 mM, path length = 1.0 cm.

Table A 1. Absorbance values at 1162 nm, log $[(A_o-A)/(A-A_\infty)]$ and log [pyridine] for $[Co(dmgBF_2)_2(H_2O)_2]$ in acetonitrile at 20 °C. [complex] = 2.0 mM, path length = 1.0 cm.

[py]/[complex]	$Abs_{1162\ nm}$	log [pyridine]	log $[(A_o-A)/(A-A_\infty)]$
0	0.2474	--	---
0.25	0.2892	-3.572	-0.8823
0.33	0.3059	-3.474	-0.7130
0.40	0.3222	-3.414	-0.5821
0.50	0.3344	-3.286	-0.4977
0.65	0.36315	-3.182	-0.3254
0.75	0.3720	-3.092	-0.2774
0.87	0.3895	-3.021	-0.1870
1.0	0.4062	-2.951	-0.1040
1.12	0.4255	-2.902	-0.0107
1.50	0.4645	-2.746	0.1800
1.75	0.4845	-2.661	0.2831
2.0	0.4949	-2.580	0.3401
2.25	0.5103	-2.517	0.4301
2.75	0.5131	-2.395	0.4473
3.0	0.5258	-2.351	0.5295
4.0	0.5495	-2.199	0.7126
5.0	0.5562	-2.082	0.7756

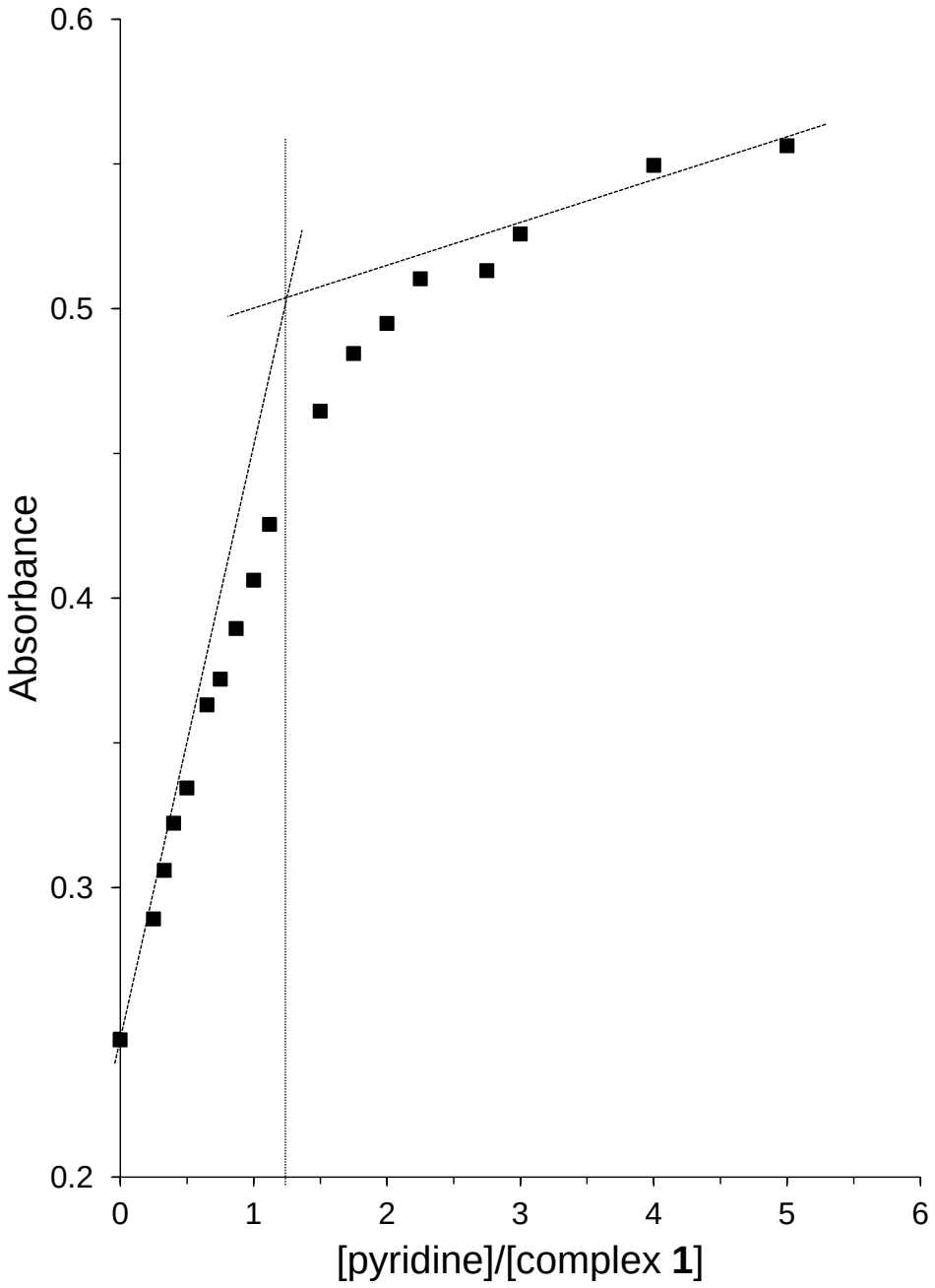

Figure A 8. Mole ratio plot for the interaction of pyridine with $[Co(dmgBF_2)_2(H_2O)_2]$ in acetonitrile. [complex] = 2.0 mM, λ = 1162 nm, T = 20 ^{o}C, path length = 1.0 cm.

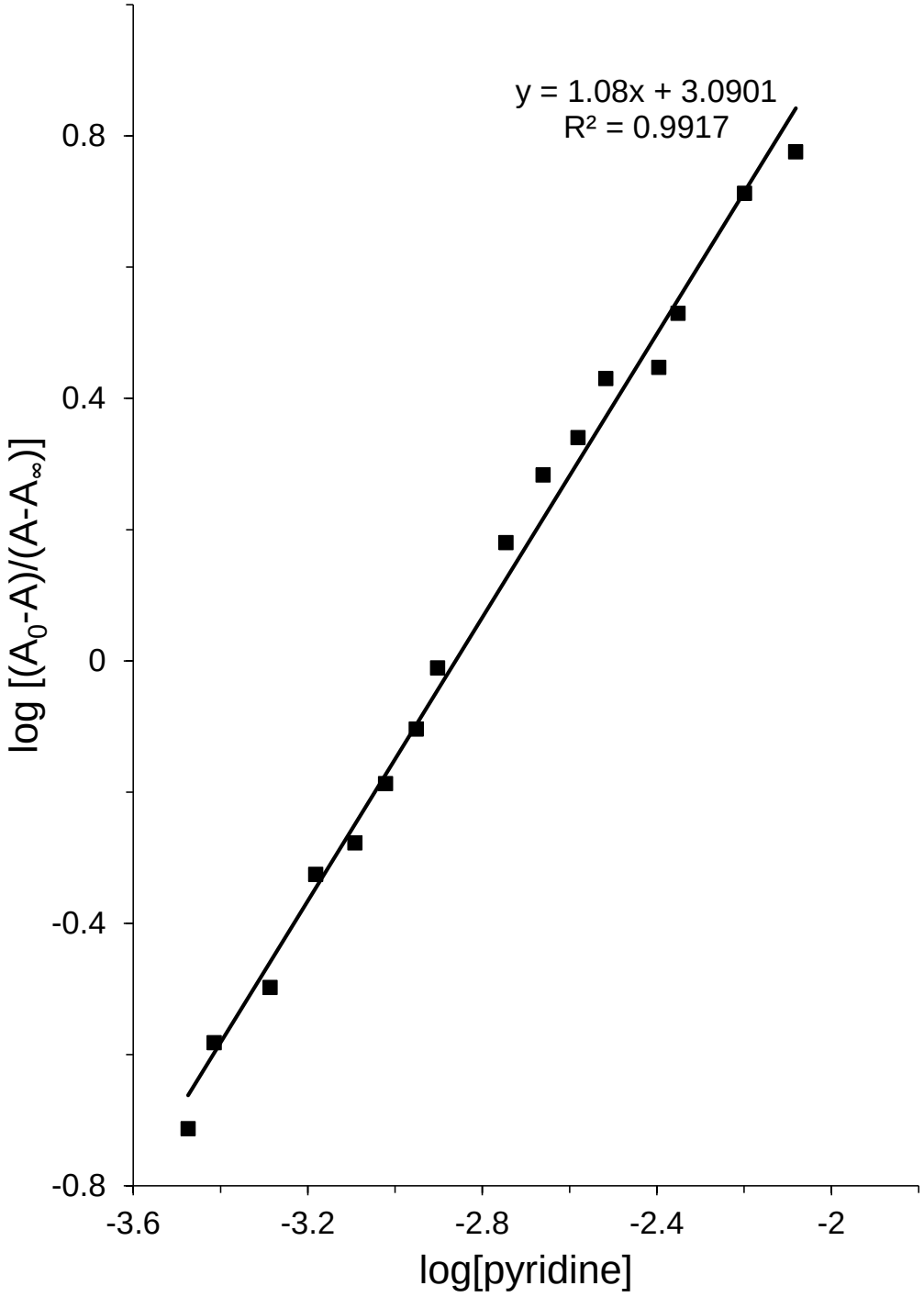

Figure A 9. A plot of log $[(A_o\text{-}A)/(A\text{-}A_\infty)]$ vs log [pyridine] for $[Co(dmgBF_2)_2(H_2O)_2]$ at 1162 nm in acetonitrile at 20 ^oC.

Table A 2. Absorbance values at 372 nm, log [$(A_o-A)/(A-A_\infty)$] and log [pyridine] for $[Co(dmgBF_2)_2(H_2O)_2]$ in acetone at 20 ^oC. [complex] = 0.10 mM, path length = 1.0 cm.

[py]/[complex]	$Abs_{372\ nm}$	log $[(A_o-A)/(A-A_\infty)]$	log [pyridine]
0	0.0922	---	---
0.50	0.1265	-0.2309	-4.886
0.87	0.1444	0.1099	-4.513
1.0	0.1497	0.2128	-4.420
1.25	0.1590	0.4103	-4.276
1.50	0.1618	0.4763	-4.125
1.75	0.1696	0.7018	-4.038
2.0	0.1724	0.8020	-3.945
4.0	0.1796	1.206	-3.514

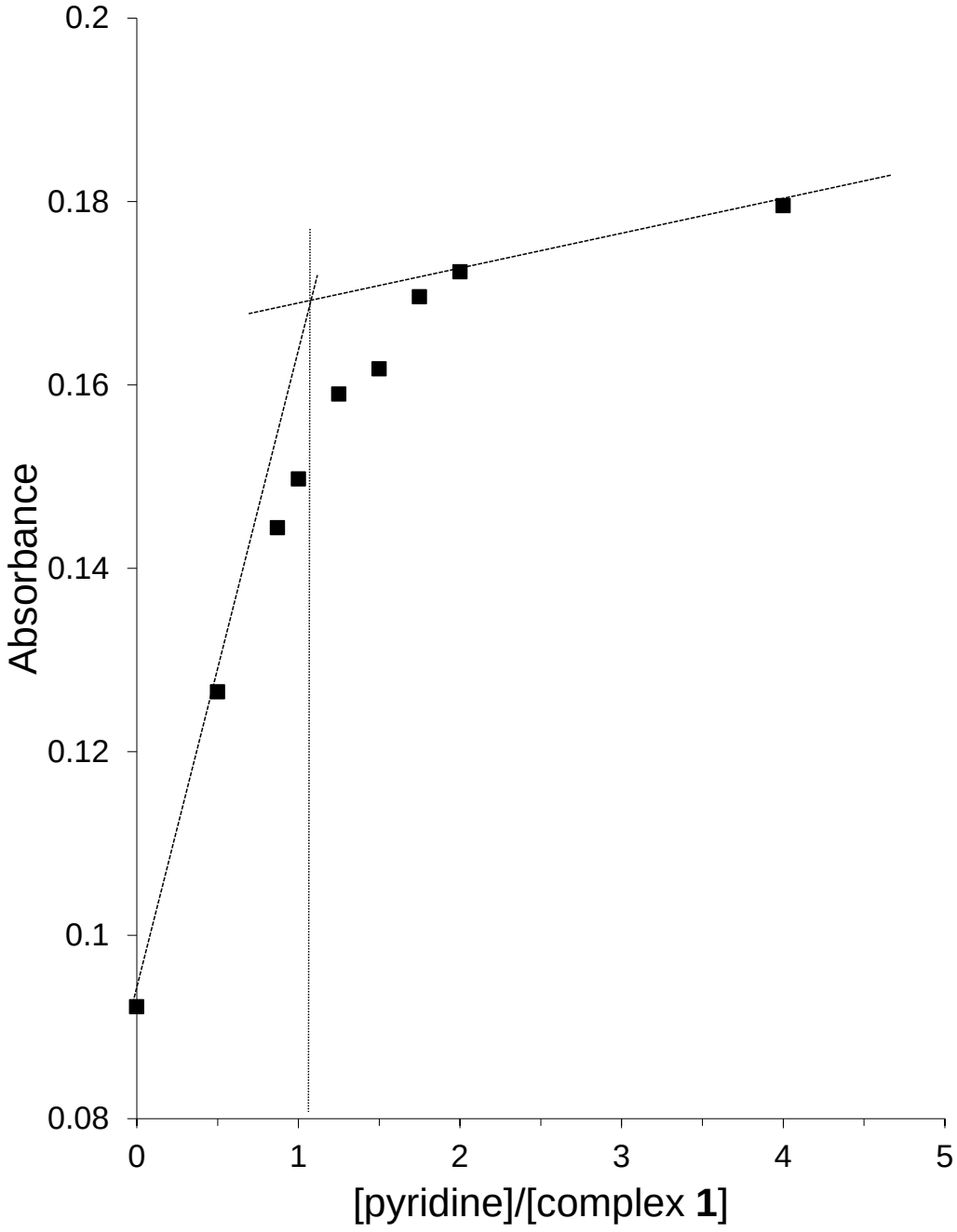

Figure A 10. Mole ratio plot for the interaction of pyridine with $[Co(dmgBF_2)_2(H_2O)_2]$ in acetone. [complex] = 0.10 mM, λ = 372 nm, T = 20 ^{o}C, path length = 1.0 cm.

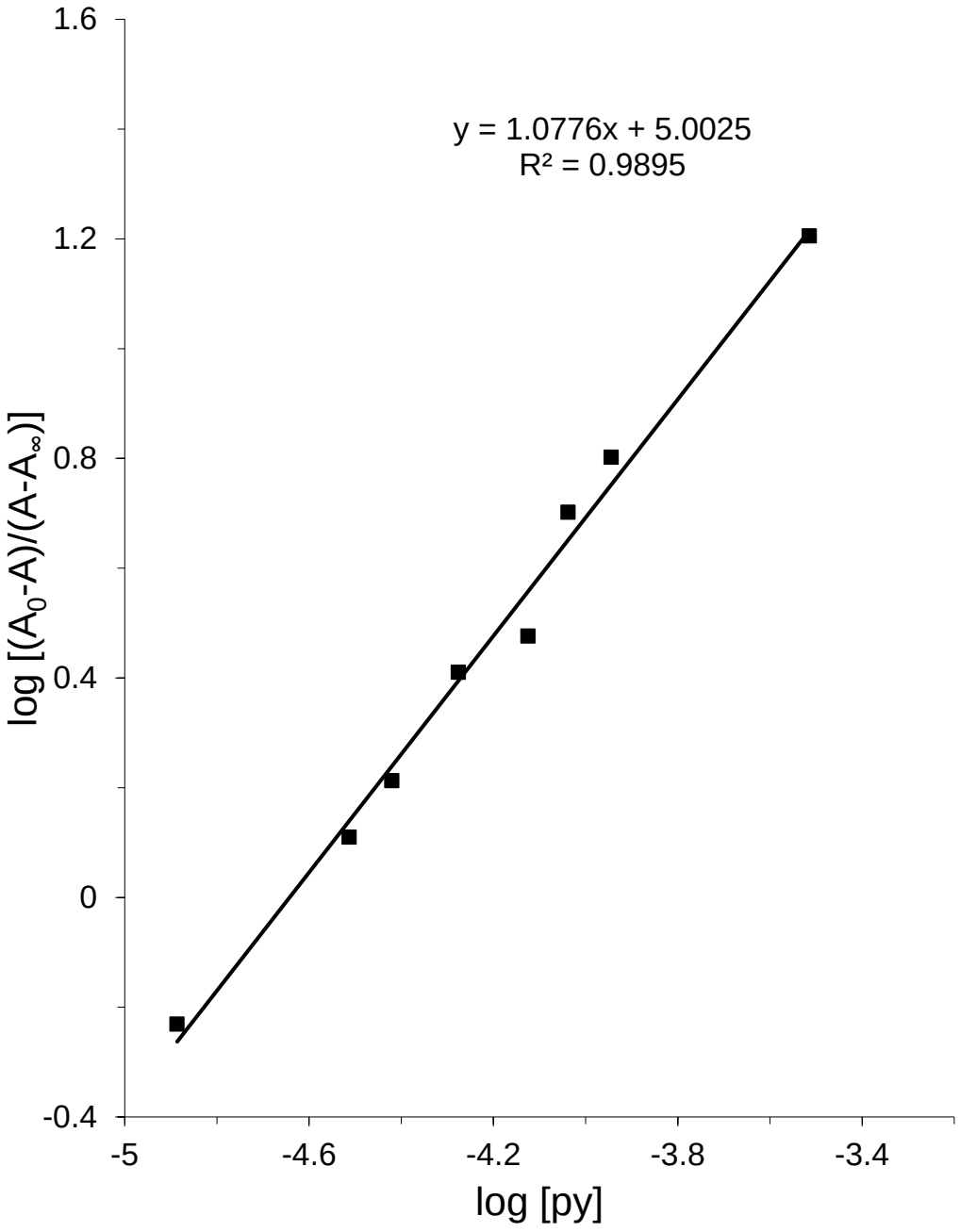

Figure A 11. A plot of log $[(A_o\text{-}A)/(A\text{-}A_\infty)]$ vs log [pyridine] for $[Co(dmgBF_2)_2(H_2O)_2]$ at 371 nm in acetone at 20 ^oC.

Table A 3. Absorbance values at 372 nm, log $[(A_o-A)/(A-A_\infty)]$ and log [pyridine] for $[Co(dmgBF_2)_2(H_2O)_2]$ in 2-butanone at 20 °C. [complex 1] = 0.10 mM, path length = 1.0 cm.

[py]/[complex]	$Abs_{372\ nm}$	log $[(A_o-A)/(A-A_\infty)]$	log [pyridine]
0	0.1045	---	---
0.50	0.1498	-4.857	-0.2480
1.0	0.1847	-4.442	0.2479
1.25	0.1973	-4.292	0.4529
1.50	0.2035	-4.148	0.5716
1.75	0.2105	-4.043	0.7357
2.0	0.2150	-3.951	0.8664
4.0	0.2244	-3.516	1.330

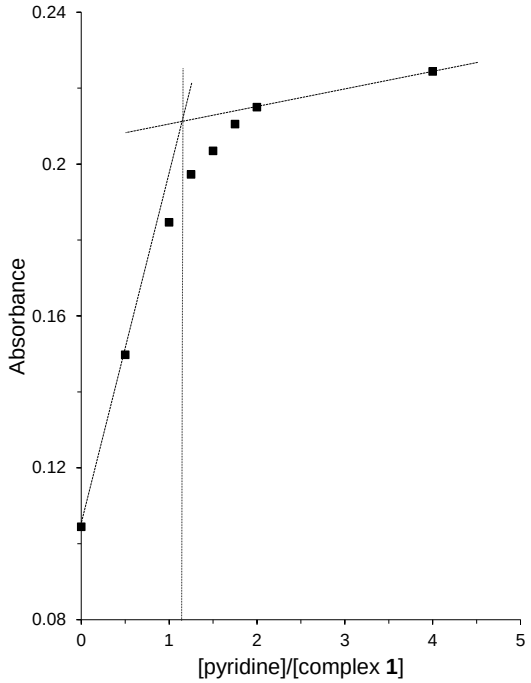

Figure A 12. Mole ratio plot for the interaction of pyridine with $[Co(dmgBF_2)_2(H_2O)_2]$ in 2-butanone. [complex] = 0.10 mM, λ = 372 nm, T = 20 °C, path length = 1.0 cm.

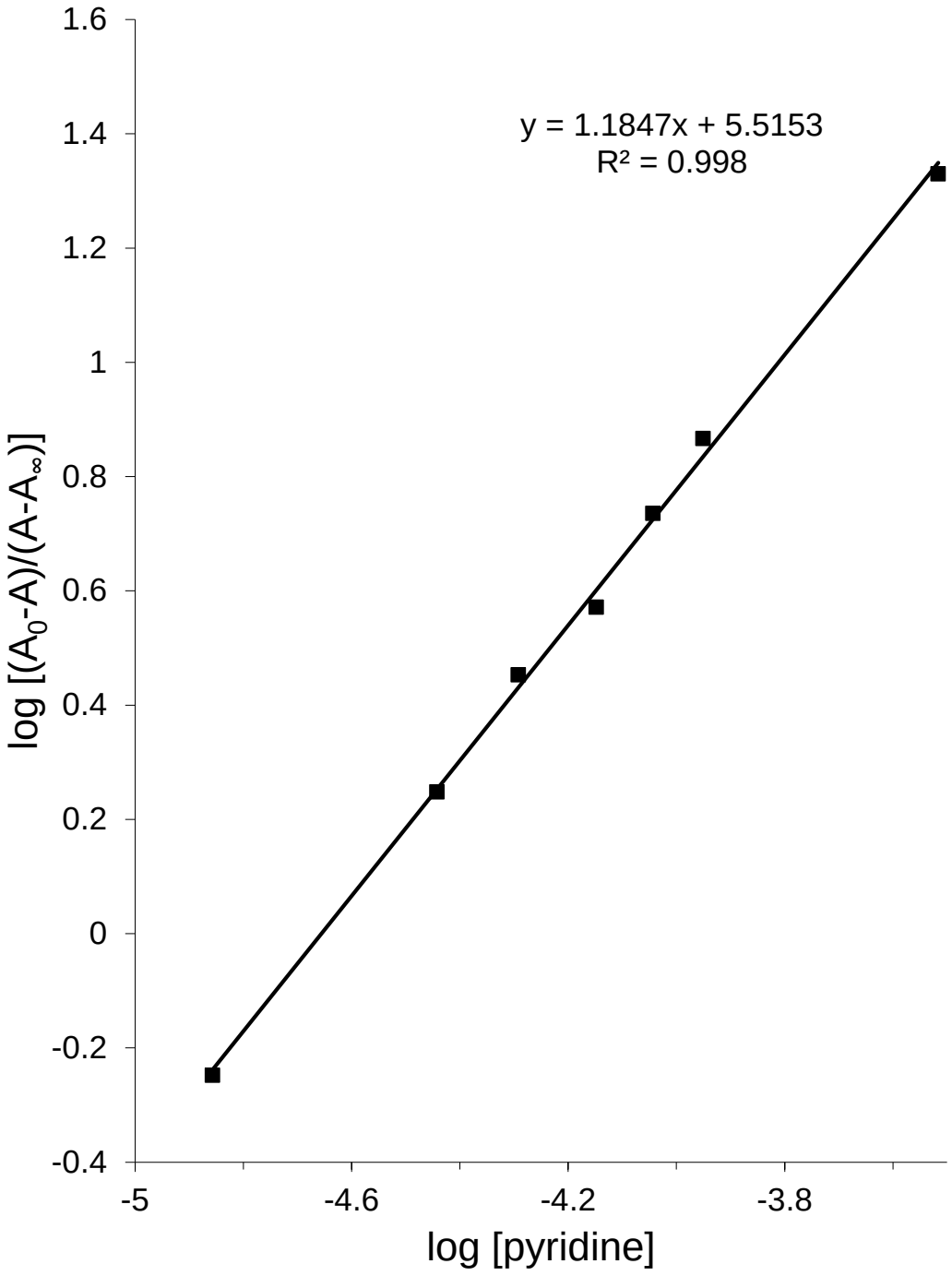

Figure A 13. A plot of log $[(A_o\text{-}A)/(A\text{-}A_\infty)]$ vs log [pyridine] for $[Co(dmgBF_2)_2(H_2O)_2]$ at 372 nm in 2-butanone at 20 ^oC.

Table A4. Absorbance values at 372 nm, log $[(A_o-A)/(A-A_\infty)]$ and log [pyridine] for $[Co(dmgBF_2)_2(H_2O)_2]$ in 1,2-difluorobenzene/acetone (4:1 v/v) at 20 ^oC. [complex] = 0.10 mM, path length = 1.0 cm.

[py]/[complex]	$Abs_{372\ nm}$	log [pyridine]	log $[(A_o-A)/(A-A_\infty)]$
0	0.1058	---	---
0.33	0.1336	-5.349	-0.3990
0.40	0.1390	-5.231	-0.2858
0.50	0.1444	-4.988	-0.1810
0.65	0.1556	-4.860	0.02092
0.75	0.1593	-4.700	0.08827
1.25	0.1817	-4.329	0.5519
1.50	0.1864	-4.173	0.6848
1.75	0.1874	-4.041	0.7184
2.5	0.1930	-3.795	0.9394
5.0	0.2011	-3.396	1.7048

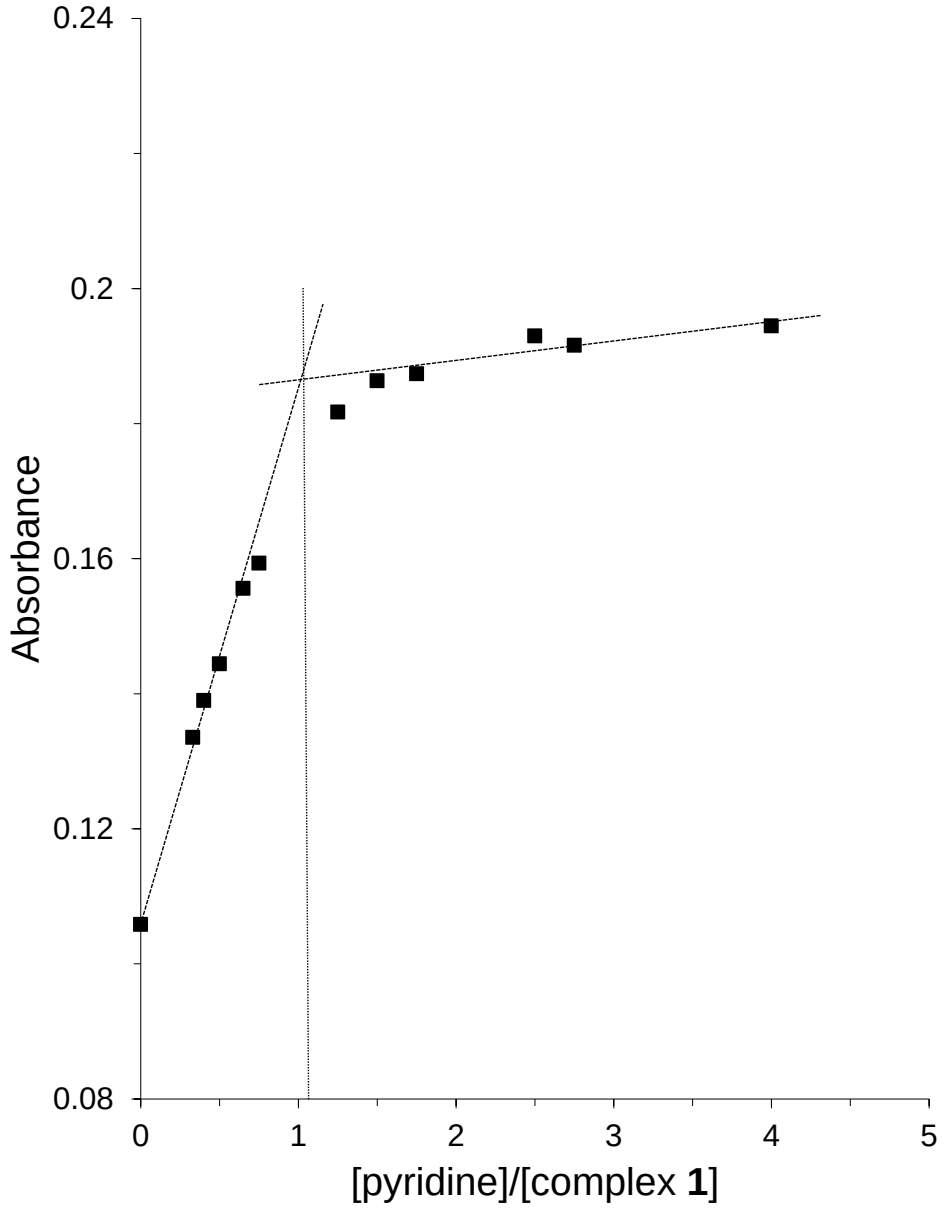

Figure A 14. Mole ratio plot for the interaction of pyridine with $[Co(dmgBF_2)_2(H_2O)_2]$ in 1,2-difluorobenzene/acetone (4:1, v/v). [complex] = 0.10 mM, λ = 372 nm, T = 20 ºC, path length = 1.0 cm.

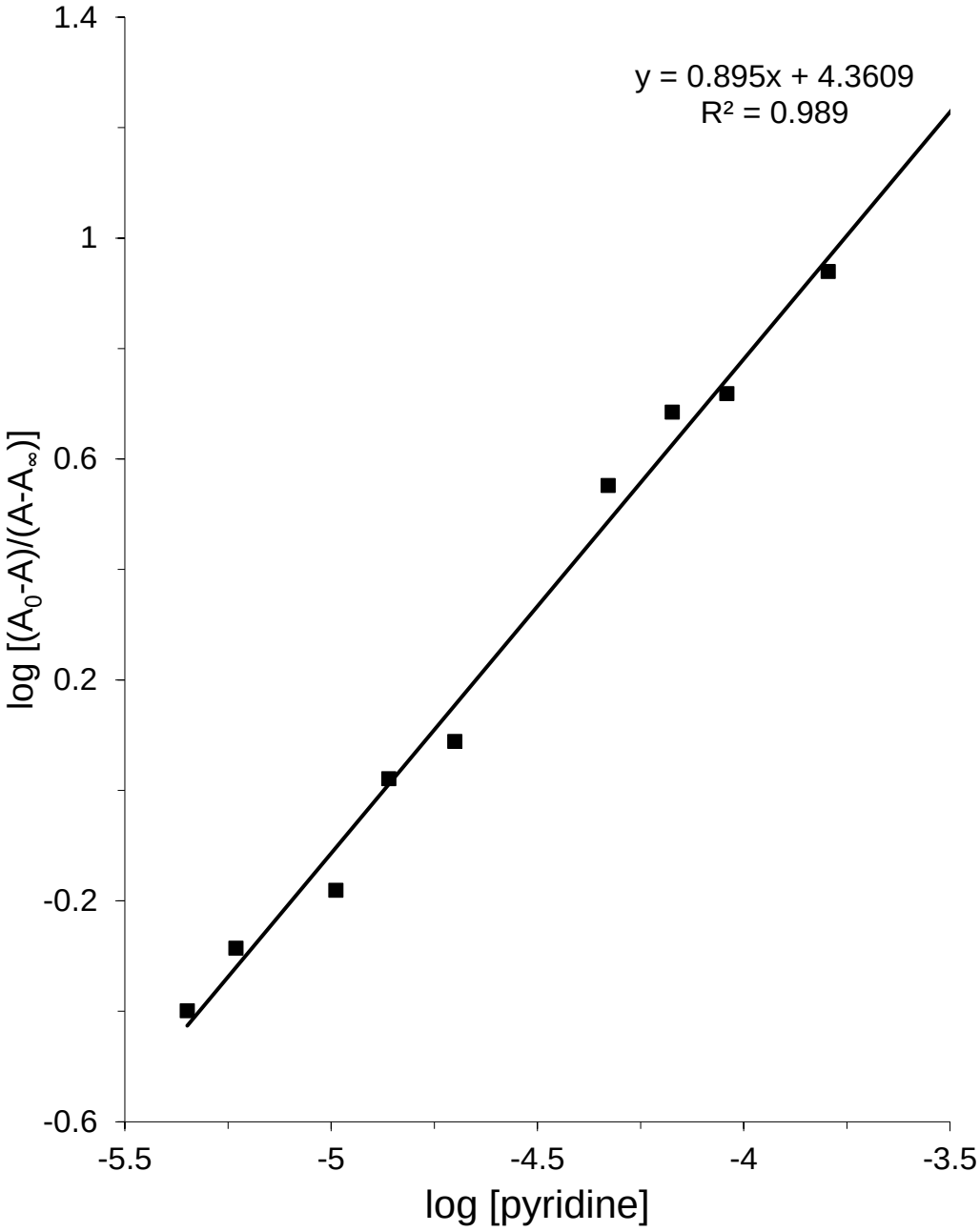

Figure A 15. A plot of log $[(A_o\text{-}A)/(A\text{-}A_\infty)]$ vs log [pyridine] for $[Co(dmgBF_2)_2(H_2O)_2]$ at 372 nm in 1,2-difluorobenzene/acetone (4:1, v/v) at 20 ^oC.

Table A5. Absorbance values at 370 nm, log $[(A_o-A)/(A-A_\infty)]$ and log [pyridine] for $[Co(dmgBF_2)_2(H_2O)_2]$ in dichloromethane at 20 °C. [complex] = 0.10 mM, path length = 1.0 cm.

[py]/[complex]	$Abs_{370\ nm}$	log [pyridine]	log $[(A_o-A)/(A-A_\infty)]$
0	0.1016	--	--
0.33	0.1341	-6.166	-0.3210
0.40	0.1409	-6.068	-0.1916
0.50	0.1506	-5.909	-0.02143
0.75	0.1738	-5.507	0.4077
0.87	0.1843	-5.330	0.6680
1.0	0.1914	-4.977	0.9282
1.12	0.1949	-4.720	1.121
1.25	0.1964	-4.514	1.226
1.5	0.1977	-4.265	1.350
2.0	0.2003	-3.993	1.755
2.25	0.1997	-3.895	1.635
2.5	0.1991	-3.816	1.531
3.0	0.2011	-3.697	2.025

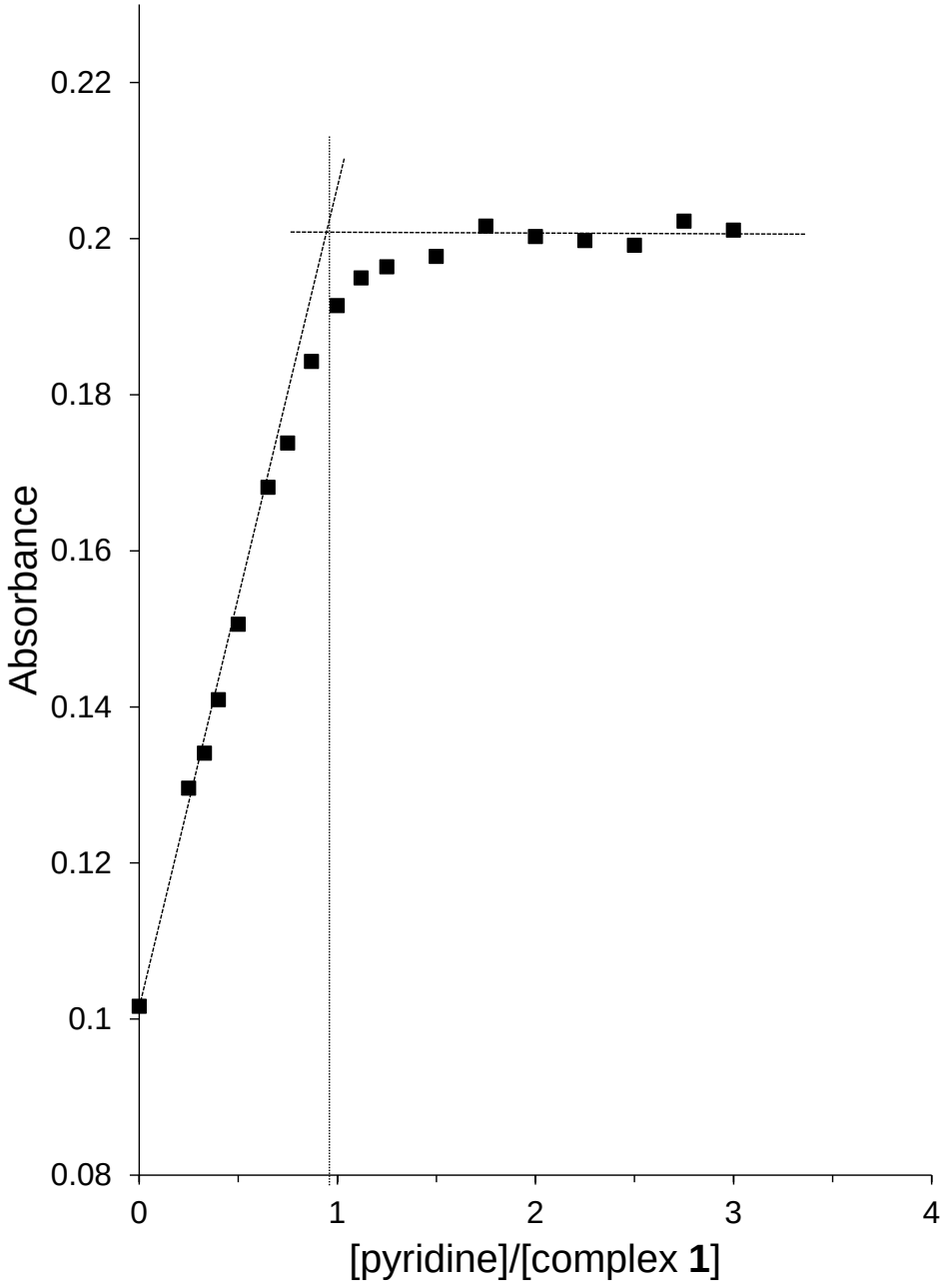

Figure A 16. Mole ratio plot for the interaction of pyridine with $[Co(dmgBF_2)_2(H_2O)_2]$ in dichloromethane. [complex] = 0.10 mM, λ = 370 nm, T = 20 ^{o}C, path length = 1.0 cm.

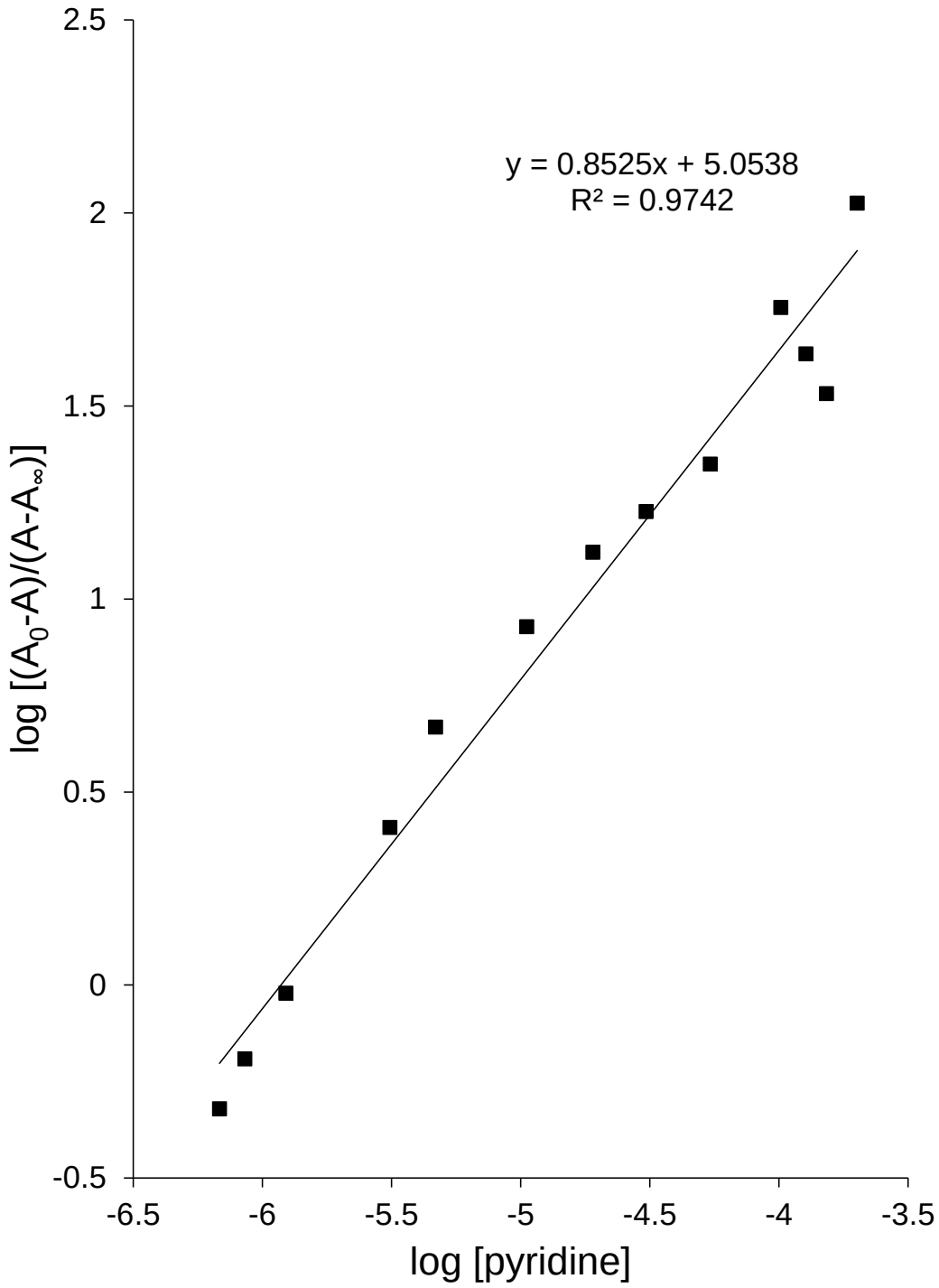

Figure A 17. A plot of log $[(A_o\text{-}A)/(A\text{-}A_\infty)]$ vs log [pyridine] for $[Co(dmgBF_2)_2(H_2O)_2]$ at 370 nm in dichloromethane at 20 ^oC.

Table A 6. Absorbance values at 447 nm, log [$(A_o-A)/(A-A_\infty)$], log [pyridine] for the [$^nBu_4N$]BH_4 reduced form of [$Co(dmgBF_2)_2(H_2O)_2$] in acetonitrile. [complex] = 1.0 mM, T = 20 ^oC, path length = 1.0 mm.

[py]/[complex]	$Abs_{447\ nm}$	log $[(A_o-A)/(A-A_\infty)]$	log [py]
0	0.1781	---	---
0.5	0.2404	-0.3440	-3.725
1.0	0.2954	0.1524	-3.384
1.5	0.3199	0.3871	-3.102
2.0	0.3433	0.6780	-2.931
2.5	0.3538	0.8610	-2.790
4.0	0.3689	1.322	-2.516

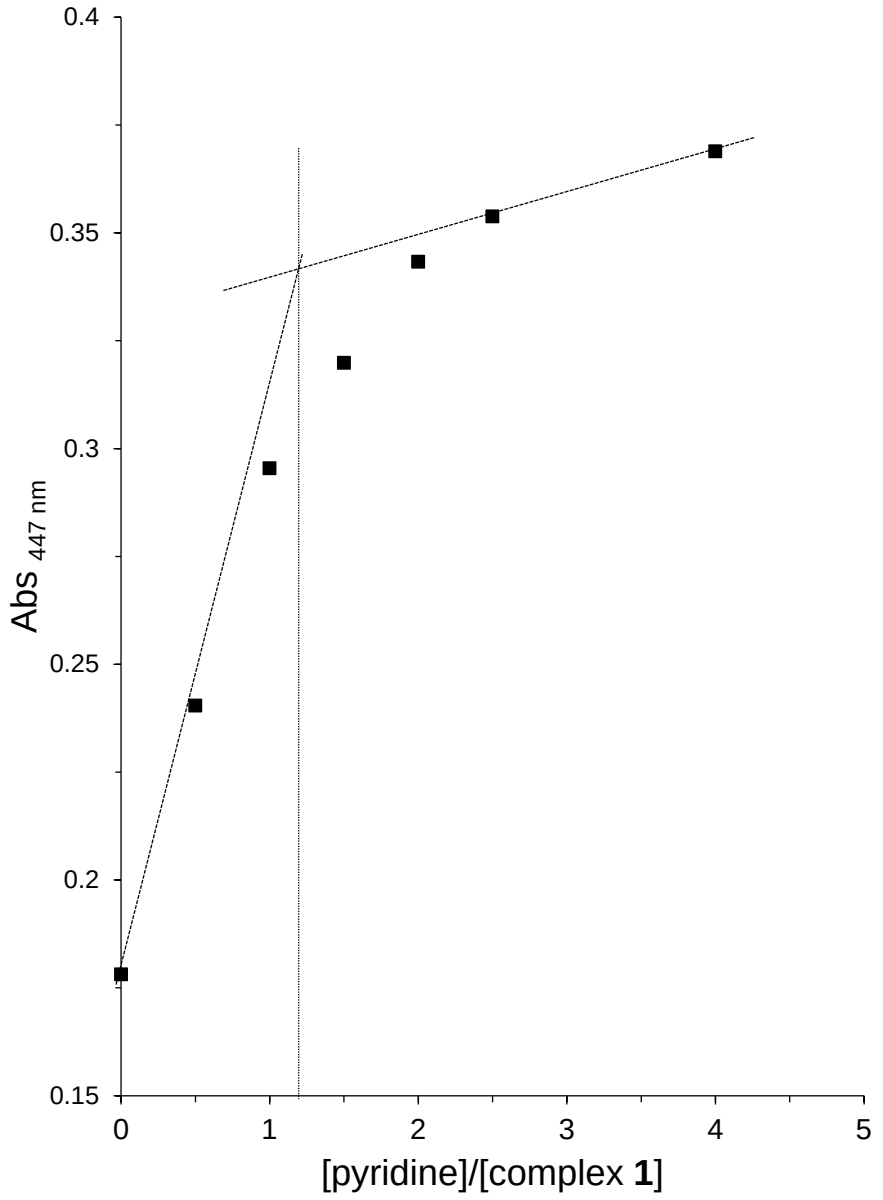

Figure A 18. Mole ratio plot for the interaction of pyridine with the $[^{n}Bu_4N]BH_4$ reduced form of $[Co(dmgBF_2)_2(H_2O)_2]$ in acetonitrile. [complex] = 1.0 mM, T = 20 ^{o}C, path length = 1.0 mm.

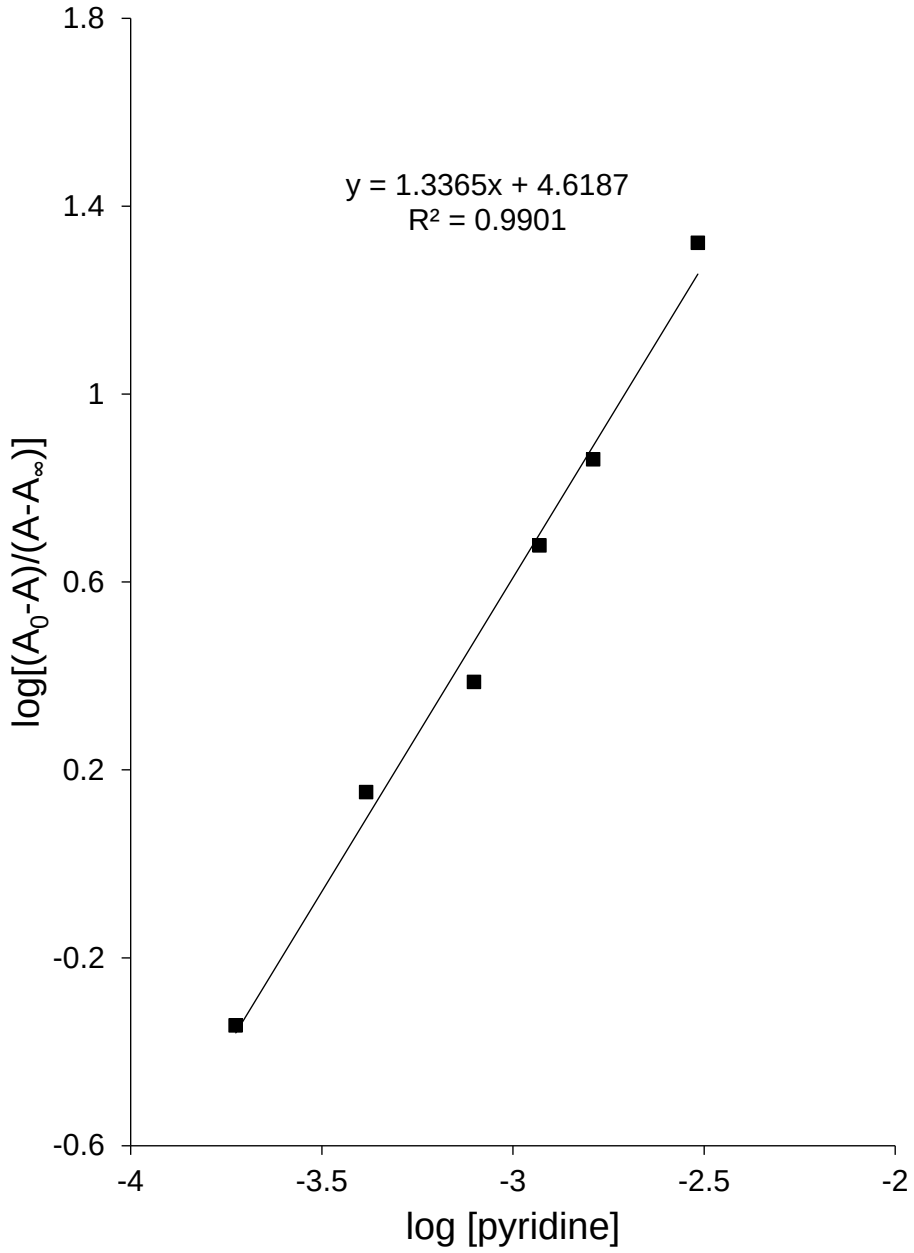

Figure A 19. A plot of log $[(A_o\text{-}A)/(A\text{-}A_\infty)]$ vs log [py] for the $[^nBu_4N]BH_4$ reduced form of $[Co(dmgBF_2)_2(H_2O)_2]$ in acetonitrile at 20 ^oC.

A4. Electrochemistry

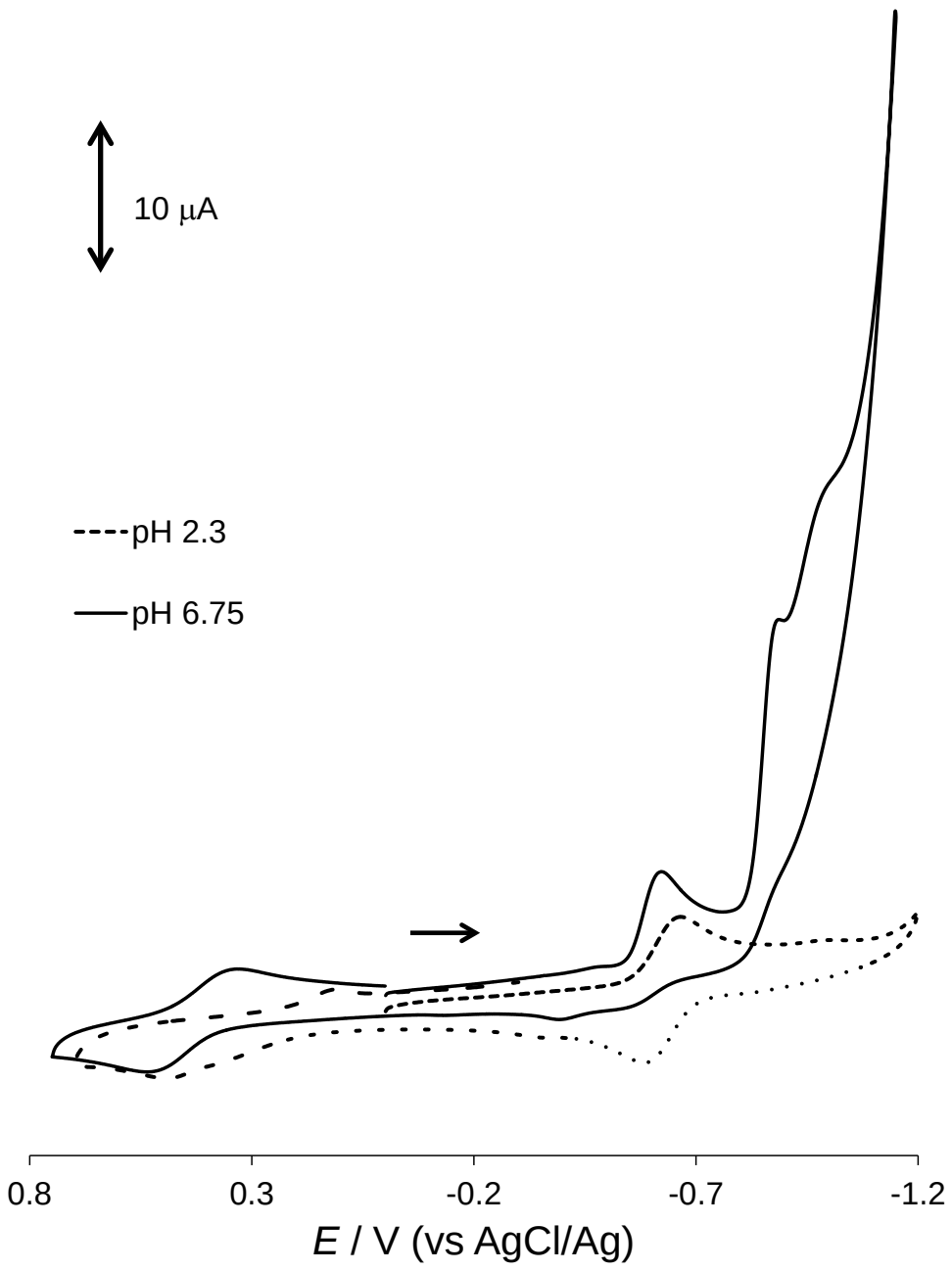

Figure A 20. Cyclic voltammograms of $[Co(dmgBF_2)_2(H_2O)_2]$ in water on a glassy carbon working electrode vs AgCl/Ag. $[Co(dmgBF_2)_2(H_2O)_2]$ = 0.64 mM, pH = 2.30 (solid lines) and pH = 6.75 (broken lines), I = 0.10 M ($NaClO_4$), and scan rate = 100 mV s^{-1}.

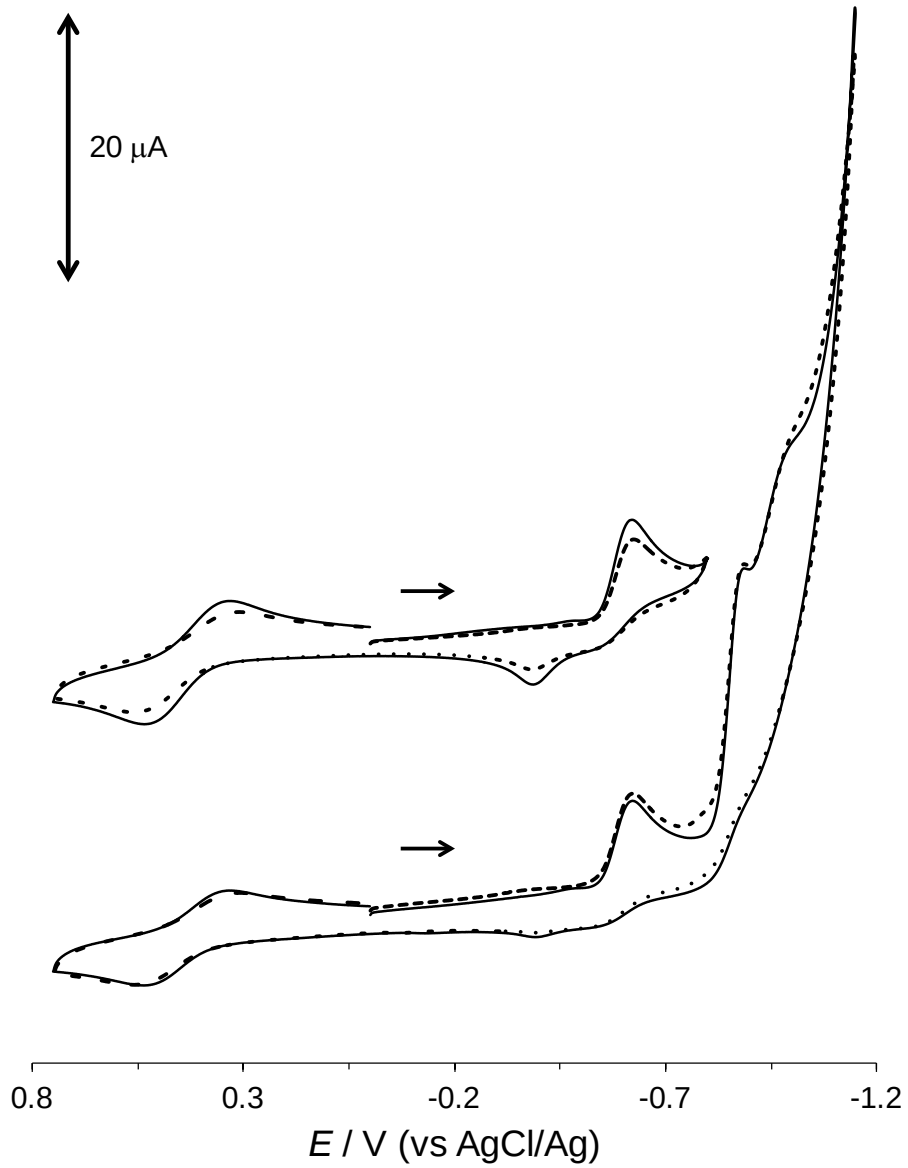

Figure A 21. Cyclic voltammograms of $[Co(dmgBF_2)_2(H_2O)_2]$ and $[Co(dmgBF_2)_2(H_2O)(py)]\bullet 0.5(CH_3)_2CO$ in water on a glassy carbon working electrode vs AgCl/Ag. $[Co(dmgBF_2)_2(H_2O)_2]$ = 0.64 mM (solid lines) and $[Co(dmgBF_2)_2(H_2O)(py)\bullet 0.5(CH_3)_2CO]$ = 0.63 mM (broken lines), pH = 2.30, I = 0.10 M $NaClO_4$, and scan rate = 100 mV s^{-1}.

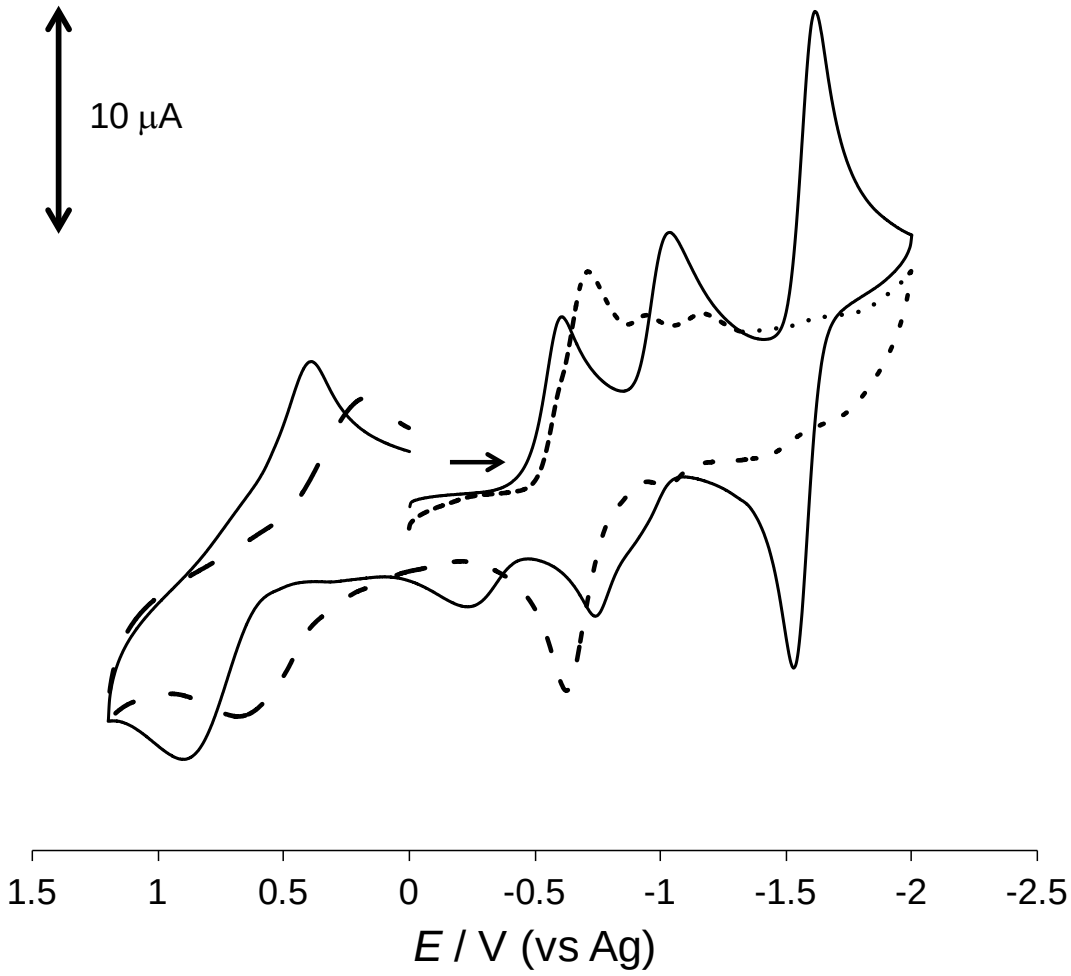

Figure A 22. Cyclic voltammograms of $[Co(dmgBF_2)_2(H_2O)_2]$ and $[Co(dmgBF_2)_2(H_2O)(py)]\bullet 0.5(CH_3)_2CO$ in 2-butanone on a glassy carbon working electrode vs Ag quasi-reference electrode. $[Co(dmgBF_2)_2(H_2O)_2]$ = 1.02 mM (solid lines) and $[Co(dmgBF_2)_2(H_2O)(py)\bullet 0.5(CH_3)_2CO]$ = 1.08 mM (broken lines), I = 0.10 M $[^nBu_4N]ClO_4$), and scan rate = 100 mV s^{-1} vs.

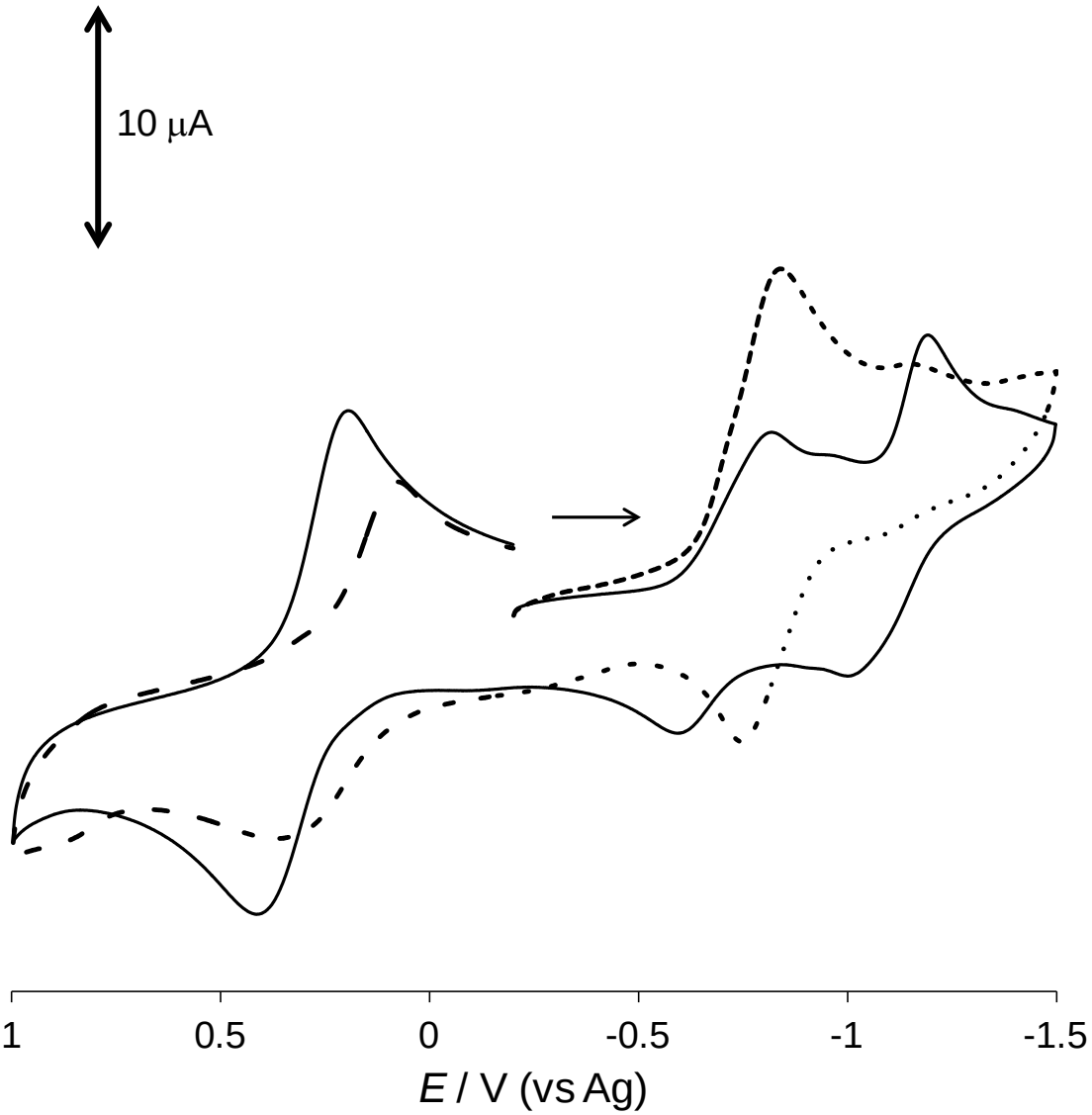

Figure A 23. Cyclic voltammograms of $[Co(dmgBF_2)_2(H_2O)_2]$ and $[Co(dmgBF_2)_2(H_2O)(py)]\bullet 0.5(CH_3)_2CO$ in 1,2-difluorobenzene/acetone (4:1 v/v) on a glassy carbon working electrode vs Ag quasi-reference electrode. $[Co(dmgBF_2)_2(H_2O)_2]$ = 1.05 mM (solid lines) and $[Co(dmgBF_2)_2(H_2O)(py)\bullet 0.5(CH_3)_2CO]$ = 1.03 mM (broken lines), I = 0.10 M ($[^nBu_4N]ClO_4$), and scan rate = 100 mV s^{-1}.

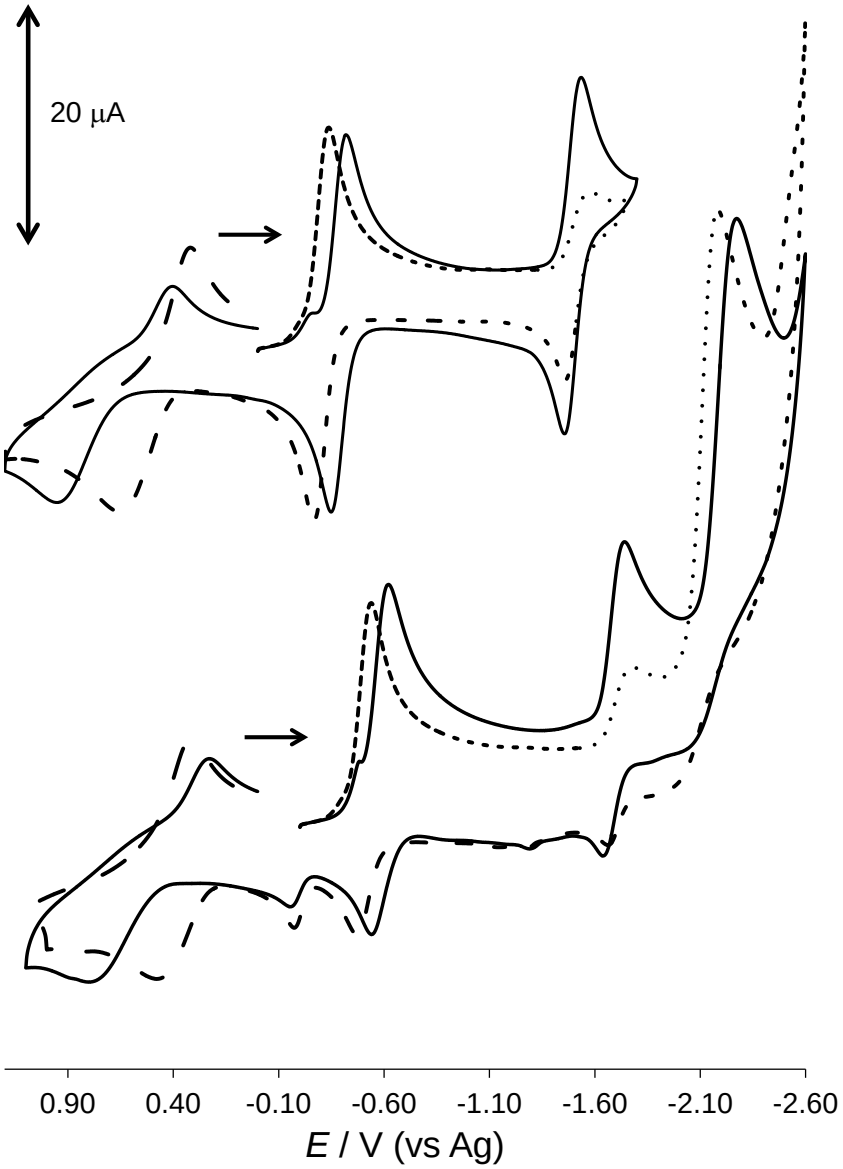

Figure A 24. Cyclic voltammograms of $[Co(dmgBF_2)_2(H_2O)_2]$ in CH_3CN on a glassy carbon working electrode vs Ag quasi-reference electrode. [complex] = 1.04 mM (solid lines) and [complex] = 1.04 mM with 5.09 mM pyridine (broken lines), I = 0.10 M ($[^nBu_4N]ClO_4$), and scan rate = 100 mV s^{-1}.

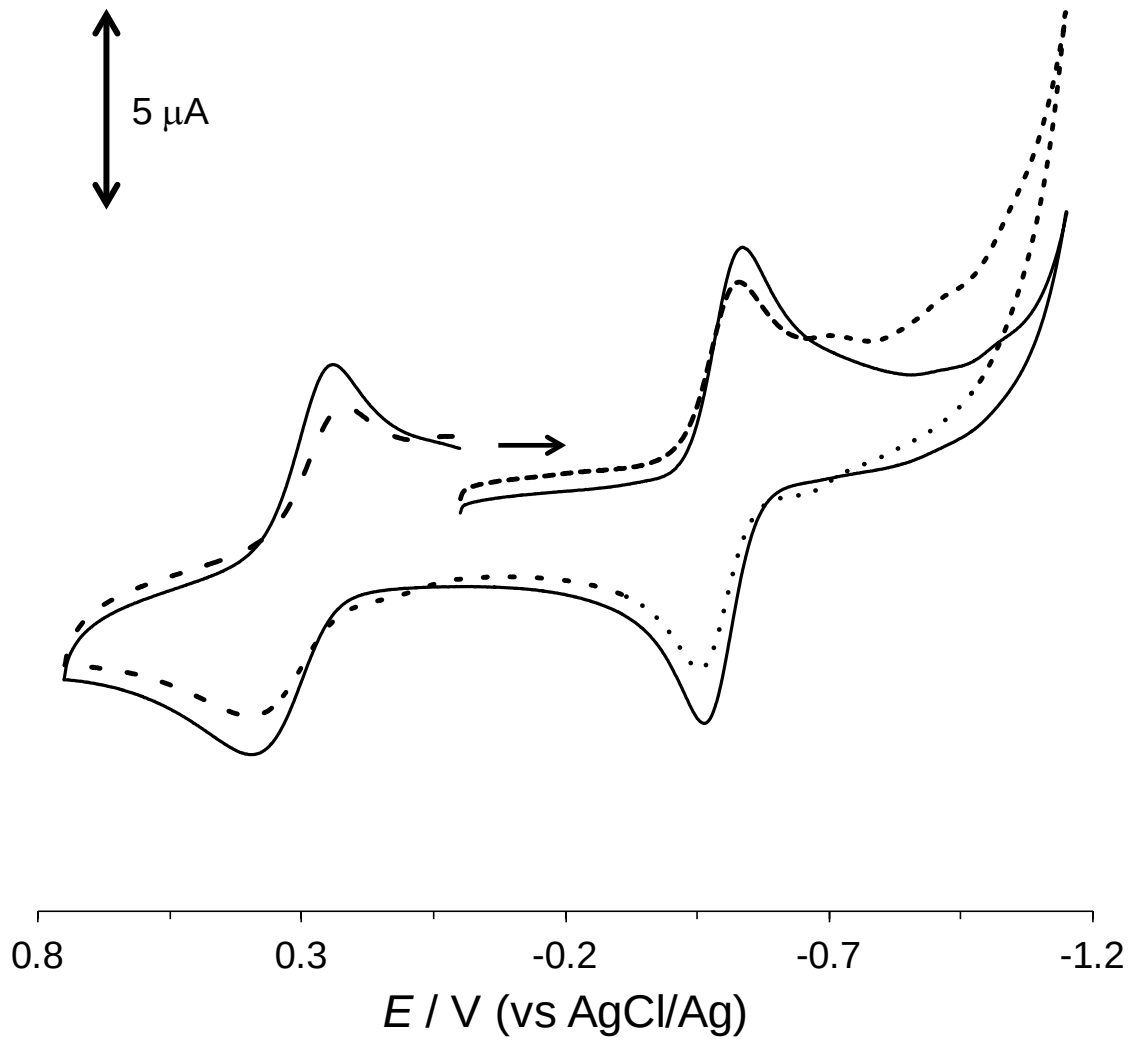

Figure A 25. Cyclic voltammograms of $[Co(dmgBF_2)_2(H_2O)_2]$ and $[Co(dmgBF_2)_2(H_2O)(py)]\bullet 0.5(CH_3)_2CO$ in water with pyridine on a glassy carbon working electrode vs AgCl/Ag. $[Co(dmgBF_2)_2(H_2O)_2]$ = 0.64 mM with 5.21 mM pyridine (solid lines) and $[Co(dmgBF_2)_2(H_2O)(py)\bullet 0.5(CH_3)_2CO]$ = 0.63 mM with 5.21 mM pyridine (broken lines), I = 0.10 M ($NaClO_4$), and scan rate = 100 mV s^{-1}.

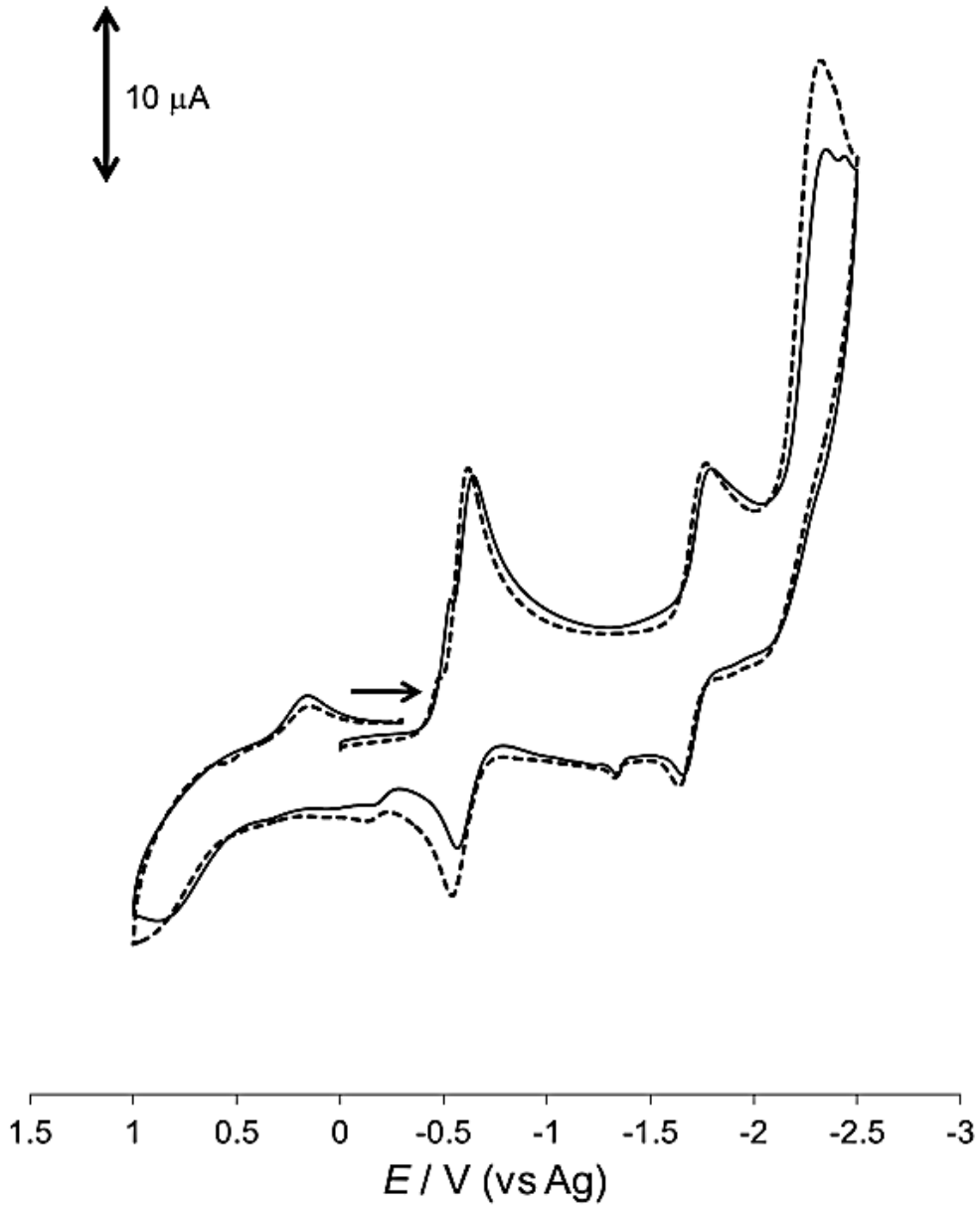

Figure A 26. Cyclic voltammograms $[Co(dmgBF_2)_2(H_2O)_2]$ in CH_3CN on a glassy carbon working electrode vs Ag quasi-reference electrode. [complex] = 1.02 mM (solid lines) and [complex] = 1.02 mM with 15.0 mM 2-methylpyridine (broken lines), I = 0.10 M ($[^nBu_4N]ClO_4$), and scan rate = 100 mV s^{-1}.

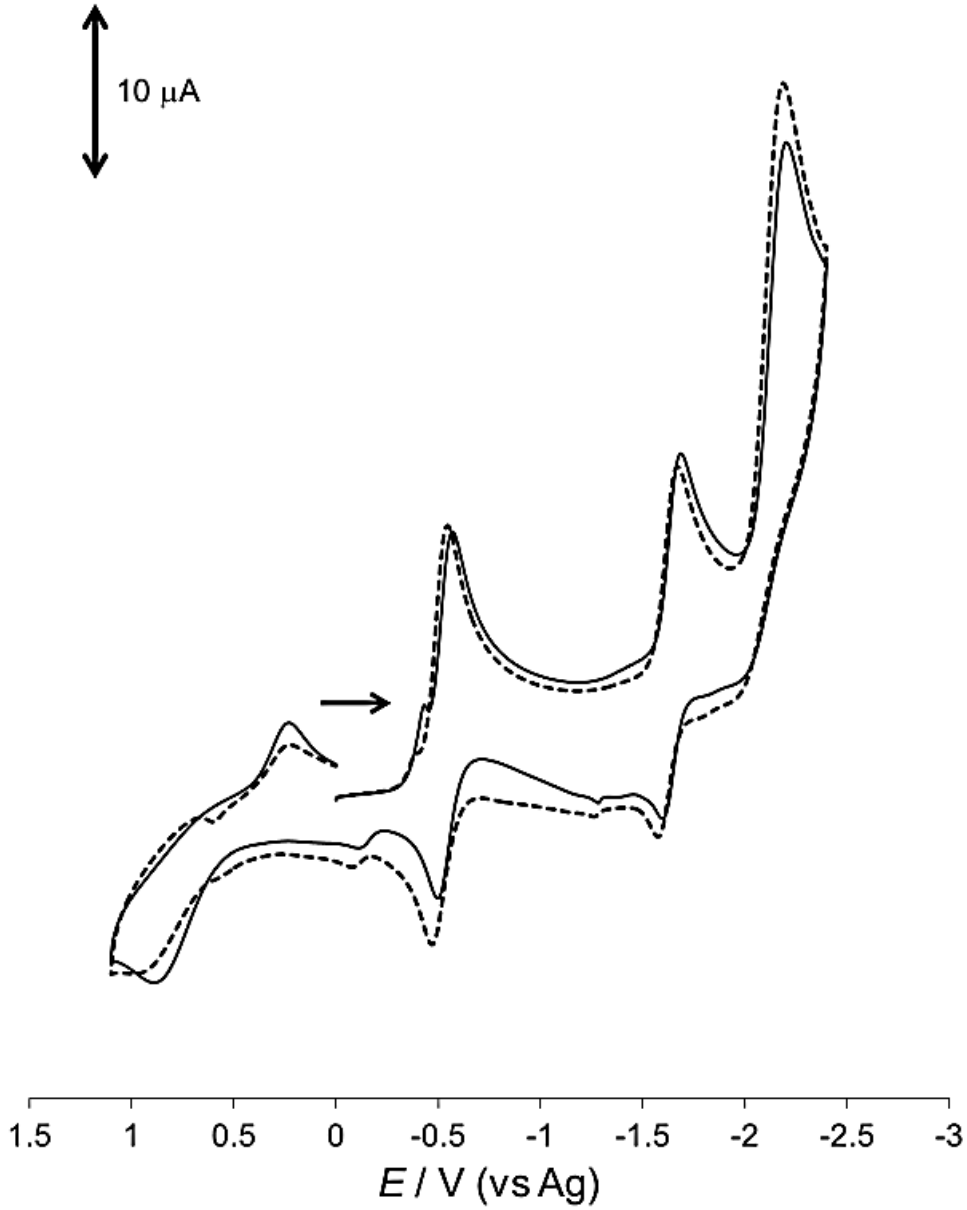

Figure A 27. Cyclic voltammograms of $[Co(dmgBF_2)_2(H_2O)_2]$ in CH_3CN on a glassy carbon working electrode vs Ag quasi-reference electrode. [complex] = 1.02 mM (solid lines) and [complex] = 1.02 mM with 15.1 mM 2,6-dimethylpyridine (broken lines), I = 0.10 M ($[^nBu_4N]ClO_4$), and scan rate = 100 mV s^{-1}.

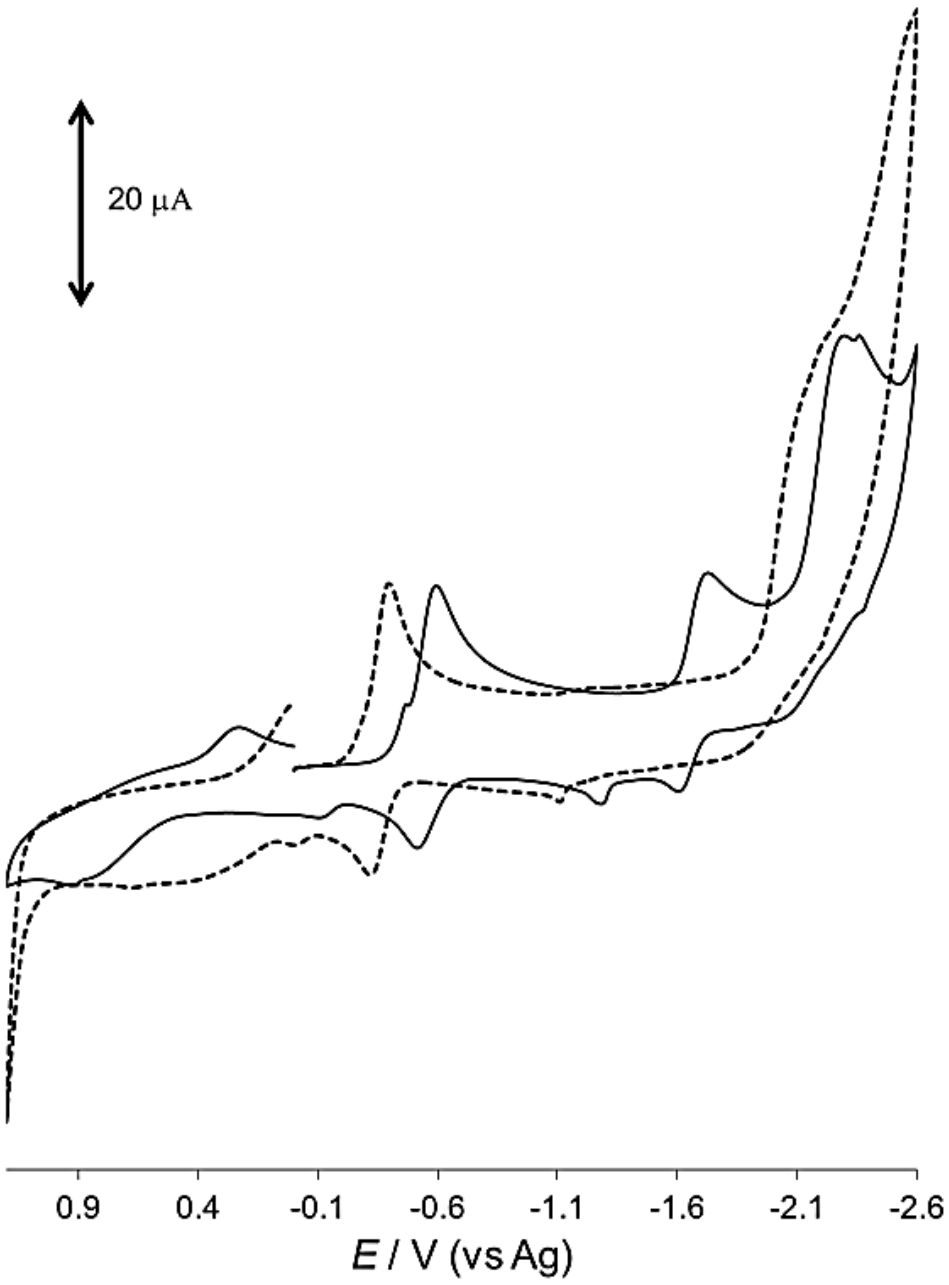

Figure A 28. Cyclic voltammograms of $[Co(dmgBF_2)_2(H_2O)_2]$ in acetonitrile on a glassy carbon working electrode vs Ag quasi-reference electrode. [complex] = 1.05 mM (solid lines) and [complex] = 1.05 mM with [2-aminopyridine] = 5.10 mM (broken lines), *I* = 0.10 M ($^{n}Bu_4N]ClO_4$, and scan rate = 100 mV s^{-1}.

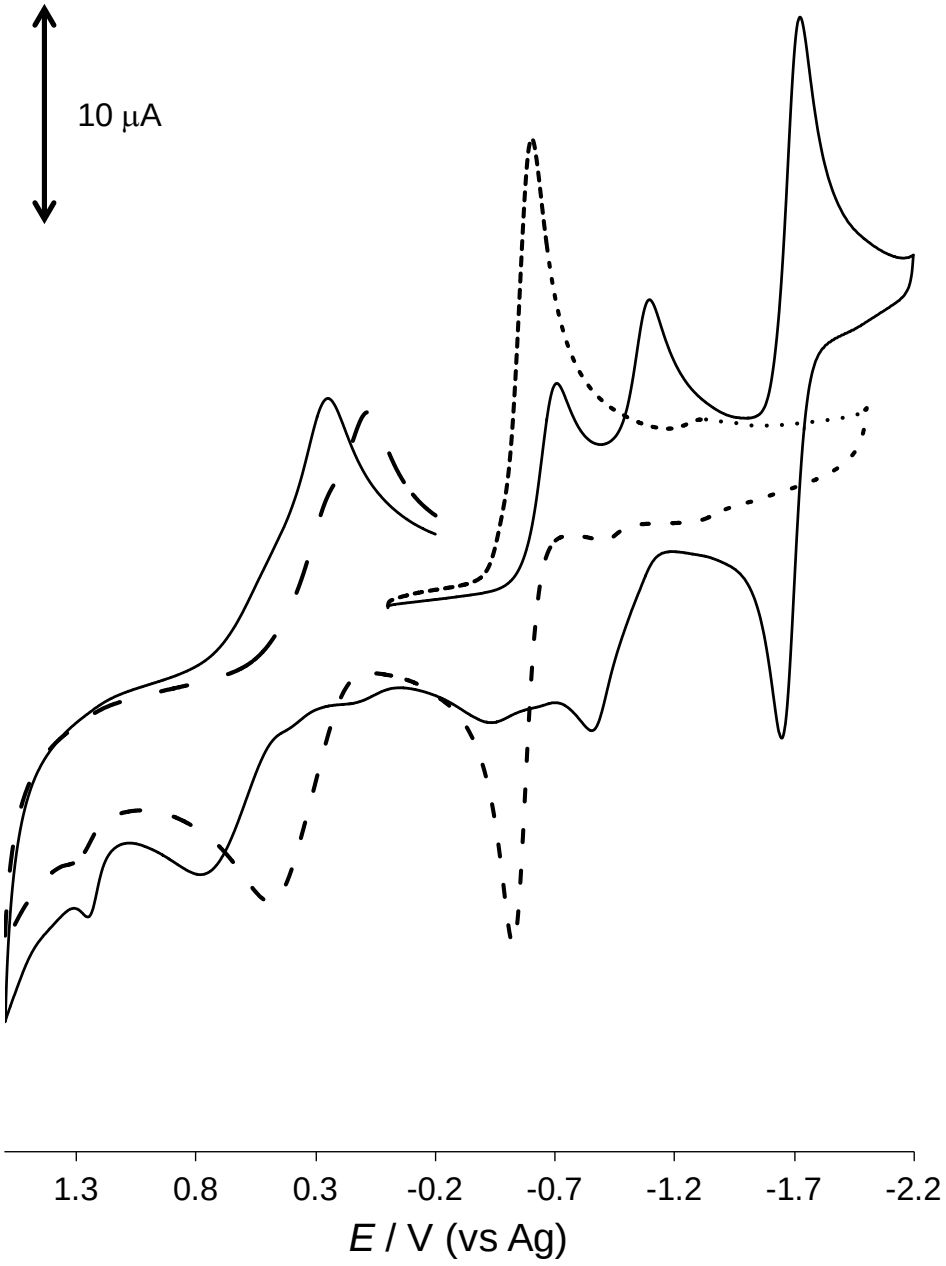

Figure A 29. Cyclic voltammograms of $[Co(dmgBF_2)_2(H_2O)_2]$ in acetone on a glassy carbon working electrode vs Ag quasi-reference electrode. [complex] = 1.04 mM (solid lines) and [complex] = 1.04 mM with 5.09 mM of pyridine (broken lines), I = 0.10 M ($[^nBu_4N]ClO_4$), and scan rate = 100 mV s^{-1}.

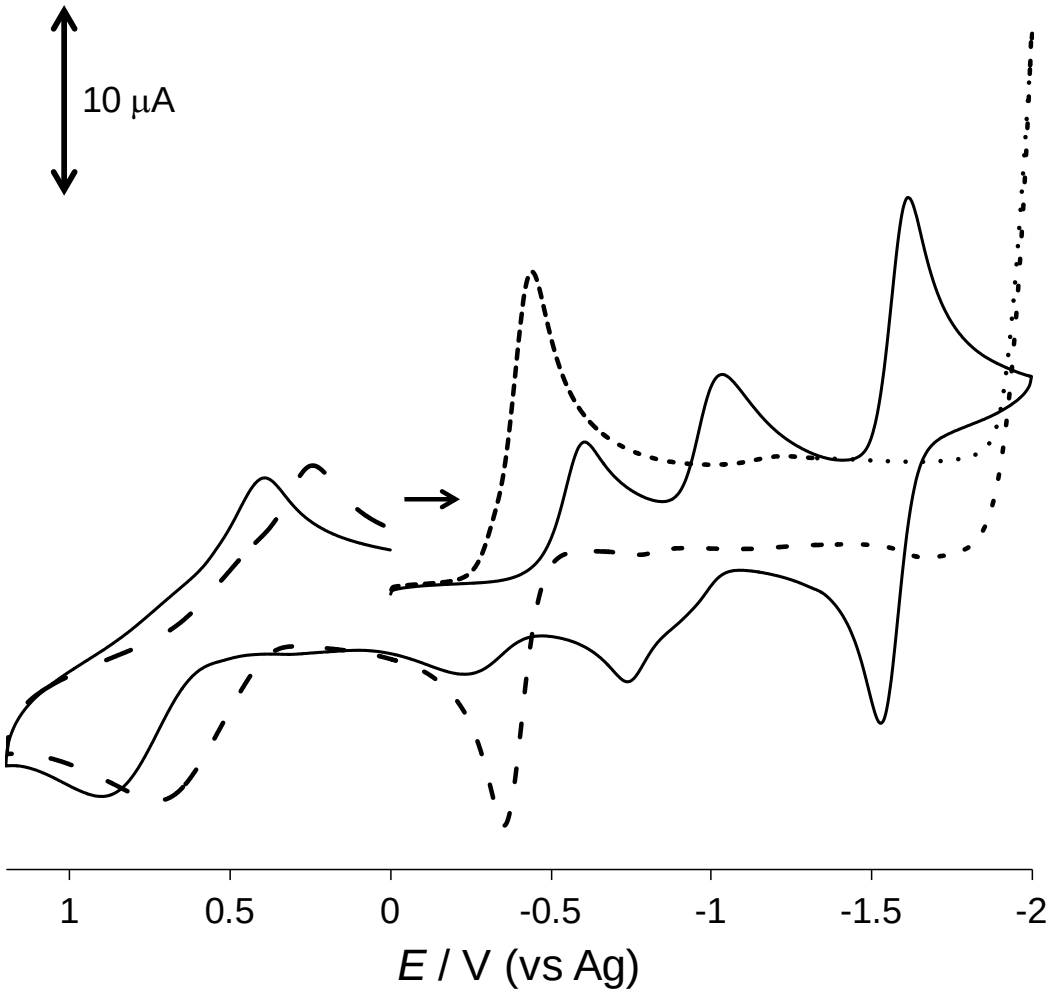

Figure A 30. Cyclic voltammograms of $[Co(dmgBF_2)_2(H_2O)_2]$ in 2-butanone on a glassy carbon working electrode vs Ag quasi-reference electrode. [complex] = 1.02 mM (solid lines) and [complex] = 1.02 mM with 5.09 mM of pyridine (broken lines), I = 0.10 M ($[^nBu_4N]ClO_4$), and scan rate = 100 mV s^{-1}.

A5. ^{19}F NMR spectroscopy

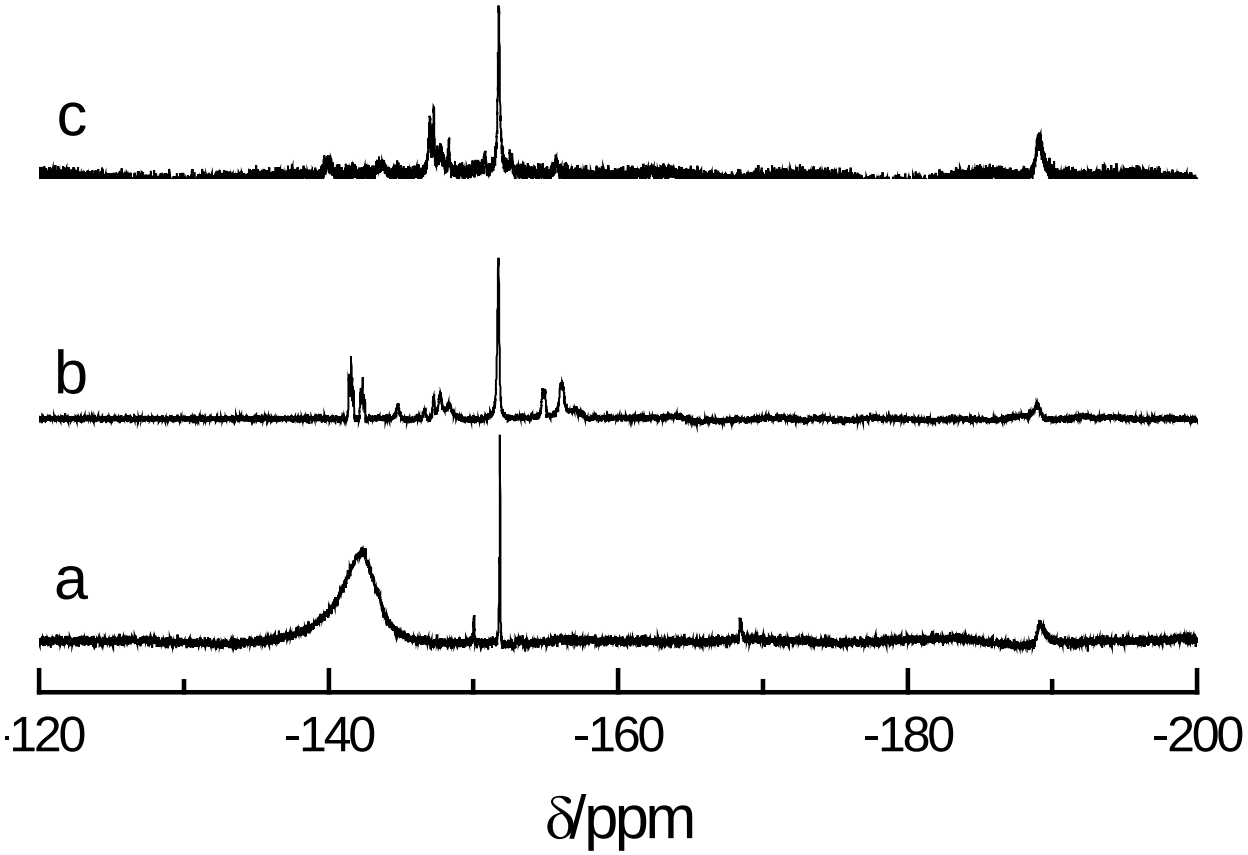

Figure A 31. ^{19}F NMR spectra in acetonitrile-d_3 of (a) 50 mM [Co(dmgBF$_2$)$_2$(H$_2$O)$_2$], (b) 50 mM [Co(dmgBF$_2$)$_2$(H$_2$O)(py)]•0.5(CH$_3$)$_2$CO, (c) 50 mM [Co(dmgBF$_2$)$_2$(H$_2$O)$_2$] with 250 mM pyridine.

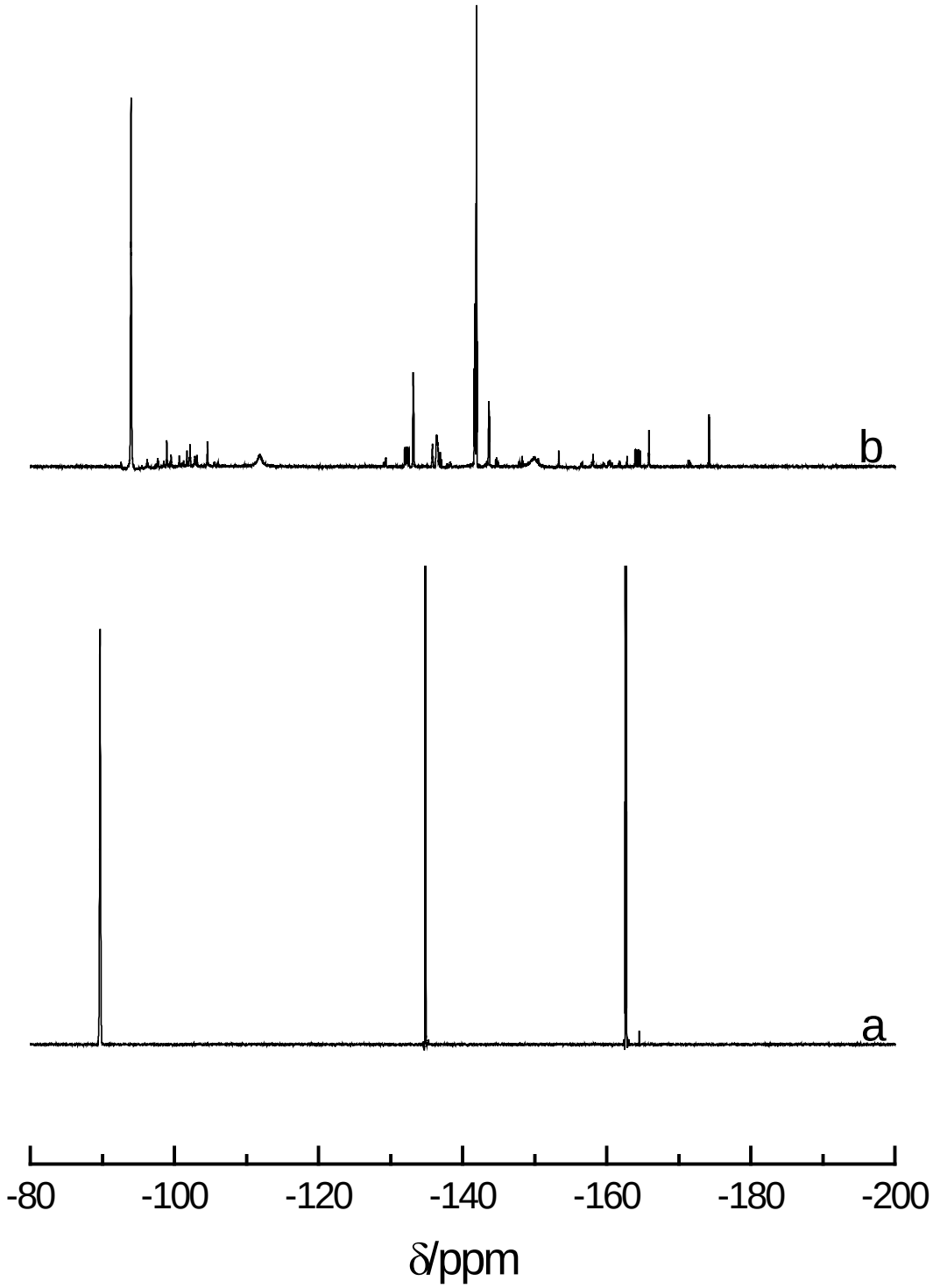

Figure A 32. ^{19}F NMR spectra in acetonitrile-d_3 of (a) 250 mM pentafluoropyridine and (b) 250 mM pentafluoropyridine with 500 mM $[^{n}BuN]BH_4$.

A6. Spectroelectrochemistry

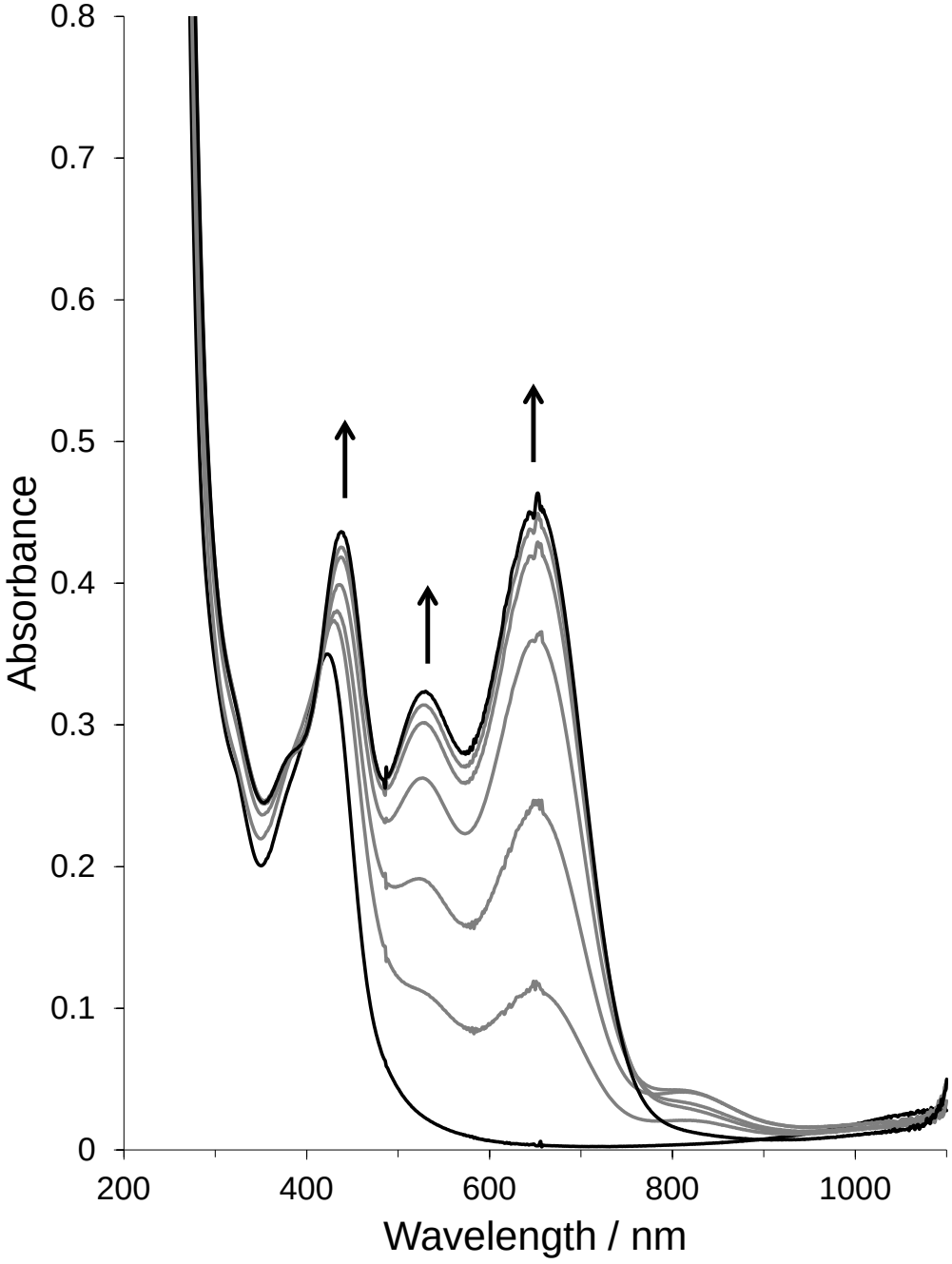

Figure A 33. Absorbance changes in the UV-visible spectra of $[Co(dmgBF_2)_2(H_2O)_2]$ with pyridine in acetonitrile at a constant potential of −1.0 V *vs* Ag. [complex] = 1.05 mM, [pyridine] = 5.09 mM, I = 0.10 M ($[^nBu_4N]ClO_4$), path length = 1 mm.

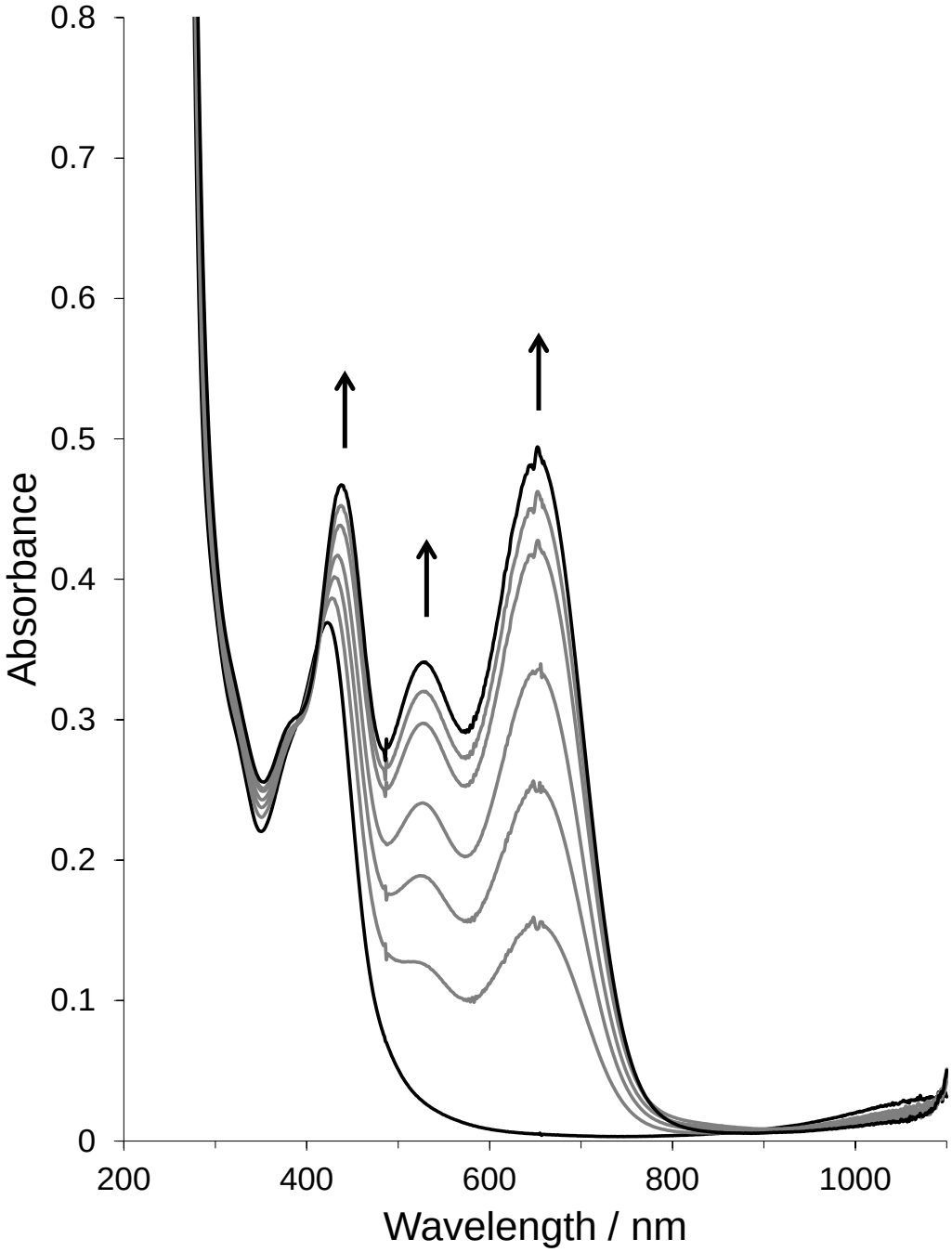

Figure A 34. Absorbance changes in the UV-visible spectra of $[Co(dmgBF_2)_2(H_2O)_2]$ with pyridine in acetonitrile at a constant potential of −1.0 V *vs* Ag. [complex] = 1.05 mM, [pyridine] = 10.18 mM, I = 0.10 M ($[^nBu_4N]ClO_4$), path length = 1 mm.

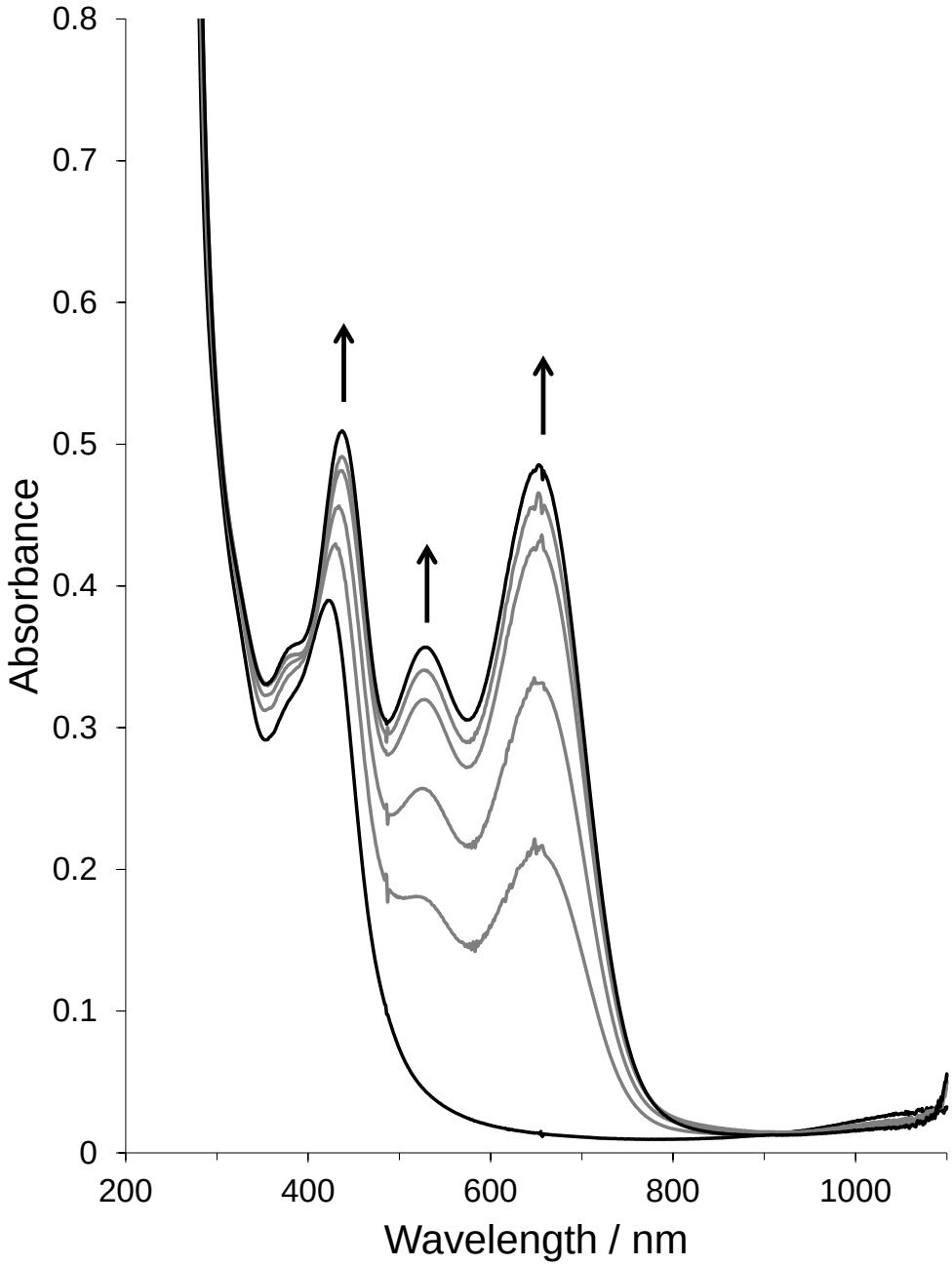

Figure A 35. Absorbance changes in the UV-visible spectra of $[Co(dmgBF_2)_2(H_2O)(py)]\bullet 0.5(CH_3)_2CO$ with pyridine in acetonitrile at a constant potential of −1.0 V *vs* Ag. [complex] = 1.02 mM, [pyridine] = 10.18 mM, I = 0.10 M ($[^nBu_4N]ClO_4$), path length = 1 mm.

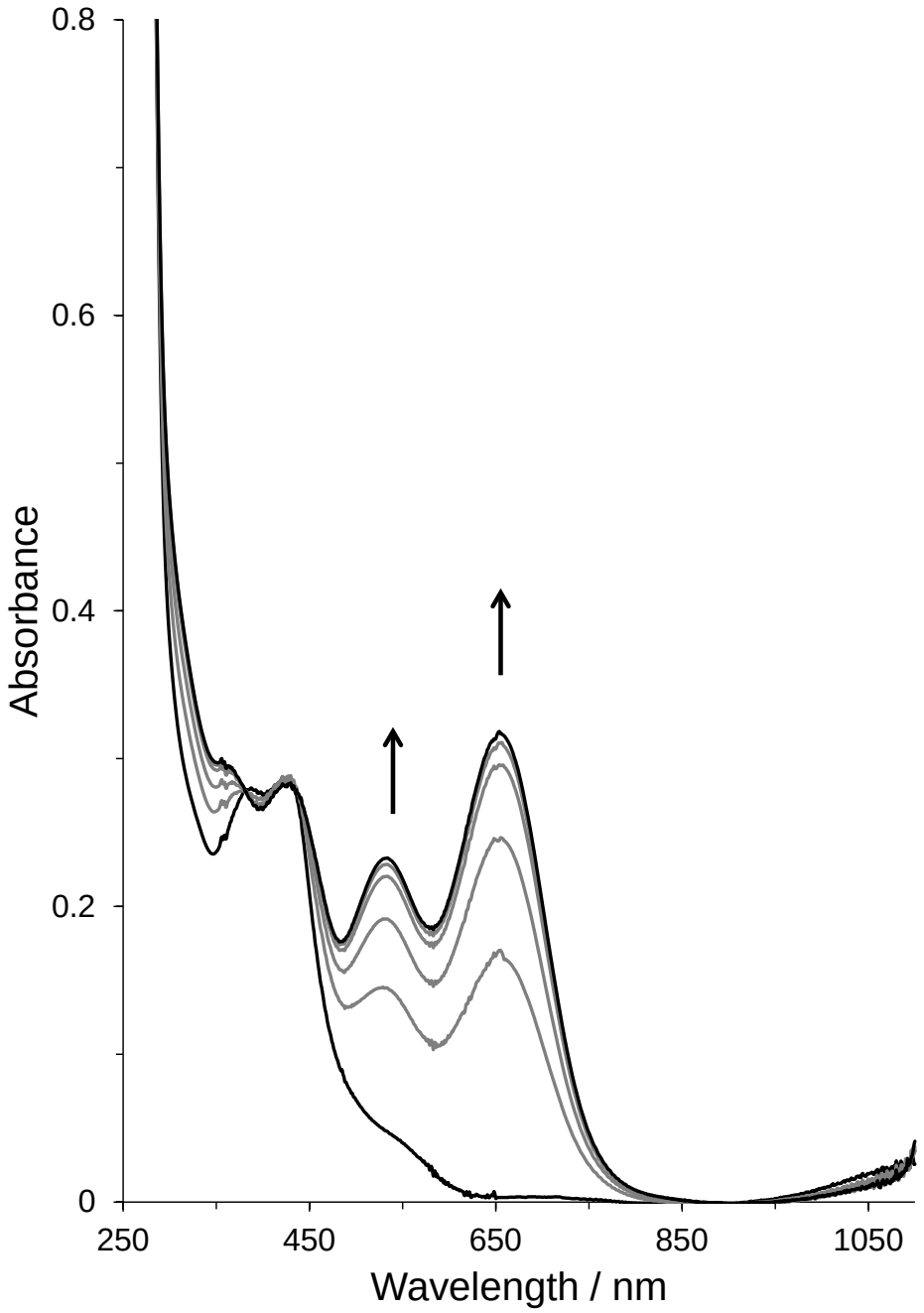

Figure A 36. Absorbance changes in the UV-visible spectra of $[Co(dmgBF_2)_2(H_2O)_2]$ with 2-aminopyridine in acetonitrile at a constant potential of −1.0 V *vs* Ag. [complex] = 1.05 mM, [pyridine] = 5.10 mM, I = 0.10 M ($[^nBu_4N]ClO_4$), path length = 1 mm.

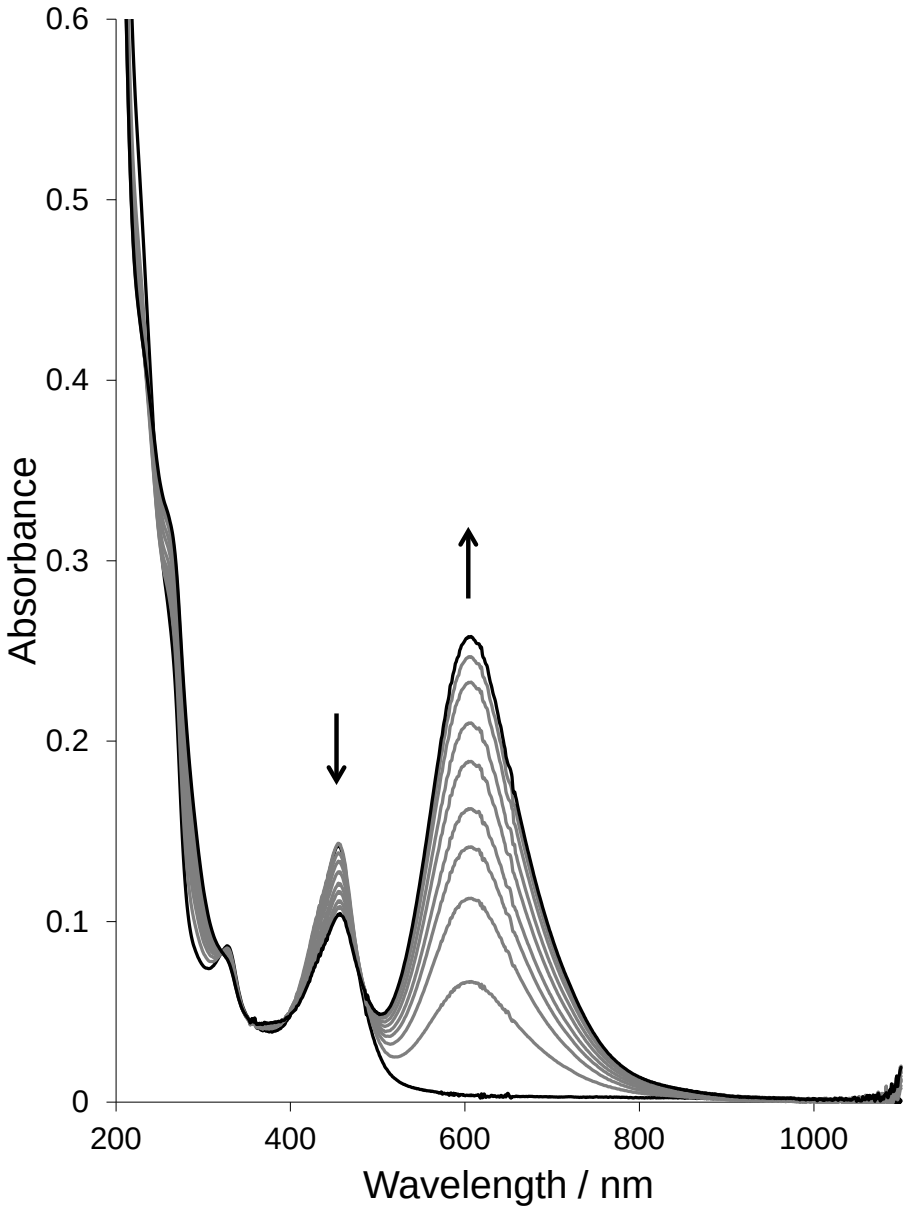

Figure A 37. Absorbance changes in the UV-visible spectra of $[Co(dmgBF_2)_2(H_2O)_2]$ in water at a constant potential of −0.75 V vs AgCl/Ag. [complex] = 0.51 mM, I = 0.10 M ($NaClO_4$), pH = 5.79, path length = 1 mm. *Note: At low pH (e.g. 2.30) the evolution of hydrogen is observed. The use of a buffer was avoided to eliminate substitution of the axial water molecules.*

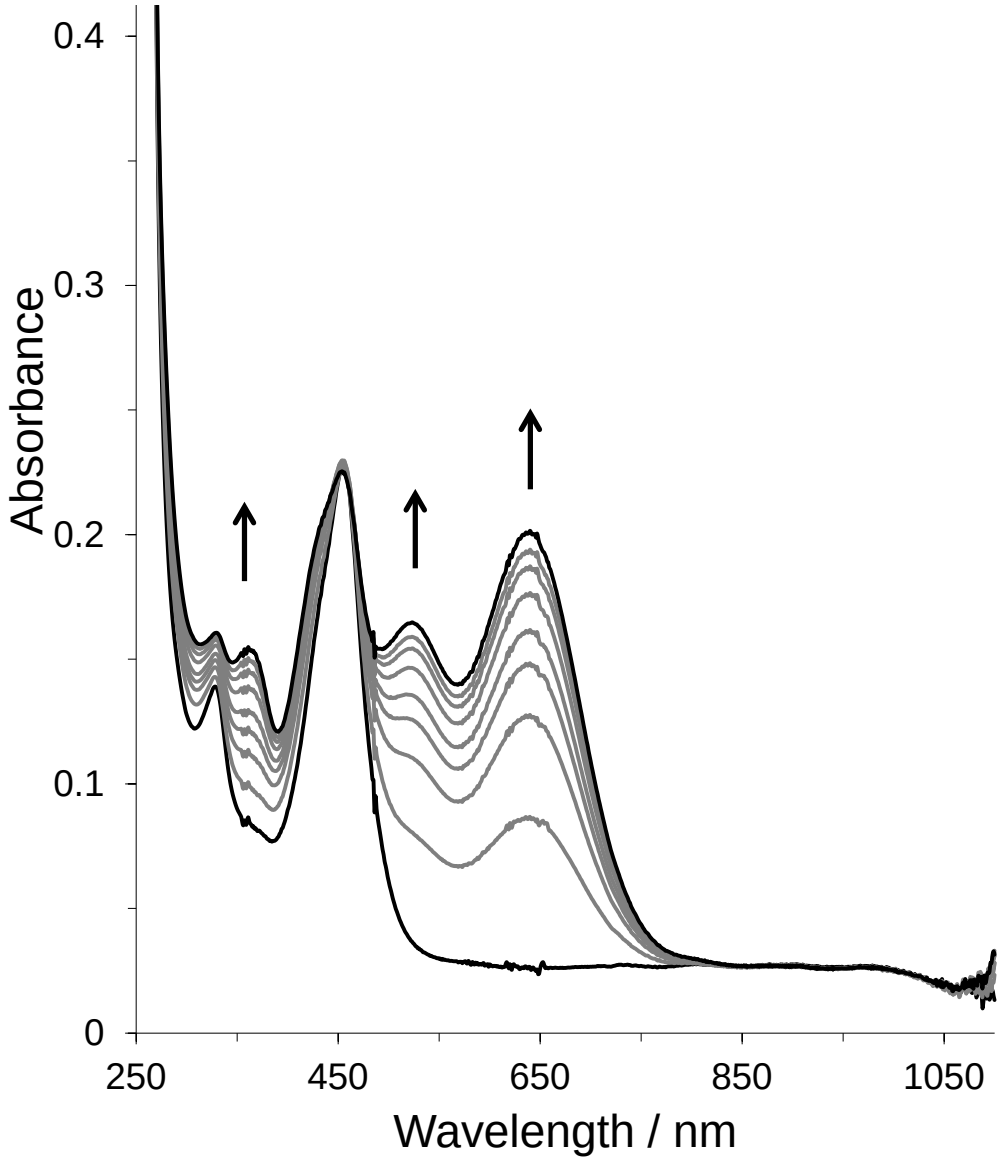

Figure A 38. Absorbance changes in the UV-visible spectra of $[Co(dmgBF_2)_2(H_2O)_2]$ in water at a constant potential of −0.7 V vs Ag. [complex] = 0.60 mM, [pyridine] = 5.21 mM, I = 0.10 M ($NaClO_4$), pH = 4.58, path length = 1 mm.

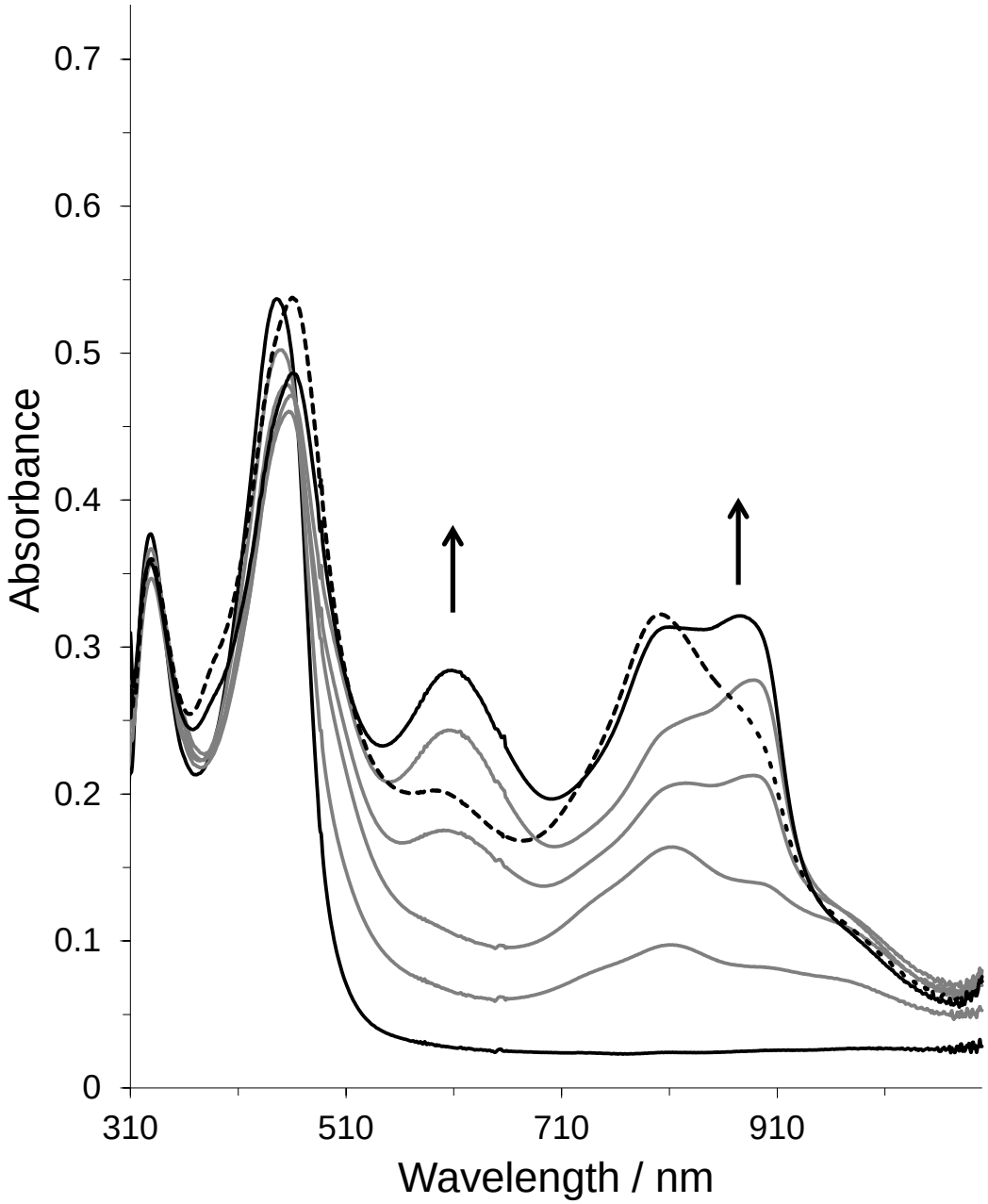

Figure A 39. Absorbance changes in the UV-visible spectra of $[Co(dmgBF_2)_2(H_2O)_2]$ in acetone at a constant potential of −1.30 V vs Ag. [complex] = 1.14 mM, I = 0.10 M ($[^nBu_4N]ClO_4$), path length = 1 mm. Broken line illustrates the spectrum after an extended time.

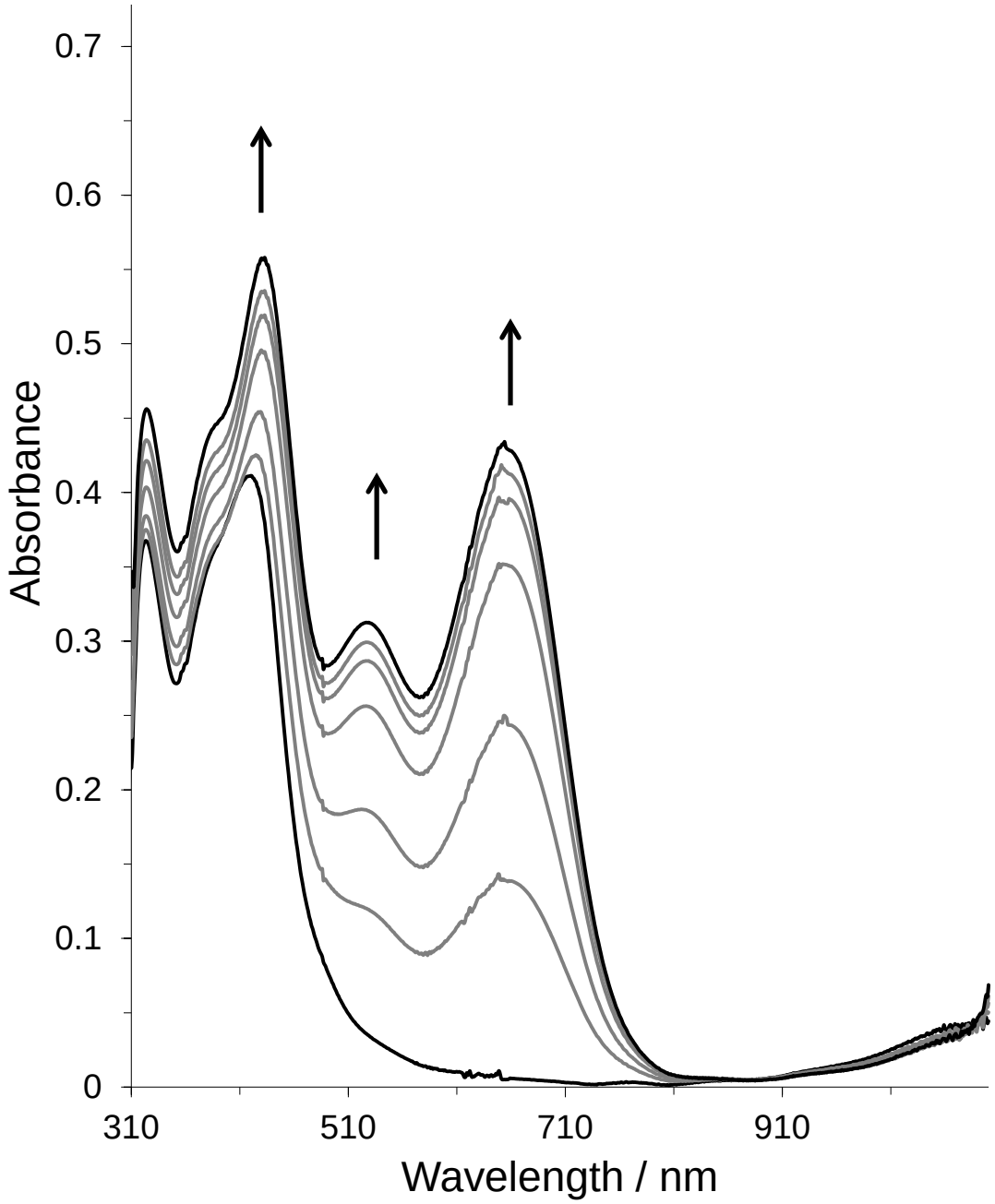

Figure A 40. Absorbance changes in the UV-visible spectra of $[Co(dmgBF_2)_2(H_2O)_2]$ with pyridine in acetone at a constant potential of −0.90 V vs Ag. [complex] = 1.14 mM, [pyridine] = 5.09 mM at a constant potential of, I = 0.10 M ($[^nBu_4N]ClO_4$), path length = 1 mm.

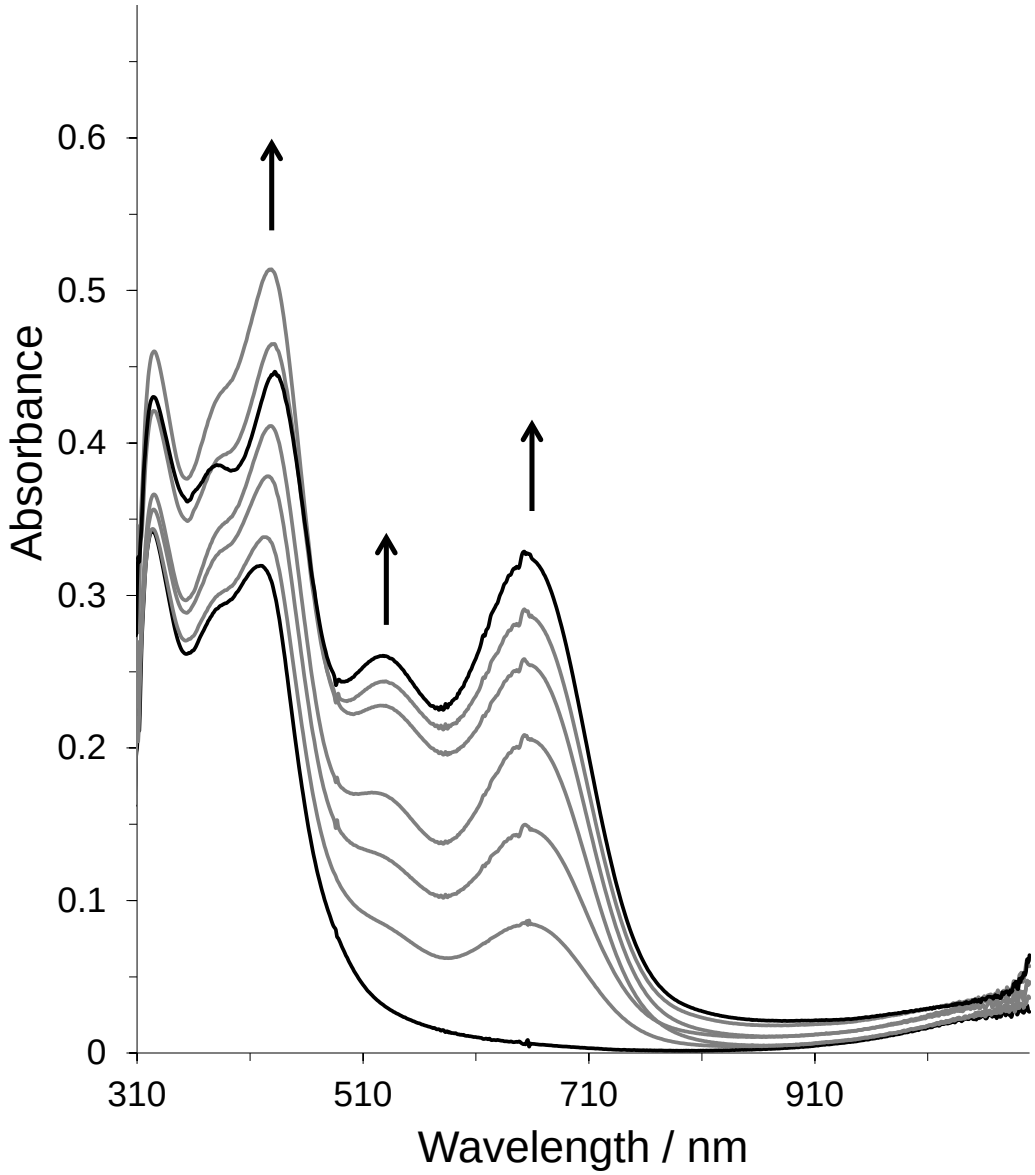

Figure A 41. Absorbance changes in the UV-visible spectra of $[Co(dmgBF_2)_2(H_2O)(py)]\bullet 0.5(CH_3)_2CO$ with pyridine in acetone at a constant potential of −0.90 V vs Ag. [complex] =1.08 mM, [pyridine] = 5.09 mM, I = 0.10 M ($[^nBu_4N]ClO_4$), path length = 1 mm.

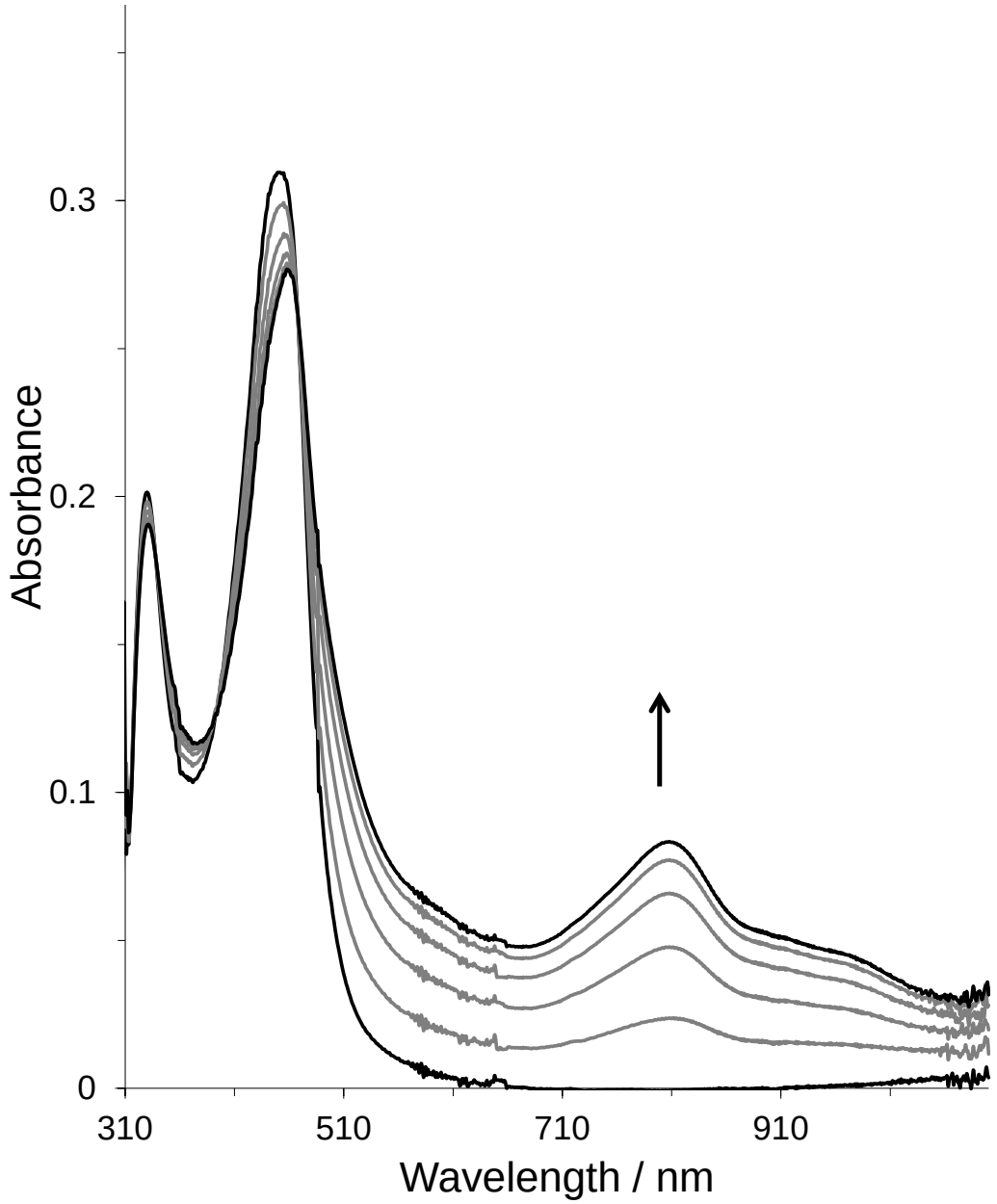

Figure A 42. Absorbance changes in the UV-visible spectra of $[Co(dmgBF_2)_2(H_2O)_2]$ in 2-butanone at a constant potential of −0.70 V vs Ag. [complex] = 1.04 mM, I = 0.10 M ($[^nBu_4N]ClO_4$), path length = 1 mm.

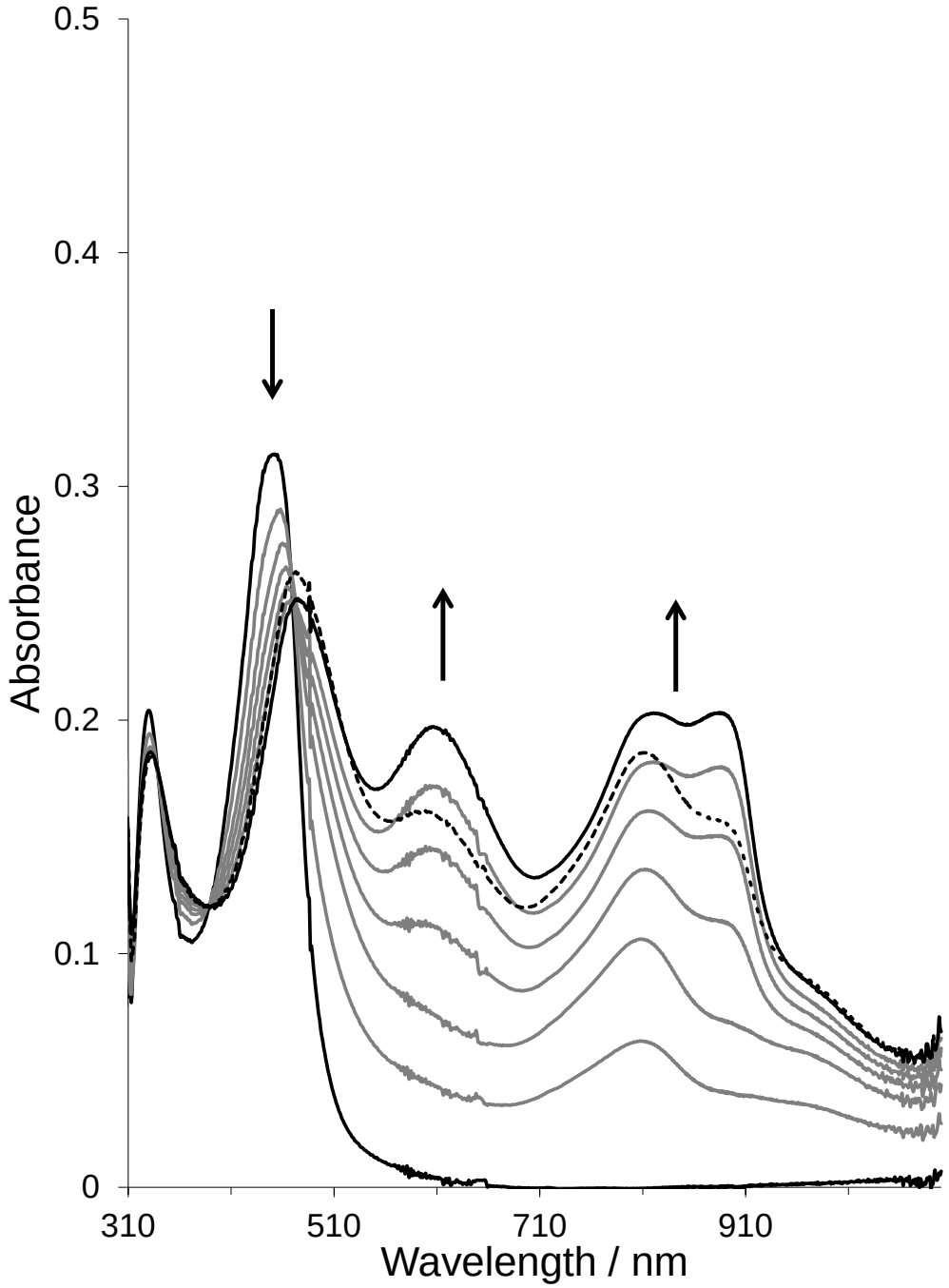

Figure A 43. Absorbance changes in the UV-visible spectra of $[Co(dmgBF_2)_2(H_2O)_2]$ 1 in 2-butanone at a constant potential of −1.10 V vs Ag. [complex] = 1.04 mM, I = 0.10 M ($[^nBu_4N]ClO_4$), path length = 1 mm. Broken line illustrates the spectrum after an extended time.

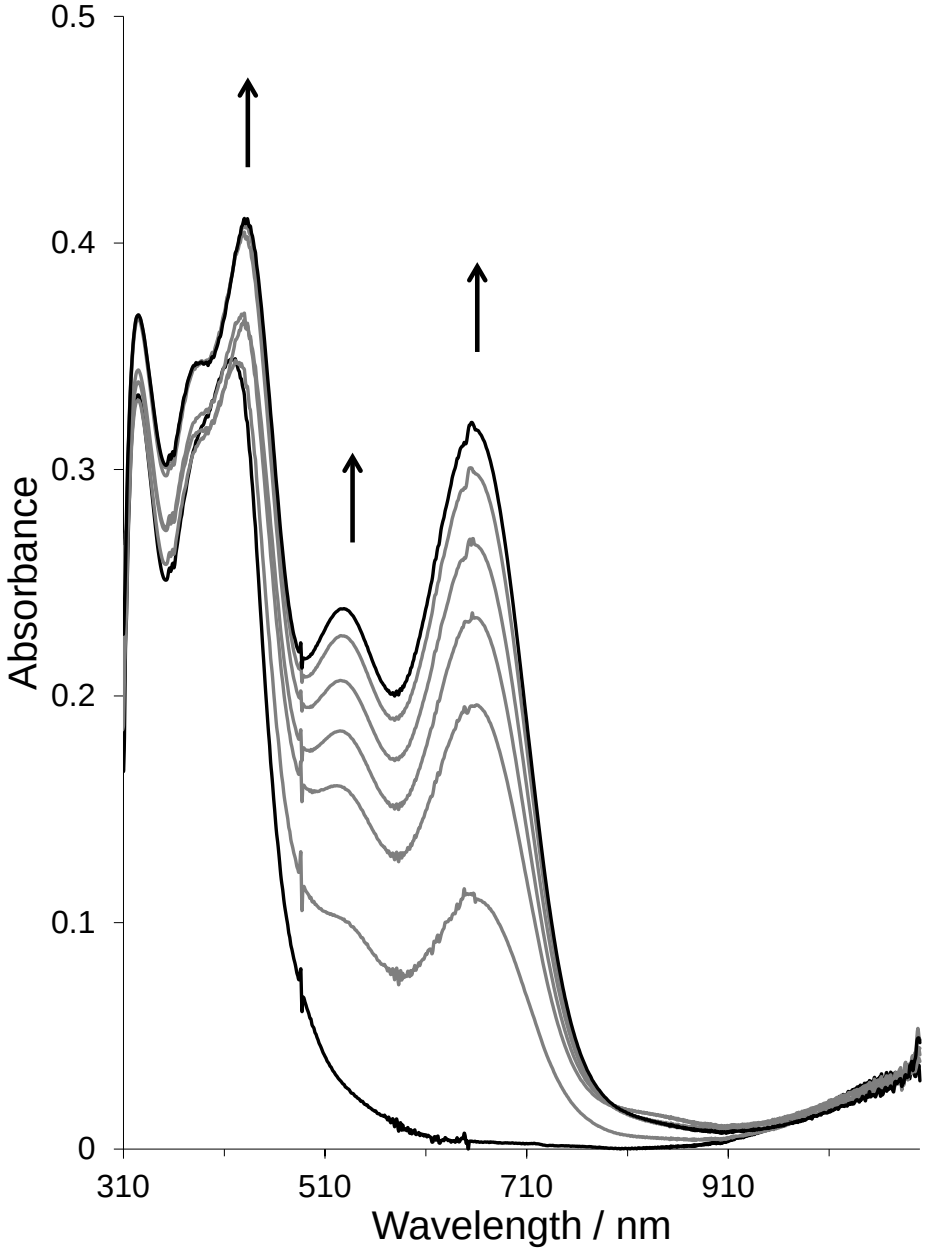

Figure A 44. Absorbance changes in the UV-visible spectra of $[Co(dmgBF_2)_2(H_2O)_2]$ with pyridine in 2-butanone at a constant potential of −0.70 V vs Ag. [complex] =1.04 mM, [pyridine] = 5.09 mM, I = 0.10 M ($[^nBu_4N]ClO_4$), path length = 1 mm.

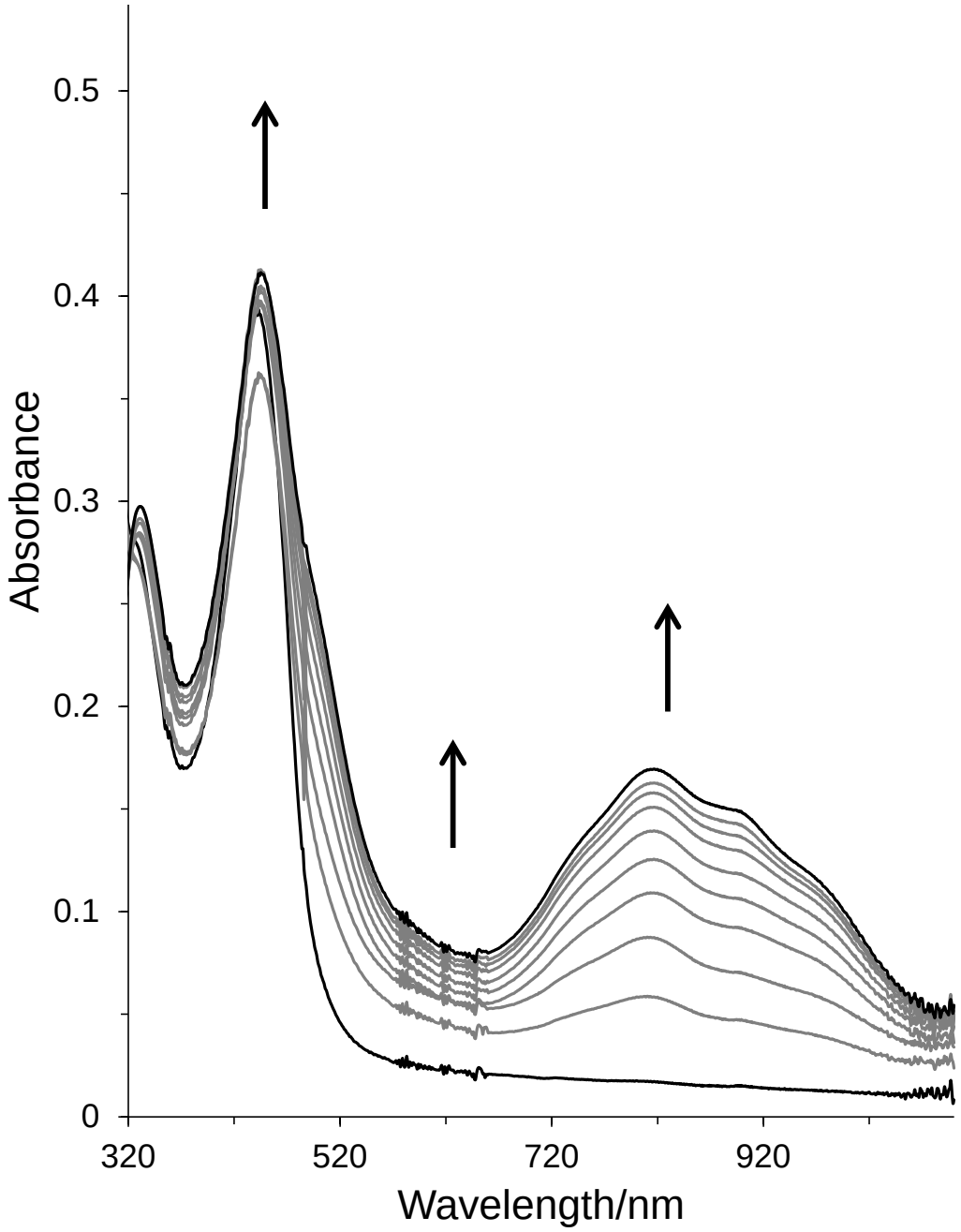

Figure A 45. Absorbance changes in the UV-visible spectra of $[Co(dmgBF_2)_2(H_2O)_2]$ in 1,2-difluorobenzene/acetone (4:1 v/v) at a constant potential of −0.90 V *vs* Ag. [complex] = 1.05 mM, I = 0.10 M ($[^nBu_4N]ClO_4$), path length = 1 mm.

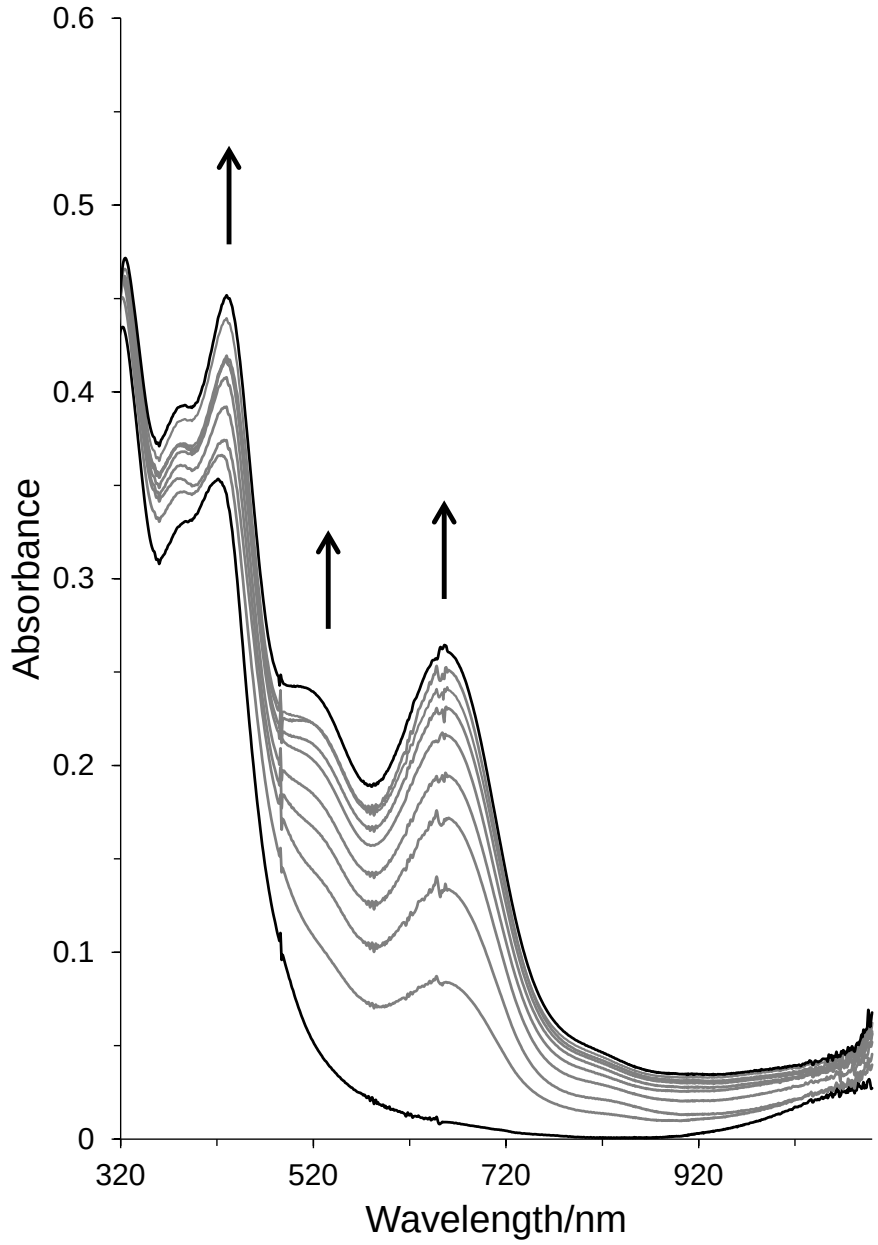

Figure A 46. Absorbance changes in the UV-visible spectra of $[Co(dmgBF_2)_2(H_2O)(py)]\bullet 0.5(CH_3)_2CO$ in 1,2-difluorobenzene/acetone (4:1 v/v) at a constant potential of −0.90 V *vs* Ag. [complex] = 1.03 mM, I = 0.10 M ($[^nBu_4N]ClO_4$), path length = 1 mm.

A7. Electrocatalytic behavior

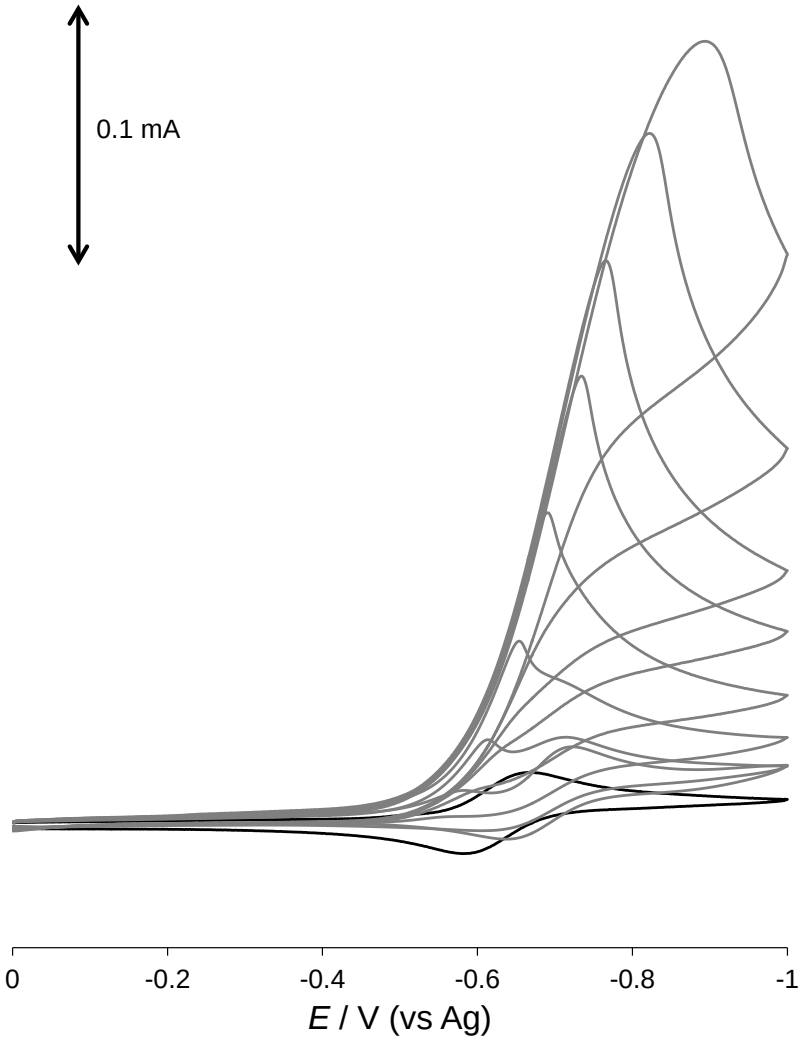

Figure A 47. Cyclic voltammograms involving electrocatalysis with $[Co(dmgBF_2)_2(H_2O)(py)]\bullet 0.5(CH_3)_2CO$ in CH_3CN. [complex] = 1.08 mM in the absence (black) and presence (3.21, 5.54, 9.52, 13.8, 19.6, 25.3, 34.5, and 44.7 mM all others) of *p*-cyanoanilinium tetrafluoroborate, support electrolyte = 0.10 M $[^nBu_4N]ClO_4$, and scan rate = 100 mV s^{-1} at a glassy carbon working electrode *vs* Ag quasi-reference electrode.

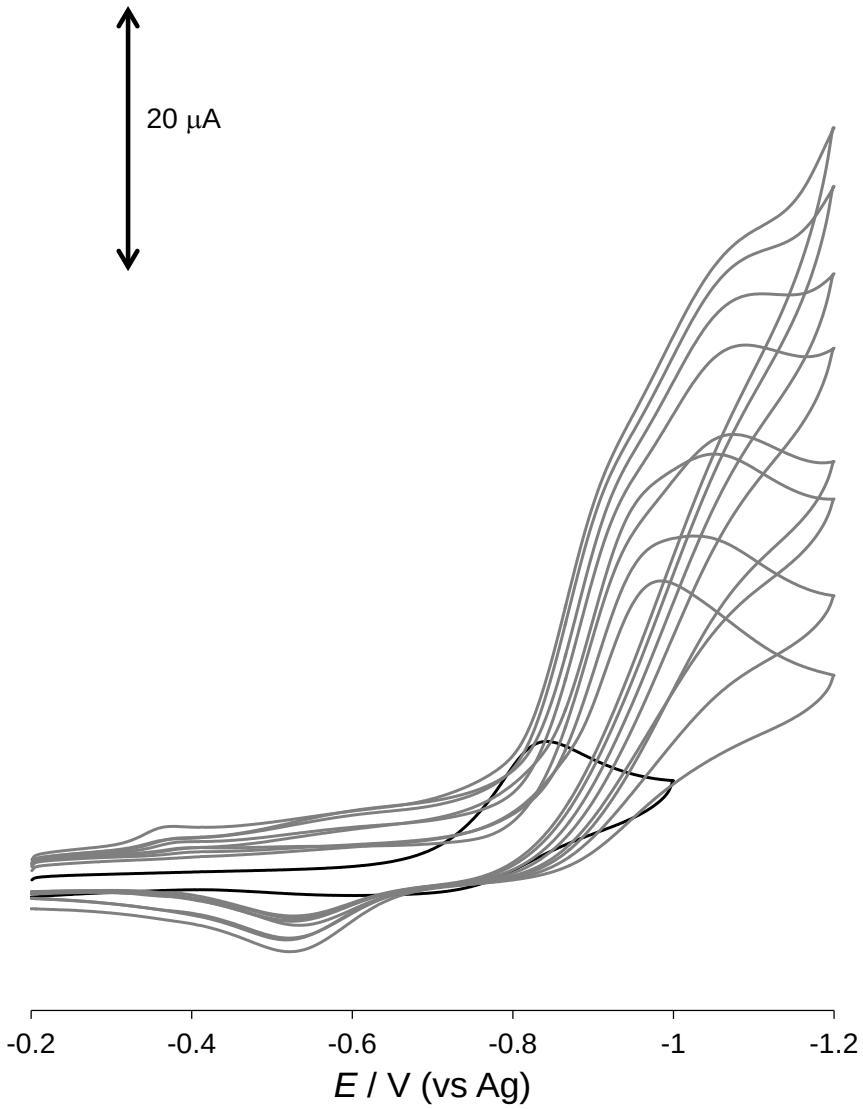

Figure A 48. Cyclic voltammograms involving electrocatalysis with $[Co(dmgBF_2)_2(H_2O)_2]$ in acetone. [complex] = 1.08 mM in the absence (black) and presence (1.80, 3.16, 4.52, 6.17, 8.74, 11.2, 14.9, and 18.6 mM all others) of *p*-cyanoanilinium tetrafluoroborate, support electrolyte = 0.10 M $[^nBu_4N]ClO_4$, and scan rate = 100 mV s^{-1} at a glassy carbon working electrode *vs* Ag quasi-reference electrode.

Figure A 49. Cyclic voltammograms involving electrocatalysis with $[Co(dmgBF_2)_2(H_2O)(py)]\bullet 0.5(CH_3)_2CO$ in acetone. [complex] = 1.08 mM in the absence (black) and presence (1.70, 3.54, 5.24, 7.28, 9.42, 12.4, 16.1, and 18.7 mM all others) of *p*-cyanoanilinium tetrafluoroborate, support electrolyte = 0.10 M $[^nBu_4N]ClO_4$, and scan rate = 100 mV s^{-1} at a glassy carbon working electrode *vs* Ag quasi-reference electrode.

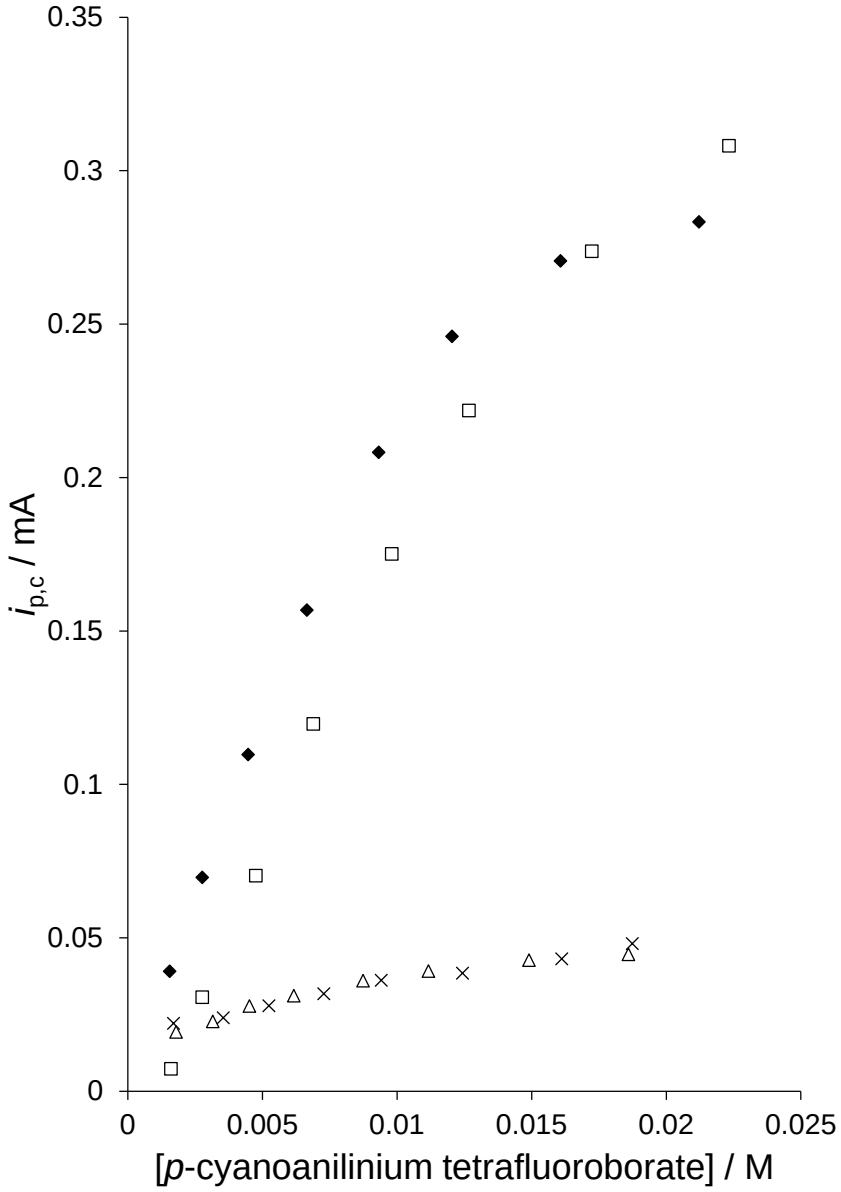

Figure A 50. Dependence of the catalytic peak current ($i_{pc,1}$) on the concentration of *p*-cyanoanilium tetrafluoroborate at a scan rate of 100 mV s^{-1} for $[Co(dmgBF_2)_2(H_2O)_2]$ (♦: in CH_3CN, Δ: in acetone) and complex 2 (□: in CH_3CN, ×: acetone) in 0.10 M $[^nBu_4N]ClO_4$, at a glassy carbon working electrode vs Ag.

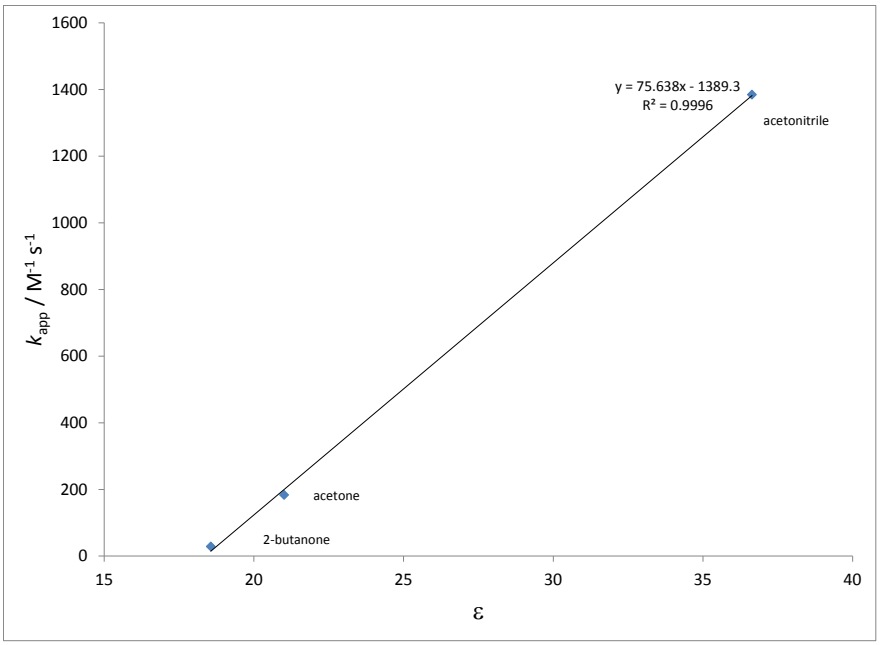

Figure A 51. The effect of dielectric constant on k_{app} (Table 12) for $[Co(dmgBF_2)_2(H_2O)_2]$.

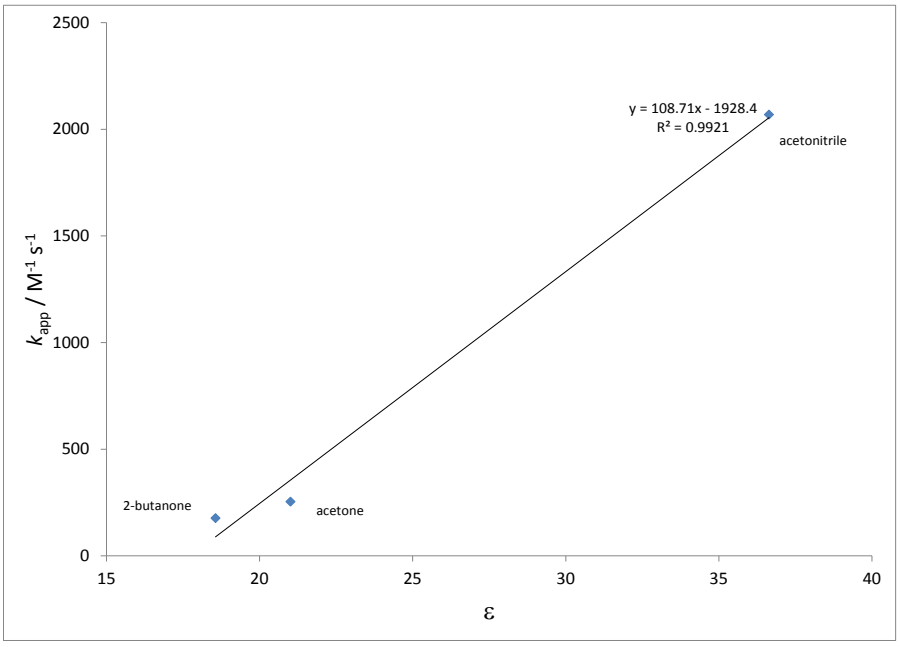

Figure A 52. The effect of dielectric constant on k_{app} (Table 12) for $[Co(dmgBF_2)_2(H_2O)(py)]\bullet 0.5(CH_3)_2CO$.

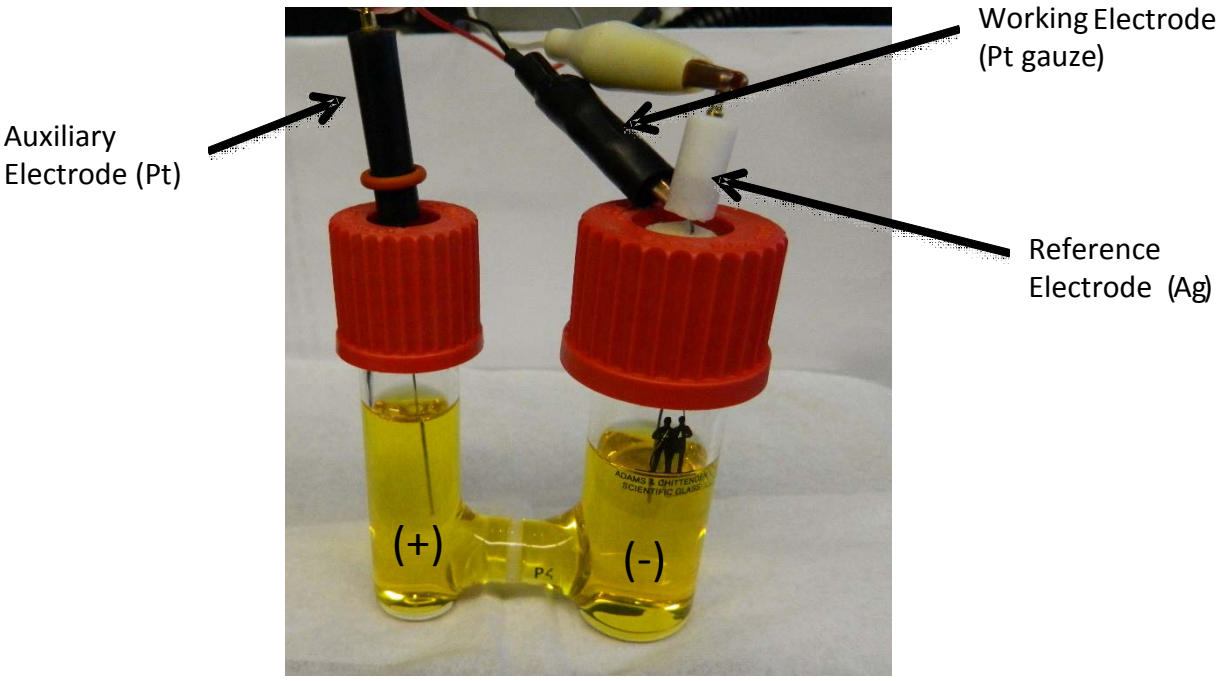

Figure A 53. Set-up of the H-Cell used for the electrocatalytic generation of hydrogen.

VITA

Michael J. Celestine

Department of Chemistry and Biochemistry mcele002@odu.edu

Old Dominion Univeristy

Norfolk, VA 23529

Education

May 2012 ……**B.S. Chemistry**, University of the Virgin Islands, Charlotte Amalie, St. Thomas, U.S. Virgin Islands

August 2015……**M.S. Chemistry**, Old Dominion University, Norfolk, Virginia, U.S.A.

Presentations

Celestine, M.; Ledbetter, A.; Corey, T.; Tippie, A.; Wishart, J.; Miller, J.; Holder, A. "Electrochemical and Radiolytic Studies of Cobalt(II)- and Ruthenium(II)-containing Complexes." Gordon Research Conference: Electrochemistry, Ventura, California, March, 2014

Celestine, M.; Ledbetter, A.; Corey, T.; Tippie, A.; Wishart, J.; Miller, J.; Holder, A. "Electrochemical and Radiolytic Studies of Cobalt(II)- and Ruthenium(II)-containing Complexes." 247th American Chemical Society conference, Dallas, Texas, March, 2014

Book Chapters

Celestine, M.J.; Bullock, J.L.; Holder, A.A. "Solving Some of the World's Problems with Ruthenium Complexes: Their Role in Imaging and Biomedical Application." p. 61 – 89. NOVA Publishers. ISBN: 978-1-63321-657-0

Bullock, J.L.; Celestine, M.J.; Holder, A.A. "Solving Some of the World's Problems with Ruthenium Complexes: Their Use in Solar Energy Capture and Production of Hydrogen." p. 1 – 60. NOVA Publishers. ISBN: 978-1-63321-657-0

Publication

Lawrence, M.A.; Celestine, M.J.; Artis, E.T.; Joseph, L.S.; Esquivel, D.L.; Ledbetter, A.J.; Cropek, D.M.; Holder, A.A. "Spectroscopic and Electrochemical Studies of two Mononuclear Cobaloximes: The influence of an axial pyridine on the redox behavior and evidences for pyridine coordinated to cobalt(I) and cobalt(II) metal centers." Manuscript in progress.